EPS Metop-B Product Validation Report: GOME-2 Level 1

Doc.No.	:	EUM/OPS-EPS/DOC/12/0760
Issue	:	v3A
Date	:	17 May 2013
WBS	:	

EUMETSAT
Eumetsat-Allee 1, D-64295 Darmstadt, Germany
Tel: +49 6151 807-7
Fax: +49 6151 807 555
http://www.eumetsat.int

This page intentionally left blank.

Document Change Record

Issue / Revision	*Date*	*DCN. No*	*Changed Pages / Paragraphs*
v1	04/12/2012		First issue for trial dissemination
v2A	07/02/2013		Issue for pre-operational validation status: The following sections have been considerably updated: 4.3 Dark signal correction 4.5.1 Results on stability and consistency of the spectral calibration 4.9.3 Earthshine Stokes fractions as compared to V-LIDORT model results 4.9.5 Q-Stokes fractions derived from solar measurements 4.11.2.1 Earthshine and reflectivity 4.11.2.2 Metop-A/B global individual co-locations 4.11.2.3 Metop-A/B comparison in the target boxes 4.11.3 Comparison to forward model data (V-Lidort) 4.12 Signal levels (A4.3.5) 5. External Partner Validation
v2B	12/02/1213		Update following PVRB board on pre-operational status All: Clean-up Metop-A / FM3 and Metop-B / FM2 and M01/M02 tags. Section 4.3. Added explanation on larger scatter in noise values between 18th October and 11th November. Section 4.5.1: Updated pre-disperser prism temperature plot and text editing. Section 4.9.5: Added explanation ion the use of Stokes fractions from solar measurements. Section 4.11.2.1: Reference to AR 14557 on GOME-2 FM2 Metop-B scan-angle dependent offset in reflectivity.

Issue / Revision	Date	DCN. No	Changed Pages / Paragraphs
			Figure 102: Titles removed and caption updated. Section 6.1 Added overall conclusion in comparison to Metop-A FM3 pre-operational status
v3	30/04/1213		Issue for operational status: The following sections have been updated or add (according to the Cal-Val planning): Section 1: Update of auxiliary file update history table Section 4.6: Update on FWHM monitoring Section 4.8: Update on overlap point monitoring Section 4.9: New section on the “cleaning” of key-data for the removal of spectral artefacts for on-ground measurements and its impact on level-2 retrievals Section 4.10.3: Updated Section on comparison between Stokes fraction and forward model results Section 4.12.2.4: Completely new section on the identification of the residual co-location structure with degradation residual signals. Section 4.12.3.: Updated conclusion on the reflectivity comparisons to forward model results. Section 4.13: Updated status on the signal level monitoring and updated conclusions on the inter-comparison to Metop-A. Section 5.2.1/2/ Editorial changes Section 5.2.3: New section on a level-2 product performance status summary covering the summaries as collected at the two GSAG meetings in February and April 2013 (48th and 49th). Section 6: Updated concluding remarks, outstanding tasks list, and status and recommendations.
v3A	03/05/2013		Editorial changes after PVRB

Table of Contents

Table of Figures

Table of Tables

1 INTRODUCTION

1.1 Purpose and Scope

This Product Validation Report provides the results of the calibration and validation testing of the following product(s) in the context of the EUMETSAT Polar System (EPS) Metop-B satellite and the GOME-2 Metop-B Flight Model 2 (FM2) level 1 product commissioning:

GOME_xxx_1A_M01 (GOME-2 Metop-B / FM2 level 1A data product)
GOME_xxx_1B_M01 (GOME-2 Metop-B / FM2 level 1B data product)

The Metop-B satellite was launched from Baikonur on 17 September 2012. The satellite commissioning, including Cal-Val testing, aims to verify the satellite and ground segment capability to provide operational services with the required levels of availability, timeliness, and quality. The main objective of Cal-Val testing is to ensure that the quality of the products satisfies the operational requirements.

This report is submitted to the Product Validation Review Board in order to decide on the validation status of the GOME-2 level 1 products. It is intended for the members of the Science and Products Validation Team (SPVT), as well as to the Metop-B commissioning management.

For the validation of GOME-2 Metop-B / FM2 level 1 products, comparisons are frequently made and documented in this report with the currently operational GOME-2 instrument (FM3) flying on board Metop-A and to the corresponding level 1 products:

GOME_xxx_1A_M02 (GOME-2 Metop-A / FM3 level 1A data product)
GOME_xxx_1B_M02 (GOME-2 Metop-A / FM3 level 1A data product)

1.2 Applicable and Reference Documents

1.2.1 Applicable Documents

AD 1 EPS Programme Calibration and Validation Overall Plan, EUM.EPS.SYS.PLN.02.004
AD 2 GOME-2 Calibration and Validation Plan, EPS.SYS.PLN.01.010, issue 3.1
AD 3 GOME-2 Level 1 Product Generation Specification, EPS.SYS.SPE.990011 v7
AD 4 GOME-2 Level 1 Product Format Specification, EPS.MIS.SPE.97232 v9
AD 5 GOME-2 / Metop-B instrument, PPF Auxiliary-data Change history, EUM/OPS-EPS/TEN/09/0616, v2
AD 6 Metop-B / GOME-2 PMD band definitions and PMD Calibration, EUM/OPS-EPS/DOC/12/0714, v1A
AD 7 TNO Space Systems Engineering Gome 2 FM2-2 Instrument Calibration, MO-AD-TPD-GO-0022, I. 2
AD 8 MetOp GOME-2 In-Orbit Verification: Final Report

1.2.2 Reference Documents

[RD1] MetOp GOME-2 In-Orbit Verification Plan, MO.PL.ESA.SY.0920, issue 1.2

[RD2] GOME-2 Level 1B Product Validation Report No. 3: Operational Status, EUM/MET/REP/08/0103, 1A

[RD3] EPS Metop-B GOME SIOV Operations Implementation Plan, EUM/OPS-EPS/PLN/11/0273, v2C

[RD4] GOME2 PPF 5.3 Software Release Note, EUM/OPS-EPS/DOC/09/0609, 1C

[RD5] EPS Generic Product Format Specification (GPFS), EPS.GGS.SPE.96167, v. 6.6

[RD6] GOME-2 SPA/PQE Software User Manual, EUM/OPS/SUM/11/2479, v1

[RD7] Investigation on GOME-2 throughput degradation, EUM/LEO/REP/09/0732

[RD8] GOME-2 / Metop-A Level 1B Product Validation Report No. 5: Status at Reprocessing G2RP-R2, EUM/OPS-EPS/REP/09/0619, 1F

[RD9] GOME Annual In-Flight Performance Review 2011, EUM/OPS-EPS/REP/11/0057,

[RD10] Auxiliary Data Inventory Update GOME2 - Product Processing Facility version 5, EUM/OPS-EPS/DOC/09/0573, v1B.

[RD11] GOME-2 PMD Band Definitions 3.0 and PMD Calibration, EUM/OPS-EPS/DOC/07/0601, v8

[RD12] Cai, et al, Characterization and Correction of Global Ozone Monitoring Experiment-2 Ultraviolet Measurements and Application to Ozone Profile Retrievals, JGR, submitted, 2012.

[RD13] Cloud retrieval algorithm for GOME-2: FRESCO+, EUM/CO/09/4600000655/RM, 2011.

[RD14] Support for upgrade to FRESCO+ in the GOME-2 PPF: Final Report, EUM/CO/09/4600000655/RM, 2011.

[RD15] GOME-2 Error Assessment Study Final Report, Phases I—IV, EUM/CO/01/901/DK, December 2002

[RD16] GOME-2 Error Assessment Study Final Report, Phase V, EUM/CO/01/901/DK, April 2004

[RD17] Hartmann, H.W., C.P. Tanzi, J.M. Krijger, and I. Aben, GOME-2 Polarisation Study - Phase C/D: Final Report, RP-GOME2-003SR, SRON, Utrecht, The Netherlands

[RD18] Koelemeijer, R.B.A., P. Stammes, J.W. Hovenier and J.F. de Haan, “A fast method for retrieval of cloud parameters using oxygen A-Band measurements from GOME”, JGR, Vol 106, 3475-3490, 2001

[RD19] Wang, P. and P. Stammes, FRESCO-GOME2 project “Additions to EPS/MetOp RAO project #3060” EUM/CO/06/1536/FM, Final Report, September 2007.

[RD20] O3M SAF VALIDATION REPORT, O3M SAF VALIDATION REPORT, issue 3, 2009.

[RD21] Final Report for RfQ 10/202689: Support for (V)LIDORT Implementation at EUMETSAT, with Statement of Work (SoW) EUM/MET/SOW/10/0301, 31 December 20.

[RD22] A. Serdyuchenko *et al.,* High spectral resolution ozone absorption cross-sections: Part I. Measurements, data analysis and comparison around 293K, JQSRT, 2012.

[RD23] A. Serdyuchenko *et al.,* High spectral resolution ozone absorption cross-sections: Part II. Temperature dependence, JQSRT, 2012.

[RD24] R. Siddans, B.G. Latter, Analysis of GOME-2 (FM202-2), Slit function Measurements, Final Report Eumetsat Contract No. EUM/CO/04/1298/RM, version 1.0, RAL, 2013.

[RD25] 48th GSAG, Minutes of Meeting, EUM/RSP/MIN/13/691056, version 1, 2013.

[RD26] 49th GSAG, Minutes of Meeting, 2013.

1.3 Acronyms and Abbreviations Used in this Document

Acronym	*Meaning*
AVHRR	Advanced Very High Resolution Radiometer
BUFR	Binary Universal Form for the Representation of meteorological data
CFR	Cloud FRactions
FFT	fast Fourier transform
FWHM	Full Width at Half Maximum
IFOV	Instantaneous Field of View
KNMI	Koninklijk Nederlands Meteorologisch Instituut (Royal Netherlands Meteorological Institute)
LIDORT	LInearized Discrere Ordinate Radiative Trasfer
NESDIS	National Environmental Satellite and Data Information Service
NOAA	National Oceanic and Atmospheric Administration
NRT	Near Real-Time
PDU	Product Dissemination Unit
PMD	polarization measurement device
PPF	level 0 to 1 Product Processing Facility
SMR	Solar Mean Reference
SZA	Solar Zenith Angle
SIOV	Satellite In-Orbit Verification Phase
WLS	White Light Source

1.4 Description of Validation Environment

The product validation has been performed with the following elements:

EUMETSAT Central Ground Segment (CGS):
EPS GS1 running GOME-2 PPF 5.3.0
EPS GS2 running GOME-2 PPF 5.3.0

See 0 for details of the PPF configuration, including auxiliary files and instrument operation changes. [RD4] contains a description of the PPF 5.3.0 history and changes.

EUMETSAT offline environment MPSTAR:
EPQM-SPQA and jmonx version 1.0.

All analysis makes use of the MPSTAR monitoring database and uses data from the OPE GOME database instance on fodbss02 and its EPS rolling archive [RD6].

1.4.1 EUMETSAT technical computing environment (TCE)

The PPF 5.3.0 is run offline (reprocessing) on TCE (/leo/rlang/proc/PPF-GOME-INST and /leo/rlang/proc/working_root_M01/) for dedicated analysis where necessary. A suite of MATLAB prototype and analysis tools is used for most of the analysis presented in this document. This includes, fetching data from the MPSTAR GOME OPE database and direct reading of data from level 1 data files either provided by the tcdras rolling archive (RA) of MPSTAR (/tcc1/fbf/tcdras/store/) or from offline reprocessed data (see before). All analysis scripts are available under */leo/rlang/proc/matlab/procedures*.

Dedicated results and data analysed are stored in */leo/rlang/data/MetopB/*.

1.4.2 Instrument key-data (FM2-2)

The results of the on-ground re-calibration measurements (FM2-2) are gathered in the “key-data” auxiliary file (GOME_CAL_xx_M01*), which is then used during level 0 to 1B processing. The initial set of key-data from the ground campaign has been used directly after launch and was contained in V 1.00 of the GOME_CAL_xx_M01 auxiliary file. Updates to key-data and this auxiliary file are discussed in Section 4. If not otherwise specified (because of such updates), the calibration auxiliary file contains the results of the FM2-2 on-ground calibration campaign carried out by TNO/Selex Galileo/ESA SSST from October 2010 to July 2011 with a final delivery of data in February 2012. All documentation along with the key-data set that was used is available here:

ftp://ftp.eumetsat.int/pub/EPS/out/GOME/Calibration-Data-Sets/Calibration-Key-Data/FM2-Metop-B/

The calibration FM2-2 is the follow-on to the initial FM2 calibration (FM2-1) carried out during 2004–2005. Details of this initial calibration are in 0.

1.4.3 Auxiliary data used for level 0 to 1B processing

Here we list the initial set of key-data used directly after launch and their subsequent updates. See Section 4 for a description of the updates.

Date	*Processor Version*	*AUX data version*	*PFS version*	*PGS version*
22/09/2012	5.3.0	STA_FM3_104	9	7
Launch		INS_FM2_100		
		COR_FM2_100		
		CAL_FM2_100		
16/10/2012	5.3.0	STA_FM3_104	9	7
GIOV		INS_FM2_101		
		COR_FM2_100		
		CAL_FM2_100		
28/11/2012	5.3.0	STA_FM3_104	9	7
CALVAL		INS_FM2_102		
Phase 1		COR_FM2_100		
		CAL_FM2_101		
17/12/2012	5.3.0	STA_FM2_100	9	7
CALVAL		INS_FM2_102		
Phase 1		COR_FM2_100		
		CAL_FM2_102		
07/05/2012	5.3.0	STA_FM2_100	9	7
CALVAL		INS_FM2_103		
Phase 2		COR_FM2_100		
		CAL_FM2_103		

Table 1: Metop-B / FM2 / GOME-2 Processor and Auxiliary data version update for CGS1/EUMETCast/UMARF. Changes are indicated in blue.

For a description of the auxiliary data types and content, see [RD10].

2 THE INSTRUMENT

The Global Ozone Monitoring Experiment–2 (GOME-2) is an optical spectrometer fed by a scan mirror which enables across-track scanning in nadir, as well as sideways viewing for polar coverage and instrument characterisation measurements using the moon. GOME-2 senses the earth's backscattered radiance and extraterrestrial solar irradiance in the ultraviolet and visible part of the spectrum (240–790 nm) at a high spectral resolution between 0.26–0.51 nm. There are 4096 spectral points from four detector channels transferred per individual GOME-2 measurement (see Figure 1).

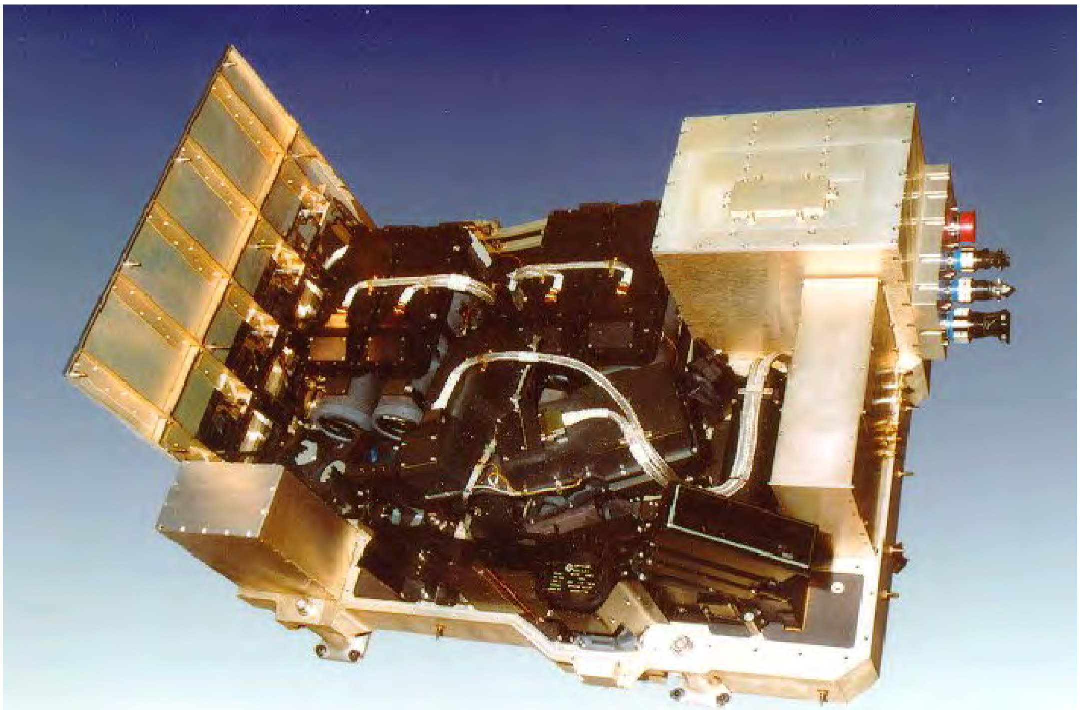

Figure 1: The Global Ozone Monitoring Experiment–2 (GOME-2) Instrument

The footprint size is 80 × 40 km for main channel data. The instrument also measures the state of linear polarisation of the backscattered earthshine radiances in two perpendicular directions. The polarisation data is down-linked in 15 spectral bands covering the region from 312 nm–800 nm for both polarisation directions with a footprint of 10 × 40 km.

The recorded spectra are used to derive a detailed picture of the total atmospheric content of ozone and the vertical ozone profile in the atmosphere. They also provide accurate information on the total column amount of nitrogen dioxide, sulphur dioxide, water vapour, oxygen /oxygen dimer, bromine oxide and other trace gases, as well as aerosols and cloud optical properties (Figure 2).

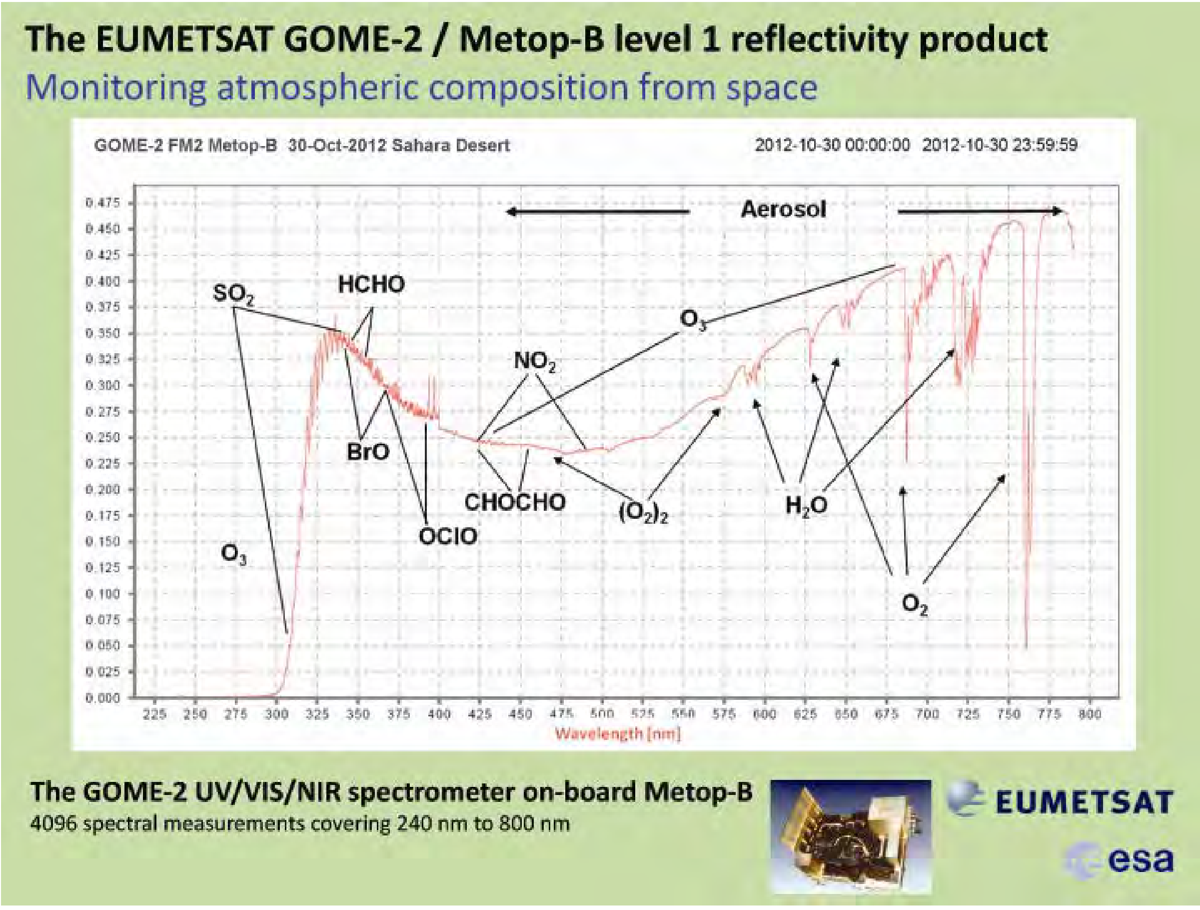

Figure 2: GOME-2 Metop-B / FM2 transmittance as derived from the GOME-2 level 1b M01 radiance product. Selected spectral regions with absorption signatures used for various trace gas products as derived from GOME-2 level-1b radiances are shown.

The GOME-2 instrument has been developed by SELEX/Galileo Avionica in Florence, Italy, under a joint contract with EUMETSAT and ESA.

2.1 GOME-2 Optical Layout ([AD2])

The four main channels of the GOME-2 instrument provide continuous spectral coverage of the wavelengths between 240 nm and 790 nm with a spectral resolution full width at half maximum (FWHM) between 0.26 nm and 0.51 nm. Channel characteristics are listed in Table 1. The optical configuration of the instrument is shown in Figure 3. Light enters the two-mirror telescope system via the scan mirror. The telescope projects the light beam onto the slit, which determines the instantaneous field-of-view (IFOV) of $0.28^o \times 2.8^o$ (across-track $\times$ along-track). After it has passed the slit, the beam is collimated again and enters a double Brewster prism for partial split-off to PMD-S, followed by the pre-disperser prism which has two functions. Brewster reflection at the back of the prism splits off part of the p-polarisation direction to PMD-P. The prism furthermore forms a low-dispersion spectrum which is subsequently separated at the channel separator prism into three parts that go to Channel 1 (transmitted beam), Channel 2 (reflected beam), and Channels 3 and 4, respectively. The separation between channels 3 and 4 is performed by a dichroic filter.

A grating in each channel then further disperses the light, which is subsequently focused onto the detector array. Each PMD channel contains a dispersion prism and two additional folding prisms and collimating lenses. PMD-P measures intensity polarised parallel to the spectrometer’s slit, and PMD-S measures intensity polarised perpendicular to the spectrometer’s slit. The two PMD channels are designed to ensure maximum similarity in their optical properties. The wavelength-dependent dispersion of the prisms causes a much higher spectral resolution in the ultraviolet than in the red part of the spectrum.

Table 2 gives values for GOME-2 FM2. For the overlap regions between the main channels, the wavelengths are given for the 10 % intensity points. For example, at 310 nm, 10 % of the signal is registered in channel 2, and 90 % is registered in channel 1. At 314 nm, 10 % of the signal is registered in channel 1, and 90 % is registered in channel 2. Spectral resolution varies slightly across each main channel; the given values are channel averages.

Channel	*Spectral range [nm]*	*Detector Pixel size [nm]*	*FWHM [nm]*
1	239 – 312	0.1	0.29
2	308 – 402	0.1	0.28
3	395 – 604	0.2	0.55
4	593 – 791	0.2	0.5
PMD-P PMD-S	312 – 790	0.62 (312 nm)–8.8 (790 nm)	2.9 (312 nm)–37 (790 nm)

Table 2: Channel characteristics of GOME-2 FM2 spectral coverage and resolution (in-flight situation; see also Section 4.8)

The GOME-2 channels can be separated in different bands operating at different integration times. The latter can also vary over the orbit. Nominal integration times in band 1A are 1.5 seconds (6 seconds at high solar zenith angles) and 0.1875 seconds for band 1B to band 4 (1.5 and 0.75 seconds at high SZA). For details on the exact integration times per band during one instrument timeline series, see the GOME-2 monitoring pages in the *timelines* sub-section at this address:

gome.eumetsat.int.-> *Metop-B*

The separation between band 1A and band 1B remains for Metop-B / FM2 at the same position as for FM3 on Metop-A, where it was set to detector pixel number 659 on 10 December 2008. This is in accordance with the GOME-1 and SCIAMACHY instrument specifications.

Channel	*1*	*1*	*2*	*2*	*3*	*4*	*5/6*
Band	1A	1B	2A	2B	3	4	PMD P/S
Used Pixels	659	365	71	953	1024	1024	256
Valid Spectral Range (nm)	240-283	283-309.7	not valid[1]	309.8-397.7	397.7-598.4	598.4-790	290-790
nm/pixel	0.07	0.07	0.09	0.09	0.2	0.2	2[2]

[1] Because detector pixels are all outside the valid range
[2] Variable over the channels

Table 3: Main channel band settings of GOME-2 FM2 Metop-B.

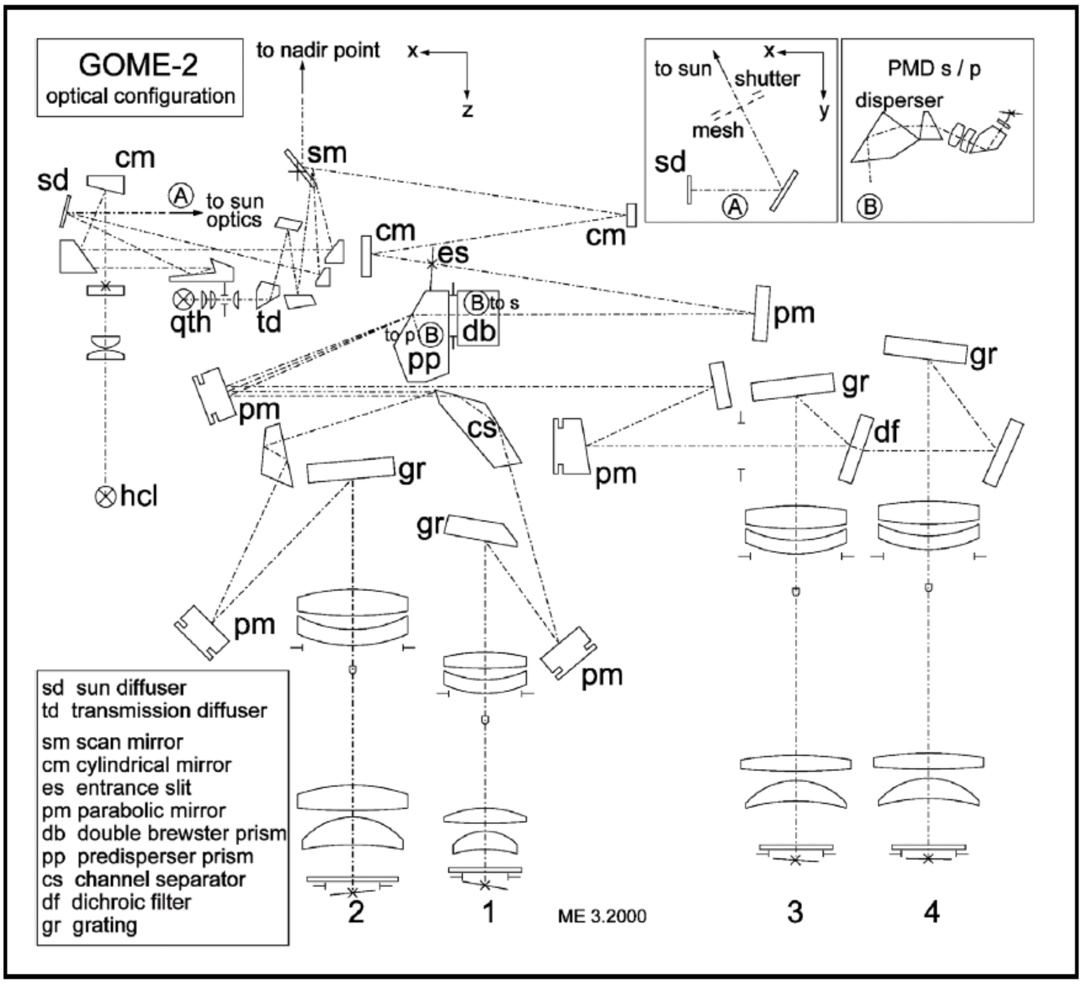

Figure 3: GOME-2 optical layout. The optics lie in one plane (except insets A and B). Nadir is in −Z direction.

2.1.1 Polarisation Measurement Device (PMD) band settings

The 256 detector pixels of both PMD devices of block C, D, and E (see 0 for specifications) are co-added on board in spectral space and for nominal earthshine measurements in 15 PMD spectral bands. After launch, the PMD settings from version 3.1 from Metop-A/FM3 have been used and are tagged as versions 1.0. These settings were updated during SIOV at 29/10/2012:18:11:30 during orbit 598 to achieve an optimal co-registration between both PMD detectors.

PMD-P					*PMD-S*				
Band Nr	*Start pixel with respect to Block C*	*Width*	*Start*	*End*	*Band Nr*	*Start pixel with respect to Block C*	*Width*	*Start*	*End*
0	23	5	312.001	314.516	0	22	5	311.875	314.375
1	31	4	317.102	319.090	1	30	4	316.948	318.926
2	38	12	321.807	329.675	2	37	12	321.634	329.514
3	51	6	331.172	335.020	3	50	6	331.016	334.872
4	57	6	335.808	339.848	4	56	6	335.661	339.698
5	85	17	360.825	378.308	5	84	17	360.644	378.138
6	103	4	380.706	384.399	6	102	4	380.515	384.170
7	118	19	400.383	428.763	7	117	19	400.059	428.350
8	140	27	435.971	493.963	8	139	27	435.521	493.181
9	167	18	496.683	550.625	9	166	18	495.886	549.510
10	185	2	554.330	558.106	10	184	2	553.192	556.944
11	189	11	569.885	614.699	11	188	11	568.637	612.854
12	200	8	619.714	658.343	12	199	8	617.781	656.047
13	219	4	739.726	763.366	13	218	4	737.179	760.682
14	225	2	788.551	797.300	14	224	2	785.719	794.415

Table 4: GOME-2 Metop-B/FM2 PMD band definitions (v2.0) valid from 29/10/2012 18:11:30 (orbit 598).

For more details on the PMD calibration and PMD band settings details, see 0 and the summary provided in Section 4.1.

2.2 GOME-2 Metop-B / FM2 Specifications Summary

Item	*Specification*
Spectral band (nm)	240-790
Spectral resolution (nm)	0.26-0.51
Spatial resolution (km2)	80 × 40 (main channels) 80 × 10 (PMD)
Earth coverage (km)	120-1920
Spectral channels	4096 (in four separated optical channels)
Polarization channels	30 (in two separated optical channels)
Calibration system	Spectral lamp, white lamp, solar diffuser
Dimensions	600 mm × 800 mm × 500 mm
Weight	68 kg
Main bus voltage	22-37 V
Power consumption	50 W
Data rate interface	400 kbit

2.3 GOME-2 Level 1b products

- sun-normalised nadir radiance
- absolute nadir radiance
- absolute sun radiance
- spectral calibration parameters
- sun mean reference spectrum
- effective cloud fraction
- cloud-top pressure
- geo-reference parameters

2.4 GOME-2 Level 2 Products

The Satellite Application Facility (SAF) on Ozone Monitoring (O3MSAF) has the responsibility for extraction of meteorological or geophysical (level 2) products from GOME. Details are at this address:

o3msaf.fmi.fi/

For detailed validation of GOME-2 level-2 products, both offline and online, see the web page:

http://lap.physics.auth.gr/eumetsat/index.php

A collection of “quick-look” imagery of GOME-2 level 2 data is available here:

http://atmos.caf.dlr.de/gome2/index.html

Table 5 contains a product and format cross-reference. The product format type, either HDF5 and/or binary universal form for the representation of meteorological data (BUFR), is given for each product:

Product	***Format Type***
Total column ozone	HDF5 and BUFR
Ozone profiles	HDF5 and BUFR
NO2	HDF5
NO2 tropics	HDF5
BrO, SO2	HDF5
HCHO	HDF5
OClO, Aerosol Absorbing Index	HDF5
Clear Sky UV fields	HDF5
UV fields with Clouds and Albedo	HDF5
Total Water Vapour Column	HDF5

Table 5: Product and format type list

Level 2 products being planned for future operational provision by the O3MSAF include the following: tropospheric ozone, BrO, and CHOCHO, among others.

2.5 Other Useful links

All of the detailed description and specifications are in the GOME-2 Product Guide and on the ESA GOME-2 page. The GOME-2 Product Quality Monitoring website provides summarized information on availability, daily and orbit reports, timelines in use, and product quality. Here is the primary intranet address:

Home > Service Status > Product Quality Monitoring > GOME-2 instrument

3 GOME FM2 IOV ACTIVITIES

GOME FM2 IOV activities area have been carried out between the LEOP hand-over of the satellite to EUMETSAT/SSST 3 days after launch and the final SIOV meeting on 9 November 2012. The final report issued by ESA-SSST and Selex/Galileo contains all the results of the basic functional and instrument performance tests carried out according to the SIOV plan [RD3]. The results are summarised in the SIOV FM2 report 0.

With respect to the purpose of commissioning and calibration/validation activities for the GOME-2 FM2 level 1B product, during this initial IOV phase a couple of essential measures have been implemented predominantly related to the collection of all required data in the MPSTAR OPE and VAL databases for GOME-2/FM2.

In addition to the collection of data and to make sure that all functional requirements for the extraction dn analysis of data for level 1b Cal-Val are in place, two additional joint CalVal/IOV activities have been carried out.

1. Adjustment of the on-board PMD band settings.
2. Monitoring and preliminary evaluation of the FM2 IOV phase 4 (cooling down) and the phase 7 throughput-test activities.

A summary of the analysis (point 1) is provided in Section 4.6. The detailed analysis is provided in 0. A summary of the observed signals during the phase 7 test (point 2) and a preliminary summary on the overall signal (throughput) performance is provided in Section 4.10.

Table 6 shows the sequence of timelines which have been issued during the course of the Metop-B / FM2 IOV campaign, as a reference for the current and for future calibration/validation activities, which may involve this timeframe.

GOME-2 Metop-B FM2 IOV timeline schedule

Phase	Day L+		1st Timeline start	JD (1-1-2000)	Orbit	1	2	3	4	5	6	7	8	9	10	11	12	13	14	15	# Orbits per day
1+2	6											*Switch-on and functional tests*									
3	7	Mon 24/09	268-00:09:13	4650	90	G11W	G11W	G11W	**CAL4W**	1920W	change r/o	G11W	G11W	**CAL4W**	change r/o	G11W	G11W	G11W	G11W	G11W	15
	8	Tue 25/09	269-01:25:58	4651	105	G11W	G11W	G11W	G11W	G11W	G12W	G12W	G12W	CAL4W	G12W	G12W	G12W	G12W	G12W		14
	9	Wed 26/09	270-01:01:36	4652	119	G27W	1920W	NADIRW	CAL4WQ40	CAL4WQ38	CAL4W	NADIRW	NADIRW	NADIRW	NADIRW	NADIRW	NADIRW	NADIRW	NADIRW		14
	10	Thu 27/09	271-00:37:14	4653	133	NADIRW	NADIRW	NADIRW	CAL4W	NADIRW	**CAL6W**	960W	manoeuvre	manouver	manouver	manouver	manouver	manouver	manouver		14
	11	Fri 28/09	272-00:12:51	4654	147	manouver	manouver	manouver	manouver	manouver	manouver	manouver	manouver	960W	960W	960W	960W	960W	960W	960W	15
	12	Sat 29/09	273-01:29:36	4655	162	960W	960W	960W	CAL4W	960W	CAL6W	960W	960W	G71W	G71W	G71W	G71W	G71W	G71W		14
	13	Sun 30/09	274-01:14:15	4656	176	G71W	G71W	G71W	CAL4W	G71W	CAL6W	G72W	G72W	G73W	G73W	G73W	G74W	G74W	G74W		14
	14	Mon 01/10	275-00:53:27	4657	190	NSW	NSW	NSW	CAL4W	NSW	CAL6W	NSW	NSW	NSW	NSW	NSW	NSW	NSW	NSW		14
	15	Tue 02/10	276-00:32:38	4658	204	1920W	1920W	1920W	1920W	1920W	CAL6W	1920W	1920W	1920W	1920W	1920W	1920W	1920W	1920W		14
	16	Wed 03/10	277-00:11:49	4659	218	1920W	1920W	1920W	1920W	1920W	CAL6W	1920W	1920W	1920W	1920W	1920W	1920W	1920W	1920W	1920W	15
	17	Thu 04/10	278-01:32:22	4660	233	1920W	1920W	1920W	1920W	1920W	CAL6W	1920W	1920W	1920W	1920W	1920W	1920W	1920W	1920W		14
	18	Fri 05/10	279-01:11:33	4661	247	1920W	1920W	1920W	1920W	1920W	CAL6W	1920W	1920W	MOON1W	MOON1W	MOON1W	MOON1W	MOON1W	MOON1W		14
	19	Sat 06/10	280-00:50:44	4662	261	MOON1W	MOON1W	MOON1W	MOON1W	MOON1W	MOON1W	MOON1W	MOON1W	MOON1W	1920W	1920W	1920W	1920W	1920W		14
	20	Sun 07/10	281-00:29:55	4663	275	1920W	1920W	1920W	1920W	1920W	CAL6W	1920W	1920W	1920W	1920W	1920W	1920W	1920W	1920W		14
	21	Mon 08/10	282-00:09:06	4664	289	1920W	1920W	1920W	1920W	1920W	CAL6W	1920W	THERM3	THERM5	1920W	1920W	1920W	1920W	1920W	1920W	15
	22	Tue 09/10	283-01:29:39	4665	304	1920W	1920W	1920W	1920W	1920W	CAL6W	1920W	1920W	1920W	1920W	1920W	1920W	1920W	1920W		14
	23	Wed 10/10	284-01:08:50	4666	318	1920W	1920W	1920W	1920W	1920W	CAL6W	1920W	1920W	1920W	1920W	1920W	1920W	1920W	1920W		14
	24	Thu 11/10	285-00:48:00	4667	332	1920W	1920W	1920W	CAL4WQ40	CAL4WQ38	CAL4W	1920W	1920W	1920W	1920W	1920W	1920W	1920W	1920W		14
	25	Fri 12/10	286-00:27:11	4668	346	1920W	1920W	1920W	1920W	1920W	CAL6W	1920W	DSM set	1920W	1920W	1920W	1920W	1920W	1920W		14
	26	Sat 13/10	287-00:06:22	4669	360	1920W	1920W	1920W	1920W	1920W	CAL6W	1920W	1920W	1920W	1920W	1920W	1920W	1920W	1920W	1920W	15
	27	Sun 14/10	288-01:26:55	4670	375	1920W	1920W	1920W	1920W	1920W	CAL6W	1920W	1920W	1920W	1920W	1920W	1920W	1920W	1920W		14
	28	Mon 15/10	289-01:06:05	4671	389	1920W	1920W	1920W	1920W	1920W	CAL6W	1920W	1920W	1920W	1920W	1920W	1920W	1920W	1920W		14
	29	Tue 16/10	290-00:45:15	4672	403	1920W	1920W	1920W	1920W	1920W	CAL6W	1920W	1920W	1920W	1920W	1920W	1920W	1920W	1920W		14
4	30	Wed 17/10	291-00:24:26	4673	417	1920W	1920W	1920W	MOON1W	255K THRUPH4	THRUPH4	THRUPH4	250K THRUPH4	THRUPH4	THRUPH4	245K THRUPH4	THRUPH4	THRUPH4	THRUPH4		14
	31	Thu 18/10	292-00:03:36	4674	431	THRUPH4	THRUPH4	240K THRUPH4	THRUPH4	THRUPH4	235K THRUPH4	THRUPH4	THRUPH4	THRUPH4	THRUPH4	THRUPH4	THRUPH4	THRUPH4	THRUPH4	THRUPH4	15
5	32	Fri 19/10	293-01:24:08	4675	446	Change r/o	G11	G11	**CAL4**	Change r/o	G11	G11	G11	G11	G11	G11	G11	G11	G11		14
	33	Sat 20/10	294-01:03:18	4676	460	G11	G11	G11	CAL4	G11	G12	G12	G12	G12	G12	G12	G12	G12	G12		14
	34	Sun 21/10	295-00:42:28	4677	474	G12	G12	G12	G12	G12	**CAL6**	G27	G21D	G22D	G23D	G24D	G25D	G26D	G21		14
	35	Mon 22/10	296-00:21:38	4678	488	G22	G23	G24	G25	G26	CAL6	1920	NADIR	NADIR	NADIR	NADIR	NADIR	NADIR	NADIR		14
	36	Tue 23/10	297-00:00:48	4679	502	NADIR	NADIR	NADIR	NADIR	NADIR	CAL6	NADIR	NADIR	960	960	960	960	960	960	960	15
	37	Wed 24/10	298-01:21:20	4680	517	960	960	960	CAL4Q40	CAL4Q38	CAL4	960	960	960	G71	G71	G71	G71	G71		14
	38	Thu 25/10	299-01:00:30	4681	531	G71	G71	G71	CAL4	**CAL5**	CAL6	G71	G71	G71	G71	G72	G72	G72	G72		14
	39	Fri 26/10	300-00:39:40	4682	545	G72	G72	G72	CAL4	G72	CAL6	G72	G72	G72	G72	G72	G73	G73	G73		14
	40	Sat 27/10	301-00:18:50	4683	559	PMDRAW	PMDRAW	PMDRAW	CAL4	NS	CAL6	NS	NS	1920	1920	1920	1920	1920	1920		15
	41	Sun 28/10	302-01:39:22	4684	574	1920	1920	1920	CAL4	1920	CAL6	1920	1920	1920	1920	1920	1920	1920	1920	1920	14
6	42	Mon 29/10	303-01:18:32	4685	588	1920	1920	1920	CAL4	1920	CAL6	SHUTTER	CAL0	1920	1920	1920	1920	1920	1920		14
	43	Tue 30/10	304-00:57:41	4686	602	1920	1920	1920	CAL4	CAL5	CAL6	CAL0	1920	1920	1920	1920	1920	1920	1920		14
7	44	Wed 31/10	305-00:36:51	4687	616	1920	1920	1920	CAL4	CAL5	CAL6	CAL0	1920	1920	NADIR	NADIR	PMDRAW	1920	1920		14
	45	Thu 01/11	306-00:16:00	4688	630	1920	1920	1920	1920	1920	CAL6	CAL0	1920	1920	1920	1920	1920	1920	1920	1920	15
	46	Fri 02/11	307-01:36:32	4689	645	1920	1920	1920	1920	1920	CAL6	CAL0	1920	1920	1920	1920	1920	1920	1920		14
	47	Sat 03/11	308-01:15:41	4690	659	1920	1920	1920	CAL4	CAL5	CAL6	CAL0	1920	1920	1920	1920	1920	1920	1920		14
	48	Sun 04/11	309-00:54:50	4691	673	1920	1920	1920	CAL4	MOON2	MOON2	MOON2	MOON2	MOON2	MOON2	MOON2	MOON2	MOON2	MOON2		14
	49	Mon 05/11	310-00:33:59	4692	687	MOON2	MOON2	MOON2	CAL4	CAL5	CAL6	CAL0	1920	1920	1920	1920	1920	1920	1920		14
	50	Tue 06/11	311-00:13:08	4693	701	1920	1920	CAL4	DSM set	235K THRUPH6	THRUPH6	THRUPH6	240K THRUPH6	THRUPH6	THRUPH6	245K THRUPH6	THRUPH6	THRUPH6	THRUPH6	THRUPH6	15
	51	Wed 07/11	312-01:33:39	4694	716	THRUPH6	THRUPH6	250K THRUPH6	THRUPH6	THRUPH6	255K THRUPH6	THRUPH6	THRUPH6	250K THRUPH6	THRUPH6	THRUPH6	245K THRUPH6	THRUPH6	THRUPH6		14
	52	Thu 08/11	313-01:12:48	4695	730	THRUPH6	THRUPH6	240K THRUPH6	THRUPH6	THRUPH6	235K THRUPH6	THRUPH6	THRUPH6	THRUPH6	THRUPH6	THRUPH6	THRUPH6	THRUPH6	THRUPH6		14
	53	Fri 09/11	314-00:51:57	4696	744	1920	1920	1920	CAL4	CAL5	CAL6	CAL0	1920	1920	1920	1920	1920	1920	1920		14
	54	Sat 10/11	315-00:31:05	4697	758	**Ops timeline start using the common 29 days sequence, starting at orbit offset 246 in order to be in sync with Metop-A**															

Table 6: GOME-2 Metop-B / FM2 IOV timeline schedule as run.

4 INTERNAL EUMETSAT VALIDATION

4.1 Monitoring of House-keeping Data (A4.1)

For the monitoring of housekeeping data like thermal, electrical, and scanning statistics, please see SIOV report 0

4.2 Monitoring Signals from internal Light sources (A4.2)

The monitoring of the signals of the internal light sources has been carried out during SIOV 0 and has been done on a regular basis since start of the routine monitoring activities on MPSTAR OPE and VAL as of 26 September 2012. Orbit, daily and long-term reports are available on the GOME-2 monitoring web site:

http://gome.eumetsat.int

The daily reports comprise the average daily white light source (WLS) measurement, the spectral light source measurements (SLS) and the monthly LED measurements (for details see 0). For the signal performance of the calibration sources, see Section 4.2. The figures that follow we show some exemplary results for signal and standard deviation of a daily measurement taken on 25 November 2012 in Figure 4 and for a spectral light source measurement in Figure 5. In Figure 6, we present the same results for a monthly LED measurement. The mean signals and standard deviations are within the expected ranges (see also SIOV report [AD8]).

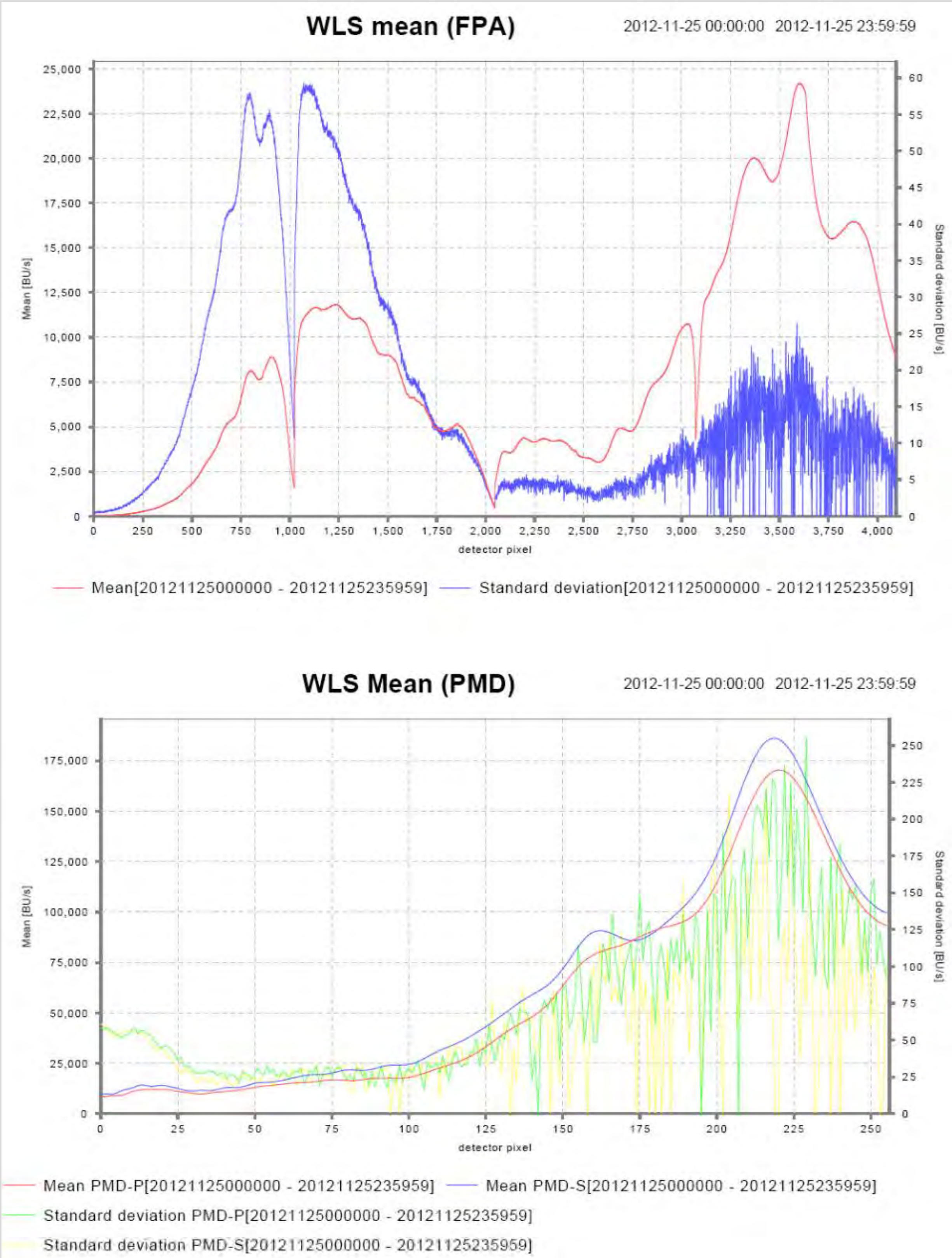

Figure 4: White-light source daily averaged measurements from main channels (upper panel) and PMD channels (lower panel).

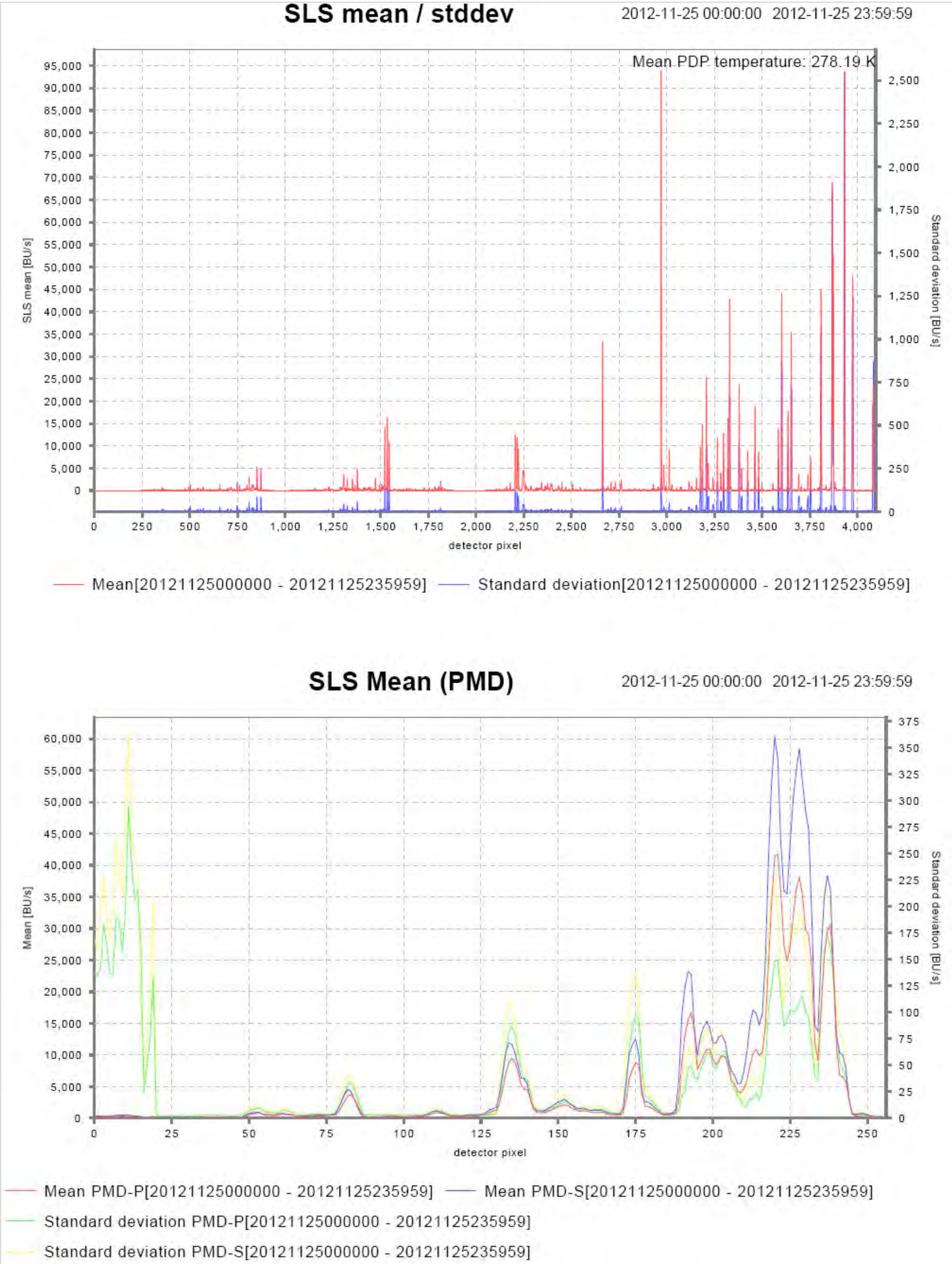

Figure 5: Spectral light source daily averaged measurements from main channels (upper panel) and PMD channels (lower panel).

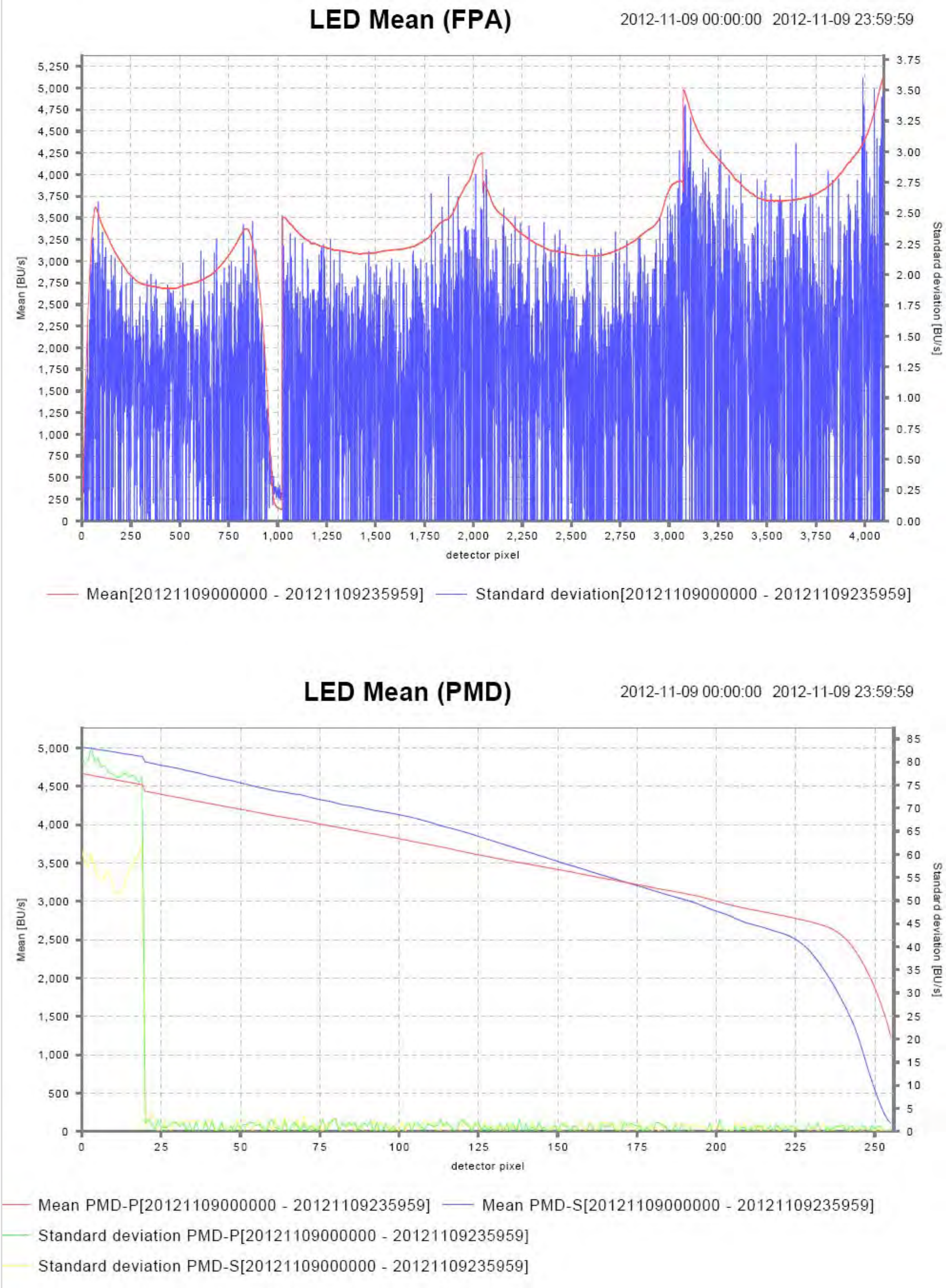

Figure 6: LED-averaged monthly measurements from main channels (upper panel) and PMD channels (lower panel).

4.3 Dark signal correction (A4.3.1)

Since 26 September 2012, dark signals have been routinely monitored and reported for Metop-B / FM2. The orbit and daily reports are available on this web page:

http://gome.eumetsat.int

A detailed evaluation of the dark-signal performance of FM2 is provided with the IOV report [AD8]. We also provide the longer-term performance of the electronic offset, the leakage current and the dark signal noise.

4.3.1 Dark signal offset

Here we provide the dark signals for the main channel and the PMDs at their most common integration times and at nominal detector temperatures

The mean values provided in Table 7 have been derived from the IOV analysis of dark signals. These values are also used as "default" dark offset values for the processing in the case where no valid dark measurements would be available for a given integration time and detector temperature.

Channel	***1***	***1***	***2***	***2***	***3***	***4***	***5/6***
Band	1A	1B	2A	2B	3	4	PMD P/S
Used Pixels	659	365	71	953	1024	1024	256
Valid Spectral Range (nm)	240-283	283-309.7	not valid	309.8-397.7	397.7-598.4	598.4-790	290-790
nm/pixel	0.07	0.07	0.09	0.09	0.2	0.2	2[1]
Predefined dark signal electronic offset (BU)	1495	1495	1495	1495	1496	1495	1502/1501

1 Variable over the channels

Table 7: GOME averaged dark signal offset for main channels and PMDs

4.3.2 Dark signal components

The figures in this section show band-averaged results for dark-signal electronic offset (plotted in blue), leakage signal (plotted in green) and dark-signal noise. Note that the dark-signal measurements for different integration times per band are taken at a different part of the ascending orbit and therefore at different SZAs. Even though all dark measurements ought to be taken "well within" eclipse, recent analysis of the timelines with the new GTL builder tool at EUMETSAT indicates that some of the dark measurements may suffer from (twilight) stray light–especially when taking the variation of the "shallowness" of the eclipse over the seasonal cycle into account. The latter is likely to cause the observed seasonal cycle in the noise signals, which varies significantly with integration time (which are related to different SZA or positions within the eclipse). This effect cannot be totally avoided because there is only a finite amount of time available for which dark-measurements are well in eclipse, and the design of the in-orbit instrument timeline is therefore a trade-off between systematic errors due to stray-light levels and systematic errors related to the amount of measurements, that is to say the acquired measurements statistics and therefore the error on the averaged calibration spectrum.

After the switch to nominal detector temperatures on 18 October 2012, "monthly" calibration timelines have been issued daily till the end of the SIOV timeline sequence (11 November 2012). Therefore, during this intermediate time period, the noise values behave more similar to the noise values taken on the following monthly calibration days (like 2 December 2012). The larger scatter is due to different positions in the eclipse where the dark measurements are derived.

In the graphs in this section the data are presented as follows, unless otherwise noted:

- The band-averaged electronic offset signal range in BU is on the left axis.
- The right axis lists leakage current in BU/sec in green.
- Band-averaged dark signal noise (for all operational integration times) is in blue in BU.

Note: The Band 2A results are not reported here because the data is outside the valid spectral range. The wavelength range covered per band is again given in Table 6.

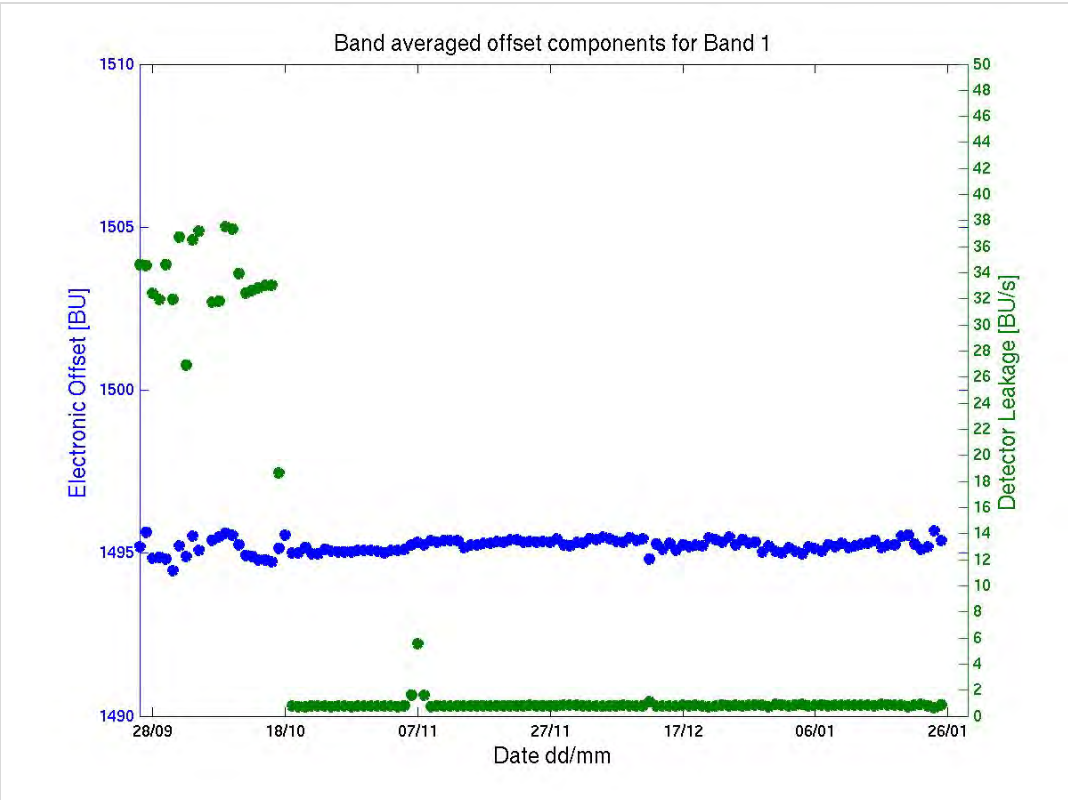

Figure 7: Band 1A averaged electronic offset (blue plots) and leakage current (green plots).

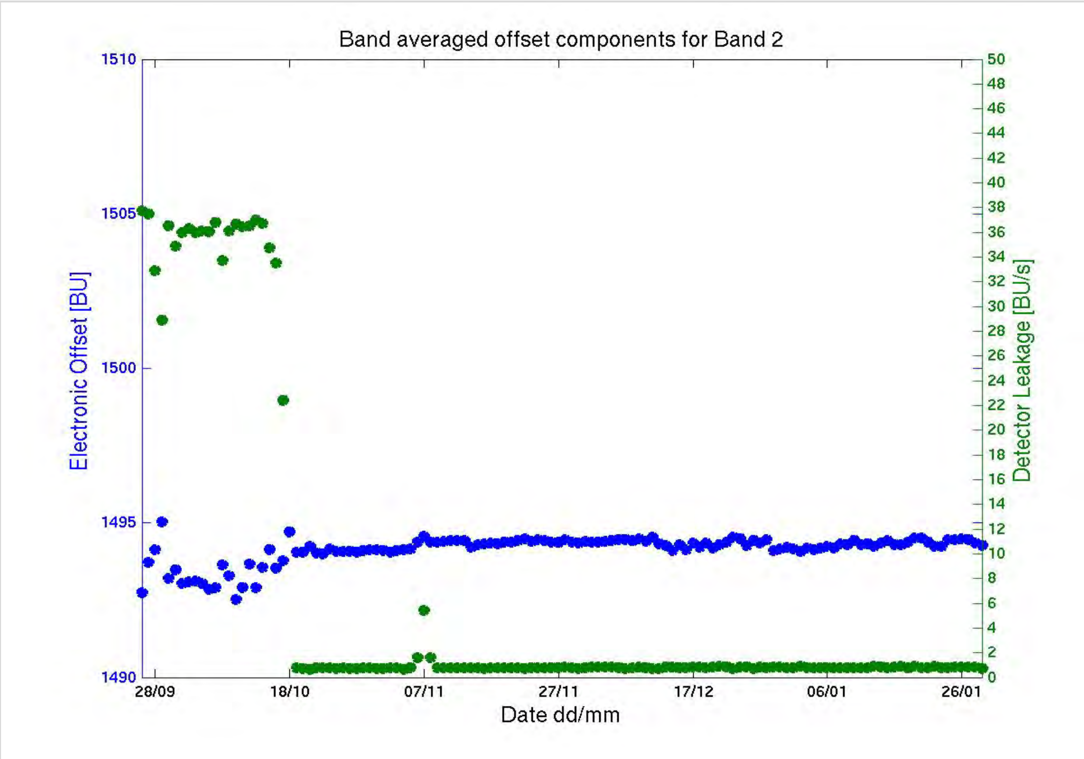

Figure 8: Band 1B averaged electronic offset (blue plots) and leakage current (green plots).

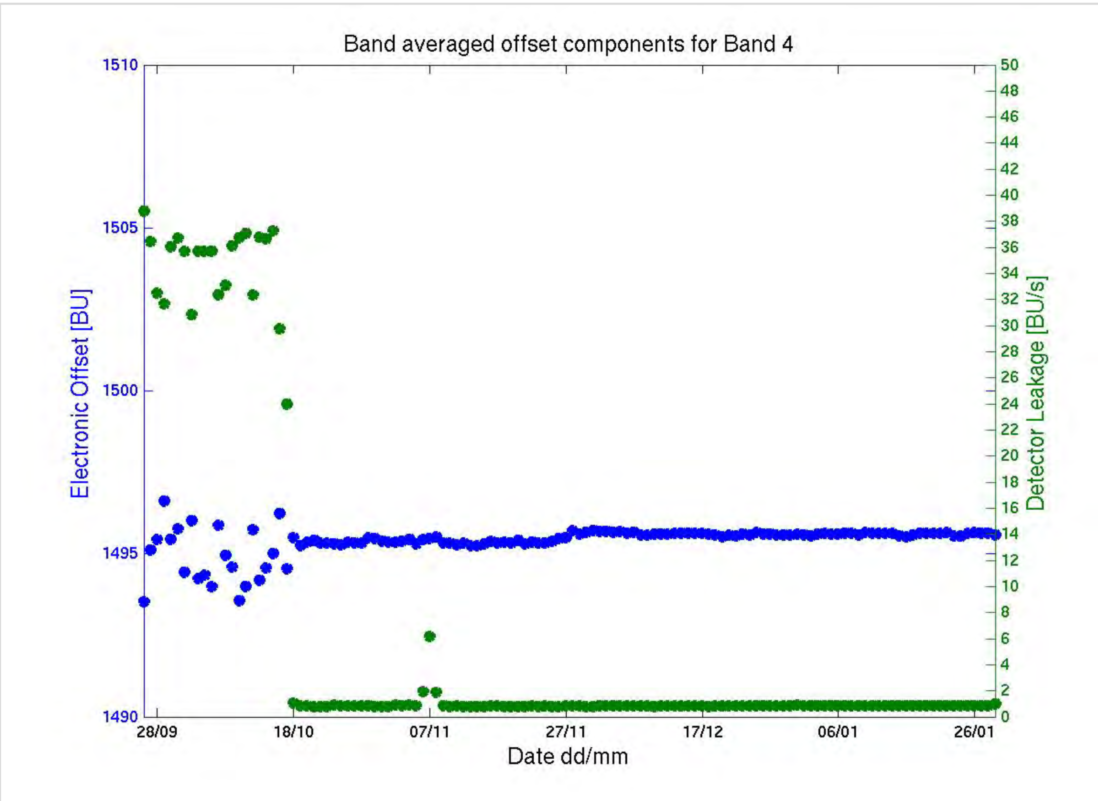

Figure 9: Band 2B averaged electronic offset (blue plots) and leakage current (green plots).

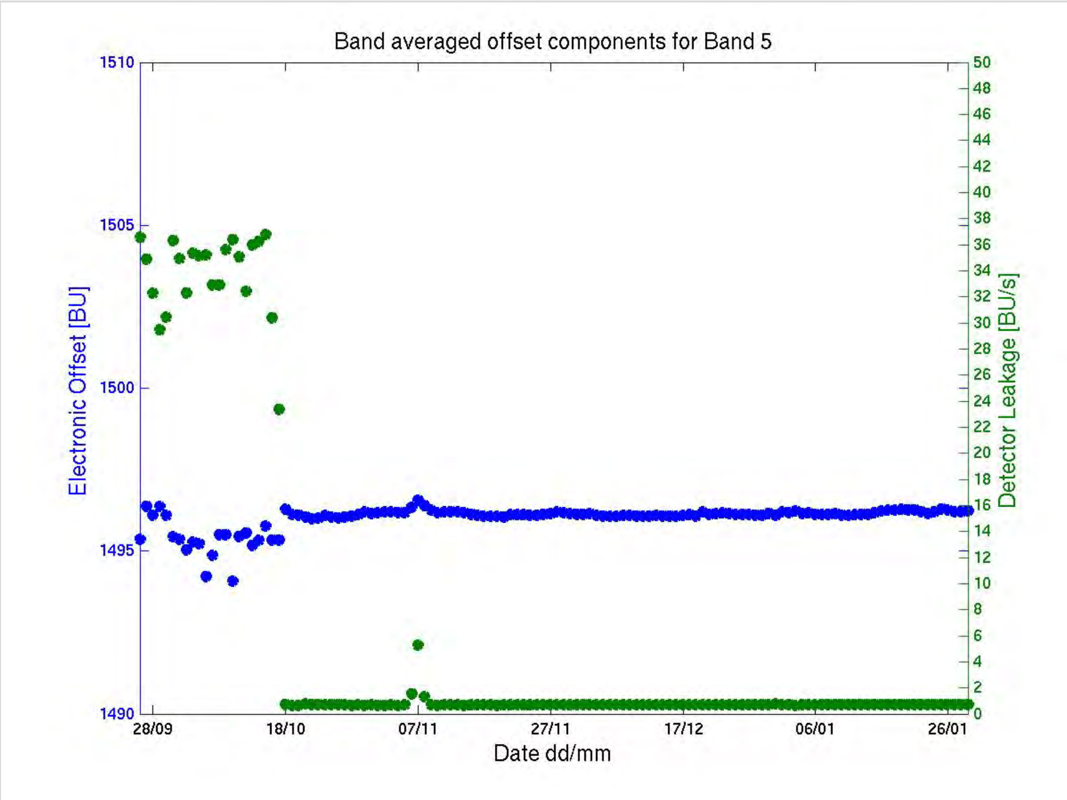

Figure 10: Band 3 averaged electronic offset (blue plots) and leakage current (green plots).

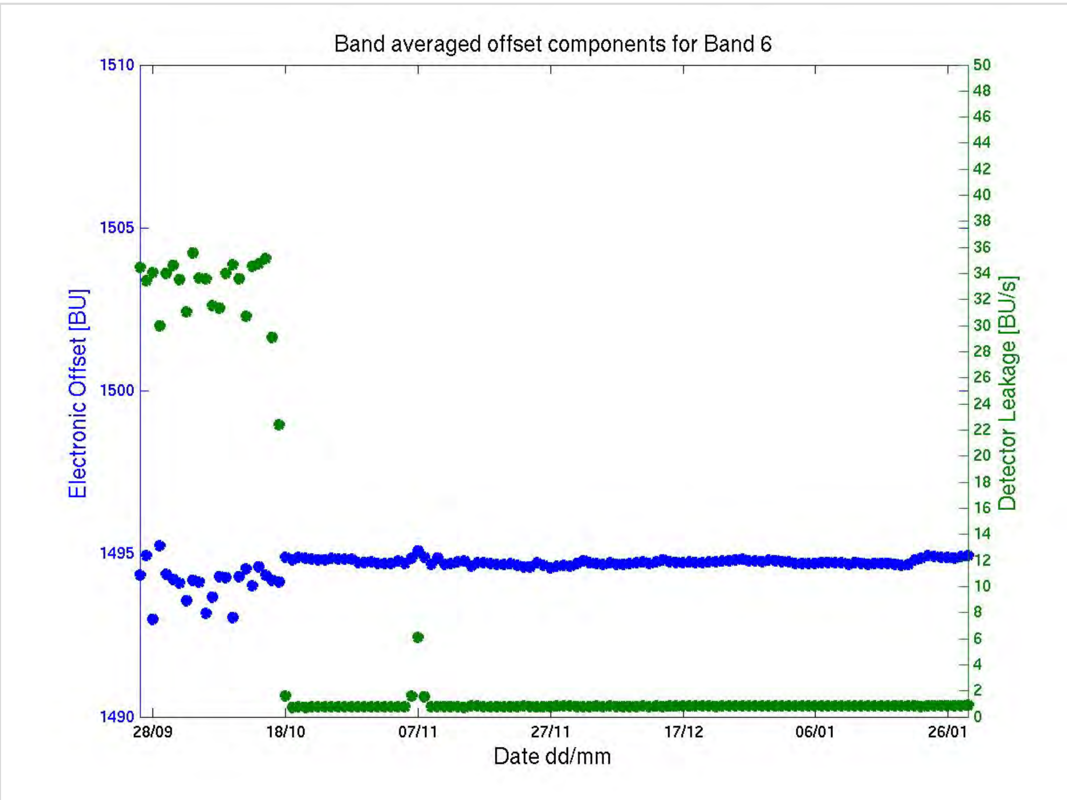

Figure 11: Band 4-averaged electronic offset (blue plots) and leakage current (green plots).

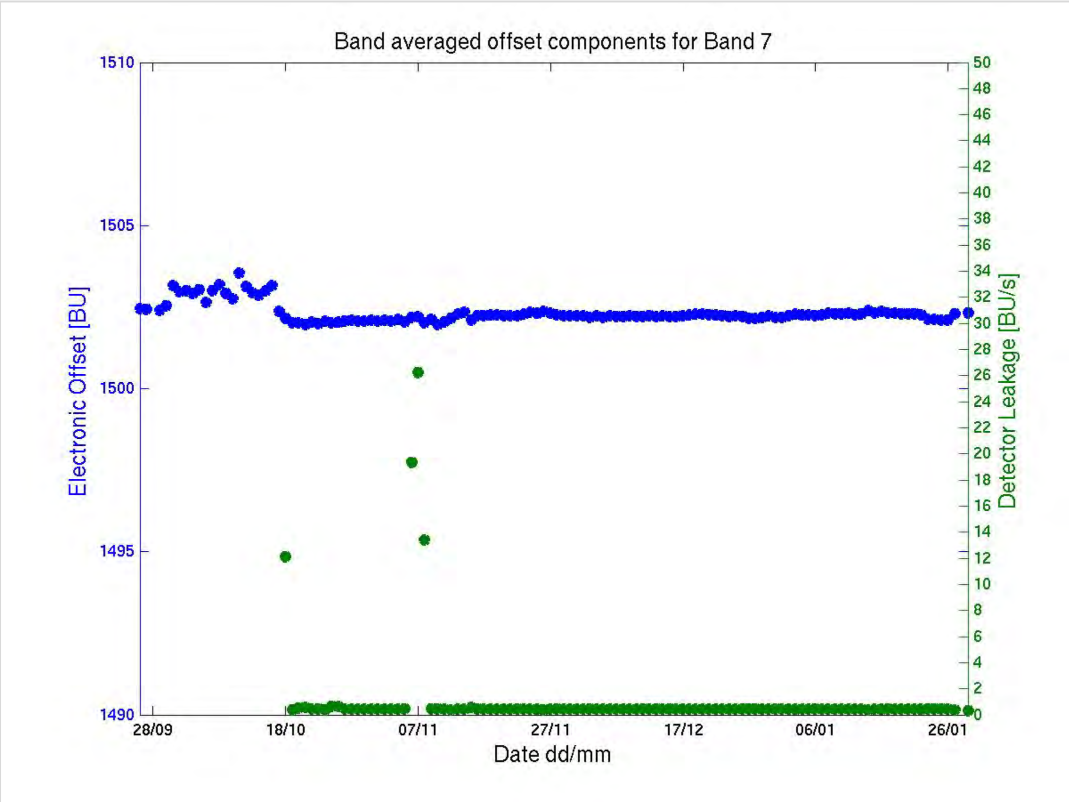

Figure 12: PMD-P-averaged electronic offset (blue plots) and leakage current (green plots).

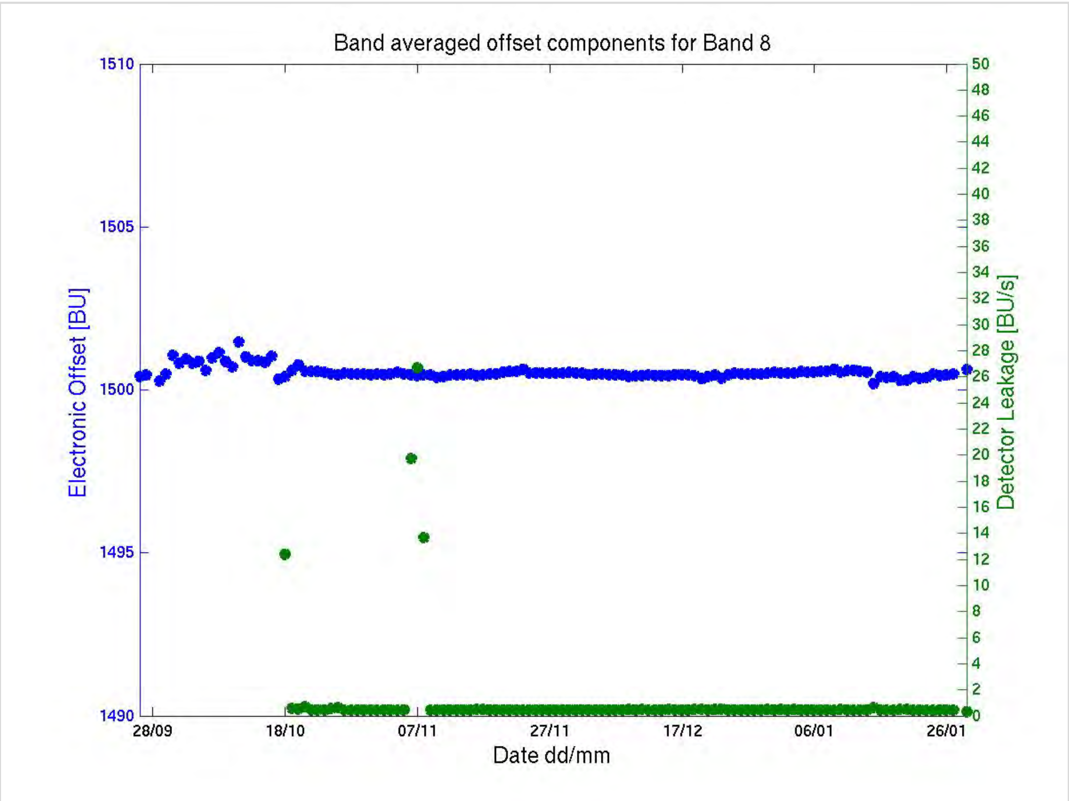

Figure 13: PMD-S-averaged electronic offset (blue plots) and leakage current (green plots).

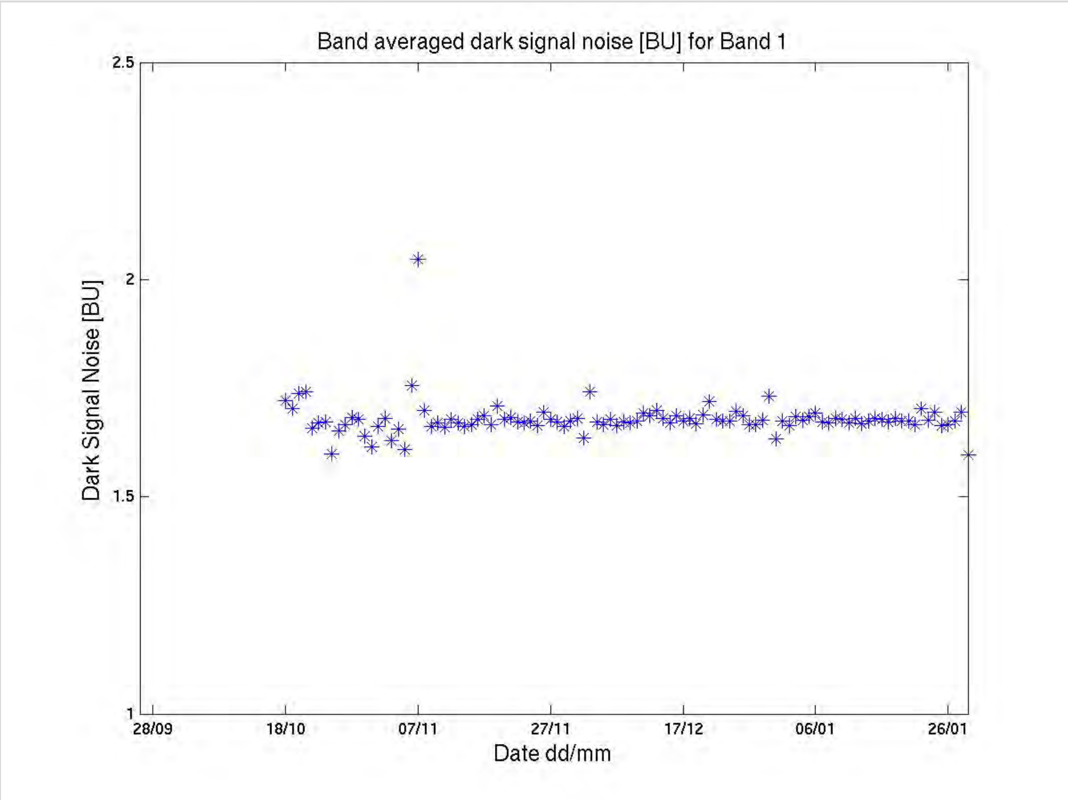

Figure 14: Band 1A-averaged noise.

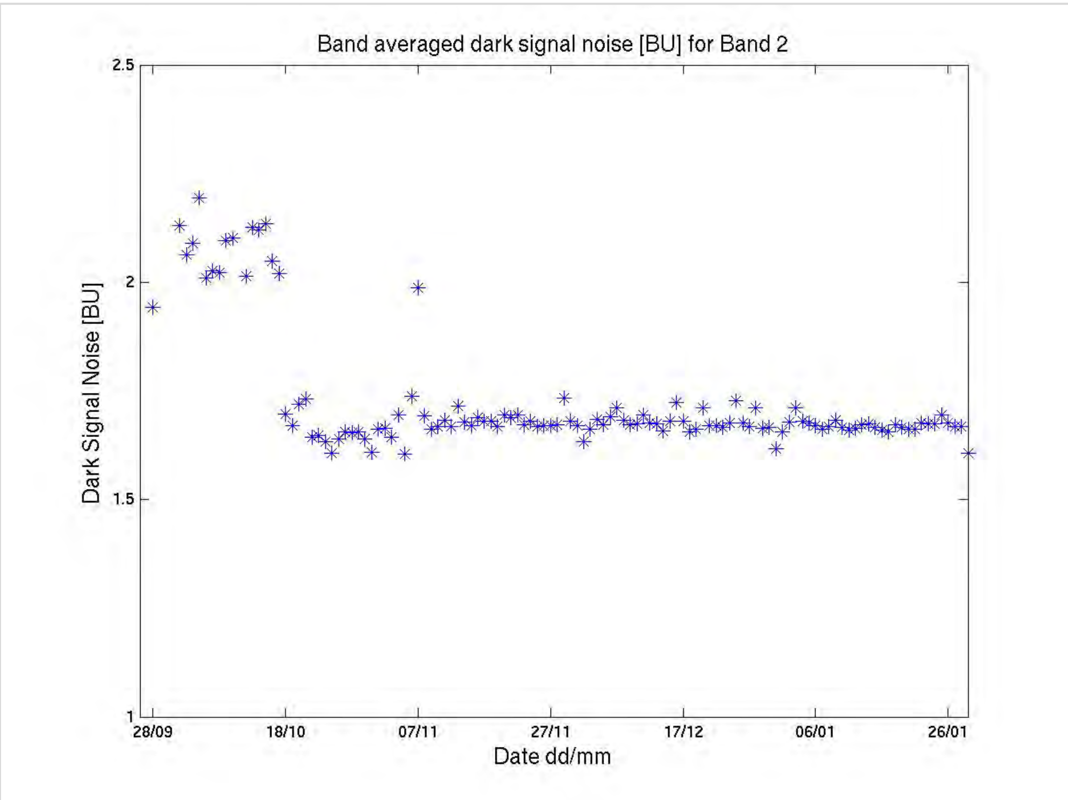

Figure 15: Band 1B-averaged noise.

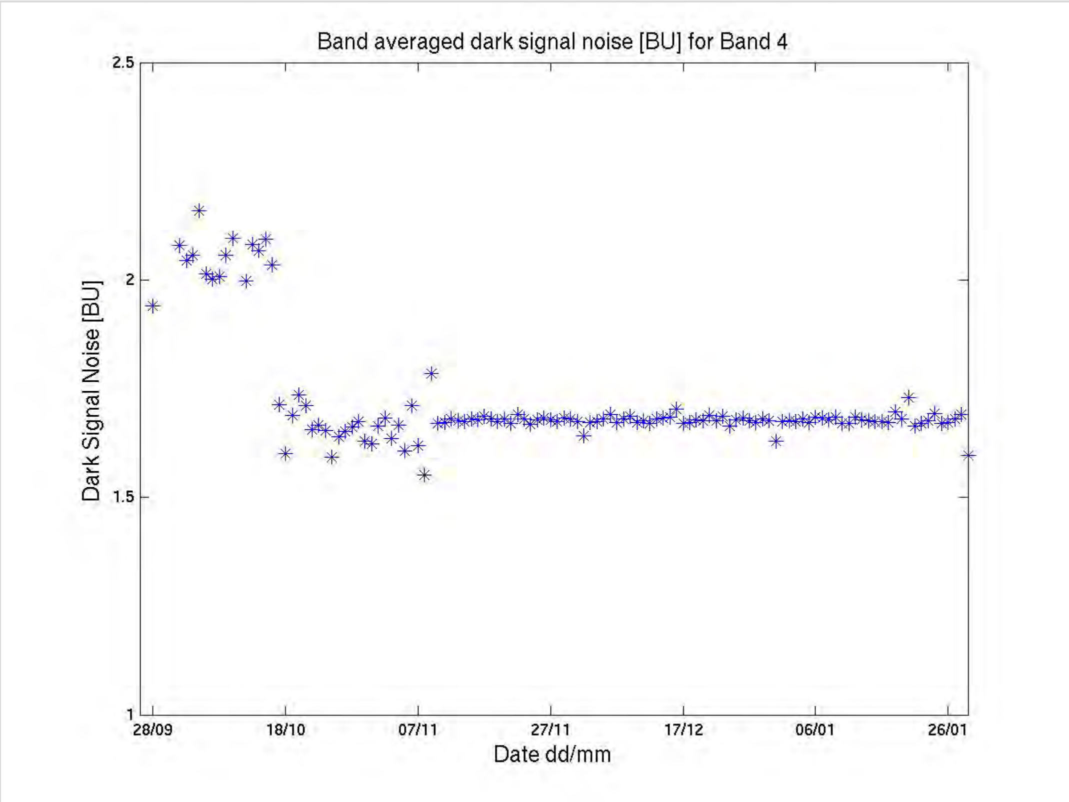

Figure 16: Band 2B-averaged noise.

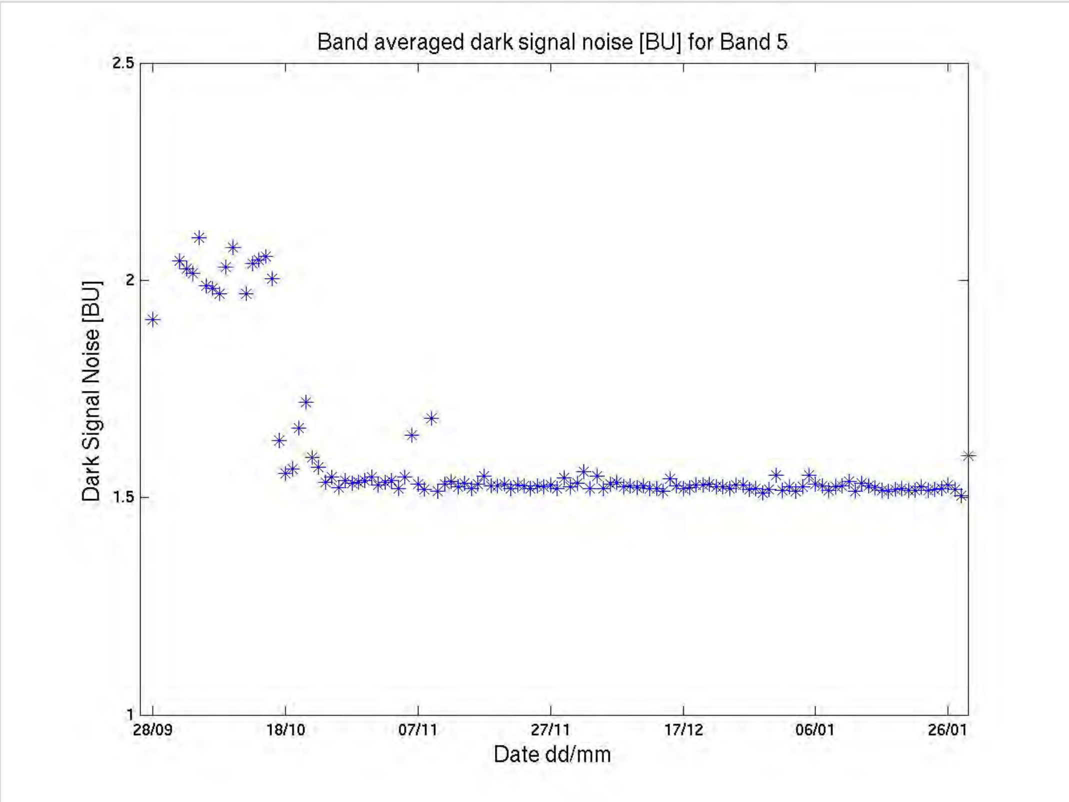

Figure 17: Band 3-averaged noise.

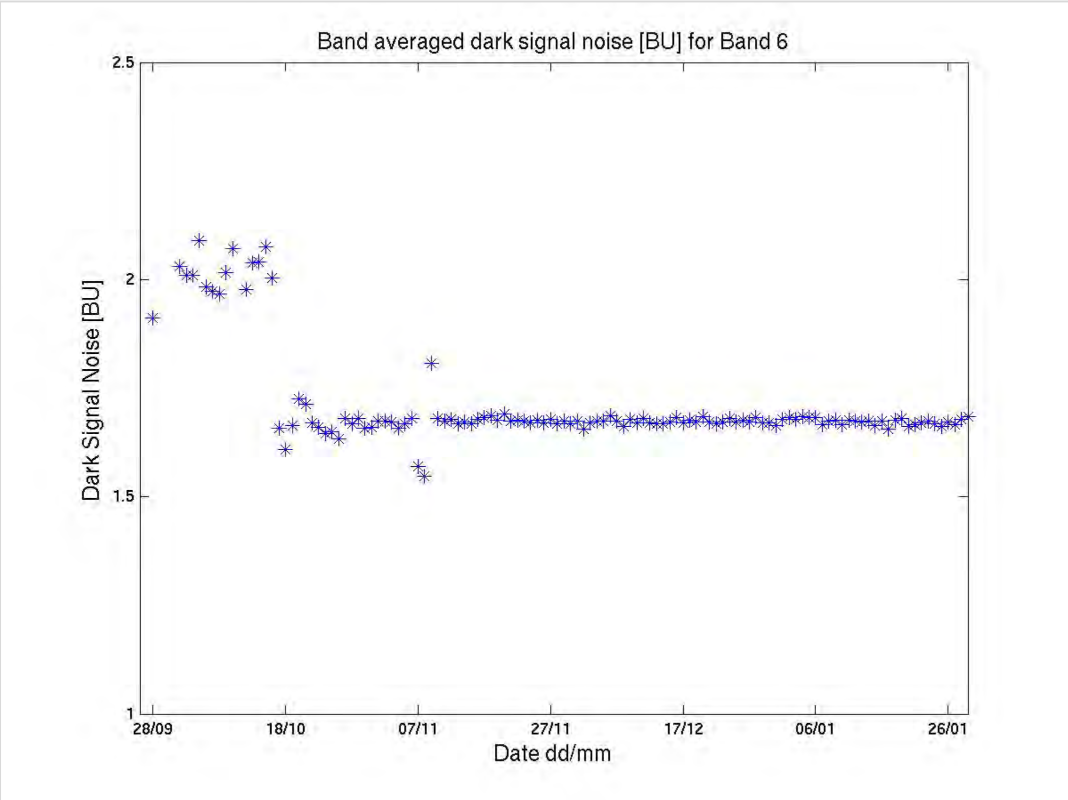

Figure 18: Band 4-averaged noise.

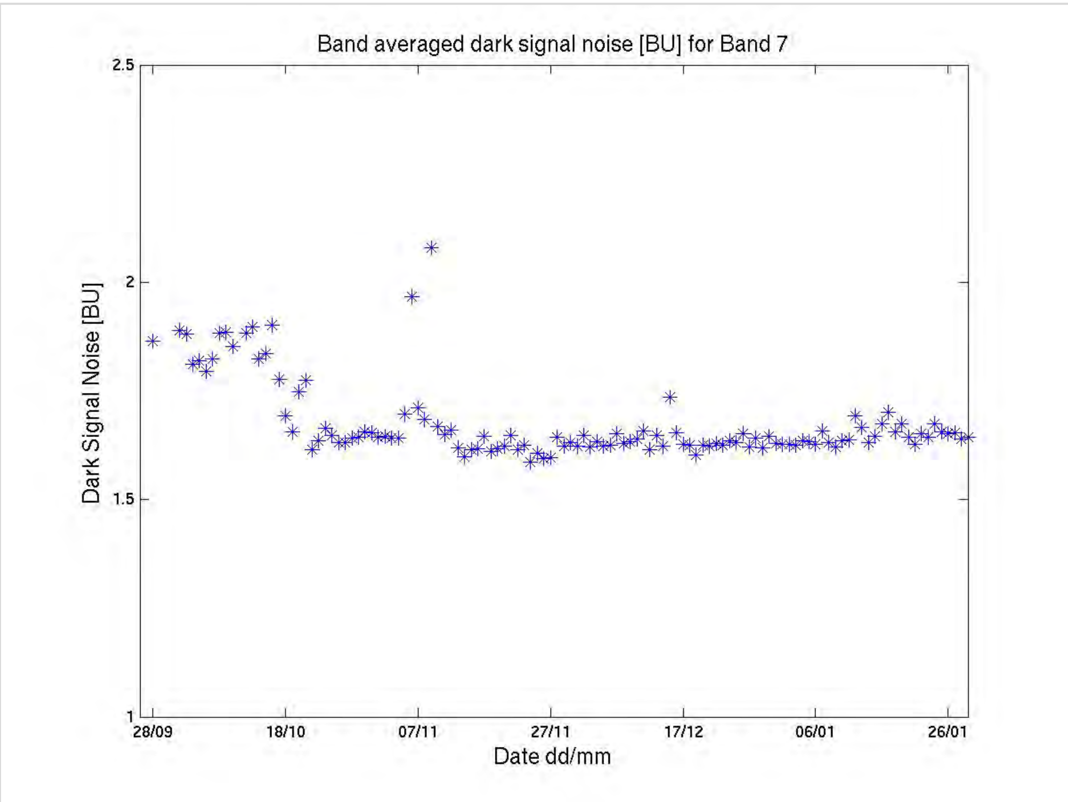

Figure 19: PMD-P-averaged noise.

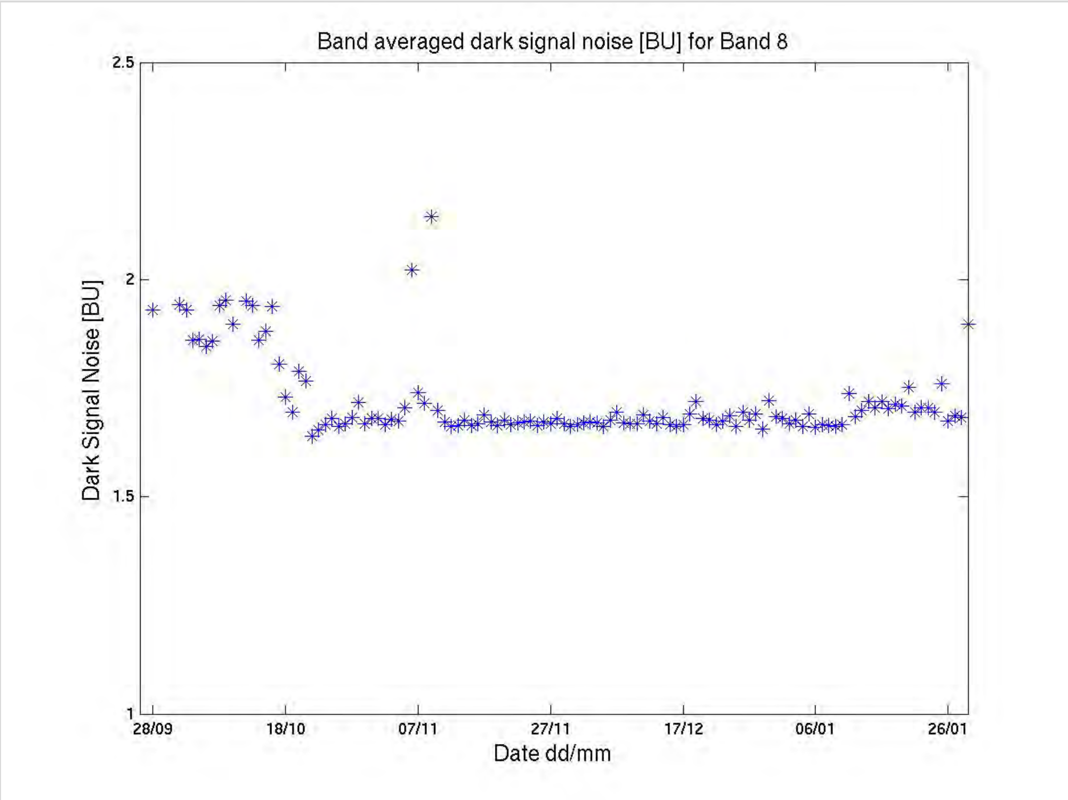

Figure 20: PMD-S-averaged noise.

4.4 PPG correction (A4.3.2)

The pixel-to-pixel gain correction is derived from the processing of averaged LED signals (see Section 4.2) by the level 0-to-1B processor. For details of this processing, see AD 3.

Figure 21and Figure 22 show the detector pixel-to-pixel gain for channels 1 to 4 and the PMDs for both Metop-A (FM3 as reference) and Metop-B (FM2). The contribution of PPG is generally to be expected at the 10^{-4} level. For Metop-A / FM3, this contribution has been increasing by the same level over the last six years (see [RD8]). This being true, we expect the PPG of FM2 to be smaller by approximately 1e-4, than the current PPG on Metop-B / FM2. The results shown in Figure 21 and Figure 22 confirm this.

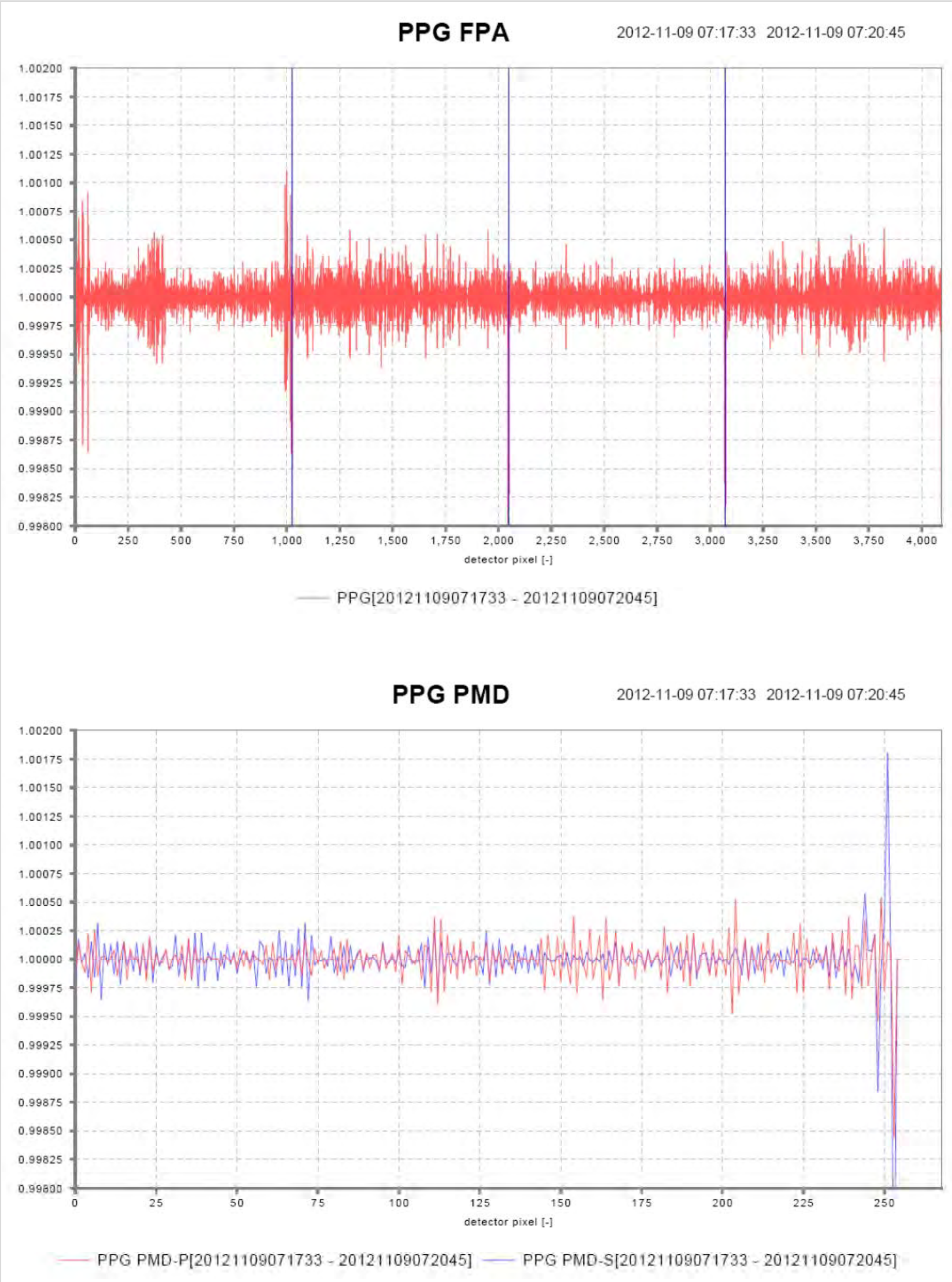

Figure 21: Metop-B / FM2 detector pixel-to-pixel gain (PPG) contribution for main channels (upper panel) and for PMD channels (lower panel) on 9 November 2012.

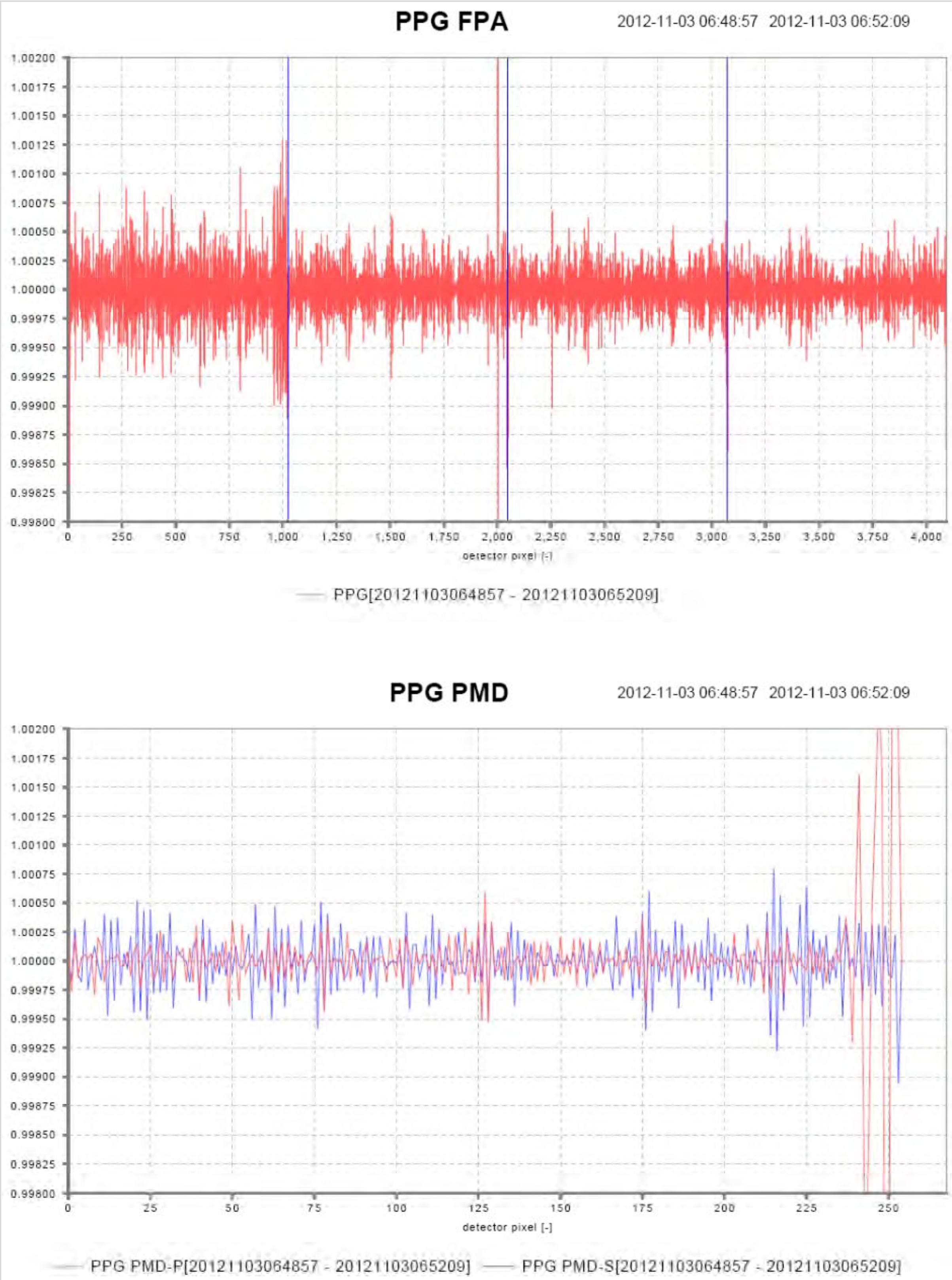

Figure 22: Metop-A / FM3 detector pixel-to-pixel gain (PPG) contribution for main channels (upper panel) and for PMD channels (lower panel) at the 3rd of November 2012.

4.5 Instrument spectral calibration and stability (A2.13-A2.15, A3.6)

GOME-2 spectral line source (SLS) measurements (see Section 4.2) are used to derive spectral calibration parameters. Under nominal operational conditions, one spectral calibration is carried out on board every day. Spectral stability in orbit, which is a function of pre-disperser prism temperature, appears to be very good for Metop-A / FM3 (see [RD8]).

The spectral stability, both in-orbit and for t on-ground to in-orbit transition, is predominantly affected by the thermal environment of the instrument and is not, or not significantly, affected by the signal strength of the lamp (e.g. by the 1g-effect). The accuracy of the spectral calibration is otherwise depending on the performance of the spectral dispersion fitting algorithm for main channels (which is the same for FM2 and FM3, see 0) and by the settings of the cross-correlation windows chosen for the mapping of the main channel spectral calibration onto the PMDs. This algorithm has been substantially been revised for Metop-A / FM3 at the beginning of the mission (see [RD11]) and is working stable since then. Optimised and dedicated cross-correlation windows have been provided for FM2 (not for FM3) by the on-ground calibration campaign (see TNO report MO-TR-TPD-GO-0118).

These cross-correlation windows have been implemented already at an early stage during FM2 IOV with INS file version 1.01.

Two dedicated measures of monitoring the on-ground to in-orbit stability and the in-orbit long-term stability, as well as the in-orbit accuracy are applied here and presented in the daily reports. First, the derived dispersion curves are compared to what has been measured on-ground. With this method we predominantly address the stability as laid out before whereas the accuracy is addressed only in so far that the on-ground measurements can be considered reliable in terms of accuracy. The latter can be considered being the case for the Metop-A / FM3 main channel on-ground characterisation but not for the FM3 PMDs.

Because of the substantial and successful revision of the PMD spectral calibration algorithm the new approach has also been applied during the on-ground calibration campaign for Metop-B / FM2, for the derivation of spectral reference key-data. We therefore expect for the latter that both main channel and PMD on-ground spectra can serve as a reasonable measure of the real changes observed between on-ground and in-flight, as well as a good measure of long-term stability.

In addition, the absolute spectral accuracy is monitored by comparing the observed position of Fraunhofer lines with their catalogued position. This can only been done for well isolated Fraunhofer lines, which however are spectrally not fully resolved by the instrument. So there is an intrinsic limitation in accuracy due to the spectral resolution of the instrument involved in this method reflected in the provided error bars on the results.

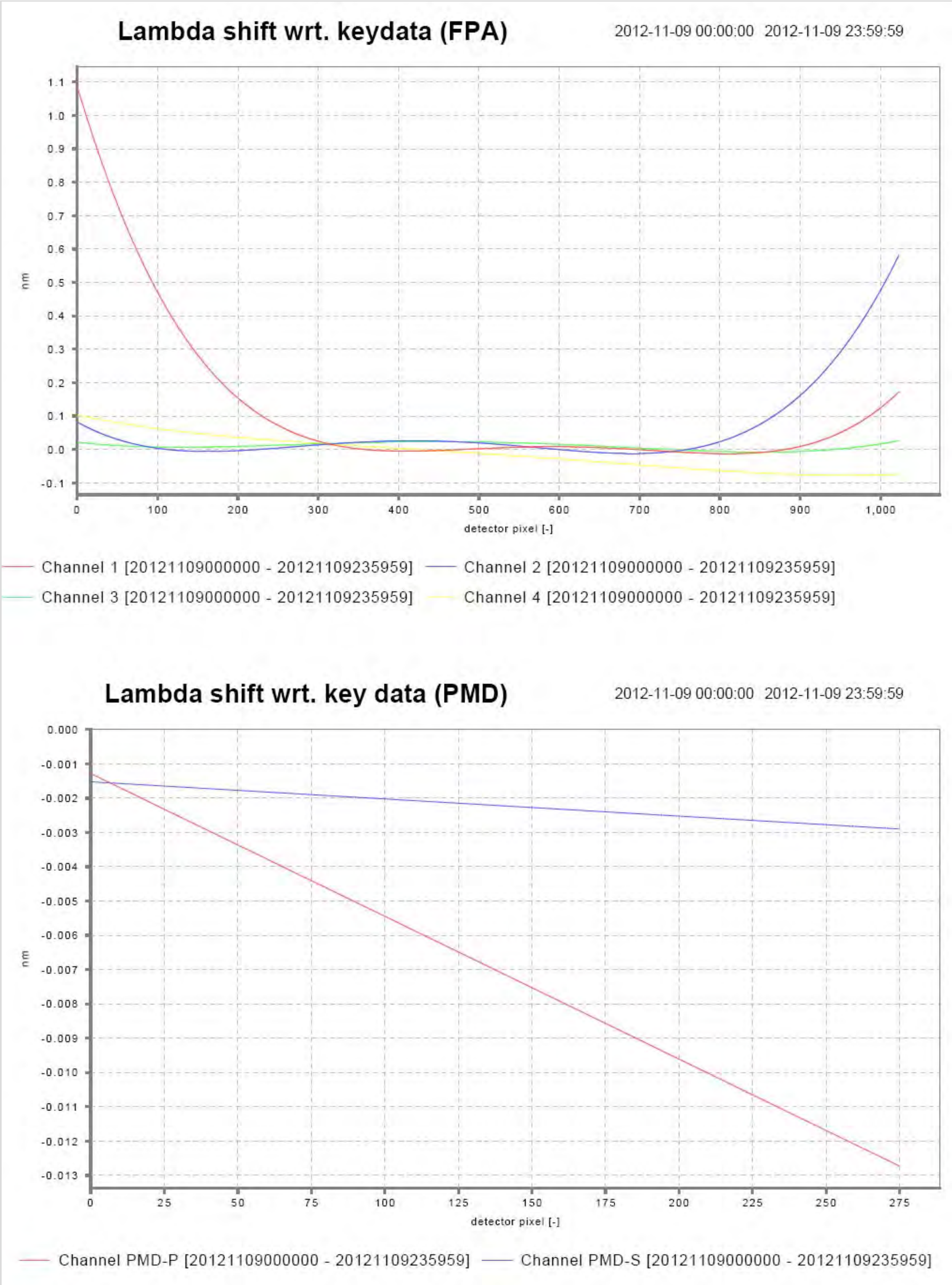

Figure 23: Metop-B / FM2 spectral dispersion curves relative to the on-ground measured dispersion during the FM2-2 calibration campaign. The top panel shows the difference in wavelength for main channels and the lower panel for PMDs on 9 November 2012.

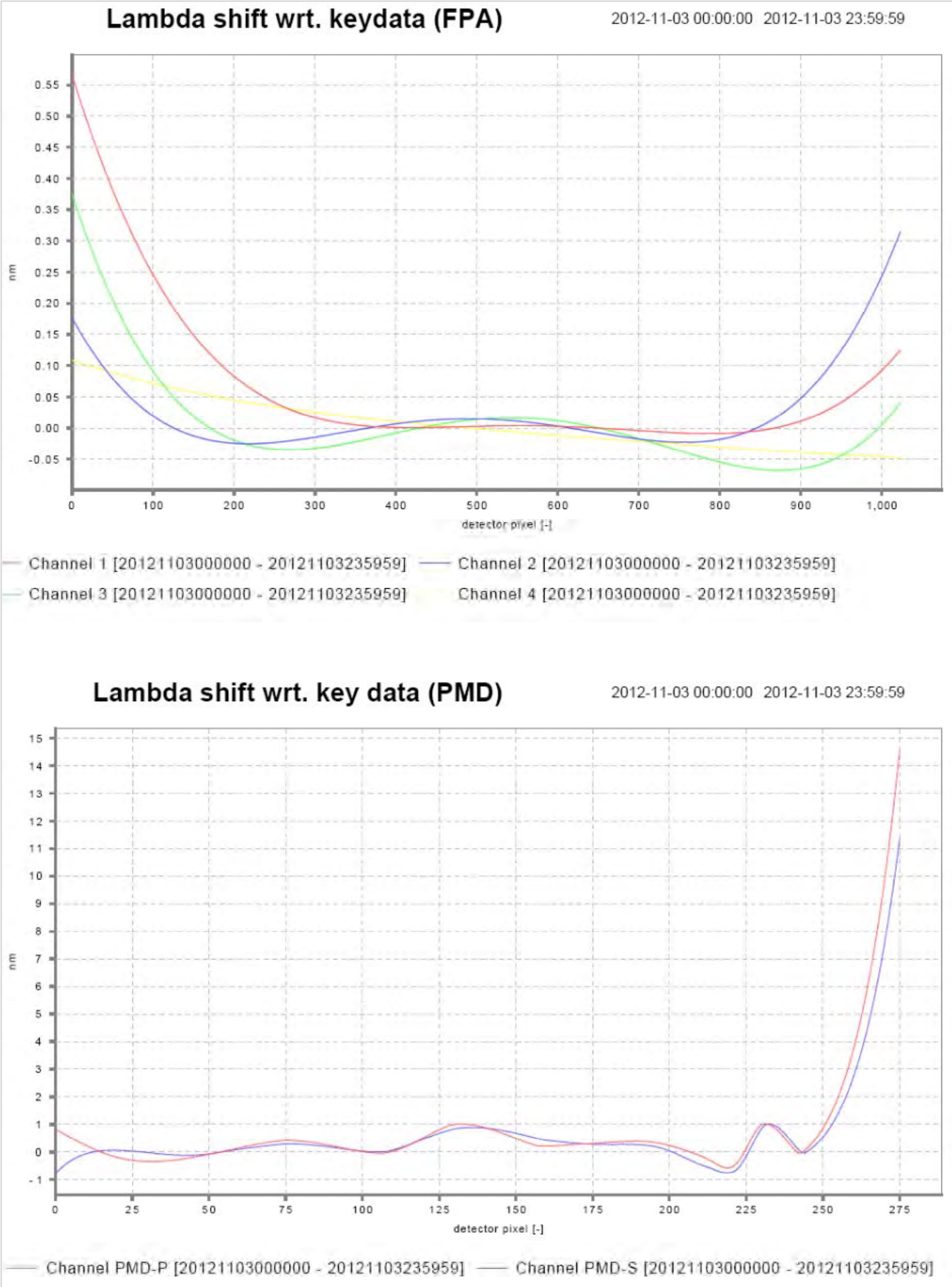

Figure 24: Metop-A / FM3 spectral dispersion curves relative to the on-ground measured dispersion during the FM3 calibration campaign. The top panel shows the difference in wavelength for main channels and the lower panel for PMDs at the 3rd of November 2012.

4.5.1 Results on stability and consistency of the spectral calibration

Figure 23 and Figure 24 show the main channel (upper panels) and the PMD channels (lower panel) differences to the on-ground measured spectral dispersion curves for both Metop-B / FM2 and Metop-A / FM3 respectively. For main channel the differences are overall quite comparable (note the difference in scale) except for channel 2, where there seems to be a larger shift after launch in the channel 2 to 3 overlap region (around 0.6 nm) than observed for FM3 (0.3 nm). This refers to an even larger movement of the overlap separation for FM2 than observed for FM3. The consequences of this shift and how to account for it are detailed in Section 4.8. As mentioned before the on-ground measured spectral reference dispersion for FM3 are not reliable as a source. From the results presented in the lower panel of Figure 23 we can however conclude that the PMD spectral calibration is very close to what has been measured on-ground, and that even though the PMDs have a very complex dispersion structure, the on-board spectral calibration processing is very close to the results achieved on-ground.

The Spectral calibration is sensitive to the thermal environment of the instrument. Figure 25 shows the pre-disperser prism temperature of Metop-B / FM2 since launch (c.f. Figure 3). Note that the on-board temperature of the platform displays a distinct seasonal cycle but is overall expected to be slowly increasing during the first two to three years.

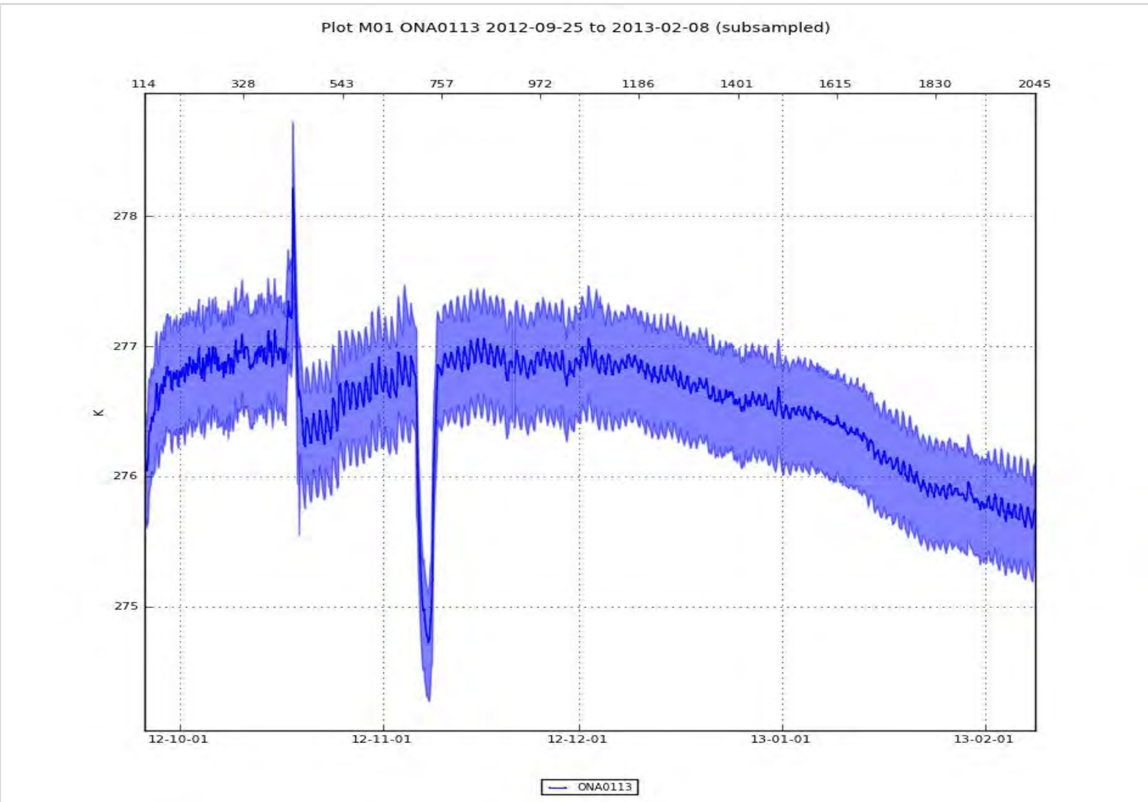

Figure 25: Metop-B / FM2 on-board pre-disperserprism temperature since launch of Metop-B.

Figure 26 shows the results derived from maximum spectral line signals and daily spectral calibrations at various wavelengths. The wavelength that is being measured by a particular pixel is calculated and that trend is displayed throughout the reporting period. The wavelength range covered per pixel is given in Table 6.

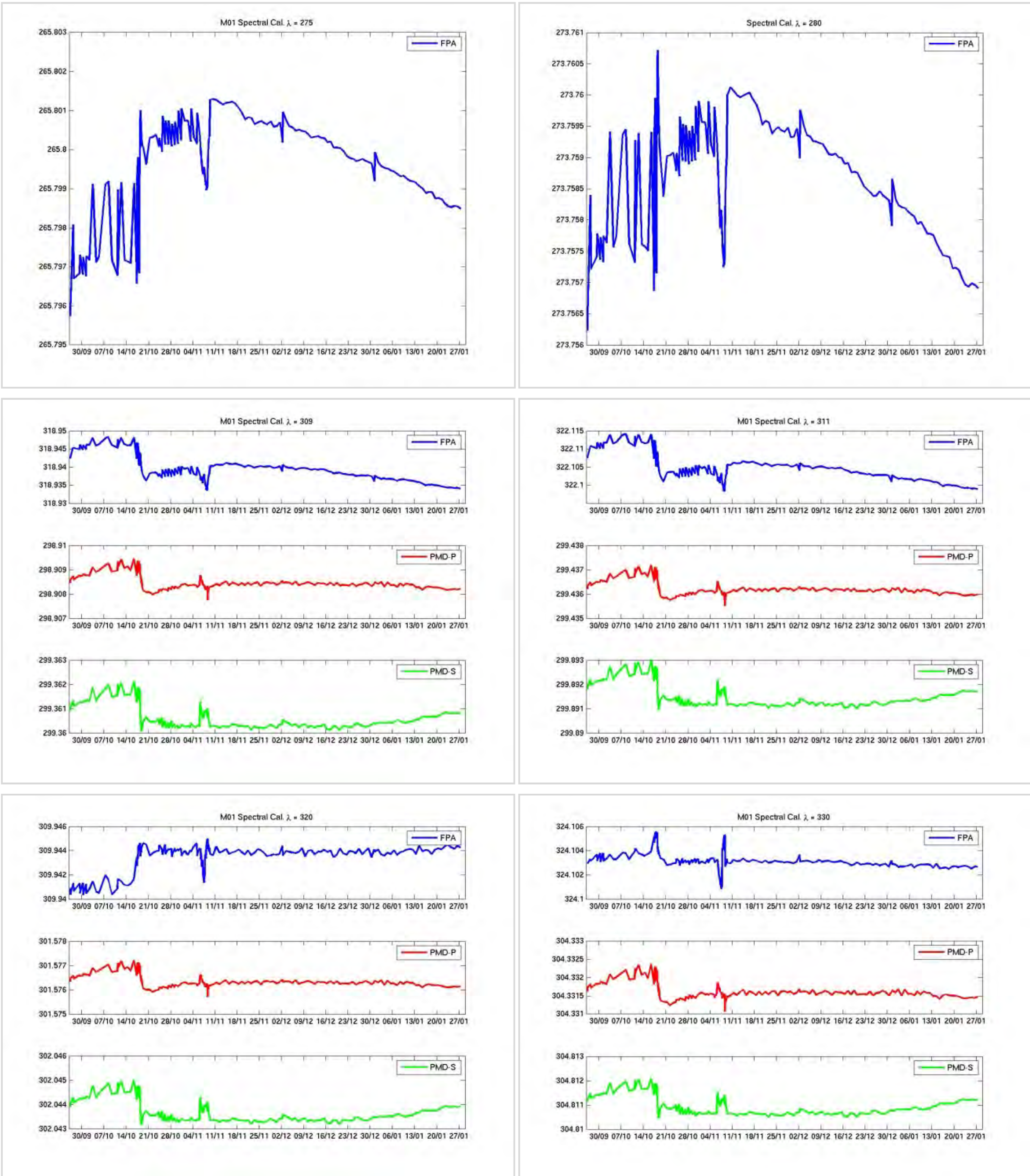
M01 Spectral Cal. λ = 275
FPA
Spectral Cal. λ = 280
FPA
M01 Spectral Cal. λ = 309
FPA
PMD-P
PMD-S
M01 Spectral Cal. λ = 311
FPA
PMD-P
PMD-S
M01 Spectral Cal. λ = 320
FPA
PMD-P
PMD-S
M01 Spectral Cal. λ = 330
FPA
PMD-P
PMD-S

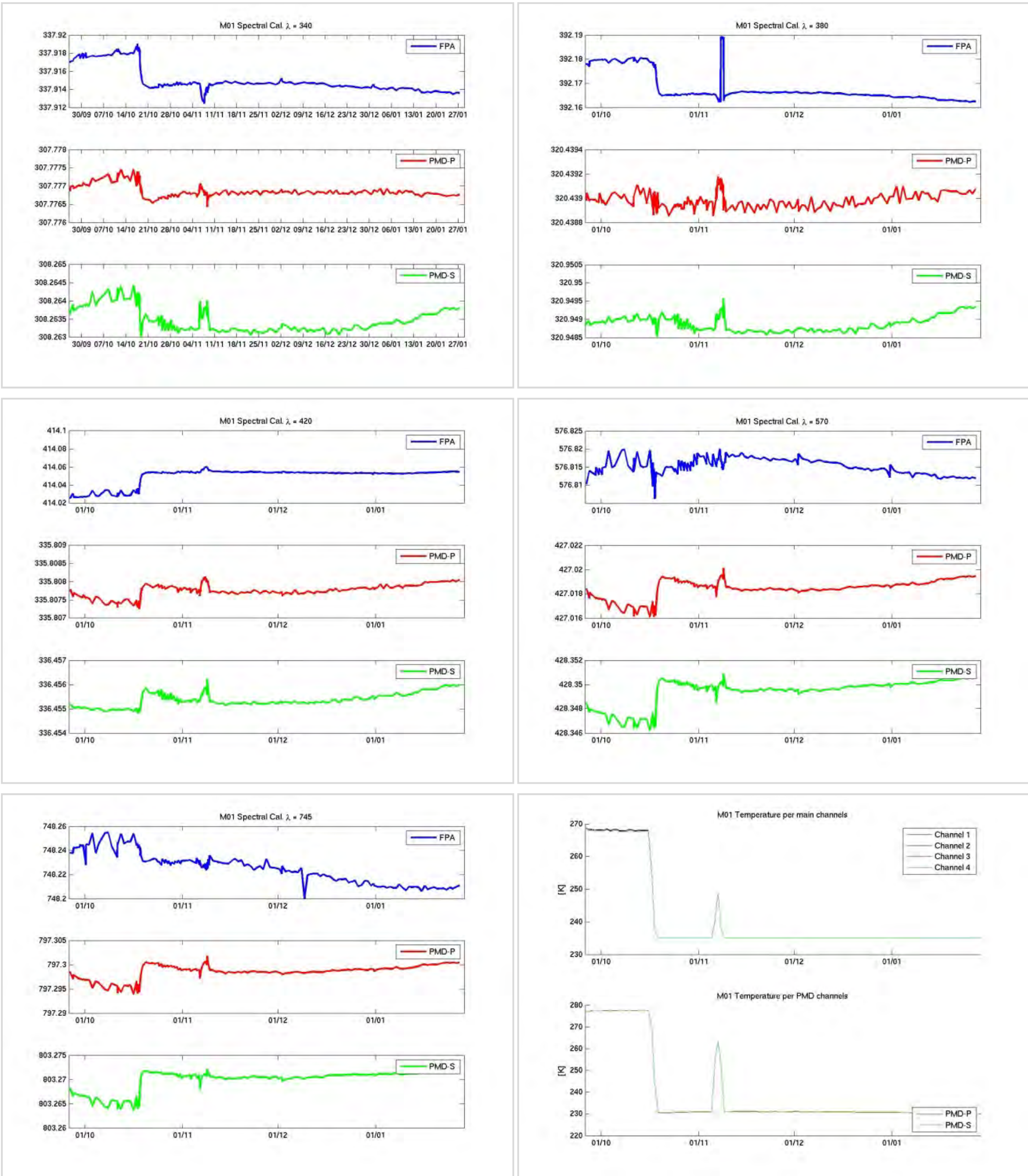

Figure 26: Spectral stability at various wavelengths between 26 September 2012 and 28 January 2013 and for main channels and PMD channels at 275, 280, 309, 311, 320, 330,340, 380, 420, 570 and 745 nm (top left to bottom left). The bottom right plot shows the detector temperatures during the same time period.

From Figure 26 it can be seen that spectral stability is high at all wavelengths and generally follows the change of the pre-disperser prism temperature, except for periods of strong temperature change or for detectors operated at higher temperature variability (uncontrolled). One such event was the warm phase of the SIOV before mid-October and another was the throughput test around 7 November 2012.

Figure 27 shows the stability of the spectral co-registration between PMD-P and S in % per detector pixel spectral width. The results demonstrate the strong stability of the co-registration outside the special events regime and its overall close relation to the on-board temperature.

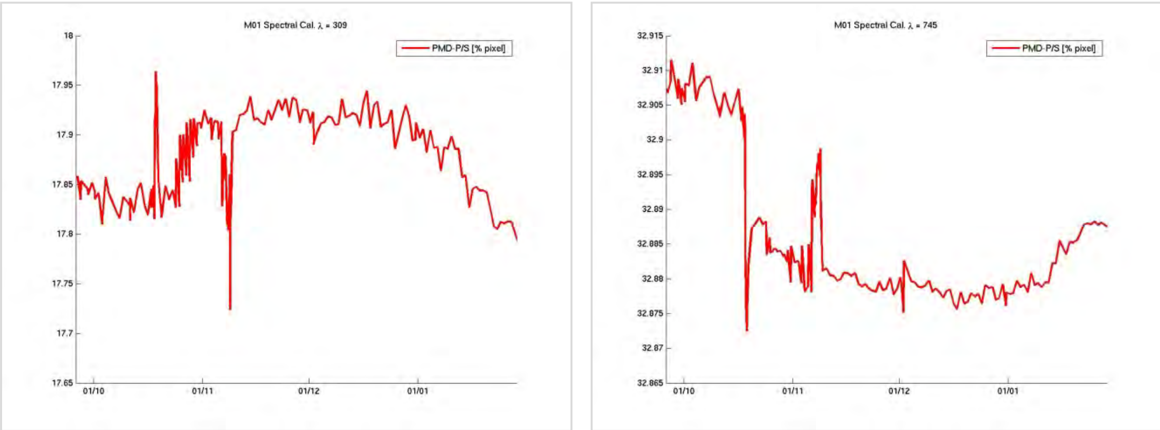

Figure 27: Spectral stability of the co-registration between PMD-P and S in percentage of fractional detector pixel around 311 & 745 nm.

The very high stability of the PMD spectral calibration is not least thanks to the significant amount of time and effort that has been spent on this part of the calibration during the FM2-2 on-ground calibration campaign.

4.5.2 Results on the accuracy of the spectral calibration

Figure 28 and Figure 29 present the results on the comparison of the spectral calibration with catalogued positions of selected (and reasonably isolated) Fraunhofer lines in the spectrum. The results present the accuracy of the spectral calibration within the limits of the method (predominantly within the limit of the spectral resolution of the instrument). For FM2/ Metop-B / FM2 the accuracy is quite good and, even better than for Metop-A / FM3, and on the order of 0.01 to 0.03 nm (note also the different scales for FM2 and FM3 results). This accuracy is well below the spectral sampling size of the instrument (0.1 nm in channels 1 and 2 and 0.2 nm in channels 3 and 4).

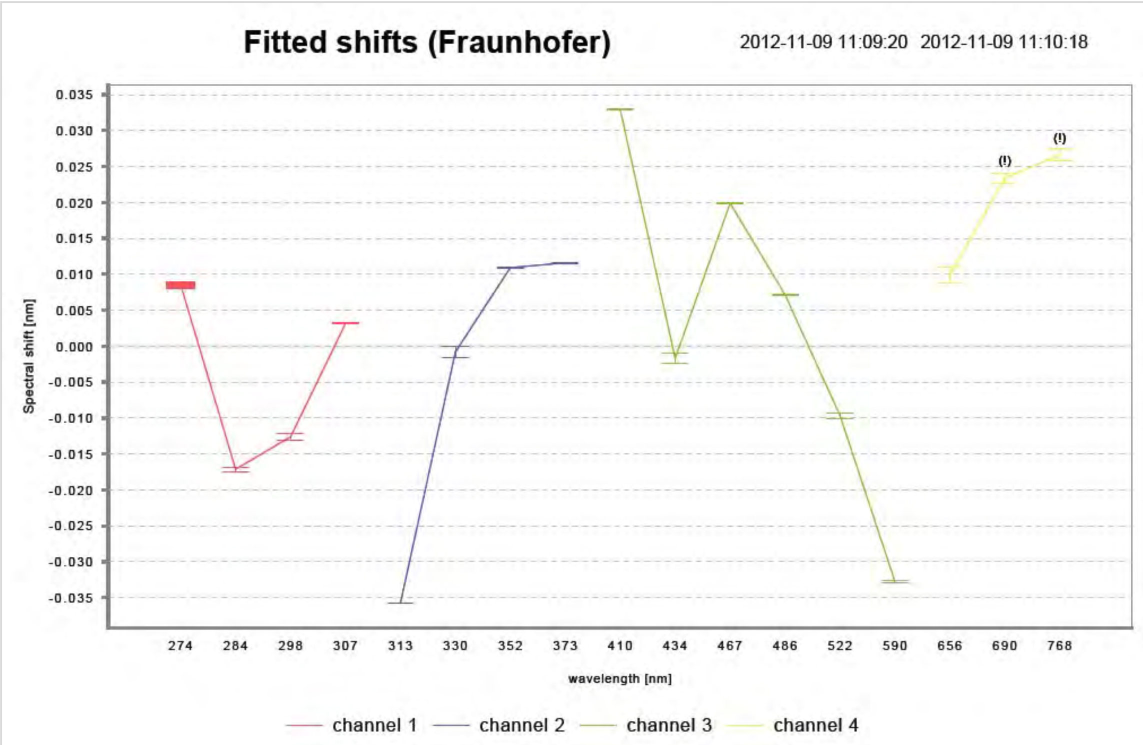

Figure 28: Metop-B / FM2 spectral calibration difference to selected Fraunhofer line positions for main channel data on 9 November 2012.

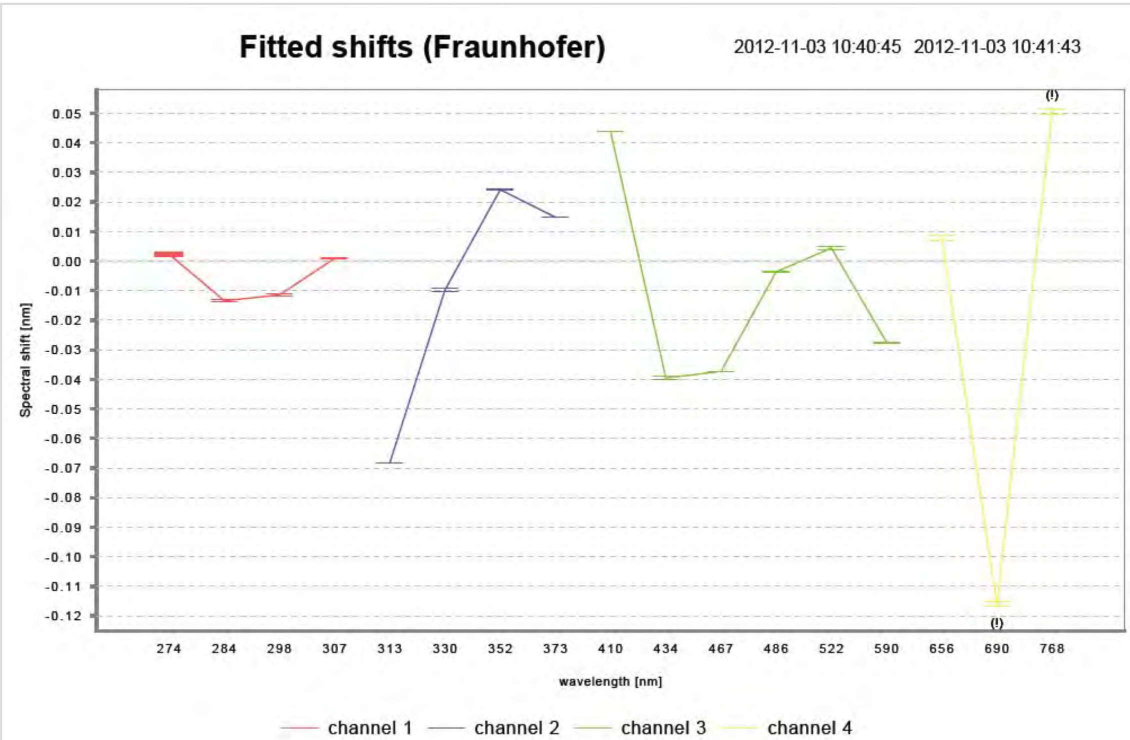

Figure 29: Metop-A / FM3 spectral calibration difference to selected Fraunhofer line positions for main channel data at the 3rd of November 2012.

4.6 Slit-function stability – FWHM monitoring

We derive the FWHM (spectral resolution) stability of the instrument applying a simple Gaussian fit to some well-isolated lines from the daily averaged SLS spectrum (see Section 4.2). Note that the slit-function response is not purely Gaussian which is why this is an approximation. However this is sufficient for the monitoring of potential changes in the FWHM. It is less accurate of course for determining the true FWHM of the instrument at any wavelength as is done by the dedicated slit-function study as carried out by RAL 0.

From the derived FWHM at certain spectral positions, both a potential on-ground to in-orbit change in the slit-function as well as a potential in-orbit long-term change can be detected.

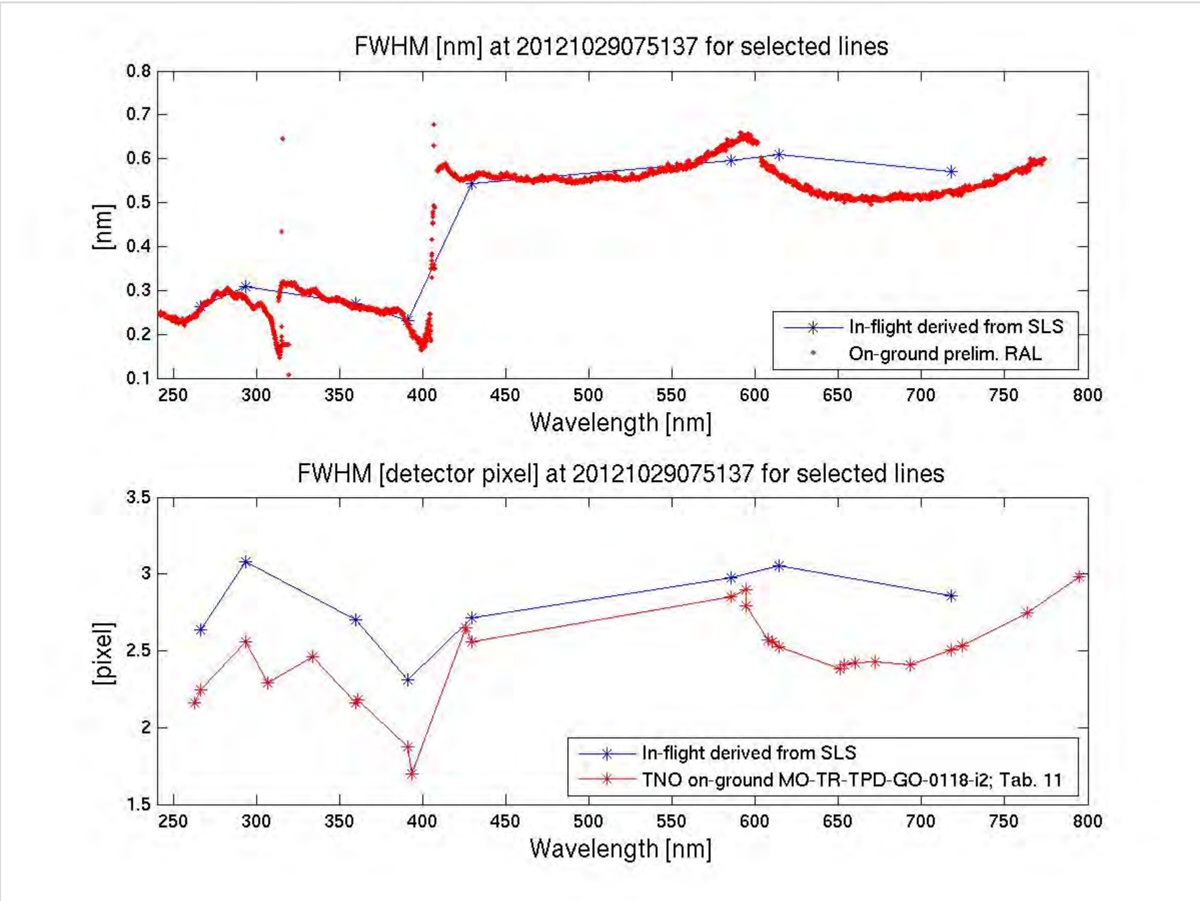

Figure 30: Metop-B / FM2 derived FWHM from a Gaussian fit to selected lines of the averaged SLS daily measurement 29 October 2012. The results are shown with the blue lines and are compared the derived FWHM from the dedicated slit-function study carried out by RAL (prelim results) in wavelength space (upper panel) using the on-ground data as derived by TNO in detector pixel space (lower panel).

In Figure 30 we compare the FWHM measured in-flight to two instalments of the on-ground measured and derived FWHM. Once the data is compared to data derived by TNO from on-ground SLS measurements during the campaign and in detector pixel space, and once we compare it to the derived FWHM from the dedicated and much more accurate slit-function campaign carried out by RAL (preliminary results from October 2012) in wavelength space.

The comparison to the RAL data results indicate that there was hardly any shift in the FWHM with respect to the on-ground situation occurring for FM2. This is in contrast to what has been observed for FM3, for which a significant shift between on-ground and in-flight in the derived FWHM has been noted.

We monitor potential changes in the FWHM as observed on Metop-A / FM3 since 28 November 2012 using the on-board spectral line source spectra (see Figure 5) making use of a selection of distinct lines (separated well enough from neighbouring lines to allow form a robust fitting). We first interpolate from the instrument spectral binning (0.1/0.2 nm), which usually is representing a line in maximum of 4 measurements, to a high resolution artificial grid using linear interpolation. Then we fit a Gaussian curve through it, assuming a symmetric slit-function. This is only a fair assumption because we are predominantly interested in the relative change of the FWHM than in its absolute values.

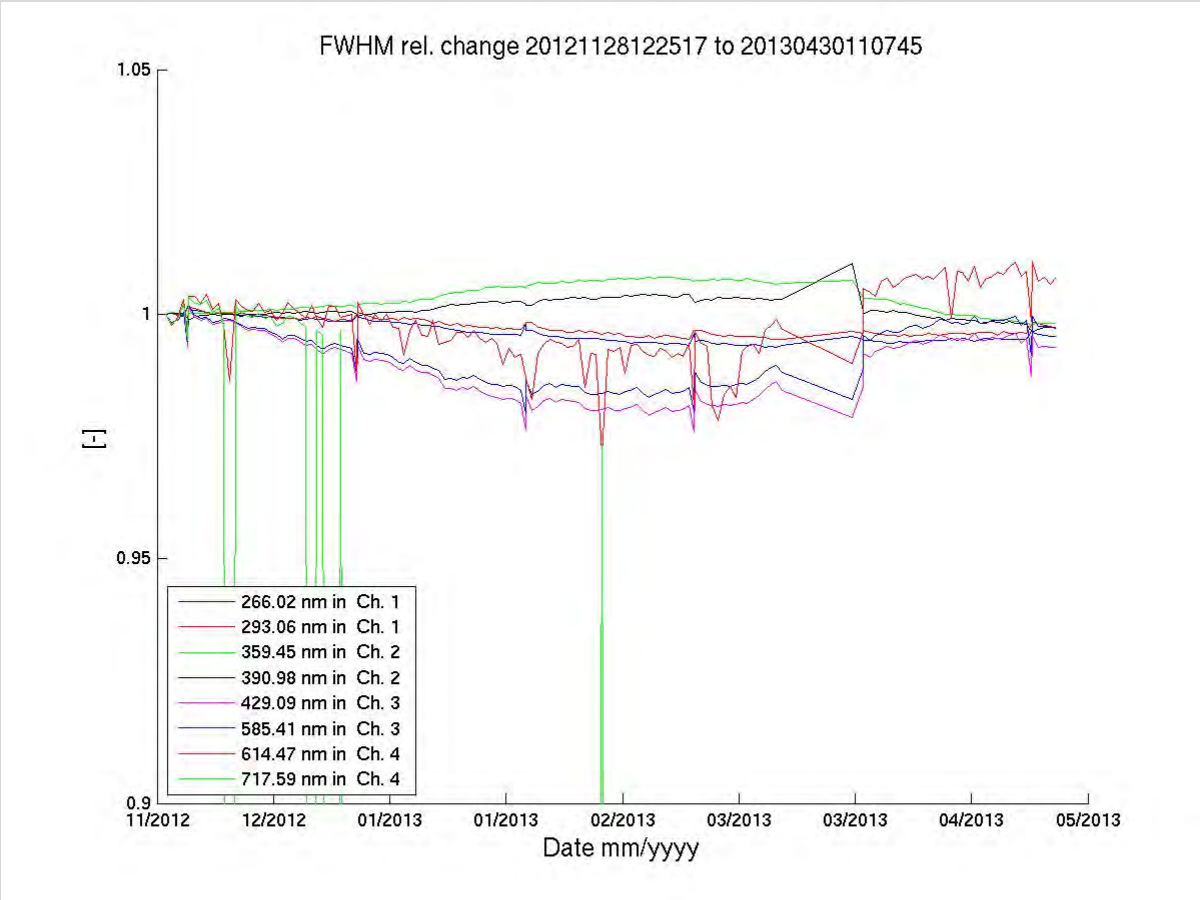

Figure 31: Metop-B / FM2 derived FWHM from a Gaussian fit to selected lines (see legend) of the averaged SLS daily measurement relative to 28 November 2012.

Figure 31 shows the result indicating a variation of the FWHM following the on-board optical bench seasonal cycle temperature. All FWHM are currently converging again after an initial spreading. While in the long-term a narrowing of FWHM values has been observed for Metop-A / FM3 [RD8] in Figure 32, currently there is only a seasonal effect evident for Metop-B / FM2, which has also been observed for Metop-A. By the end of commissioning, no long-term trend has been observed.

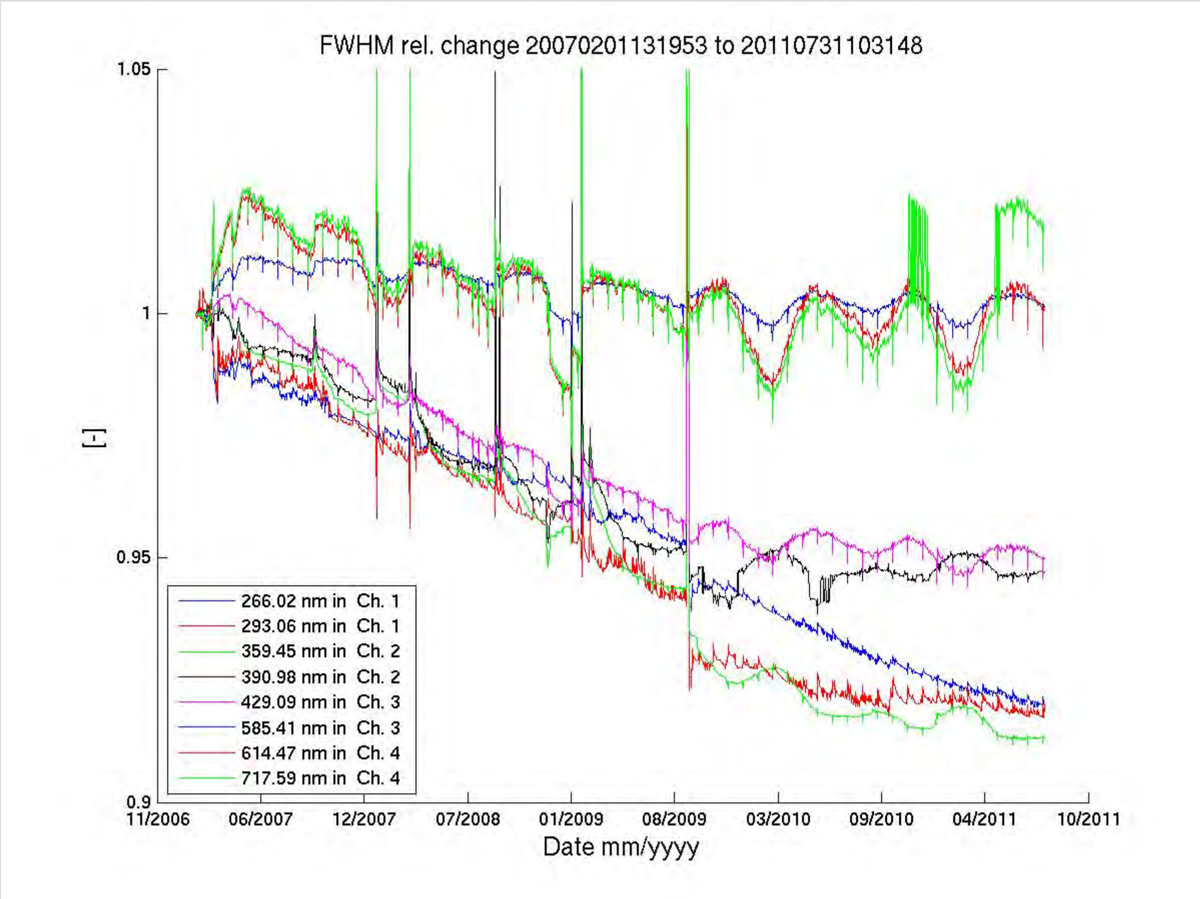

Figure 32: Same as Figure 31 but for Metop-A / FM3.

4.7 PMD co-registration and PMD band settings (IOV / CalVal task)

The co-registration between the two PMD detector band definitions is important since the closer two band values for P and S are the more accurate the derived Stokes fraction values (which in turn determine the accuracy of the polarisation correction or of retrievals making direct use of the latter). Since the definition of the bands is defined on-board in detector-pixel space, any shift of the spectral calibration between on-ground and in-orbit of in-orbit will compromise the optimal co-registration of the uploaded definitions, provided they are not adapted accordingly.

To upload the optimal settings for the PMD in-orbit situation is a “routine” task and has been foreseen in the planning of the IOV to be carried out as part of the IOV/CalVal activities (see also Section 3). The procedure which has already been applied for Metop-A / FM3 has also been used for Metop-B / FM2 [RD11] and the detailed steps and results are documented in [AD 6].

The upload of the optimised definitions versions 2.0 (see Table 3) has been carried out during orbit 598 on 29 October 2012.

Figure 33 and Figure 34 show the centre positions of the PMD bands S and P after the co-registration updated (green vertical lines) with respect to the targeted positions as suggested by the GSAG. The blue vertical lines show the positions as they were before the upload for PMD band definition version 1.0 (the current FMS definitions).

Note: Because of the detector pixel discretisation and the very low spectral resolution in the red part of the spectrum for PMDs, the optimal line position will never fully overlap the targeted positions.

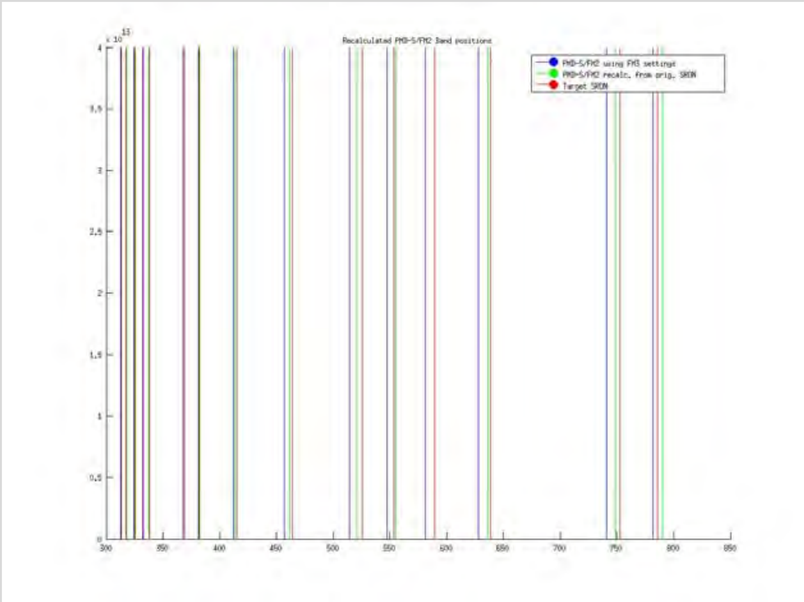

Figure 33: Centre band position of PMD-S Metop-B / FM2 after co-registration shift (green) with respect to the old position from band definitions verison 1.0 (blue) and the target positions recommended by the GSAG (red). In case only the red line is visible the green line is hidden below the red line.

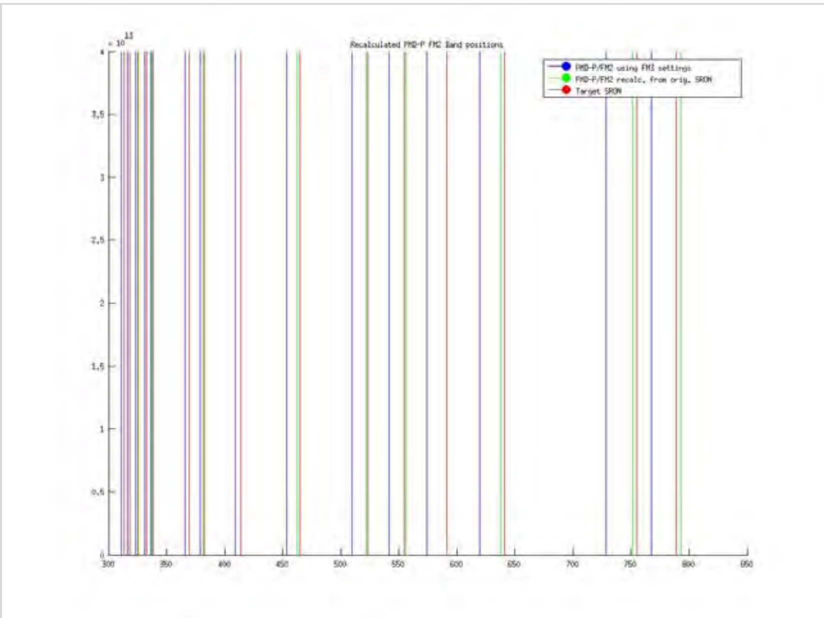

Figure 34: Centre band position of PMD-P Metop-B / FM2 after co-registration shift (green) with respect to the old position from band definitions verison 1.0 (blue) and the target positions recommended by the GSAG (red). In case only the red line is visible the green line is hidden below the red line.

Figure 35 shows that the chosen line definitions for version 2.0 are optimal in terms of spectral co-registration between the two PMDs since, both the centre and the edges of the bands are within half a detector pixel difference between PMD-P and S when translated from wavelength space back into detector pixel space.

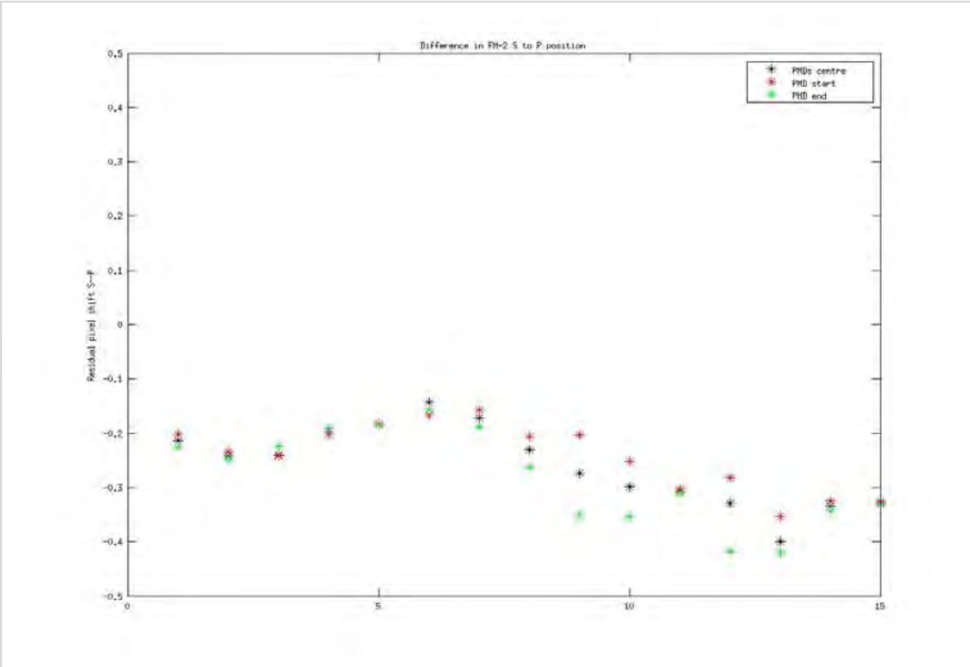

Figure 35: Band centre and edges detector pixel co-registration at sub-pixel range after adjustement of the PMD band definitions following the rules laid out in this section.

These settings then result effectively in a shift of one detector pixel between PMD-P and S over the full 279 pixel array (see Figure 36), which is what was expected from the on-ground calibration campaign (see references in [AD 6]).

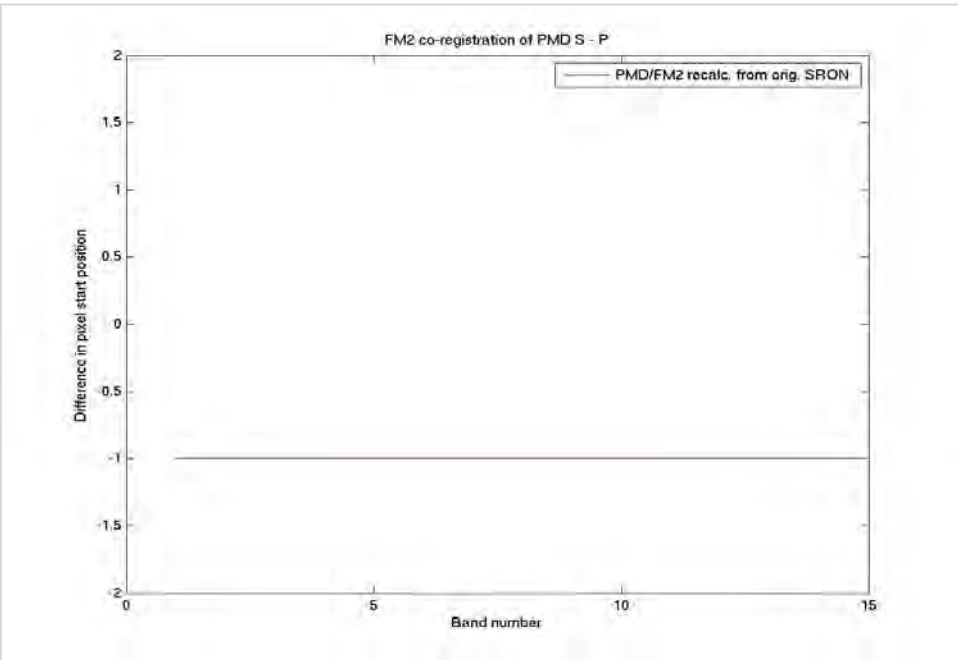

Figure 36: Detector band centre pixel co-registration for the adjustement of the PMD band definitions following the rules laid out in this section.

4.8 Channel Overlap Point Adjustment and Etalon Correction

4.8.1 Background

From our GOME-2 Metop-A / FM3 experience, we expected that the launch itself could trigger a slight shift of the channel separator prism ("cs" in Figure 3), thereby causing a shift in the projection of the dispersed beams onto the main channel detector pixel assembly (FPAs; see optical layout in Figure 3). While the centre part of the radiometric response functions measured on-ground during the calibration campaign FM2-2 (see Section 1.4) remain valid, this is not true in the channel overlap regions where the energy is distributed between the two channels changes and where, in addition, the response functions exhibit very steep gradients towards zero (see Figures of radiometric response functions below). As a result, the response functions are not valid in the overlap regions resulting in large errors in the radiometric calibration. This is clearly visible in both Earthshine and the solar spectrum. Since for solar spectrum there exist reference spectra of acceptable quality (not readily available for the earthshine spectra) the channel separation "jumps" show up in the derived residual between measured and reference spectra as shown in the lower panel of Figure 37 around 310 (channel 1 to 2 separation) and 400 nm (channel 2 to 3 separation). The "jumps" are also visible in the Earthshine spectrum (see Figure 38). No such "jump" is visible or expected between channels 3 and 4 (around 600 nm) due to use of a different channel separation mechanism.

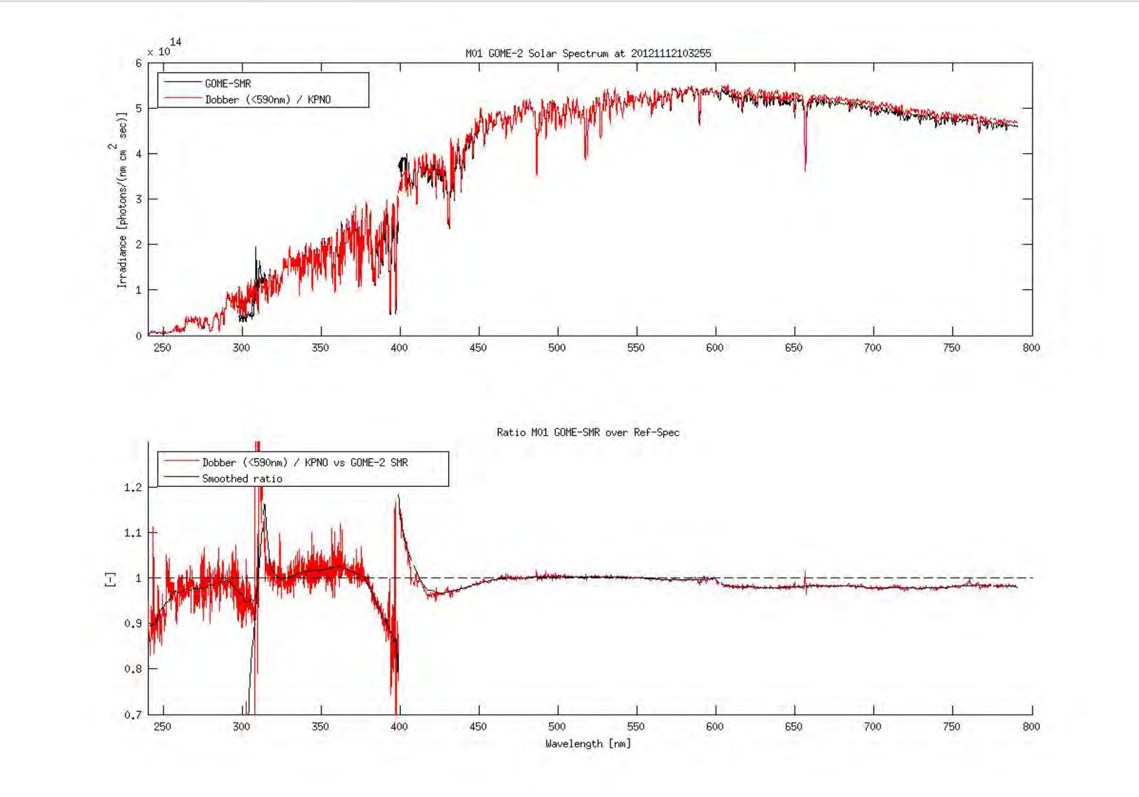

Figure 37: GOME-2 FM2 calibrated solar spectrum (upper panel; black line) compared with a reference spectrum by Dobber et al. (Solar Phys (2008) 249: 281–291) below 590 nm (upper panel, red line). Above 590 nm the KPNO/AFGL spectrum of 2004 is used. The lower panel shows the residual between both (red line) and a moving average to guide the eye.

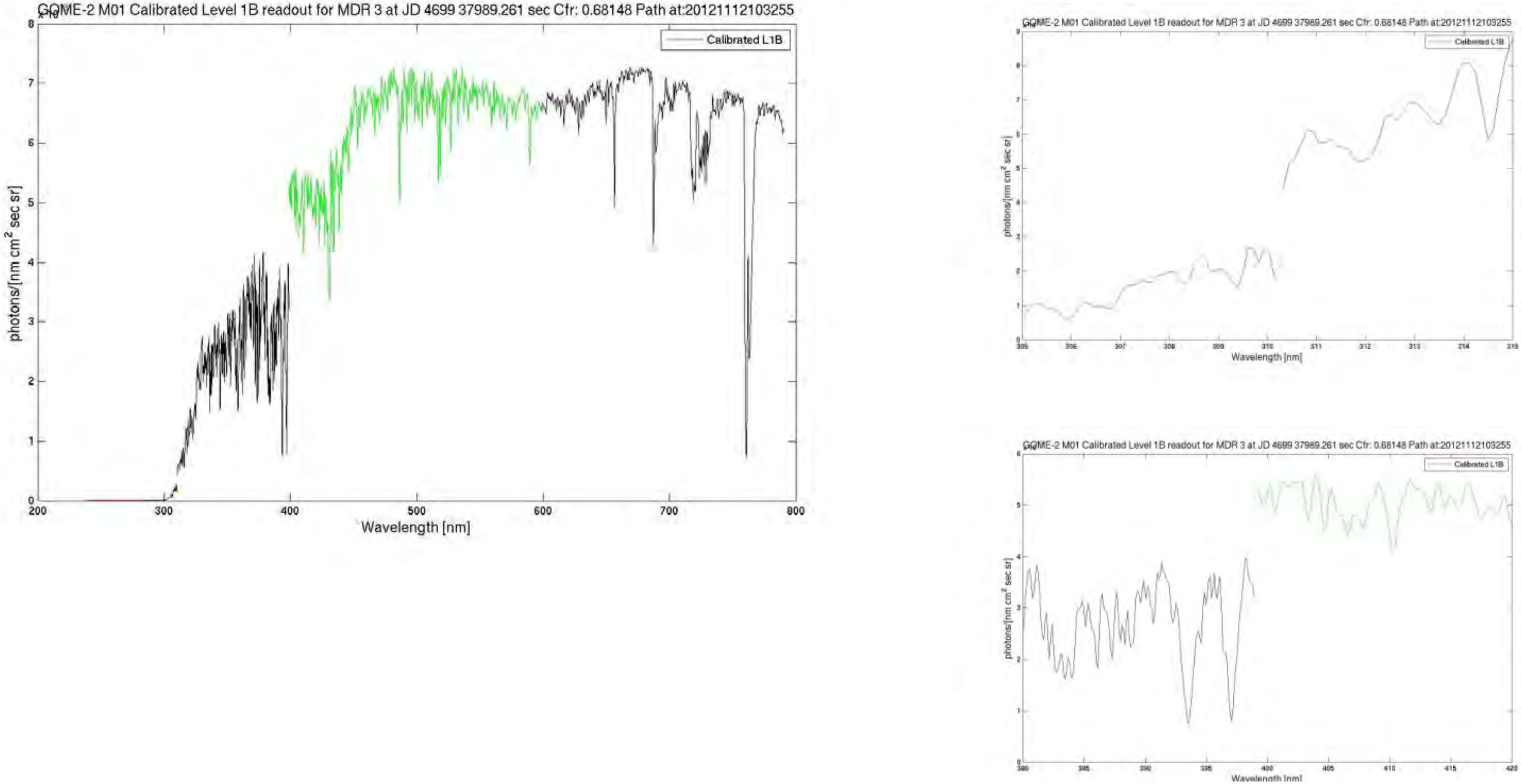

Figure 38: GOME-2 FM2 calibrated Earthshine spectrum (upper panel) with alternating colours for the different bands. The two panelsat right show "jumps" between channel 1 and 2 (top) and 2 and 3(bottom.)

For FM3 on Metop-A, a procedure has been developed by ESA/SSST (Michael Eisinger) to adjust the radiometric response functions (RA_IRR_ABS*[1], RA_RAD_ABS*, RA_SUN_CAL_IRR_ABS*[2]) together with the channel overlap positions (WL_OVERLAP) using the in-flight white-light source comparison to the on-ground measured white-light source reference spectrum (RA_WLS_*), which is also available in the key-data.

This approach, which will also be followed for FM2, was successful to the extent that it corrected the "jumps" (closing them) of the overlap regions by adequately and "smoothly" adjusting the radiometric response functions in the channel overlap regions. However, this approach had the drawback that it was applied (and still is for Metop-A / FM3) without taking an in-time varying etalon correction in these regions into account (because the approach implicitly not only fixes the response to the overlap shift but also corrects for the on-ground to in-orbit etalon effect in the region of the overlap at this, but only for this, point in time). As a result, the etalon correction derived once per day on-board from the white-light source measurements to account for both the on-ground to in-orbit etalon changes, as well as the in-flight long-term etalon changes - and which is applied during level 0 to 1B processing to all calibrated and dispersed spectra - cannot be applied anymore correctly to the overlap region (for details on the etalon correction in the level 0 to 1B processing see 0).

Therefore, for FM2, and as will be explained in detail in the following section, the adjustment procedure has been extended to also include the effect of the on-ground to in-orbit etalon change by making use of the observed etalon at the point in time when the overlap correction is derived, and apply both to the radiometric response key-data. As a consequence, the in-orbit derived etalon changes (which are then much smaller than the etalon changes including the on-ground to in-orbit transition) can be applied to the whole valid region of the detector array per channel and the overlap regions can be consequently exploited by level 2 retrievals.

This is a significant achievement considering that, for example, the region between 312.8 nm and 316.5 nm–which is important for the retrievals of, for example, ozone and SO2–could not be exploited up-to-date for Metop-A / FM3 (see Section 7.4 in [RD8]).

In the following we will show the step-by-step derivation of the radiometric adjustments needed and their impact on the spectra as shown in Figure 37 and Figure 38. The procedure will also lead to an optimised set of Etalon settings (GOME_INS_xx_M01) used for level 0 to 1B processing of FM2 data.

[1] Name of key-data files in the provided key-data set for FM2; see Section 1.4.
[2] Newly derived key-data set for FM2-2

4.8.2 Adjustment procedure

4.8.2.1 Observed overlap point shift.

Following launch, the overlap point has been monitored using the WLS spectra by the operational monitoring database.

Figure 39 shows that the overlap point is stable after launch at 309.9 nm (310.3 nm; CAL 1.00) for the channel 1 to 2 transition. The channel 2 to 3 transition at 397.76 nm (398.91 nm; CAL 1.00) is less stable and changes with the long term changes of the optical bench temperature, as has been observed for Metop-A. It remains to be seen for the long-term evaluation if the current trend is part of the seasonal cycle trend in OB temperatures or/and the warming up of the platform.

Recommendation: *Introduce a second (or more frequent) adjustment of the radiometric key-data in the overlap region, as a routine operation during the mission, at least after the platform temperatures have been stabilized (after approximately three years for Metop-A). This approach is now also followed for GOME-2 Metop-A with a second adjustment carried out in May 2013.*

The channel 3 to 4 transition at 598.43 nm (598.46 nm; CAL1.00) is significantly more stable than the channel 2 to 3 separation. The differences in stability are a consequence of the design of the channel separator prism (see Figure 3) and expected. The initial adjustment to the radiometric key-data, as discussed in the following, will account for the on-ground to in-orbit shift only.

This on-ground to in-orbit changes in the overlap points result in a shift of -0.58, -1.15 and -0.03 nm respectively, which has also be confirmed by the GIOV report 0. As a consequence, the original key-data file for the overlap point definitions in CAL 1.00 can be updated taking this shift into account in version 4.0 of WL_OVERLAP.202 key-data file to be used in CAL 1.01 (see Table 8).

Overlap	***First channel 90% point [pixel]***	***First channel 50% point [pixel]***	***First channel 10% point [pixel]***	***Wave-length 90% point [nm]***	***Wave-length 50% point [nm]***	***Wave-length 10% point [nm]***	***Second channel 10% point [pixel]***	***Second channel 50% point [pixel]***	***Second channel 90% point [pixel]***
1	883.7476	902.0548	925.4358	307.6311	309.72	312.1438	80.24069	96.17893	116.5989
2	803.9475	840.1556	869.1092	393.4376	397.76	401.0087	9.43374	28.54393	43.83267
3	957.3695	982.858	1012.033	592.6492	598.43	604.6211	36.96266	62.23039	91.53473

Table 8: Newly evaluated 90%, 50%, 10% overlap points based on the observed shift of the 50% point using the WLS on-board measurements from the operational monitoring database. To be used as version 4.0 of WL_OVERLAP in CAL 1.01.

Figure 39: GOME-2 FM2 channel overlap point monitoring results by the operational monitoring database. Upper panel channel 1 to 2, middle panel channel 2 to 3, lower panel, channel 3 to 4. Channel 2 to 3 also shows a strong response to changing optical bench temperatures during the SIOV 2nd throughput test around 7 November 2012.There is also a considerable response to the darkness test carried out during the 2nd half of March, because of data processing issues.

Figure 40 shows the newly-defined 90%, 50%, and 10% overlap point for the WLS spectrum derived on 11 November 2012.

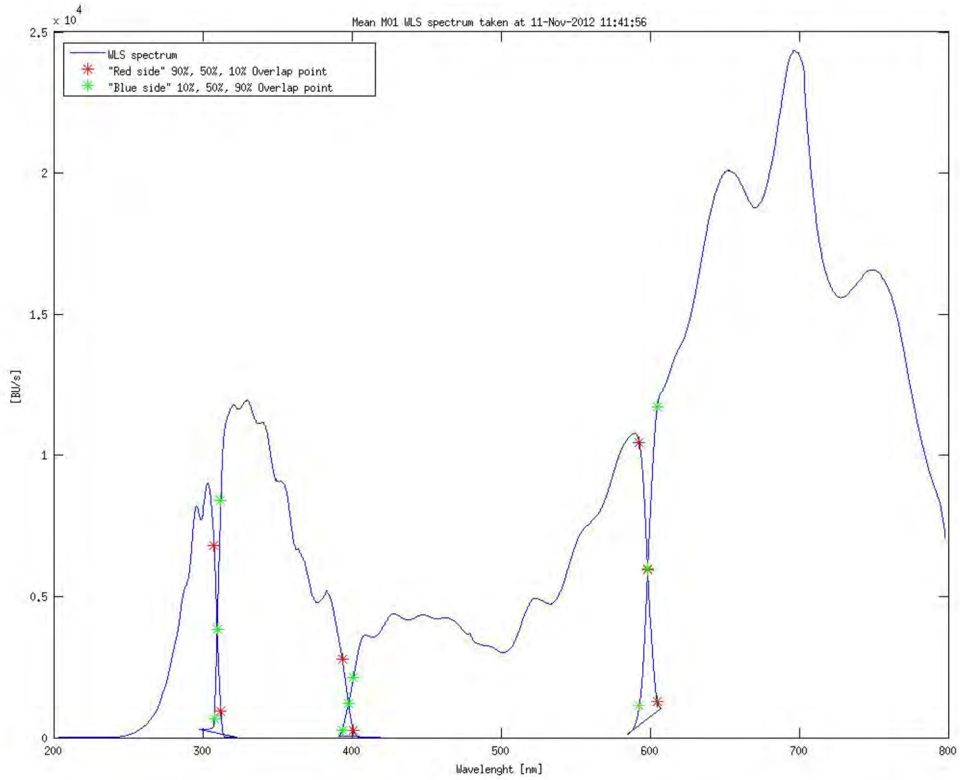

Figure 40: GOME-2 FM2 90, 50, and 10% overlap point position (stars) for a WLS spectrum as derived on-board on 11 November 2012.

4.8.2.2 Offline-derived Etalon

To be able to evaluate and adjust the derived etalon and overlap region setting, offline analysis tools in TCE are used and will be compared to the “as is” as well as to the modified PPF level 1B product results.

We start off with the initial settings of processing using version 1.01 of the INS processing settings and version 1.00 (original TNO data set) of the GOME_CAL key-data as have been used for Figure 37 and Figure 38. The etalon correction in this original configuration is derived from the in-flight and on-ground white-light source (WLS) spectrum as shown in Figure 41. The etalon correction is derived (both with the PPF and offline) according to Section 5.2.18 in [AD 3], with the only difference that for the “offline” derived etalon correction slightly modified start and end points have been used. These points fall just outside the overlap regions, taking the observed shift of the overlap points (previous section) into account. This is done so that the residual of the shifted and the un-shifted radiometric response function is lower or equal to the on-ground calibration measurement error of response functions at the start and end points (ets/ete).

Note: Finding these optimal points, which define both the regions inside and outside of the overlap regions, involves a certain amount of manual interaction. This manual interaction is not shown here.

Table 9 shows the start / stop detector pixels per channel as used for FM2 after launch as the region for which the etalon correction is derived and applied (PPF-derived etalon correction in lower panel of Figure 42; blue line). They therefore implicitly define the region of the overlap outside the etalon correction region.

	Channel 1	*Channel 2*	*Channel 3*	*Channel 4*	*PMD-P*	*PMD-S*
ets	310	210	120	85	751	750
ete	931	850	1009	989	997	998

Table 9: Start (ets) / Stop (ete) detector pixel per channel which fall outside the overlap region. Launch SIOV settings for FM2 as taken from Metop-A / FM3

In contrast, Table 10 lists the adjusted settings taking the observed mean overlap shift per channel transition into account. Consequently the offline derived etalon using these start/stop pixel definition is slightly different, especially towards the channel overlap region (see Figure 42, lower panel, red line).

	Channel 1	*Channel 2*	*Channel 3*	*Channel 4*	*PMD-P*	*PMD-S*
ets	310	180	79	85	751	750
ete	887	713	1009	989	1000	999

Table 10: Start (ets) / Stop (ete) detector pixel per channel which fall outside the overlap region. Intermediate settings used offline only for adjustment procedure

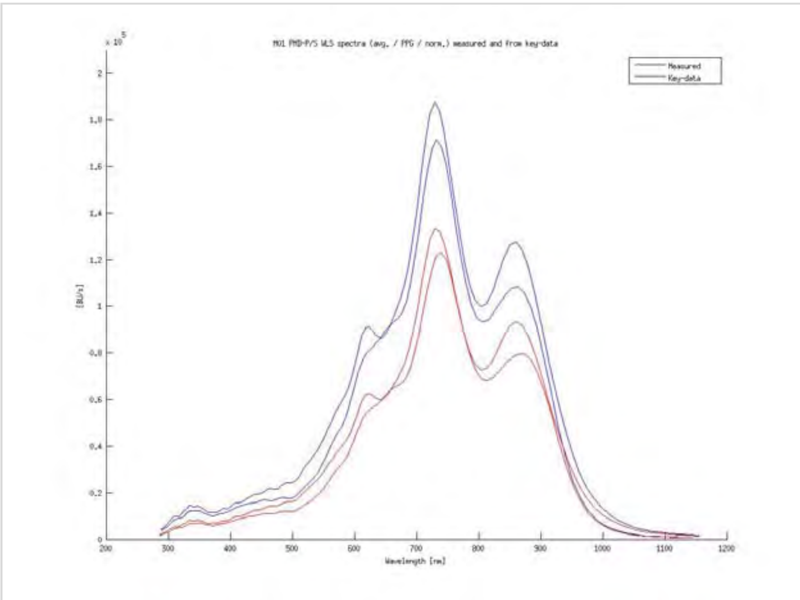

Figure 41: GOME-2 FM2 white-light source spectra measured in flight on 11 November 2012 (blue curve) and as measured on ground for the FM2-2 campaign. Note that the difference in overall signal strength is an expected 1g to 0g effect of the lamp output.

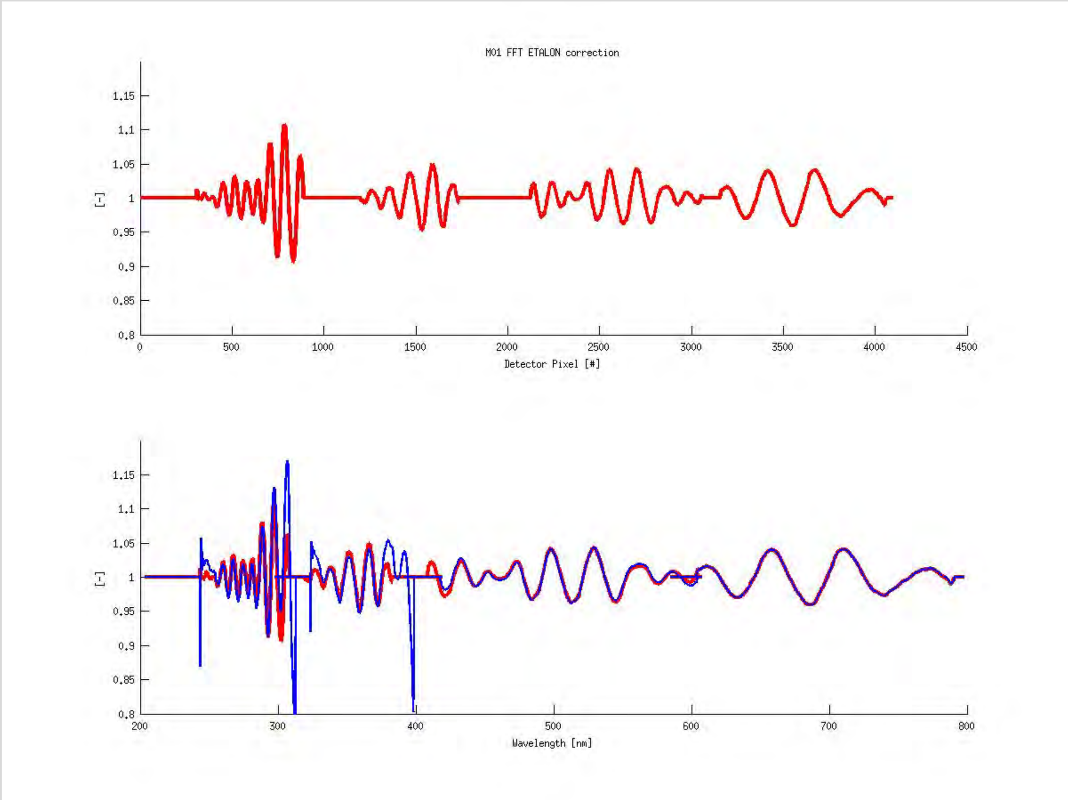

Figure 42: GOME-2 FM2 derived etalon correction from the WLS spectra in Figure 41 according to PGS 7.1. Upper panel offline derived etalon in detector pixel space using the settings in Table 10. The lower panel shows the etalon correction as derived from the PPF (blue line) using the original INS 1.01 settings Table 9) and the "offline" derived Etalon using the settings from Table 10.

Figure 43 and Figure 44 show the crossing point of the shifted and the un-shifted radiometric response functions, according to the described procedure and the position of the selected overlap region start/stop points on the derived residuals (of the shifted and un-shifted response spectra). The results show that it is difficult to reach the 3 % residual point in channel 1 (Figure 43; lower panel red star) but it works reasonably well for all other transition points. In order to make a "smooth" transition the gradient of the response functions need also to be taken into account, and this is not reflected in the residuals.

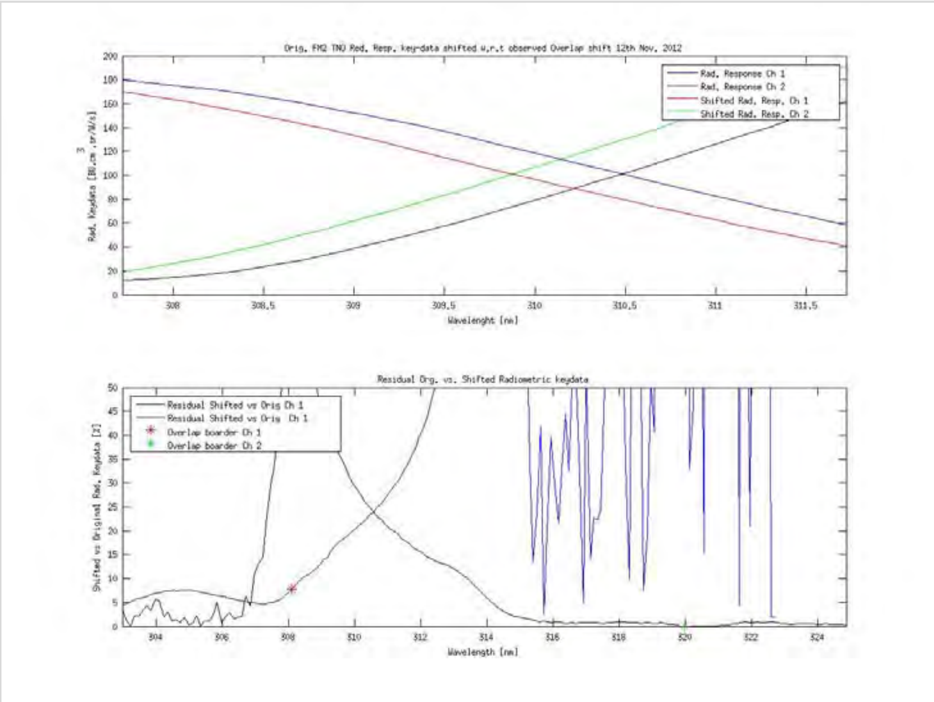

Figure 43: Shifted and un-shifted radiometric response function according to the observed overlap shift (upper panel) in the channel 1 to 2 transition region. The lower panel shows the residual of the shifted and the un-shifted spectra, as well as the position of the chosen start/stop of the overlap region. (Table 1010)

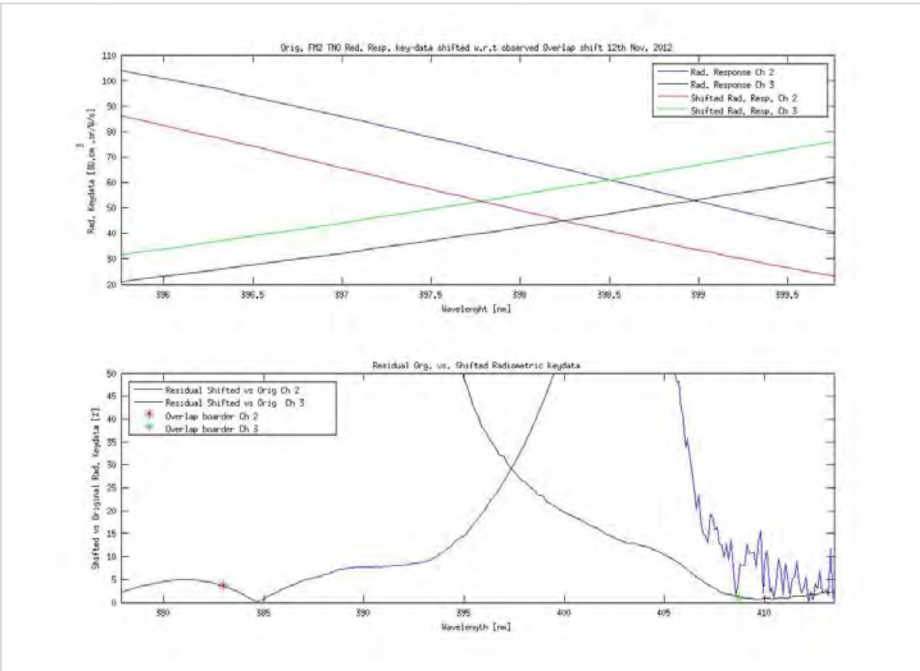

Figure 44: Shifted and un-shifted radiometric response function according to the observed overlap shift (upper panel) in the channel 2 to channel 3 transition region. The lower panel shows the residual of the shifted and the un-shifted spectra, and the position of the chosen start/stop of the overlap region (Table 10).

4.8.2.3 Derivation of the overlap region adjustment of the radiometric response functions

First the ratio of the on-ground to in-orbit WLS spectrum of Figure 41 for channels 1 and 2, and for channels 2 and 3 are combined for the treatment of the overlap region 12 and 23 respectively.

Note: In the analysis and illustrations in this section, the treatment of the channels 3 to 4 overlap is omitted since the shift is assumed to be 0 there.

From the ratio, a third order polynomial fit (same degree as for the etalon correction background fit, see PGS 7.1) is fitted to the combined ratio spectra but excluding the overlap region in the fit, as defined in Table 10 (see Figure 45). Then, this background is removed by taking the ratio of fit and combined ratio-spectra and the part of the resulting spectrum outside the overlap region is set to 1 (See Figure 46).

Finally, we replace the region outside of the overlap region (set to 1 in Figure 46) with the etalon correction derived offline in Figure 42, lower panel, red line (this is the additional step not applied to FM3 on Metop-A). The result is the final correction spectrum for the overlap region 12 and 23 as shown in Figure 47. In this way the etalon correction of the on-ground to in-flight situation on 11 November 2012 is now taken into account implicitly in the correction spectra for the radiometric response key-data. Therefore, this type of corrected key-data can only be applied if the in-flight acquired WLS spectrum of Figure 41 is used as reference WLS spectrum (RA_WLS*) in the updated key-data.

The resulting corrected radiometric and IRR-radiometric response key-data spectra are shown in Figure 48. The results also show that the choice of the overlap region start/stop definitions were adequate because there is a very smooth transition between the overlap-adjusted and etalon-adjusted regions.

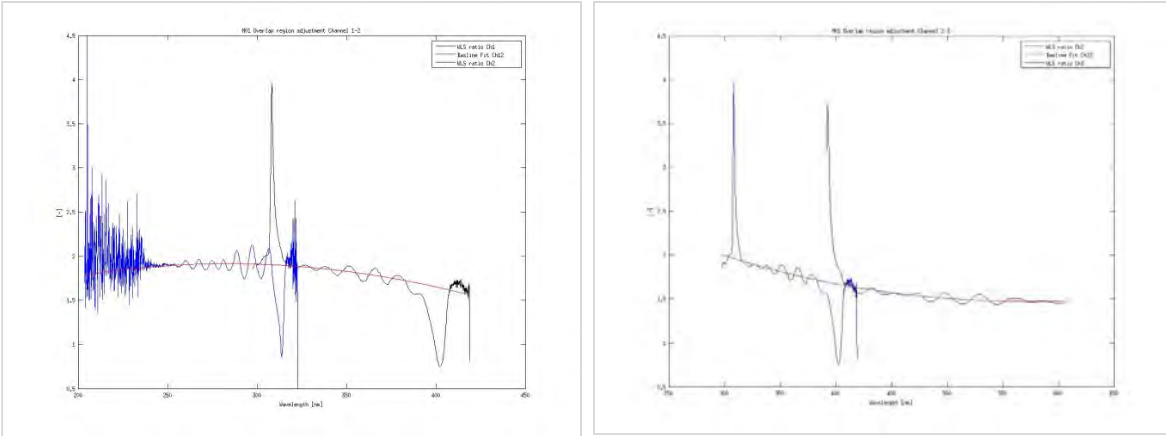

Figure 45: WLS spectra ratio between a spectrum measured on 11 November 2012 in-flight by FM2 and the on-ground measured WLS reference spectrum as contained in the CAL 1.00 key-data set (FM2-2). The figure also shows a third order polynomial fit excluding the overlap regions (red line). The left panel shows the result for channel 1 and 2 and the right panel for channel 2 and 3 (blue and black line respectively).

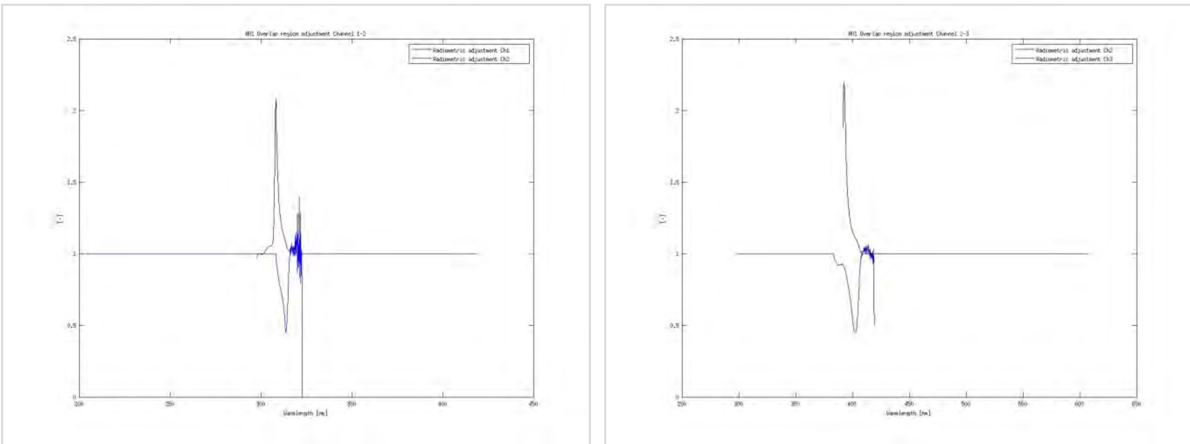

Figure 46: WLS spectra ratio between a spectrum measured on 11 November 2012 in-flight by FM2 and the on-ground measured WLS reference spectrum as contained in the CAL 1.00 key-data set (FM2-2), but the rato is to the background fit results and the part of the spectrum outside the overlap regions is set to 1.

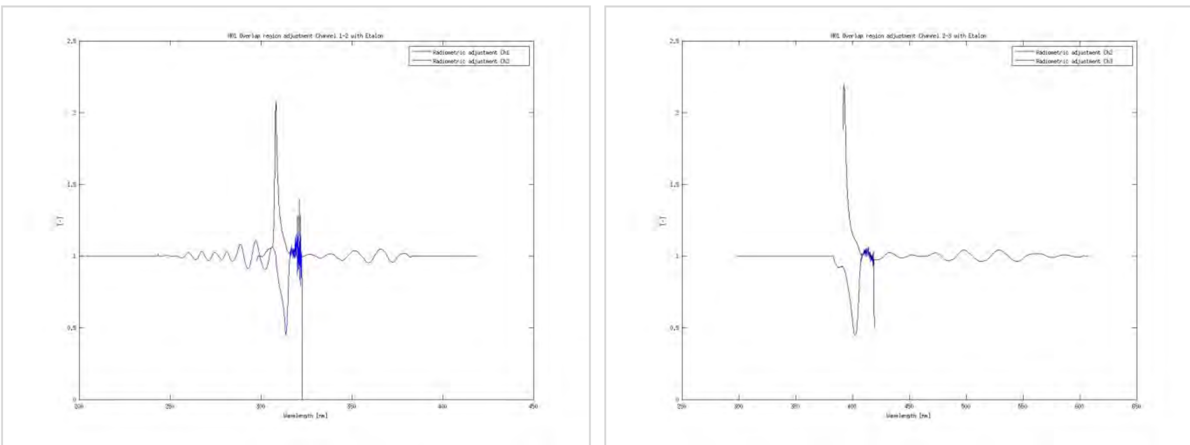

Figure 47: WLS spectra ratio between a spectrum measured on 11 November 2012 in-flight by FM2 and the on-ground measured WLS reference spectrum as contained in the CAL 1.00 key-data set (FM2-2). The region outside the overlap is replaced by the etalon correction as derived from the same date (see Figure 42).

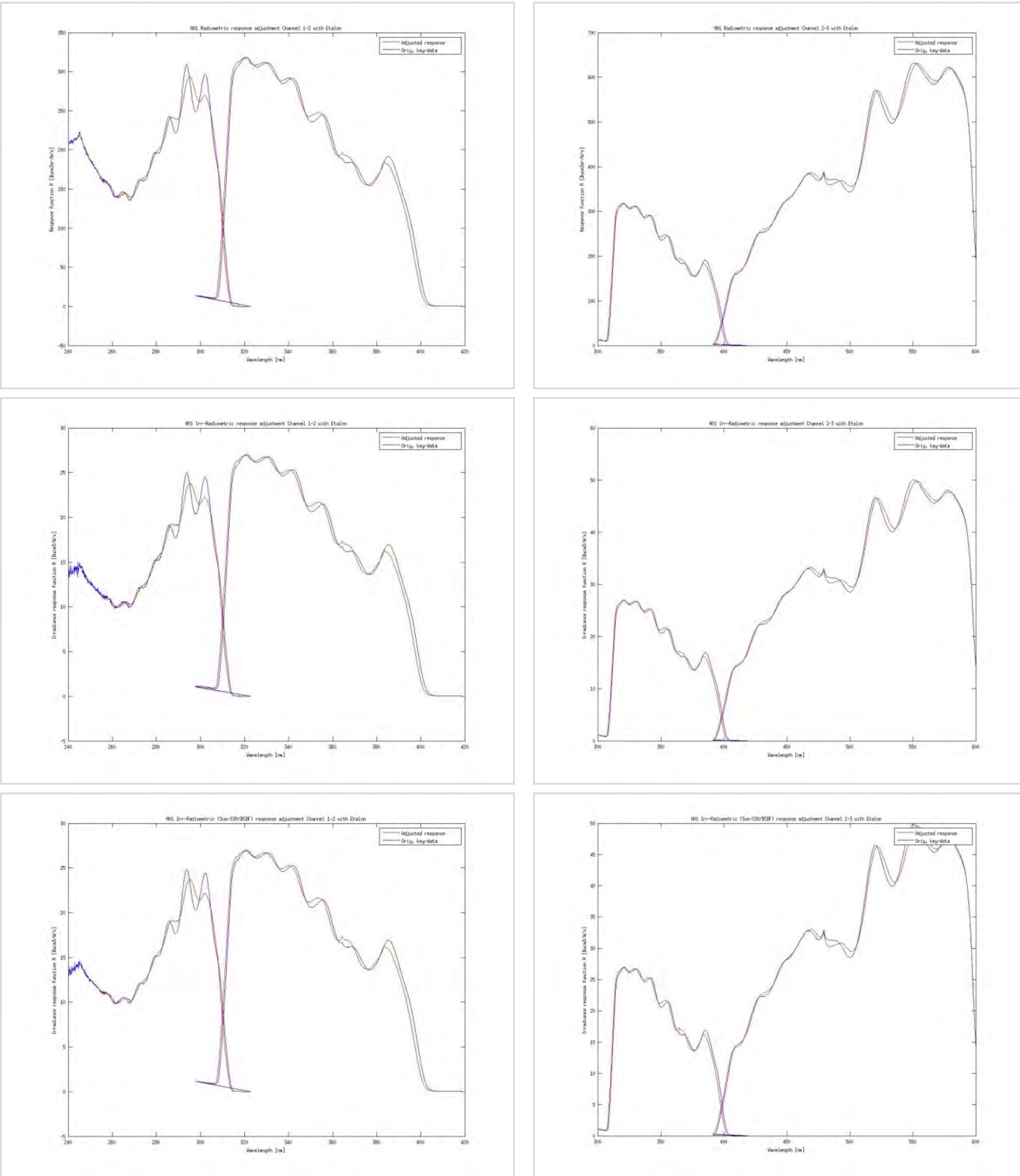

Figure 48: Adjusted set of key-data response functions (CAL 1.01) using the correction spectra of Figure 47 (red curve). The blue curve shows the original key-data response functions (CAL 1.00/ FM2-2 campaign). The left panels show the overlap 12 and the right panel the overlap 23 regions. Upper panel show the radiometric response functions (RA_ABS_RAD_MAIN), the middle panel the irr-radiometric response functions (RA_ABS_IRR_MAIN*), and the lower panel the irr-radiometric response functions as derived from the suns-simulator and the BSDF (RA_SUN_CAL_ABS_IRR_MAIN*).*

4.8.2.4 Derivation of etalon after adjustment (verification) and updated etalon settings

To verify the functional, quantitative, and qualitative performance of the adjustment, the updated radiometric response data–together with the updated WLS reference spectrum and the updated overlap definitions–has been combined in a new key-data set CAL version 1.01 (see also Section 4.8.2.6) which has then been used to derive an etalon correction from the same in-flight WLS measurement taken on 11 November 2012. At the same time, the settings for the etalon correction valid region have also been altered to be extended to the borders of the valid region of detector pixels per channel. This is in contrast with the original settings (INS 1.01; Table 8). The new settings are listed in Table 11.

	Channel 1	*Channel 2*	*Channel 3*	*Channel 4*	*PMD-P*	*PMD-S*
ets	310	85	14	37	751	750
ete	929	880	1013	991	1000	999

Table 11: Start (ets) / Stop (ete) detector pixel per channel which have been extended for the use with the adjusted response key-data set of CAL 1.01 in INS 1.02

The left panel of Figure 49 shows the result for an etalon correction on 11 November 2012 with the updated key-data set at the same scale as used for Figure 42. As required, the etalon correction is very close to 1, with some residual resulting only from the intrinsic accuracy of the background fitting, interpolation and fast-fourier-transform (fft; for details see PGS 7.1).

The right panel of Figure 51 shows an etalon correction derived on 30 October 2012. This was before the second throughput test of SIOV, whereas the etalon correction derived on 11 November 2012 was after. For this, we expect small but significant differences in etalon triggered by the temperature cycling of the detectors, as carried out during the previous testing days. Finally, Figure 52 shows a focus on the overall etalon correction as derived “offline” on 30 October 2012 (upper channel) and in the channel overlap region 12 and 23 in the lower panels.

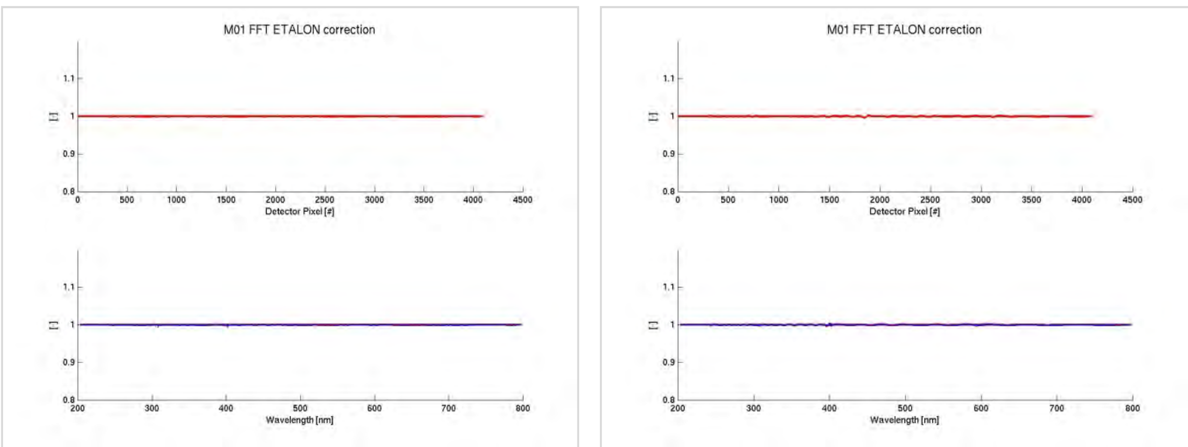

Figure 49: Left panel: Etalon correction on 11 November 2012 with the updated key-data set CAL 1.01 at the same scale as used for Figure 42. Right panel: etalon correction derived on 30 October 2012 using the same modified key-data and at the same scale.

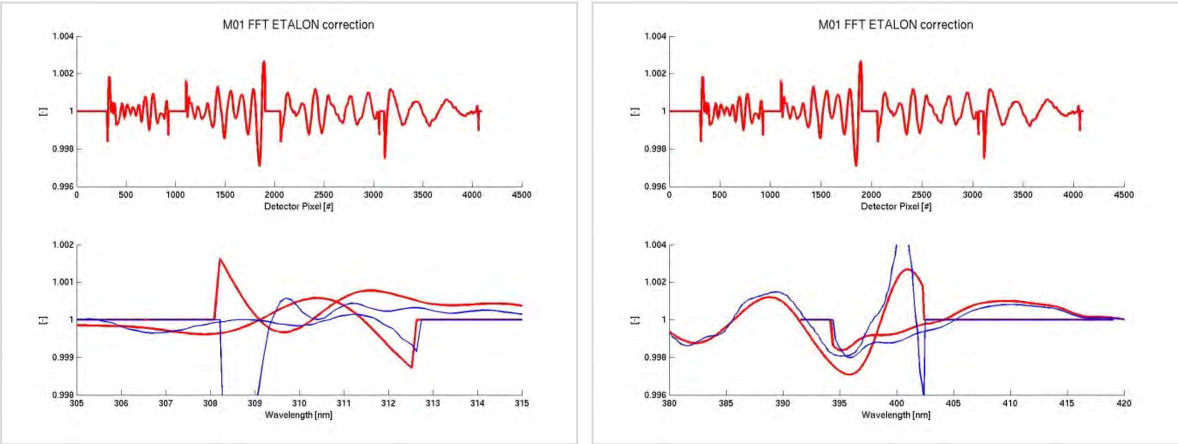

Figure 50:Same as Figure 49 but with an adjusted scale (upper panel) and in addition focused on the overlap region 12 (left lower panel) and 23 (right lower panel). The blue curve is the result from the PPF whereas the red curve is the "offline" derived correction.

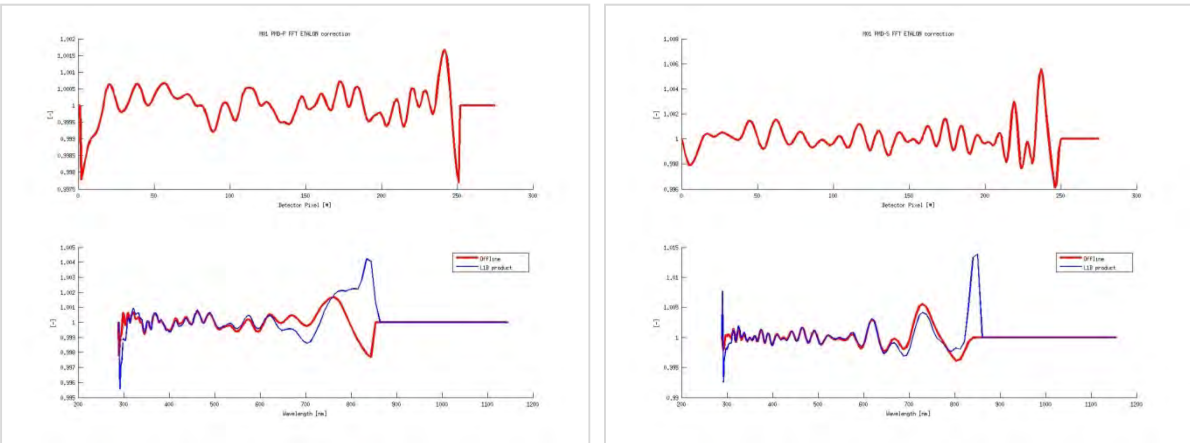

Figure 51: Derived etalon correction after the adjustment with CAL 1.01 key-data for PMD-P and S (left and right panel).

Overall, the derived etalon correction for 30 October 2012 shows the typical etalon structure though on a much smaller scale than for CAL 1.00/INS1.01 (Figure 42) as expected. It also shows that there can be small differences, especially in the overlap region between the "offline" derived and the PPF derived etalon correction due to the intrinsic background fitting and fft accuracies involved (note, that these differences are smaller than 0.1 %). However, the lower panels of Figure 50 also prove that, using this new approach, the etalon correction can meaningfully be derived in the overlap region and that the correction spectra are even overlapping.

Summary: This means that derived calibrated level 1B data can subsequently be exploited by the user up to the 50 % point as defined in Table 11. It means also that there is no need to omit part of the valuable spectrum–especially in the channel 1 to 2 transition region–as is currently still the case for FM3 data on Metop-A.

4.8.2.5 Treatment of PMD data.

To be consistent with the approach taken for the main channel data, the etalon correction derived from the 11 November 2012 WLS spectra is also applied to the radiometric response data for PMDs in the same way as described above. Of course, there is no need to carry out any overlap region adjustment. Table 11 lists the updated start /stop etalon settings for PMD that cover the complete spectral region of the PMDs.

Figure 51 shows results for the derived etalon correction after the adjustment with CAL 1.01 key-data for PMD-P and S. Note the very small vertical scale (sub-percentage level). Again, the differences between the PPF-derived and the offline-derived correction (blue and red line) are due to the intrinsic accuracies of background correction and fft.

4.8.2.6 Updated key-data set (summary)

During the course of the adjustment procedure described in the previous section, the following set of key-data has been modified, creating version 4 (CAL 1.01; see file headers) from version 3 (CAL 1.00).

Channel overlap	WL_OVERLAP
WLS reference spectrum	RA_WLS_MAIN,RA_WLS_PMD_P,RA_WLS_PMD_S
Radiometric Response	RA_ABS_RAD_MAIN, RA_ABS_RAD_PMD_P RA_ABS_RAD_PMD_S
IR radiometric Response	RA_ABS_IRR_MAIN, RA_ABS_IRR_PMD_P RA_ABS_IRR_PMD_S
IR radiometric Response-using the sun-simulater and BSDF derived data	RA_SUN_CAL_ABS_IRR_MAIN RA_SUN_CAL_ABS_IRR_PMD_P RA_SUN_CAL_ABS_IRR_PMD_S

4.8.3 Verification of Earthshine and validation of solar spectra after adjustment

In this exercise, we verify the impact on the earthshine spectrum using the new CAL 1.01 auxiliary key-data set by both visual inspection and by comparison to the spectrum displayed in Figure 38 (CAL 1.00).

Note: A more quantitative validation will be carried out in Section 4.13.

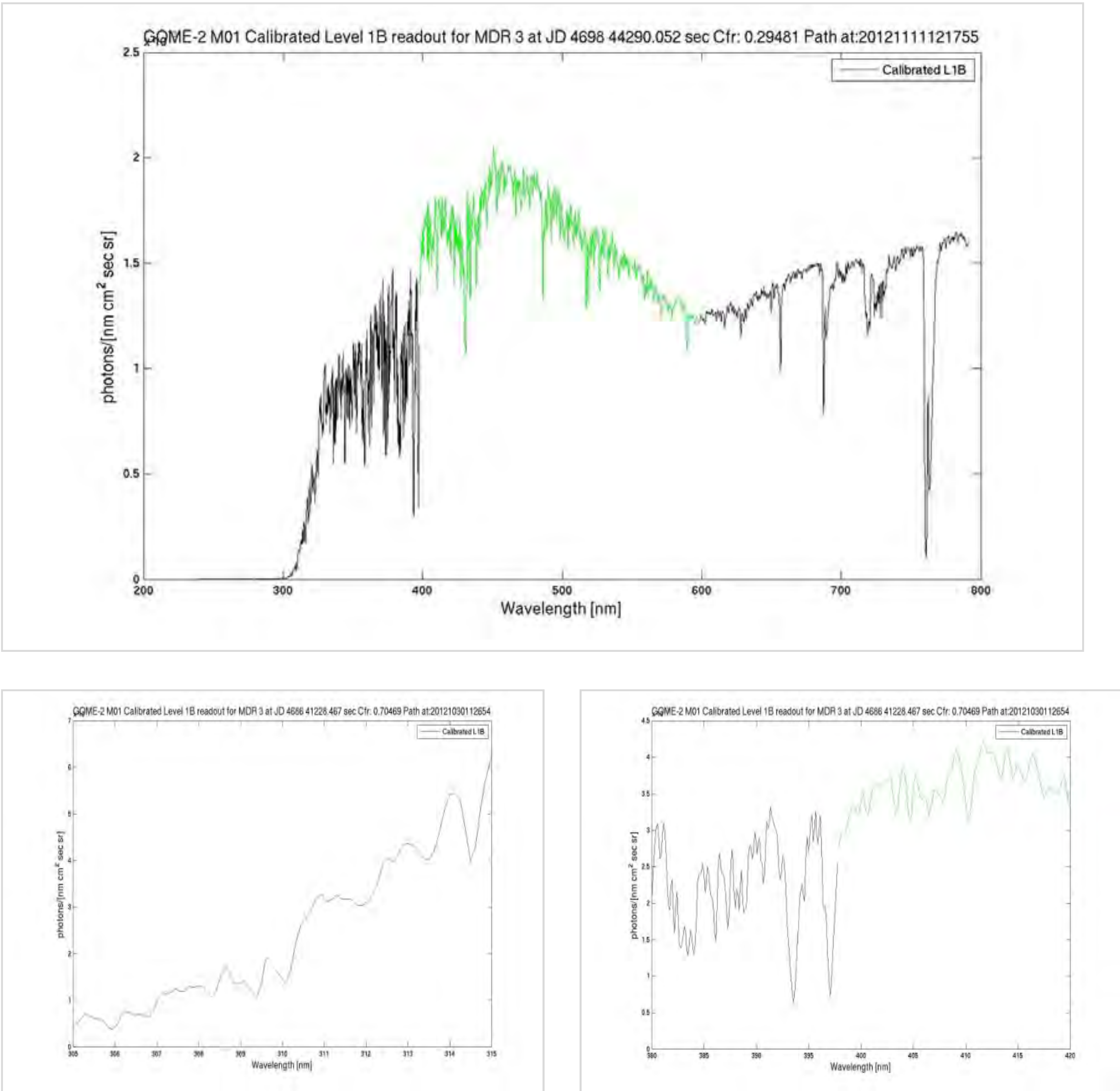

Figure 52: GOME-2 FM2 calibrated Earthshine spectrum (upper panel) with alternating colours for the different bands. The lower two panels show the focus on the channel 1 and 2 (left) and 2 and 3 (right) transitions after using the adjusted key-data set from CAL 1.01.

Figure 52 shows a calibrated level 1B earthshine spectrum taken on 30 October 2012 using the PPF and the updated key-data set CAL 1.01. Now, the focus panel on the two overlap regions show a very smooth transition between the channels. The spectra also do not show any visible etalon-residual effect.

This becomes even clearer when comparing the two spectra of Figure 38 and Figure 53. Since the net result of the etalon adjustments outside the overlap region should be zero, we expect the overlap region correction itself to be the only visible difference in the comparison, within the limits of the accuracies as described in the previous sub-sections. Indeed the residual is around 1 % outside the overlap region and on the order of the applied corrections (Figure 47) inside the overlap regions.

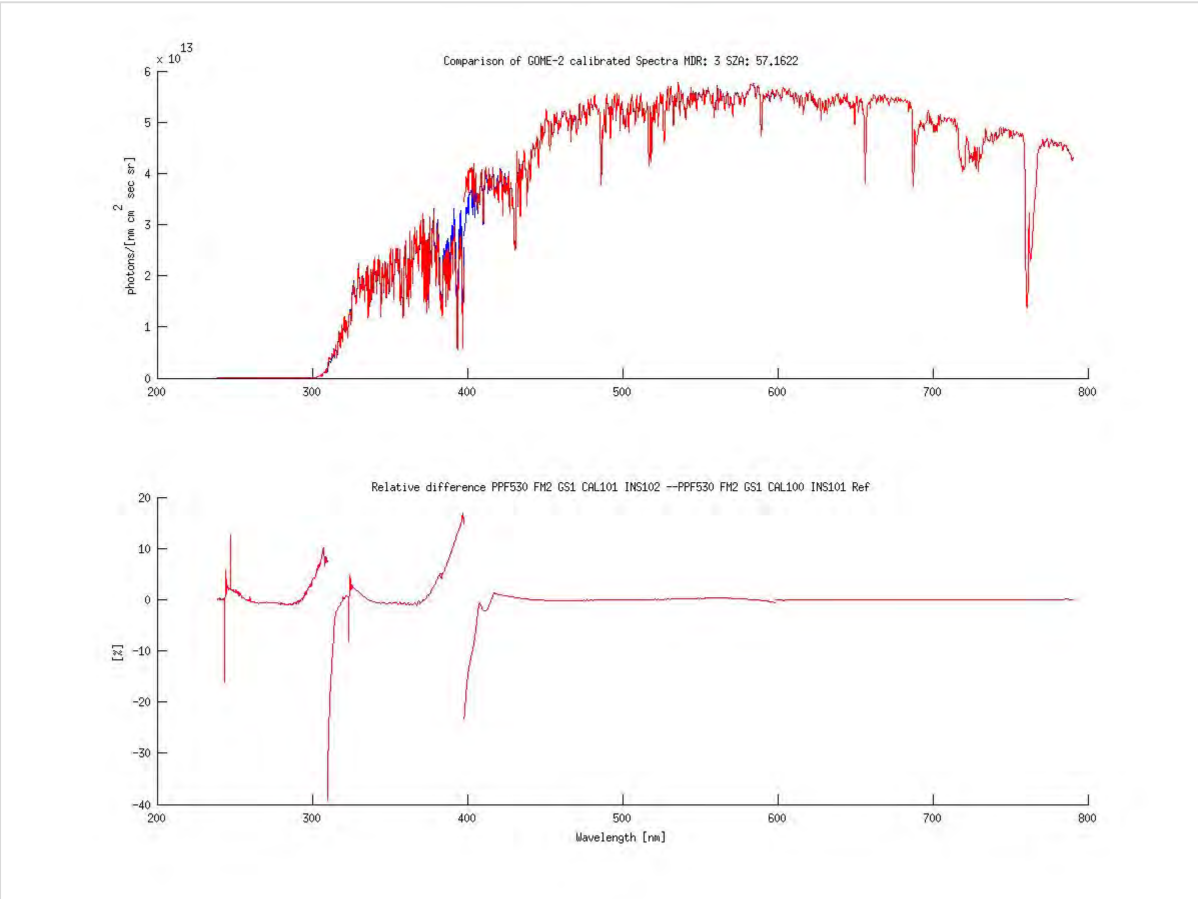

Figure 53: GOME-2 comparison of calibrated Earthshine spectrum of those spectra displayed in Figure 38

and Figure 52 (CAL 1.00/INS1.01 vs. CAL 1.01/INS1.02; upper panel). The lower panel shows the residual in percentage between both spectra.

Figure 54 shows the solar spectrum displayed already in Figure 37, but derived with the CAL 1.01/INS 1.02 setting by the level 0 to 1B processor. This compares to our standard reference spectrum by Dobber et al./KNPO (see previous sections). Indeed, the large residuals in the overlap regions are now gone or significantly reduced when compared to the result in Figure 37, demonstrating that the new approach results in both significantly improved data quality in the overlap region together with the capability of continuous correction of these regions by the derived on-board etalon according to PGS 7.1.

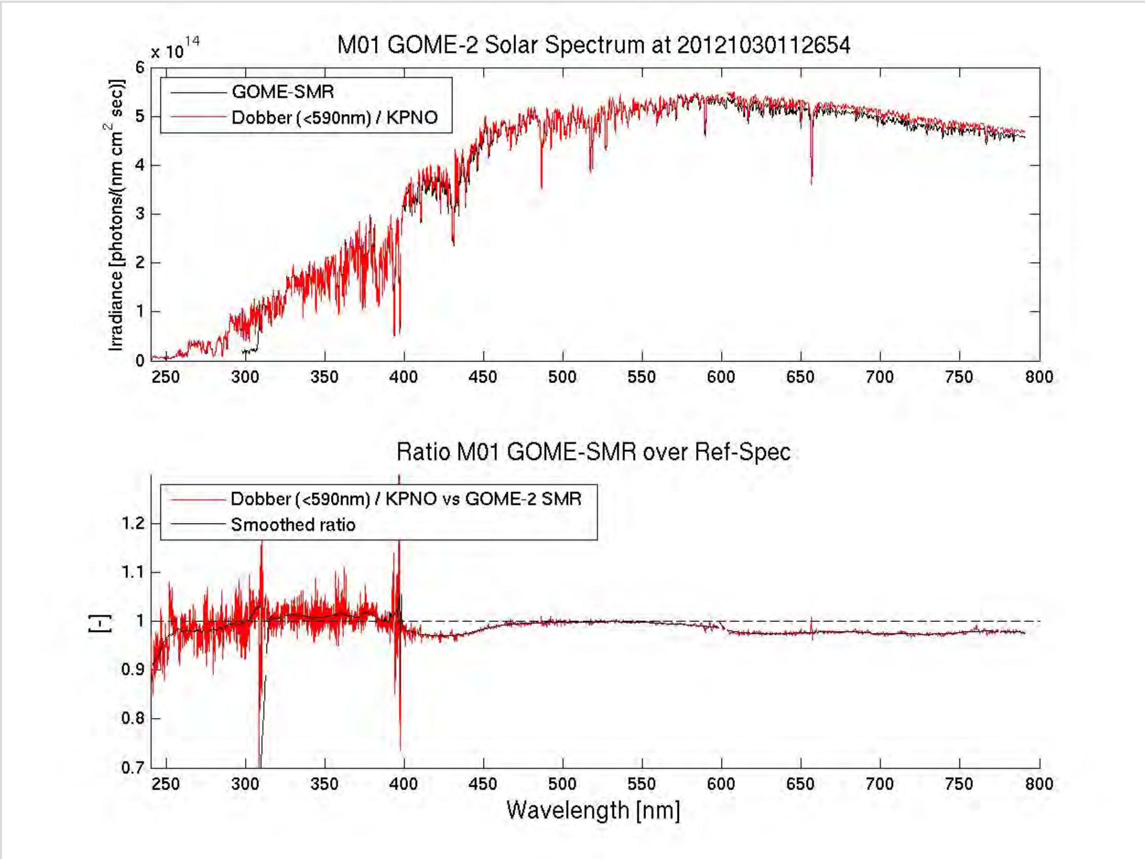

Figure 54: GOME-2 FM2 calibrated solar spectrum (upper panel; black line) compared with a reference spectrum by Dobber et al. (Solar Phys (2008) 249: 281–291) below 590 nm (upper panel, red line). Above 590 nm the KPNO/AFGL spectrum of 2004 is used. The lower panel shows the residual between both (red line) and a moving average to guide the eye.

Finally, we compare also the PMD-P to S ratios for the solar spectra data in Figure 55. This ratio should generally be close to one since the solar irradiance is un-polarised (for details see also [AD 3] on the monitoring of solar stokes fractions). Actually, this ratio has never been close to one for either FM3 on Metop-A or FM2 in the previous processor configuration (See CAL 1.00; left panel Figure 55).

With the etalon-adjusted irradiance response data for PMDs (CAL 1.01; right panel Figure 55) and the resolution of an open AR on the updated of the SUN_CAL_PMD_S irradiance response key-data on 17 December 2012 (AR 14556) the PMD-P to S ratio.

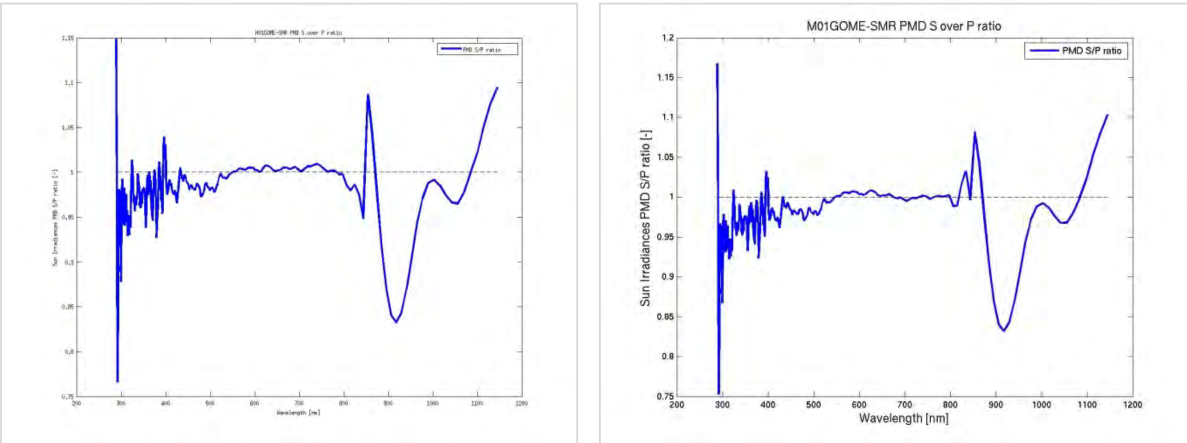

Figure 55: GOME-2 FM2 calibrated solar spectrum PMD S over P ratio. The left panel shows the results corresponding to the original CAL 1.00/ INS 1.01 settings. The right panel shows the results for the new processor and key-data configuration (CAL 1.03 / INS 1.02).

4.9 Key-data “cleaning”

During the on-ground calibration campaign for FM2-2 0 (and also for FM3 and FM1) small-scale structures which could not be fully identified as being either real instrumental spectral structures or artefacts of the on-ground measurements have already been observed in the key-data. During the initial analysis of level 2 retrieval residual spectral structures during the pre-operational commissioning phase, various partners reported on “persistent” spectral structures in the residuals which are also frequently linked to observation geometries (north-south, to the u-Stokes fraction for example; see following Section), and cloud-free pixels. Also, increased residuals at certain scan-angles have been reported, predominantly in channel 3 (see also Section 5.2.2).

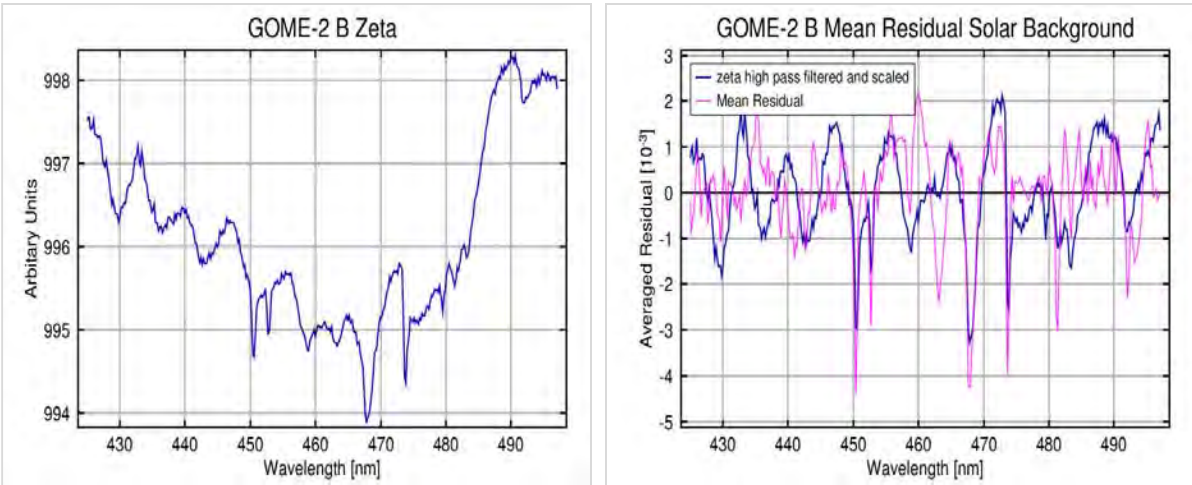

Figure 56: ζ-sensitivityof the instrument to 45 degrees polarised light (left panel). The right panel shows the latter high-pass filtered (smoothed background removed) and compared to a NO_2 fit residual (pink line). Courtesy: IUP Bremen.

Figure 56 shows the sensitivity of the instrument to 45 degree polarised light (ζ-sensitivity) and some of its very sharp spectral features (around 450 nm and 468 nm) appearing in the fit residuals of NO_2. The latter can have a substantial effect not only on the accuracy of the fit but also on the total column amount retrieved. This is shown in Figure 57, in which both results show distinct patterns at a close-to-nadir position.

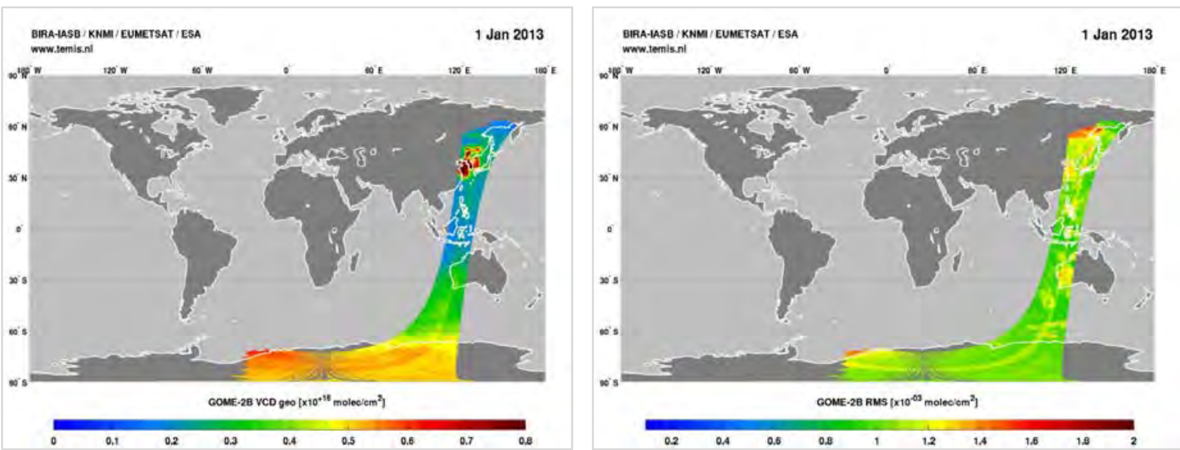

Figure 57: NO_2-total column amount (left panel) and fit-residual (right panel) using reflectivity data from channel 3 between 425 and 497 nm for the calibration key-data version 1.02. Courtesy: BIRA

The key-data provider (TNO) confirmed that the observed residual spike structures may be related to residual absorption line patterns of the Xe-lamp stimulus used during calibration of the instrument. These structures are not are not calibrated out by rationing, probably due to instability of the lamp over one measurement cycle. This is shown in Figure 58**.**

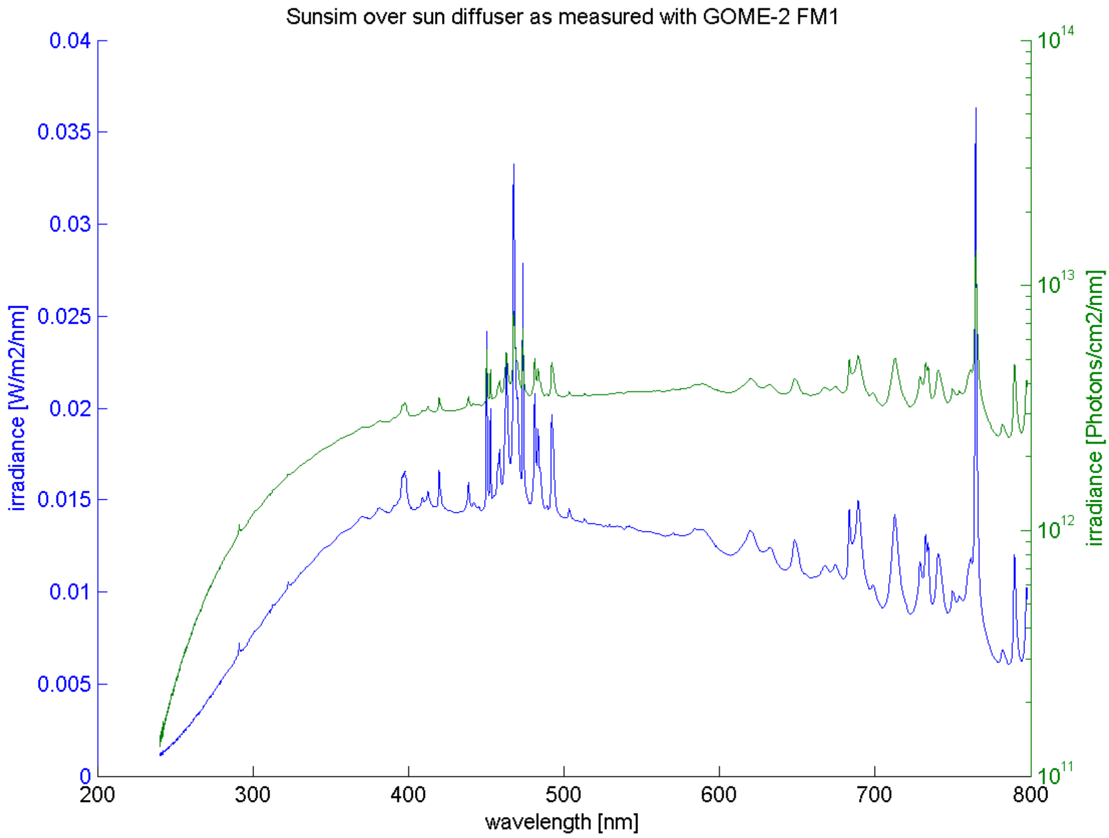

Figure 58: Xe-lamp stimulus spectra as used during the onground calibration campaign for all polarisation key-data related measurments.

While the commissioning of the source with respect to polarisation is done broad-band (and will not provide any evidence for the observed spectral features), the key-data provider considers it very likely that "...these features are indeed introduced by the calibration source". This was stated in an e-mail to TNO/TBD on 19 April 2013. They will therefore potentially affect all key-data measured with this source.

During the on-ground calibration campaign, the suggestion was made to "clean" the key-data using FFT filtering in spectral space. However, up to this point in the analysis presented during this commissioning campaign, there has been no strong evidence that such cleaning would be beneficial for the level-2 retrievals.

4.9.1 Cleaning procedure

The cleaning of key-data is carried out using a FFT type of filtering and follows the scheme specified for Etalon retrievals in the PGS, Section 5.2.18, Algorithm option 1 (A2.16.3.1). The following filter coefficients have been used (see A2.16.3.1 in [AD3]):

[0 0 25 50
0 0 25 50
0 0 25 50
0 0 25 50
0 0 25 50
0 0 25 50],

where the vertical dimension are the channel numbers for which the four coefficients are applied. Figure 59 shows the result for the applied FFT filtering in spectral space for the ζ-sensitivity key-data. Note that the mentioned sharp spectral structures around 450 nm and 468 nm are smoothed out, while the lower frequency structures are untouched.

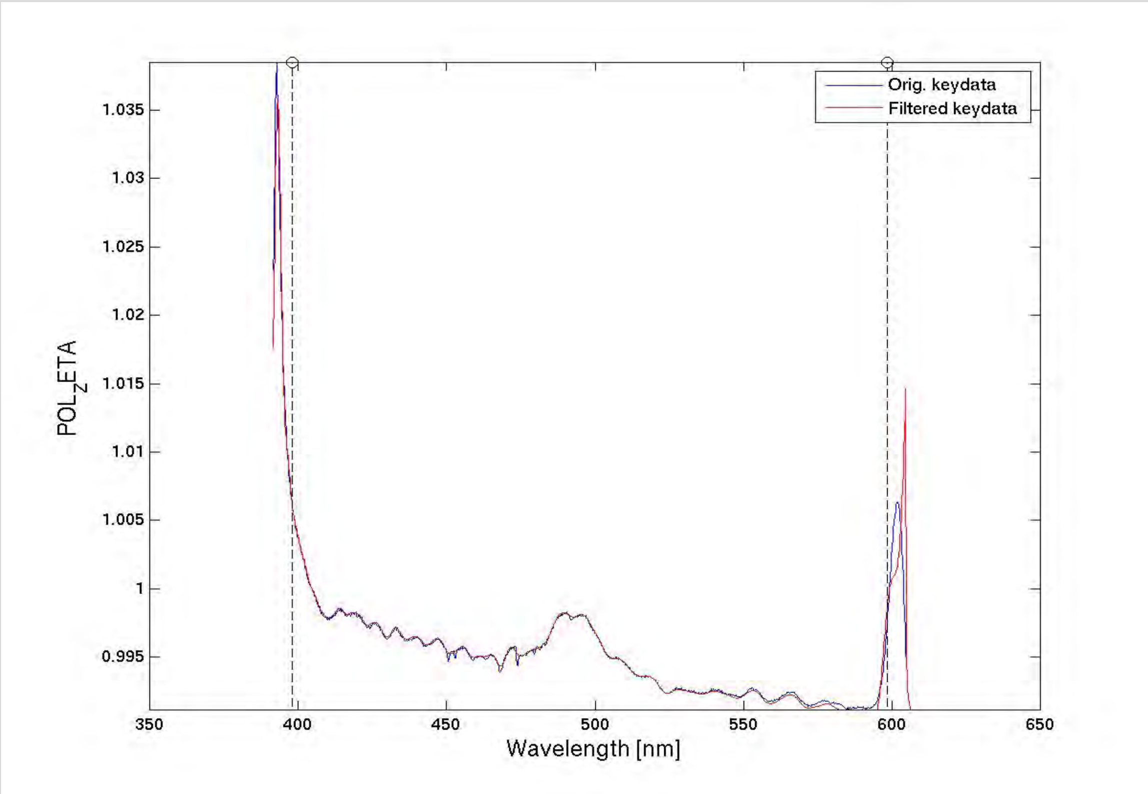

Figure 59: FFT-Filtered ζ-sensitivity key-data spectrum (red-line) as compared to the original data (blue line). Since FFT filtering my introduce artefacts at the boards, the valid key-data region is indicated by the vertical dashed lines.

The results presented in Figure 57 also indicate potential key-data deficiencies in viewing angle direction. Figure 60 shows the angular dependence key-data for ζ, called χ_ζ, for which the original key-data (underlying red lines) show some pronounced outliers in angular dimension (the key-data is measured at 28 reference angles), while one expects the key-data to be smooth in this dimension.

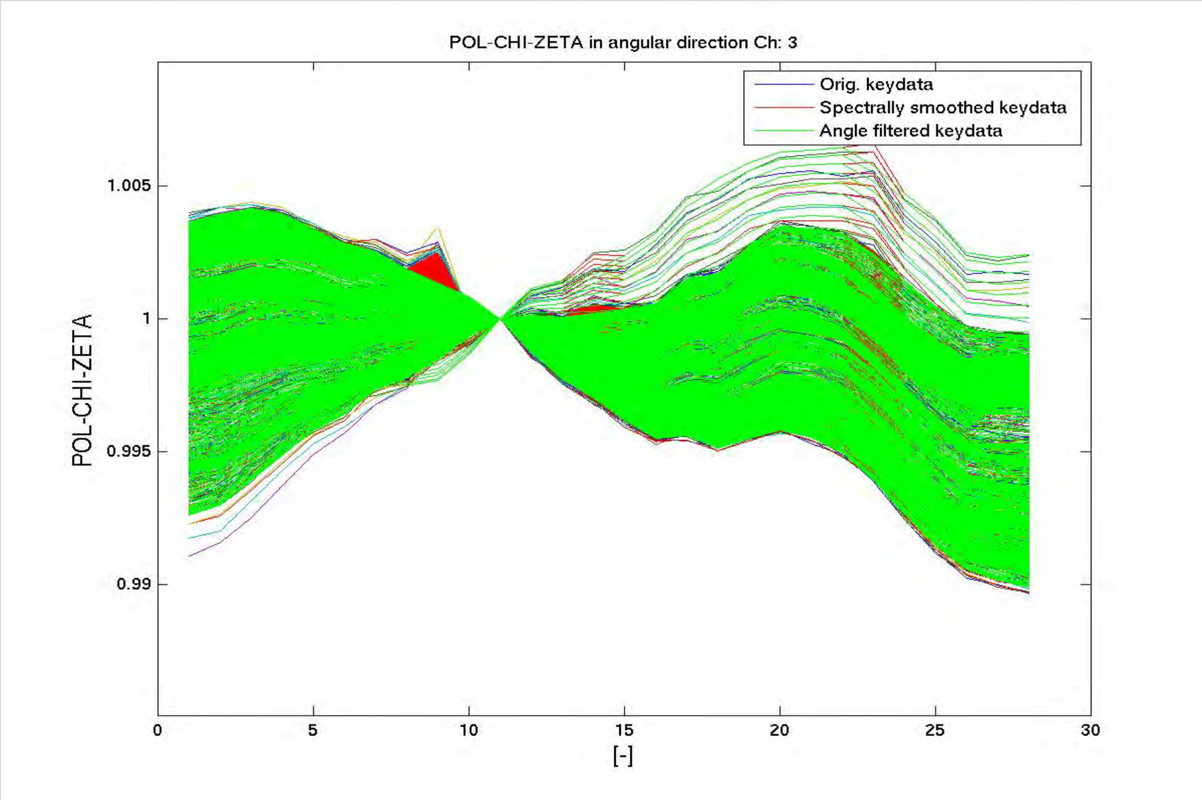

***Figure** 60: Angular dependence of ζ-sensitivity key-data for all wavlentgh (lines) over 28 reference angles .The red and colored lines show the original key-data overlaid by "spline" smoothed keydata in green (for details see body of the text).*

For "cleaning'' of key-data in the angular direction, a simple spline method has been used: identify the outliers manually and spline over these masked angular points. This is shown in Figure 60 for the "cleaned' results–in green.

Both cleaning methods have been applied consistently for all affected key-data in either one (FFT only) or two (FFT and spline) dimensions. This way, the following key-data has been cleaned:

POL_ZETA_PMD_S.202
POL_ZETA_PMD_P.202
POL_ZETA.202
POL_KAPPA_PMD_S.202
POL_KAPPA_PMD_P.202
POL_KAPPA.202
POL_GAMMA.202
POL_CHI_ZETA_PMD_S.202
POL_CHI_ZETA_PMD_P.202
POL_CHI_ZETA.202
POL_CHI_PMD_S.202
POL_CHI_PMD_P.202
POL_BETA.202
POL_ETA.202
BSDF_AIRR_PMD_S.202
BSDF_AIRR_PMD_P.202
BSDF_AIRR.202.

All key-data of this type has been measured using the Xe-lamps. The new set of key-data is comprised in an update key-data auxiliary file version 1.03.

4.9.2 Cleaning results

Figure 61 shows the result for the same level-2 retrievals as shown in Figure 57, but for the updated calibration key-data set version 1.03 for FM2. Notice that the observed residual structure is reduced or has disappeared and the total column retrieval results are smooth over the entire scan.

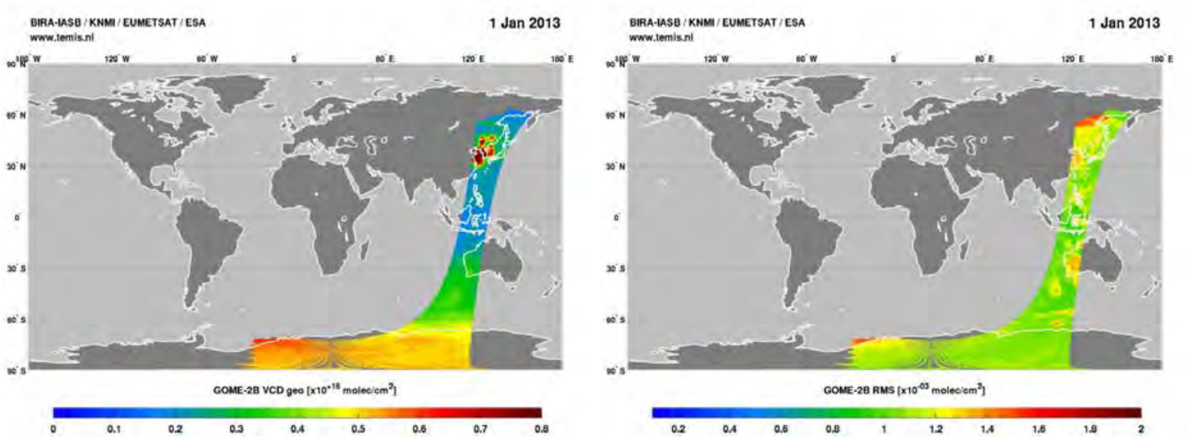

Figure 61: Total column amount (left panel) and fit-residual (right panel) using reflectivity data from channel 3 between 425 nm and 497 nm for the new "cleaned" calibration key-data set version 1.03

Finally, Figure 62 shows the impact on the reflectivity products in the level 1b product when comparing a processed version with the old "uncleaned" calibration key-data set version 1.02 to the new "cleaned" one of version 1.03. The small-scale structure differences are clearly visible, especially in channel 3. There is also some difference in angular domain visible as the result of the spline smoothing in this dimension. Overall, the broad band differences are negligible, as expected.

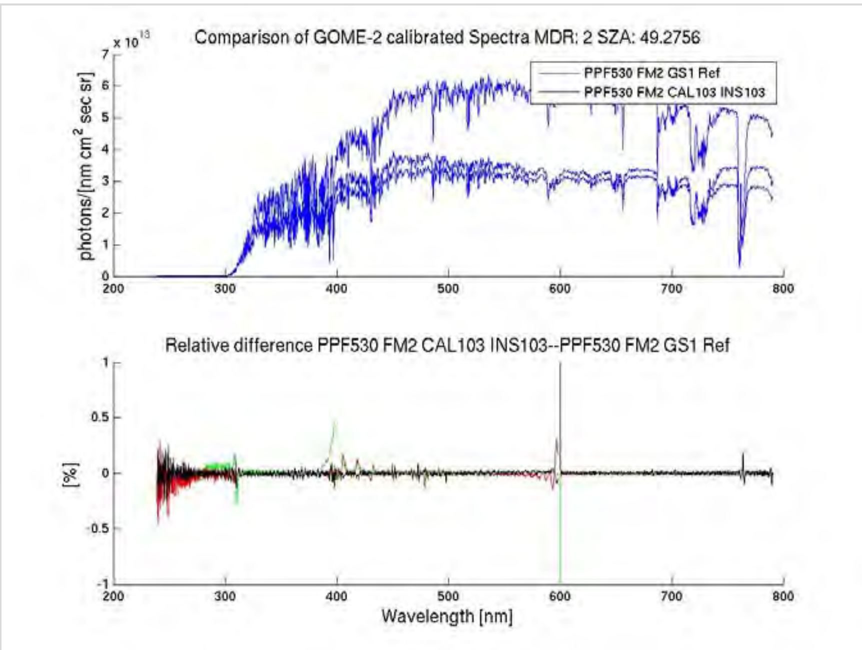

Figure 62: Reflectivity measurments at three different vieing angles (upper panel) and for the unlcleaned key-data set version 1.02 (colored lines) and the cleaned one 1.03 (blue lines) for the new "cleaned" calibration key-data set version 1.03. The lower panle shows the resiudal betwen both key-data sets applied.

4.10 Polarisation correction – Stokes fraction quality (A4.4/A5.3)

The quality of the polarisation correction of main channel data (see [AD 3]) and the quality of the derived Stokes fraction (for direct use, for example, on aerosol optical properties retrievals) is evaluated using the following measures:

- Limiting Atmosphere Method (Earthshine data)
- Stokes fractions for special geometries (Earthshine data)
- Quality flagging on missing and "degraded" Stokes fractions
- PMD S/P ratio for solar measurements
- Stokes fractions derived from solar measurements

The results shown here are derived from one orbit of Metop-B / FM2 (and Metop-A / FM3 for reference) data on 28 November 2012 using the updated auxiliary data set in Section 4.8.2.6. On 27 November 2012, the processor issued a first fully-valid online Stokes fraction correction matrix in CGS1: this to improve the Stokes fraction quality using input from three weeks of collected Stokes fractions from special geometries. For details on the PPF online Stokes fraction correction mechanism see 0. We compare the results to the corresponding operational product from Metop-A / FM3 taken at the same day 48 minutes later, approximately for the same ground track. Figure 63 shows measured and derived q-Stokes and u-Stokes fractions for both Metop-A/B orbits used in the following analysis at PMD spatial resolution. It is important to note that Stokes fractions are very sensitive to surface type and clouds; so significant differences between Metop-A and Metop -B are expected due to this 48-minute separation.

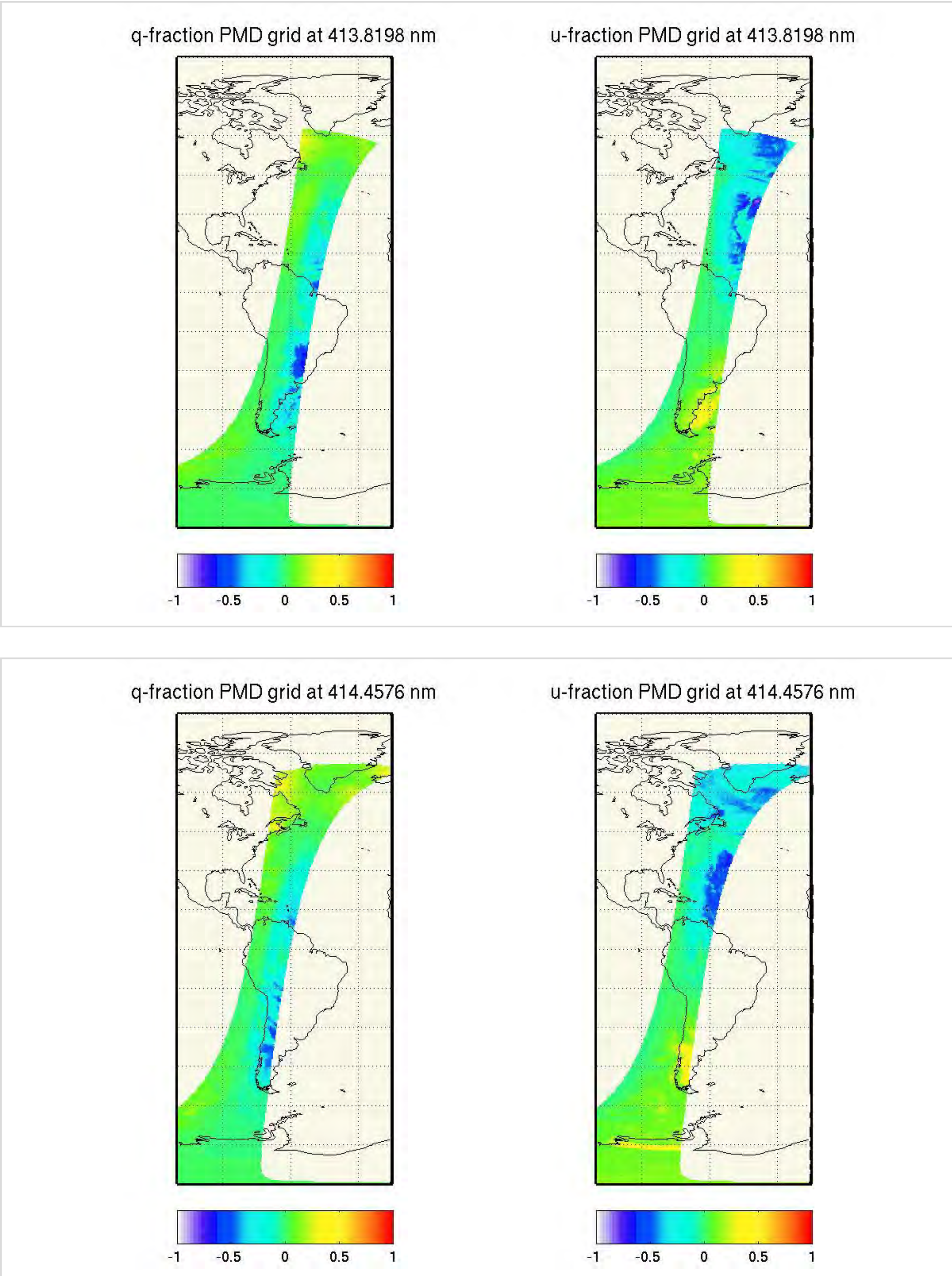

Figure 63: q-Stokes and u-Stokes fractions at PMD spatial resolution for Metop-B / FM2 (upper panels) and Metop-A / FM3 (lower panel) for one orbit on 28 November 2012

4.10.1 Limiting Atmosphere Method

To monitor and validate the measured GOME-2 Stokes fractions under all viewing conditions a general approach is used–the “Limiting-Atmosphere“ approach. This approach is based on a statistical analysis developed by SRON under contract to ESA. It can be shown that the general behaviour of the Stokes fraction, *q*, along the orbit is primarily determined by molecular (Rayleigh) scattering, in particular over dark ocean surfaces, and that variability in *q* is caused by the presence of clouds and aerosols. It has been observed that the measured polarisation values are always clearly between extreme limiting values. These limiting values lie between the Rayleigh single scattering values and $q = 0$. Furthermore, for a large number of measurements, the measured polarisation values are influenced by largely cloudy scenes, which depolarise the light leading to a measured Stokes fraction of $q = 0$. The assumption upon which the generalised validation of *q* is based is that the minimum Stokes fractions observed are representative of a *limiting atmosphere* with minimum depolarisation–a combination of minimum ground-albedo and minimum aerosol loading. In the case of little or no instrument degradation, these limiting values will be constant in time and can be used as an empirical validation method for the both short-term and long-term in-flight monitoring of polarisation measurements. Figure 64 shows Stokes fractions calculated from earthshine scanning measurements with respect to the single scattering Stokes fractions (the diagonal line) and $q = 0$. Red points lie *inside* the physically reasonable range while blue points lie *outside* the physically reasonable range. The plots show two time periods, one three-minute period (upper panels) and one full day-side orbit period (lower panels) for both instruments: FM2 in the left panels, FM3 in the right panels.

The results shown in Figure 64 clearly demonstrate that Metop-B / FM2 results are already of equal quality to those for the current Metop-A / FM3 products.

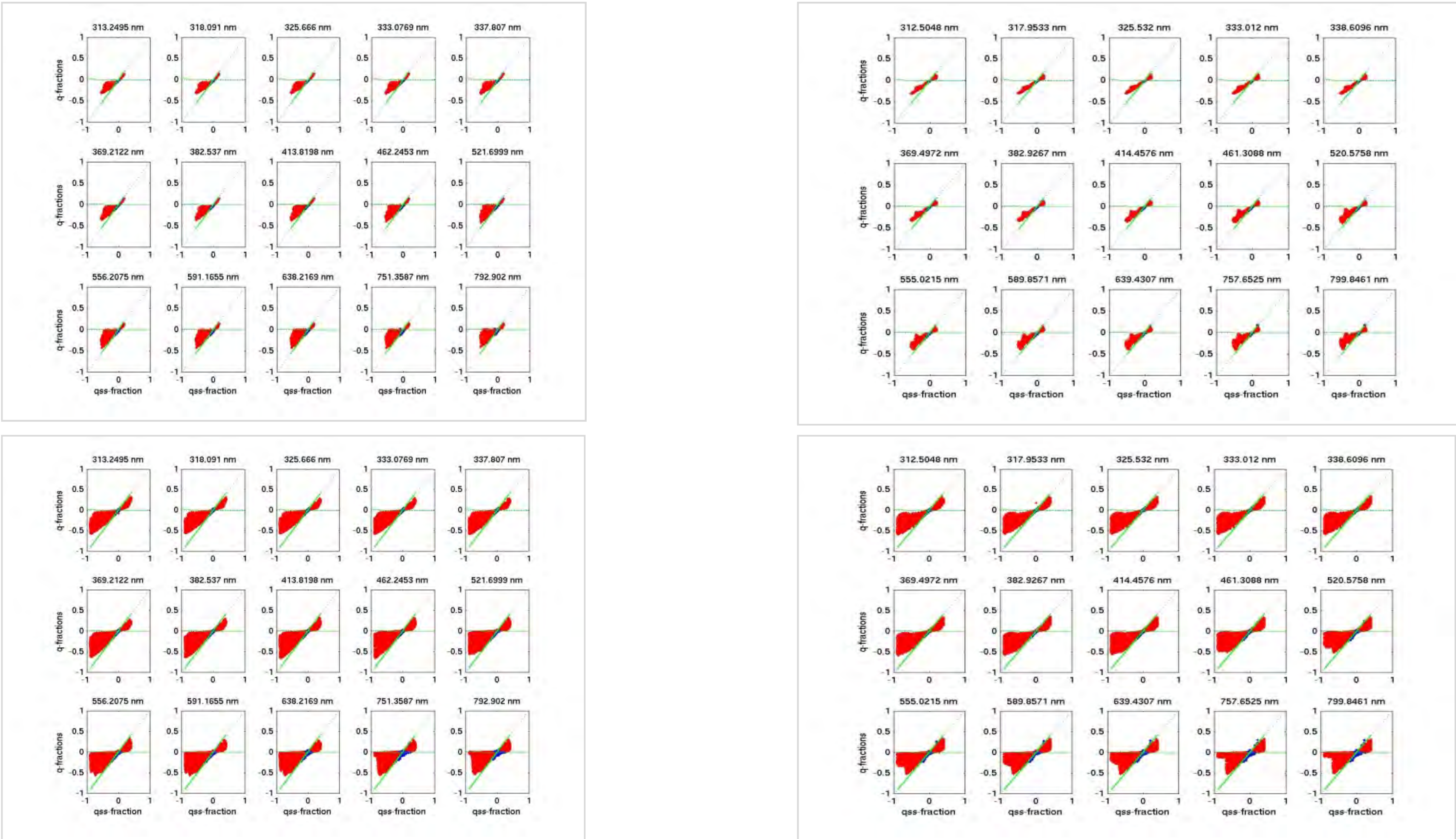

Figure 64: The plots show two time periods of one 3 minute period (upper panels) and one full day-side orbit period (lower panels) for both instruments (FM2 left panels, FM3 right panels) on 28 November 2012. Red plots are inside the required limiting atmosphere limits and blue plots are outside the required limiting atmosphere limits.

Figure 65 shows the location of those Stokes fractions which are either missing due to low PMD signal levels (below 5 BU above noise) or are flagged as “bad” because they lie outside the limiting atmosphere criteria (blue plots in lower panels in **Error! Reference source not found.**). Bad Stokes ractions are usually found in the vicinity of the area where the Stokes q-fraction approaches zero (see upper left plot), which we previously have tagged as the “c-shape” area” in which a special treatment of the “singularity”-issue for calculation of Stokes fractions is applied (see [AD 3]) and where also the “limiting-atmosphere criterion approaches a singularity. Some “bad” Stokes fractions can be expected within the “c-shape” area, but none are expected outside this area.

The results in Figure 65 show there are no bad Stokes fractions for the investigated orbit outside the “c-shape” area for Metop-B / FM2 processing. The total number of bad Stokes fractions per day approaches 23,000 and approx 13,500 are set to missing. See the summary page for daily reports on gome.eumetsat.int. The corresponding figures for Metop-A / FM3 are about 20,000 and 14,500 (status in November 2012), with the larger amount of missing Stokes fractions for FM3 being due to instrument throughput degradation. For FM2, the “bad” Stokes fraction value was 27,000 before the update of the online correction matrix on 27 November 2012. Further improvements can be expected by additional statistical data acquired over time. However, the remaining differences may be due to slightly worse performance in the comparison of Stokes fractions for special geometries for FM2 with respect to FM3.

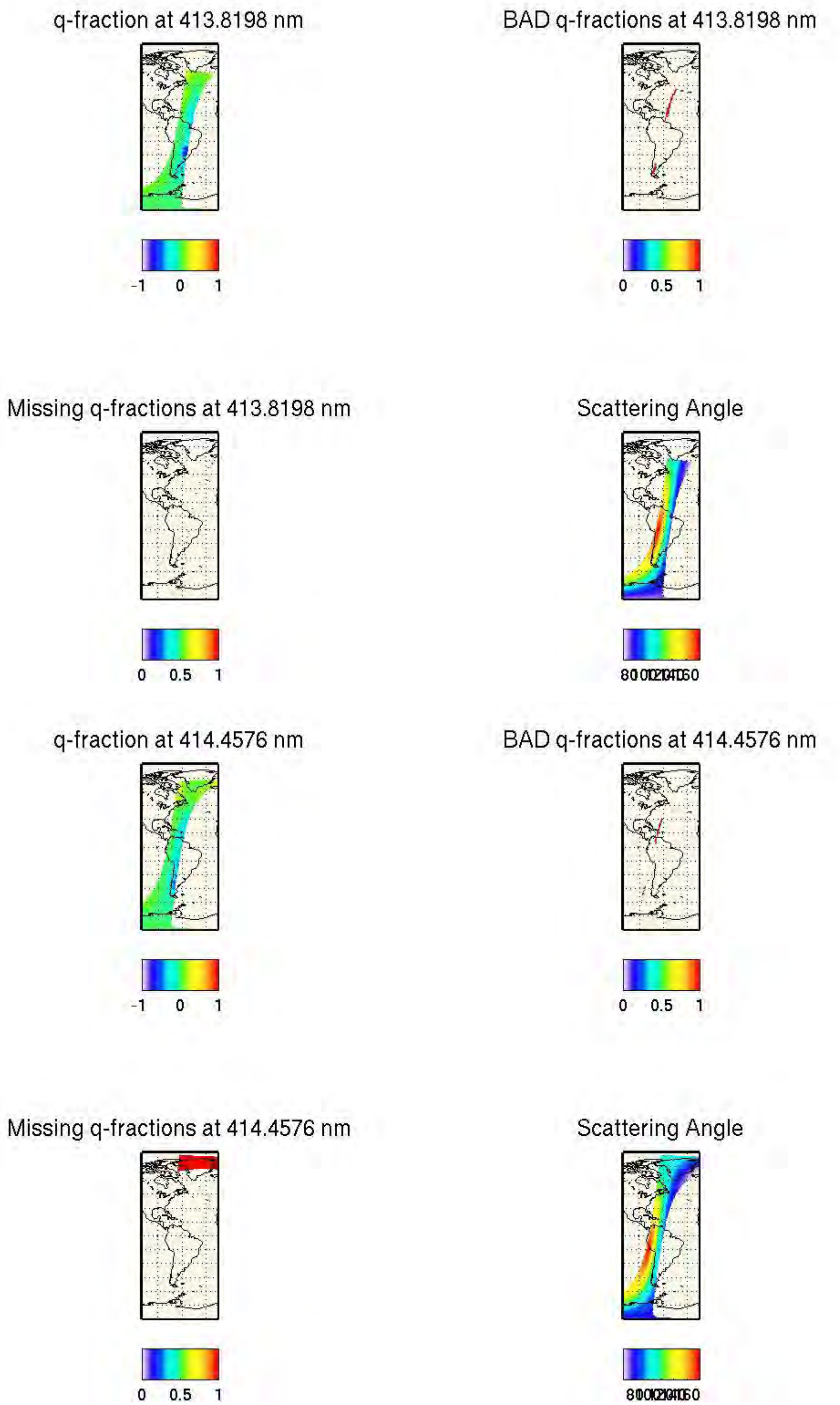

Figure 65: The upper four panels show q-Stokes fractions, "bad" Stokes fractions, missing Stokes fractions and the corresponding scatter angle for Metop-B / FM2. The lower four panel show the same but for Metop-A / FM3.

4.10.2 Stokes fractions for special geometries

The Stokes fraction q depends on the degree of linear polarisation P and the polarisation angle with respect to the reference plane χ in the form $q = P \cdot \cos 2\chi$. Assuming that the polarisation angle at all wavelengths is similar to its single scattering value, χ_{ss}, then q = 0 when $\cos(2\chi_{ss}) = 0$ independent of the degree of linear polarisation, P, and regardless of the actual atmospheric scene observed. Therefore, specific locations can be found, taking into account the illumination geometry, where the Stokes fraction q of the light reflected by the earth's atmosphere is exactly zero. Any systematic deviations from zero in spectral and viewing angle space may then be attributed to deficiencies in the calibration. This approach is also used for the online correction of Stokes fractions, which has been already applied to the results presented in the following using the most recent correction acquired by the operational processor.

The panels that follow show the results for those special geometries cases 28 November 2012 for special geometries acquired over one full orbit (Figure 66 and Figure 67).

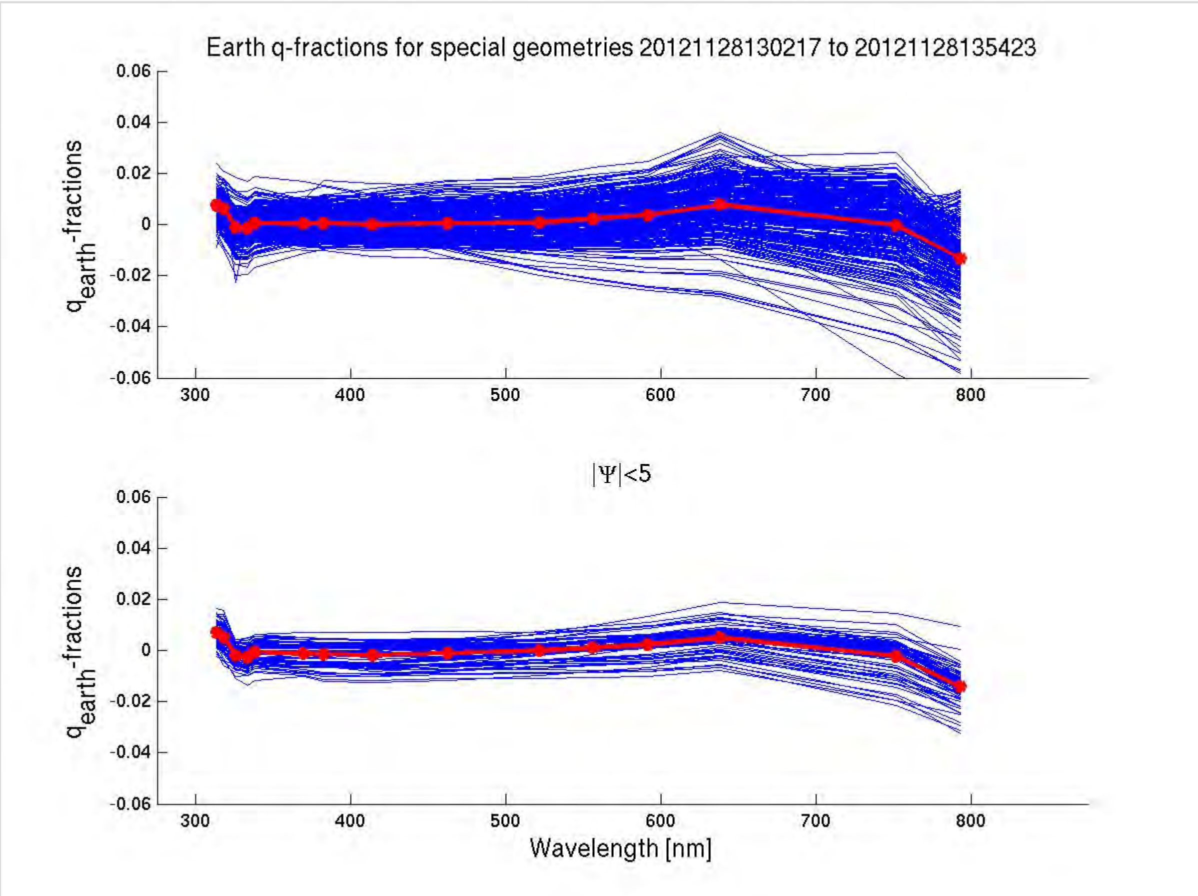

Figure 66: The plots show q-Stokes fractions for special geometries over the full Metop-B / FM2 orbit. The red line is the average over the orbit. The upper panel shows all derived special geometry Stokes fractions. The lower shows only those restricted to a viewing angle of +/-5 degrees.

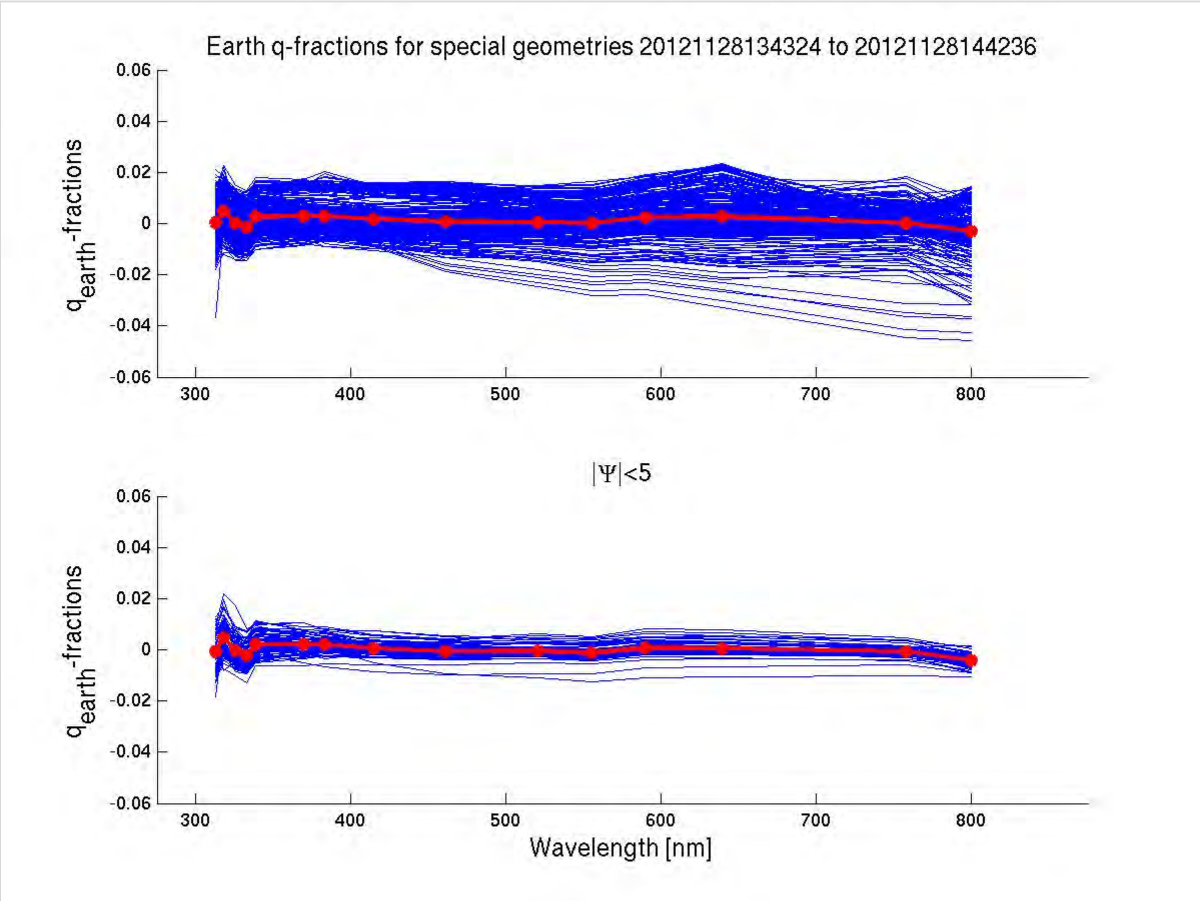

Figure 67: The plots show q-Stokes fractions for special geometries over the full Metop-A / FM3 orbit. The red line is the average over the orbit. The upper panel shows all derived special geometry Stokes fractions. The lower shows only those restricted to a viewing angle of +/-5 degrees.

The results in Figure 68 indicate that Metop-B / FM2 Stokes fractions are already, and on average, of very good quality (comparable to Metop-A / FM3) following the applied online correction. They show a slightly worse performance in the NIR than is the case for Metop-A / FM3.

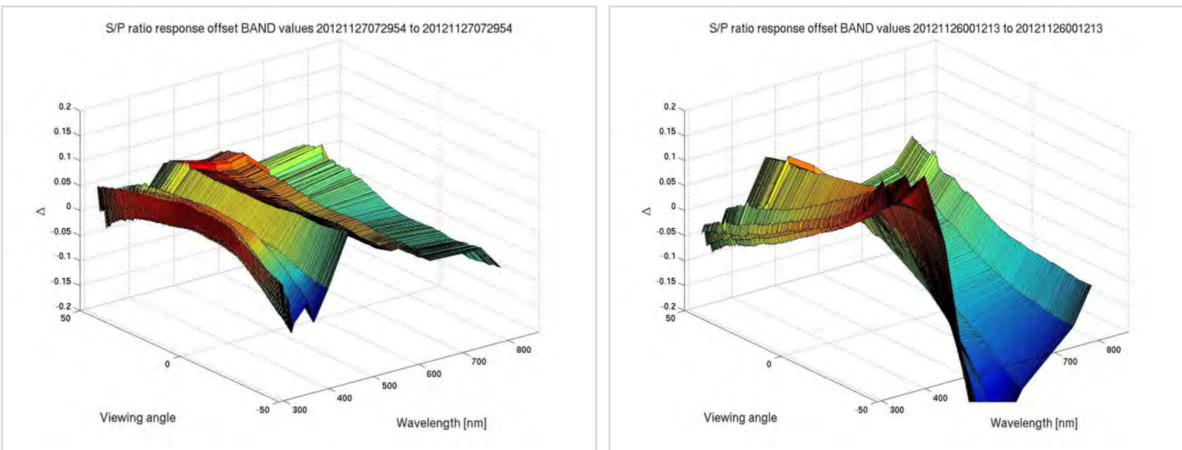

Figure 68: Online -derived PMD S over P correction surface for Metop-B / FM2 (left panel; 27 Nov 2012) and for Metop-A / FM3 (right panel, 26 Nov 2012).

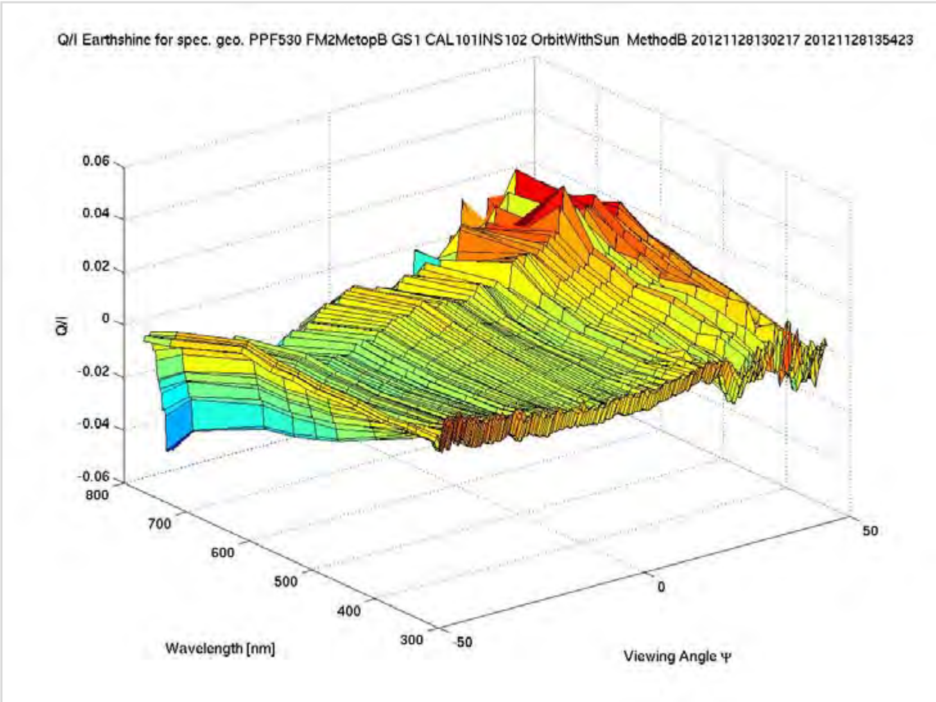

Figure 69: Averaged q-Stokes fractions for special geometry in dependence of wavelength and viewing angle and for one orbit of Metop-B / FM2 data.

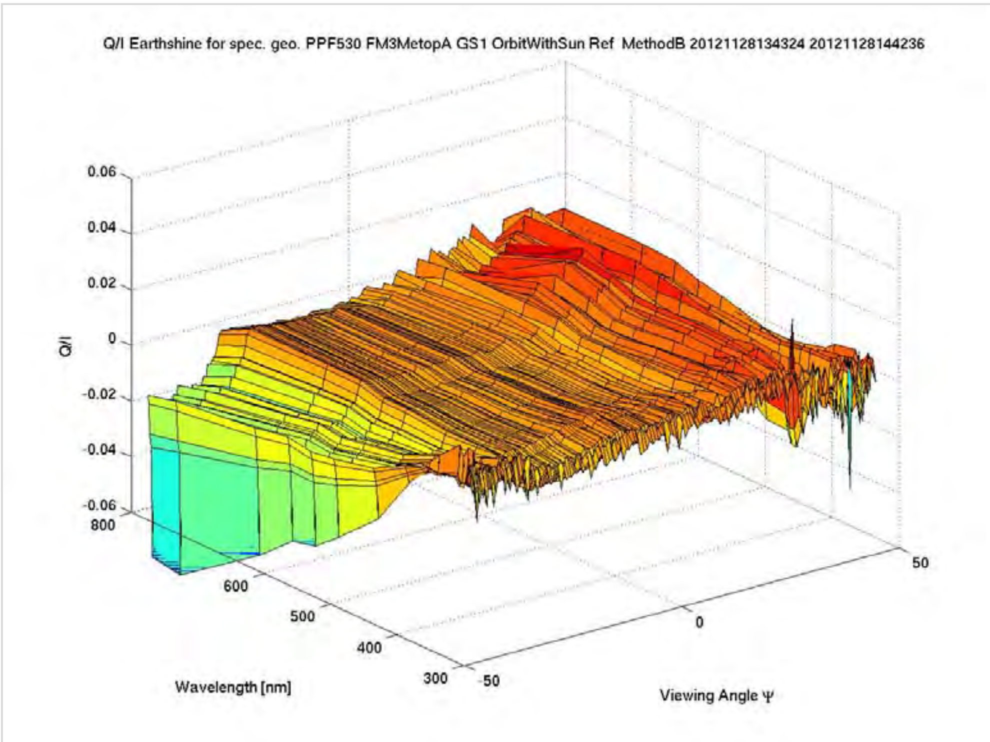

Figure 70: Averaged q-Stokes fractions for special geometry in dependence of wavelength and viewing angle and for one orbit of Metop-A / FM3 data.

Figure 69 and Figure 70 show that the origin of the deviation in the NIR comes predominantly from the most negative viewing angles. However, for Metop-B / FM2, the NIR performs worse than for Metop-A / FM3 over the whole NIR viewing angle region, even though (or because) the online derived *S over P* correction surface is much larger than for Metop-B / FM2–due to differential degradation effects between the two PMD channels. See Figure 68.

4.10.3 Earthshine Stokes fractions as compared to V-LIDORT model results

We compare Stokes fractions as measured by Metop-B / FM2 and Metop-A / FM3 within two target areas: Pacific and Sahara. For a precise definition of these areas, see Figure 83 and to the output of a vector radiative transfer model V-LIDORT version 2.5 [RD21] fed by 6 hourly ECMWF forecast model profiles in temperature , water vapour, ozone, and humidity.

This installation of V-LIDORT 2.5 uses a GOME-1-derived lowest equivalent reflection Albedo database by Koelemijer et al. [RD18], over ocean and a MERIS-based Albedo database over land surfaces (see the references in [RD19]). The model includes a Mie scattering code with bi-model phase scattering distribution functions and uses standard atmosphere LOWTRAN aerosol optical properties, which are confined to a selection of extinction coefficients, single scattering albedo, and asymmetry parameters defined for 6 wavelengths covering the GOME-2 range, and for a selection of mixed types: rural continental, maritime, background stratospheric. [RD21].

Figure 71 and Figure 72 show scatter plots of GOME-2 FM2 and FM3 measured Stokes fractions for the Pacific and Sahara target region as compared to the model Stokes fraction output for all available wavelength (310 nm – 800 nm). Different viewing geometries are encoded in different colours. Note, however, that due to the time difference and the cloud screening, as well as the differences in ground track of the two instruments, they do not necessarily observe all the same viewing geometries. Generally, agreement is very good and the observed patterns in the scatter plots are quite similar for both instruments, especially in cases of reasonably stable atmospheric conditions between the two passes.

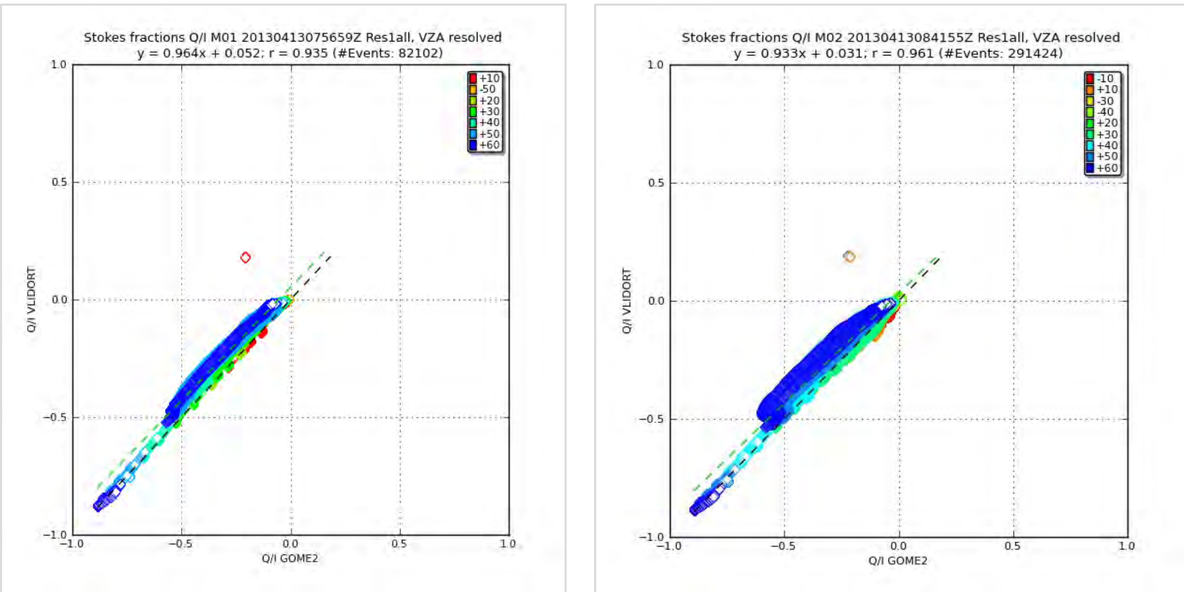

Figure 71: Metop-B / FM2 (left panel) and Metop-A / FM3 data (right panel) measured Stokes fraction (x-axis) derived for 10 January over the Sahara target area (see Figure 83) and compared with V-LIDORT 2.5 model Stokes fraction (y-axis) using 6 hourly ECMWF forecast data in ozone temperature and humidity. The scatter plot cover Stokes fractions in the region between 310 nm and 800 nm. Different colors inidcate different viewing geometries. Note that per instrument different viewing angle might be covered because of the temporal and ground track diffwerences

A much larger range of Stokes fraction values is observed for the Sahara, based on surface type and scattering conditions (single-scattering high polarisation decreasing towards increasing numbers of scattering). In contrast, the Pacific generally sees lesser degrees of scattering because the surface has a depolarising effect, depending on its roughness. This roughness depends in turn on wind speed, which is not taken into account by the model. By default, the model considers the surface scattered light to be completely depolarised. Therefore, the model has a tendency to underestimate the degree of polarisation as seen in Figure 72. Apart from a very few outliers, there are no Stokes fractions in the “forbidden” zone, save for the “Limiting-Atmospheres”, observed.

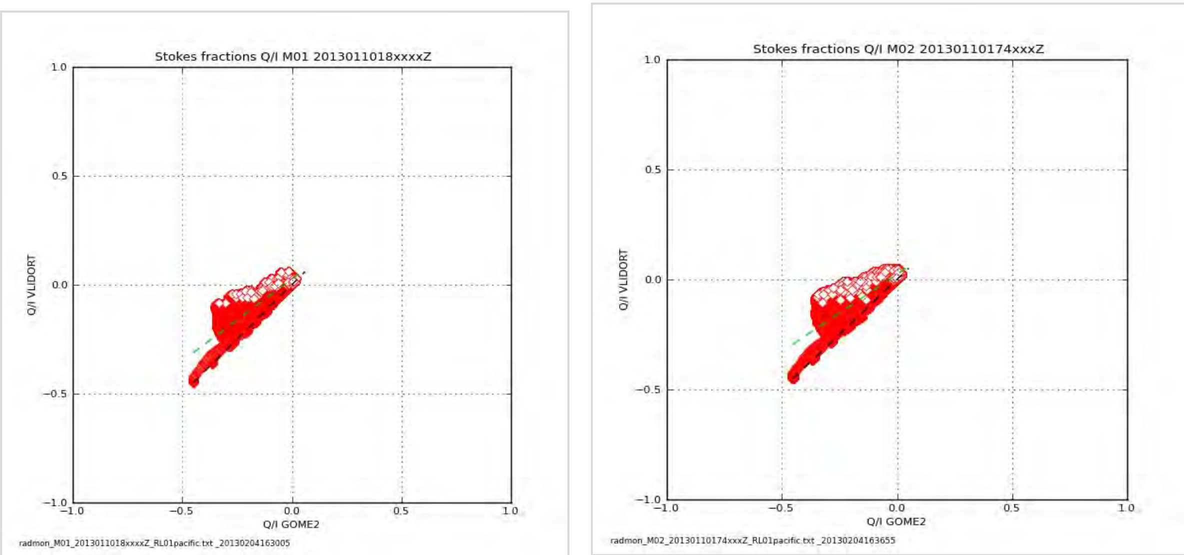

Figure 72: Metop-B / FM2 (left panel) and Metop-A / FM3 data (right panel) measured Stokes fraction (x-axis) derived for 10 January over the Pacific target area (see Figure 83) and compared with V-LIDORT 2.5 model Stokes fraction (y-axis) using 6 hourly ECMWF forecast data in ozone temperature and humidity. (See also Figure 83.).

4.10.4 PMD S over P ratio from Solar Measurements

The S over P ration from measurements of the solar spectrum using the PMDs is a measure of the calibration accuracy and quality of the individual PMD irradiance spectra. In the most optimal situation the ratio should be one, since the calibration of the radiometric response key-data for PMDs provides and end-to end calibration of the polarisation sensitivity of the optical path from the sun-port to the PMD detectors (involving the calibration unit; see Figure 3) and the solar irradiance is un-polarised. For Metop-A / FM3 it has however been observed that the ratio was never really one and always exhibited a persistent spectral pattern as shown in the example provided in Figure 73.

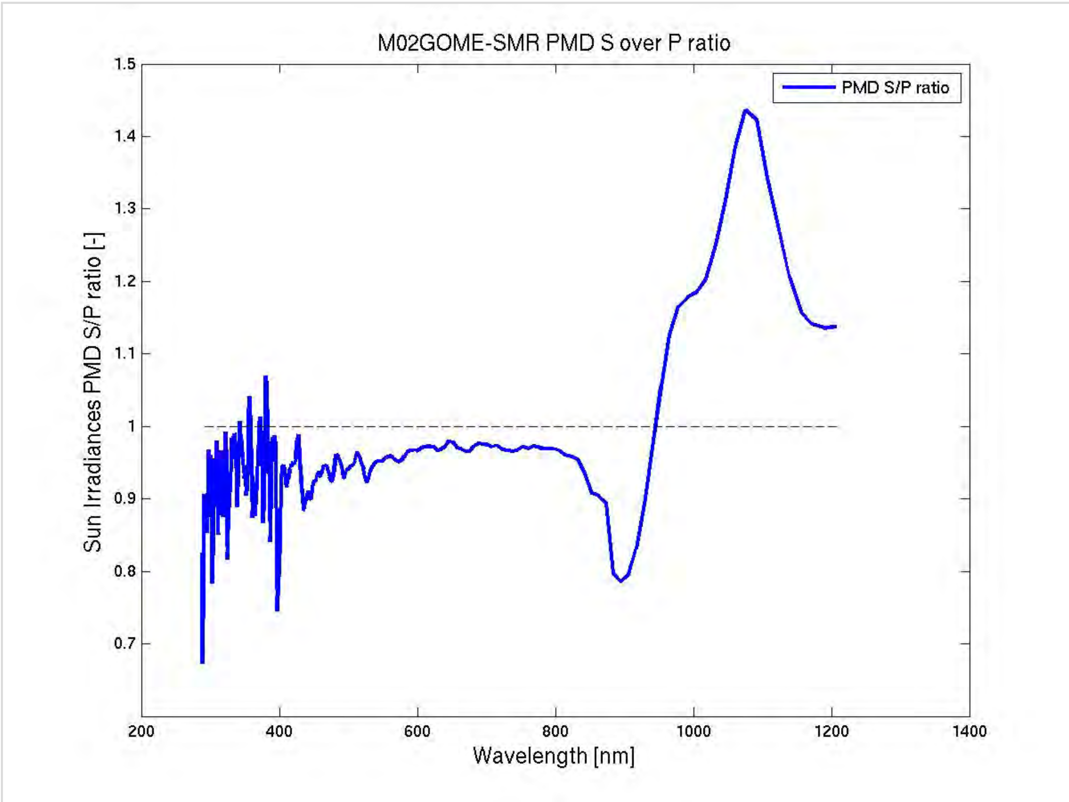

Figure 73: Metop-A/FM3 PMD S over P ratio from the solra mean reference data.

Figure 74 shows the same ratio but for Metop-B / FM2 after an issue with the IR radiometric response data for PMD-s has been solved with calibration key-data file version 1.03 (see also Section 4.8.3).

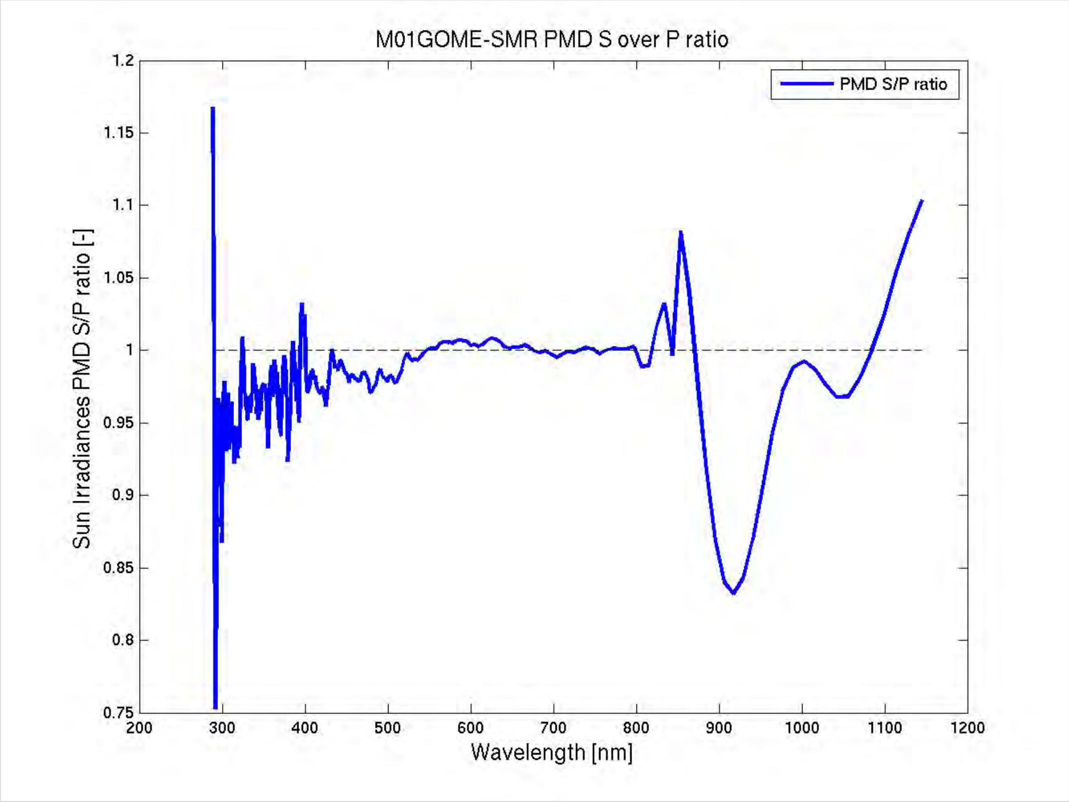

Figure 74: Metop-B/FM2 PMD S over P ratio from the solar mean reference data.

Generally, a comparison of Figure 73 and Figure 74 shows that the calibration of the irradiances from PMD measurements is better for Metop-B / FM2 than for Metop-A / FM3. The spectral fine structure below 400 nm in both results might be due to top errors in the spectral co-registration between both measurements. Note also that the calibration key-data is not valid for a wavelength higher than 800 nm, and therefore no Etalon correction is applied in this region.

4.10.5 Q-Stokes fractions derived from solar measurements

From the S over P ratio from solar measurements Stokes fraction values can be derived applying different key-data (see PGS 7.1, Section 5.2.23, Eq. 176, [AD 3]) like the relative radiometric response of S and P as well as all key-data involved in the calculation of the Mueller Matrix elements 2 and 3 (see PGS 7.1, Section 5.2.3, [AD 3]). Ideally, the solar Stokes fractions should be close to 0. However, due to residual polarisation introduced by the optics in the calibration unit, some remaining offset from 0 structures are expected. This is in contrast to the P to S ratio, for which the end-to-end calibration should take out any residual polarisation effect. In its current formulation in PGS 7, the derived Stokes fractions for solar measurements mostly used in order to monitor any long-term changes in this residual polarisation, which would invalidate the on-ground end-to-end IR radiometric calibration of the PMDs.

Figure 75 shows the derived Stokes fractions from solar measurements using three different formulations of the Sun-Stokes fraction equation. The nominal equation is provided in PGS 7, Eq. 176 AD 3 and is shown as an average over the individual measurements (red line). The other two curves are calculated by using uncorrected M1s/M1p MME key-data (see [AD 3]) for which the online correction for Stokes fractions has not been applied. The other one is using the previous formulation as provided in PGS 6.1, Eq. 229, which uses the MMEs from the end-to end solar irradiance calibration measurements.

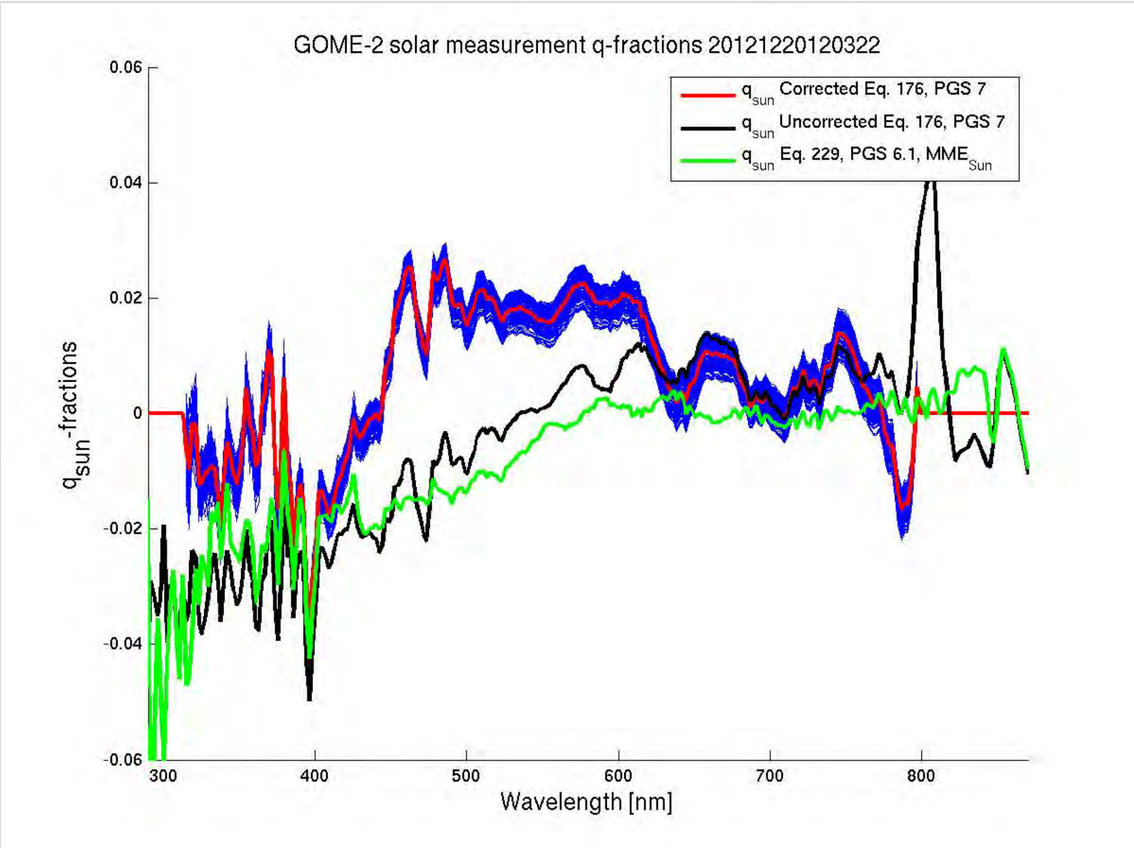

Figure 75: Metop-B/FM2 solar Stokes fraction data from individual measurments (blue line) and their average (red line) applying the definition as provided in PGS 7, Eq. 176 using the corrected M1s/M1p MME ratio.The other tow curves show the average Stokes fractions but using the uncorrected M1s/M1p MME ratio (black line) and the definition has usedpreviously in PGS 6.1 Eq. 229.

Overall, the Stokes fractions are close to 0 but also show some spectral structures and an offset in the region where the P to S ratio is essentially 0. This offset is ascribed to the residual polarisation introduced by the calibration unit and needs to be monitored over time. Similar offsets and structures have also been observed for Metop-A / FM3 data. See daily reports on Solar Stokes fractions on http://gome.eumetsat.int for both instruments).

4.11 Summary of Level 0 to 1B Calibration Steps

In this section we summarise all the most important calibration spectra applied by the level 0 to 1B processing for Metop-B / FM2 on 28 November 2012. For reference, we also provide the same for Metop-A / FM3. Note the most prominent difference is the small Etalon correction applied for Metop-B / FM2 after the overlap and the Etalon adjustment as laid out in Section 4.8 with the introduction of the CAL 1.01 and INS 1.02 auxiliary files.

Figure 76: GOME-2 Metop-B / FM2 calibration spectra for the level 0 to 1b processing of one spectra taken on 28 November 2012. Band 1a, 1b, 2b, 3 and 4 are displayed in the columns from left to right. Band 2a is ommited because all detector pixel of this band fall outside the valid region.

1st row: Raw level 0 signals.

2nd row: Dark signal offset.

3rd row: Pixel-toPixel gain

4th row: Difference between the in-fligth and the on-ground spectral calibration.

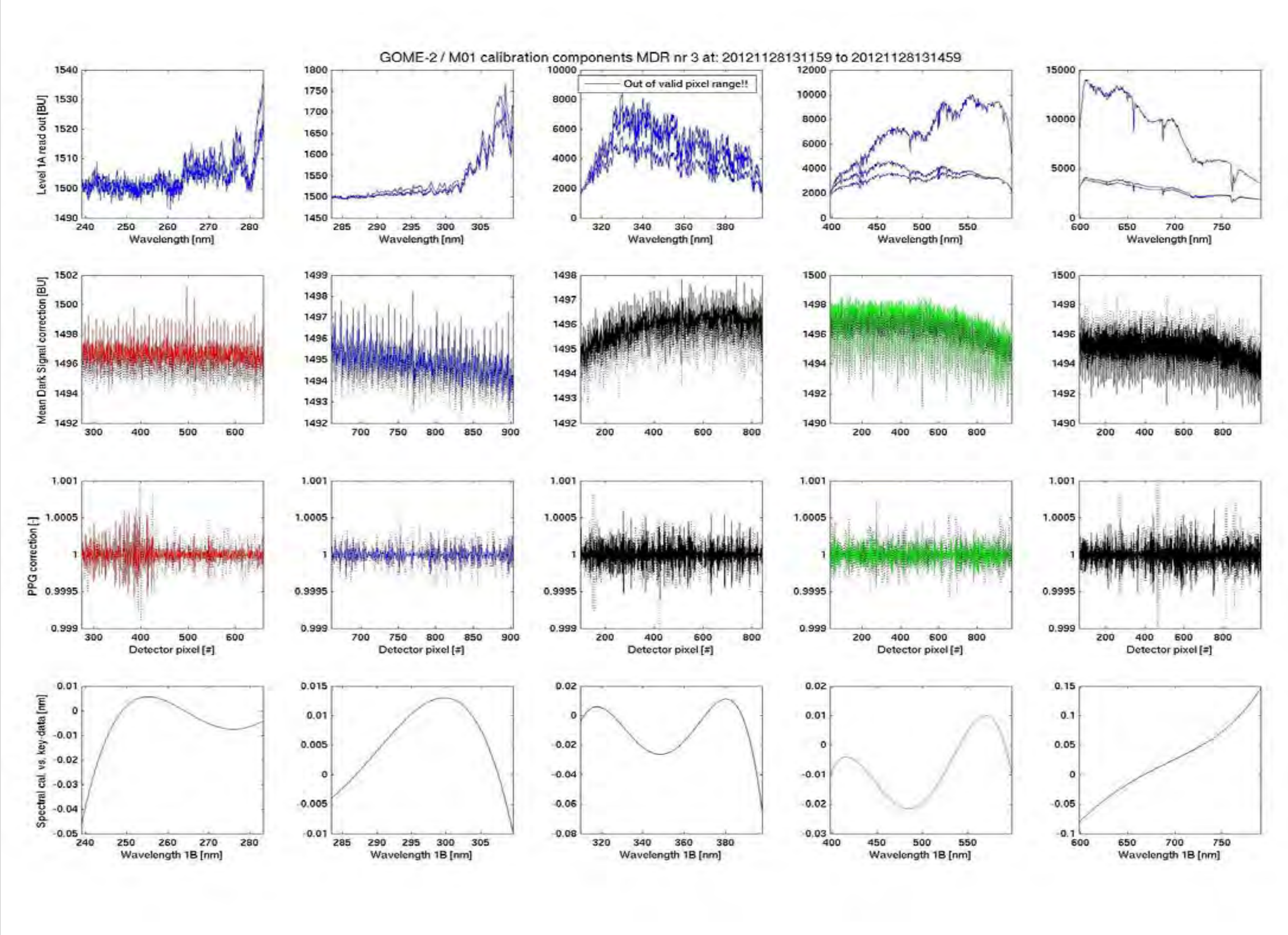

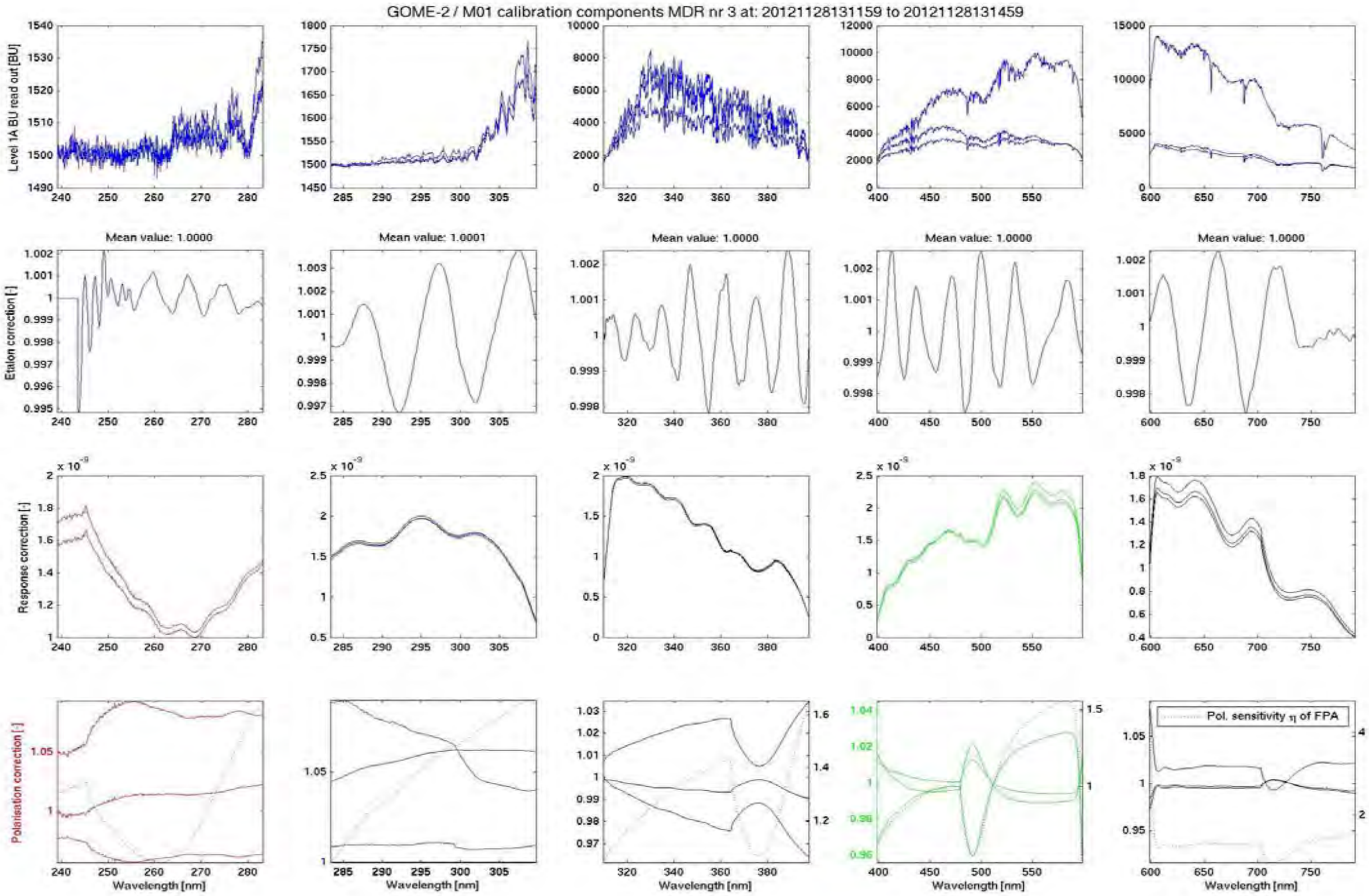

Figure 77: GOME-2 Metop-B / FM2 calibration spectra for the level 0 to 1b processing of one spectra taken on 28 November 2012. Band 1a, 1b, 2b, 3 and 4 are displayed in the columns from left to right. Band 2a is ommitted because all detector pixel of this band fall outside the valid region.

1st row: Raw level 0 signals.

2nd row: Etalon correction.

3rd row: Radiometric response correction.

4th row: Polarisation correction.

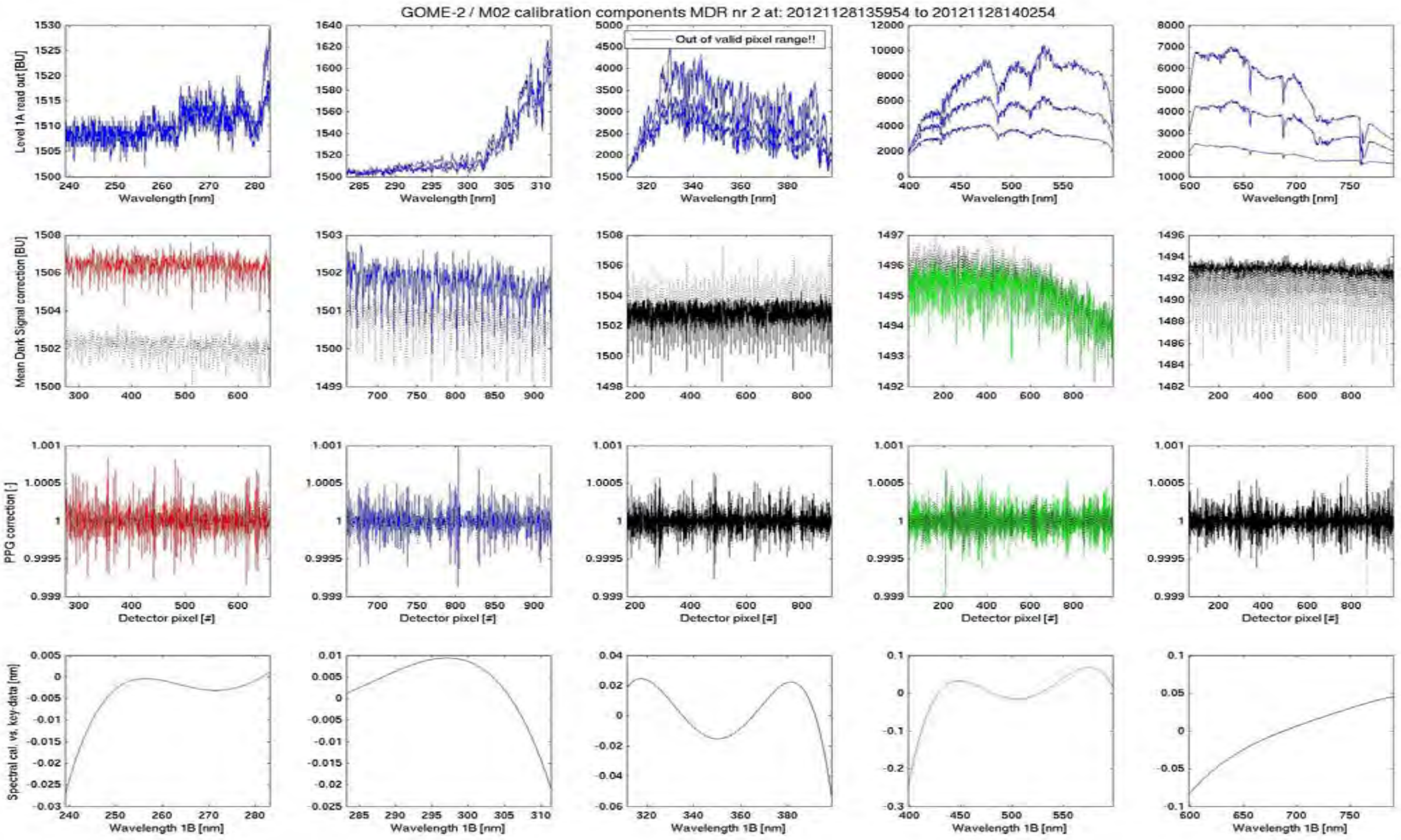

Figure 78: GOME-2 Metop-A / FM3 calibration spectra for the level 0 to 1b processing of one spectra taken on 28 November 2012. Band 1a, 1b, 2b, 3 and 4 are displayed in the columns from left to right. Band 2a is ommited because all detector pixel of this band fall outside the valid region.

1st row: Raw level 0 signals.

2nd row: Dark signal offset.

3rd row: Pixel-toPixel gain

4th row: Difference between the in-flight and the on-ground spectral calibration.

Figure 79:: GOME-2 Metop-A / FM3 calibration spectra for the level 0 to 1b processing of one spectra taken on 28 November 2012. Band 1a, 1b, 2b, 3 and 4 are displayed in the columns from left to right. Band 2a is ommitted because all detector pixels of this band fall outside the valid region.

1st row: Raw level 0 signals.

2nd row: Etalon correction.

3rd row: Radiometric response correction.

4th row: Polarisation correction.

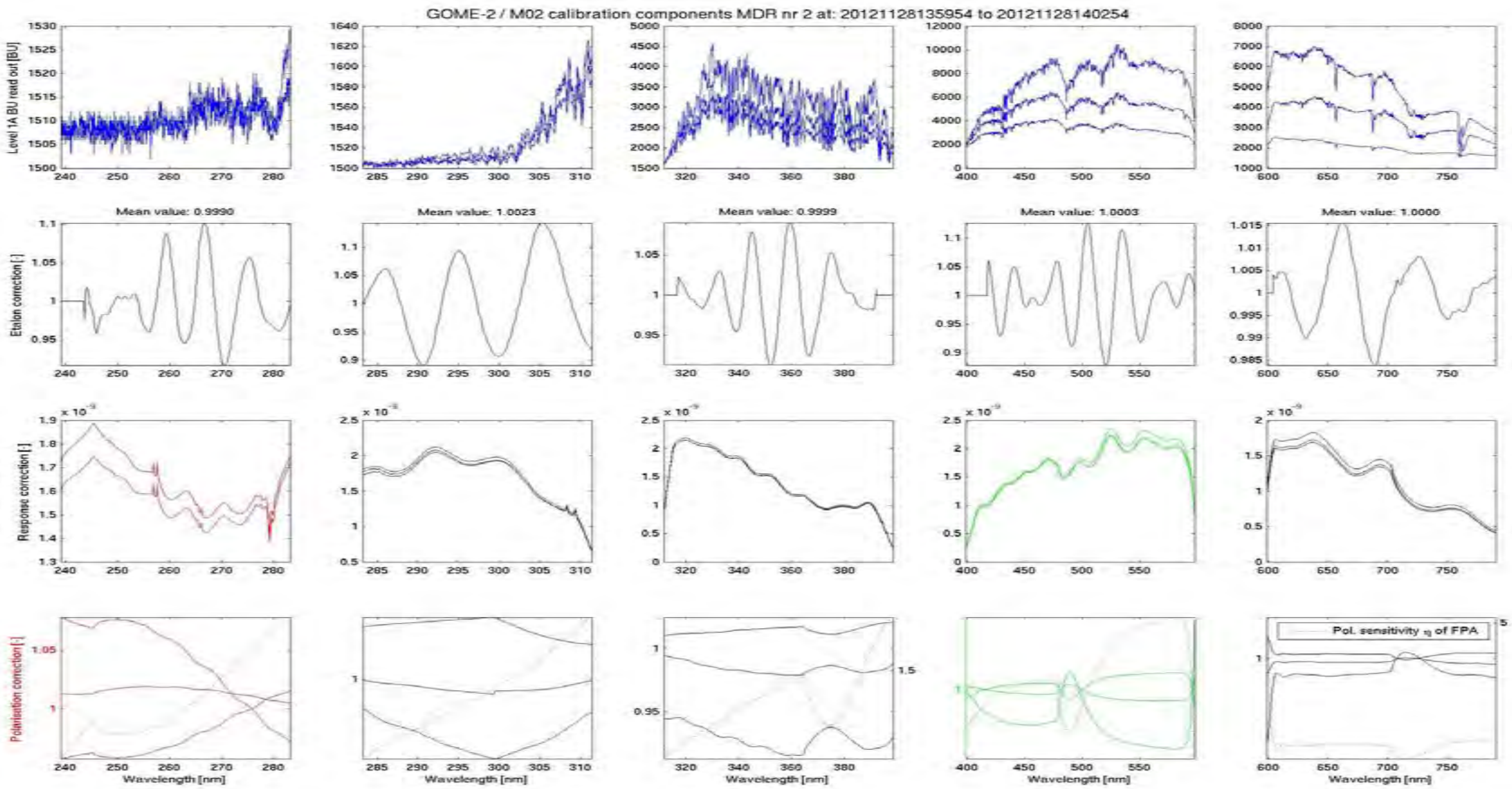

4.12 Radiometric accuracy (Solar and Earthshine) – Metop-A/B comparisons (A5.6)

4.12.1 Solar measurements

We compare the first calibrated solar measurement taken on 29 October 2012 with a solar reference spectrum by Dobber et al., (Solar Phys (2008) 249: 281–291), which has been combined above 590 nm with the Kitt-Peak National Observatory KPNO/AFGL spectrum of 2004. The measured GOME-2 spectrum has been reprocessed with the latest CAL 1.01 and INS 1.02 auxiliary files to take the new overlap region and etalon treatment into account. See also Section 4.8 for comparison with results before the auxiliary data update). We compare the results with the results derived for the first and reprocessed solar spectrum taken by Metop-A / FM3 at the 20th of December 2006. The reprocessed solar spectrum uses the latest PPF 5.3.0 and aux-data set for FM3. Both reference spectra are based on original high-resolution Kitt-Peak Fourier transform measurement data, which have been convolved with the spectral response (slit) function for the GOME-2 FM2 and FM3 instruments.

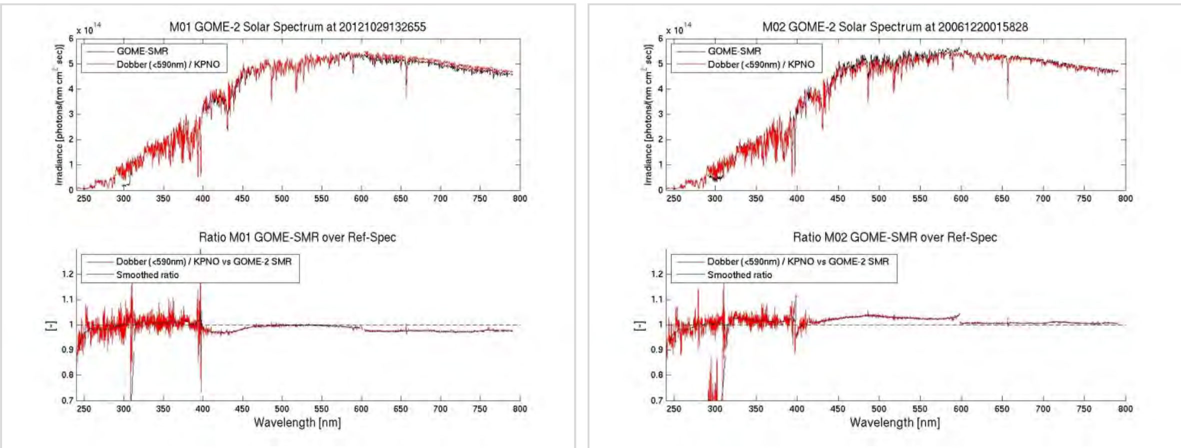

Figure 80: First solar spectrum for Metop-B / FM2 main channels (left panels) taken at the 29th of october 2012 and as compared to the reference (see text). The right panles show the corresponding first Metop-A / FM3 spectrum (reprocessed; see text) from the 20th December 2006.

Figure 80 shows that the overall differences in the residual for GOME-2 Metop-B / FM2 is slightly smaller than for Metop-A / FM3. This is probably due to improved on-ground calibration data quality and, possibly, a better treatment of the Etalon and the shifted radiometric response in the overlap region. A notable residual feature, however, is the one observed between 400 nm and 450 nm in channel 3 for FM2, which may be related to specific problems in the underlying key-data. See also the following subsection on earthshine measurements.

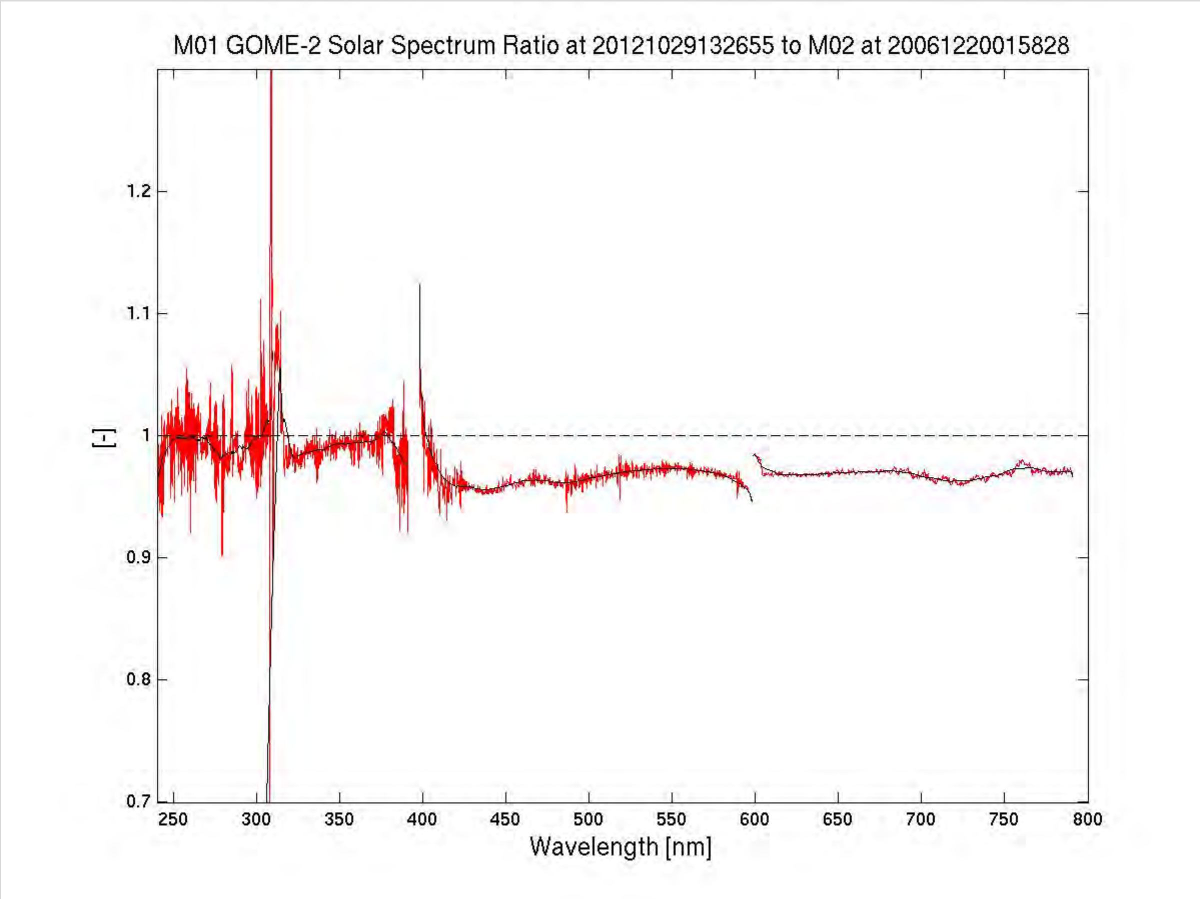

Figure 81: Ratio of the first solar spectrum for Metop-B / FM2 main channels taken at the 29th of october 2012 with the first solar spectrum of Metop-A / FM3 taken at the 20th of Decmeber 2012

The overall baseline of the reference spectrum is considered to be of higher quality for the wavelength region below 590 nm, the region of the Dobber et al. spectrum which has been developed as reference specifically for this type of instrumentation. This includes an improved UV-VIS accuracy; see Solar Phys (2008) 249: 281–291. The jump at 590 nm in the residual is therefore probably due to lower accuracy of the reference spectrum.

The ratio between the first solar spectrum of Metop-B / FM2 and the first solar spectrum of Metop-A / FM3 as displayed in Figure 81 shows that the FM3 spectrum was not only initially higher then FM3 but also that the overlap regions were (are) treated differently–with results in quite significant residuals in the region of the channels 1 and 2 overlap, and channels 2 and 3 overlap. Overall, the differences are below 5 %.

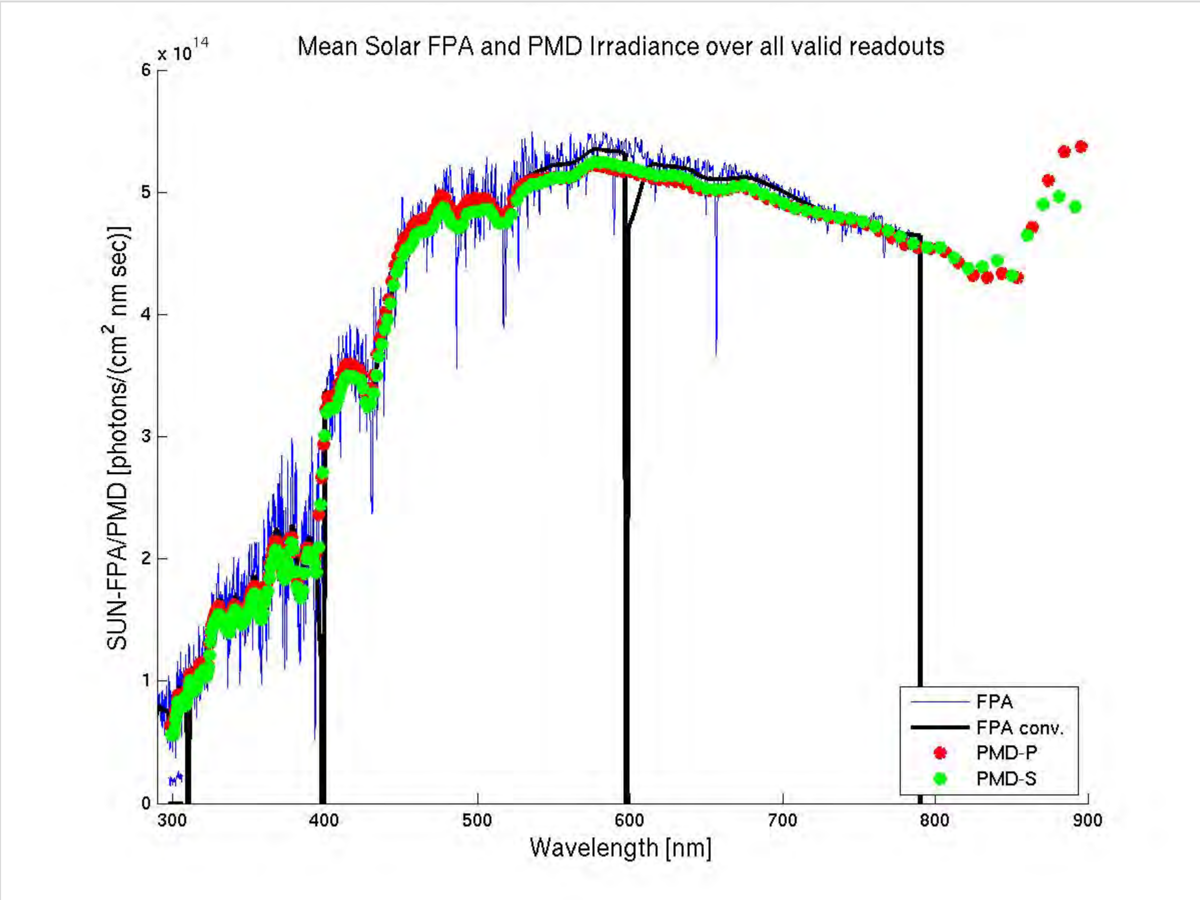

Figure 82: First solar spectrum for the Metop-B / FM2 PMD-P (red filled circles) and PMD-S (green filled circles) channel data taken at the 20th of December 2012. The spectra are compared to the main channel spectrum (blue line) and a convolved version of the main channel spectrum using the slit-function key-data definitions for PMD-P (black line).

Figure 82 shows the PMD-P and S solar spectra compared with convolved main channel spectra. For the targeted consistency between main channel data and PMDs, the differences between the convolved main channel and the PMD spectrum should be minimal. Overall this goal is achieved with the notable exception of the region between approximately 530 nm and 680 nm both for PMD-P and PMD-S.

4.12.2 Earthshine signals

The verification and validation of Earthshine radiances and reflectivity spectra are complicated by the lack of stable targets. Any selected case surface and atmospheric conditions–varying at widely different timescales–compromise the accuracy and interpretation of any comparison to independent (e.g. forward-model based) reference data.

Evaluations must be based either on measurements over certain regions known to provide relatively stable conditions during a single year and from year to year, so as to minimize the effect of seasonality, pollution events and climatological changes. These areas are used for the instrument-to-instrument comparisons, for comparison to forward model results, and for long-term radiance monitoring. Figure 83 shows some of these “stable” target regions. From these regions, we will focus on the Sahara, this being the most stable target with the least cloud interference. This delivers the best statistics especially under cloud-free conditions.

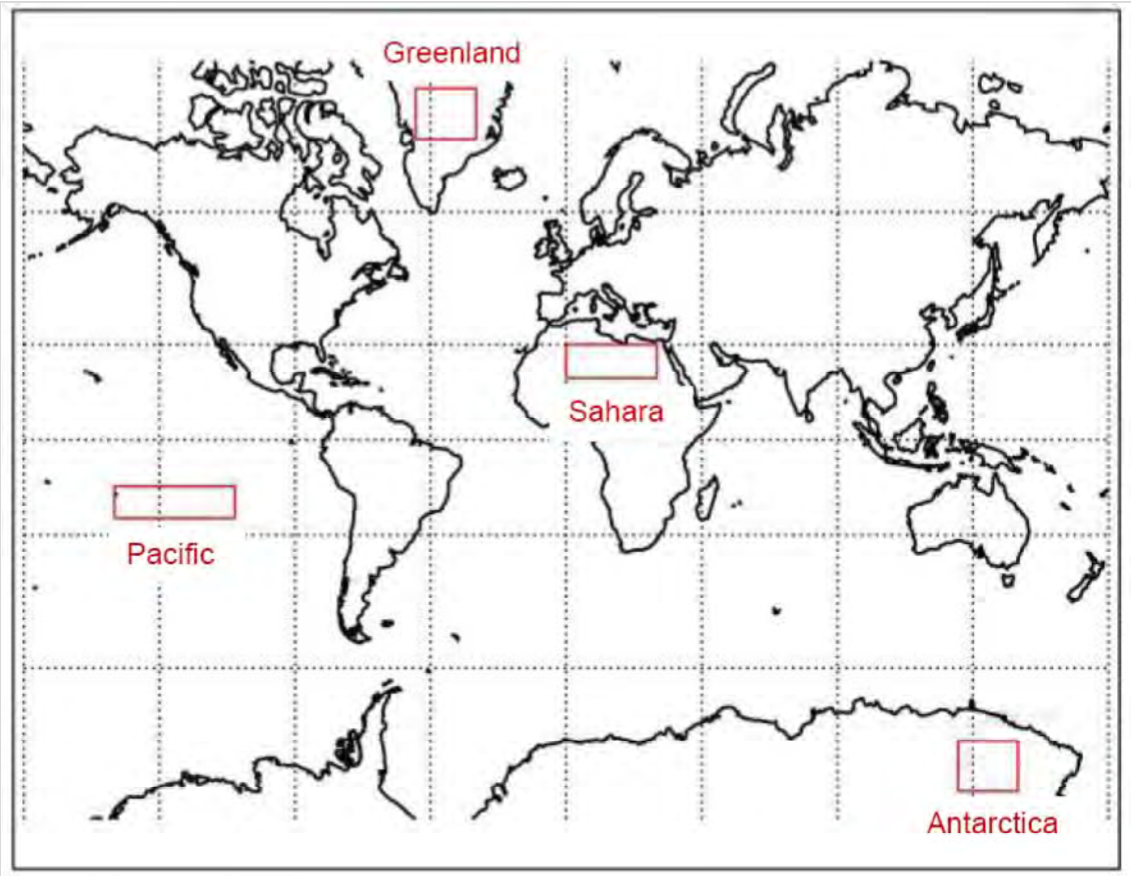

Figure 83: “Stable” (low albedo and atmospheric composition variations) target areas used for the routine NRT monitoring as well as the evaluation of reprocessed earthshine data. For the evaluation of G2RP-R2 we consider only the Sahara area, which provides the most stable situation and best statistics (most clear-sky cases).

In addition to the evaluations using stable Earthshine sources, we perform systematic evaluations. In these evaluations, results are inferred from systematic changes observed with respect to a reference parameter (like viewing angle or solar zenith angle or by intercomparison to co-located Metop-A / FM3 data, predominantly in the polar regions.

4.12.2.1 Earthshine and reflectivity

Individual earthshine and reflectivity spectra at three different viewing angles (most extreme angles and nadir) from Metop-B / FM2 after the update of the auxiliary key-data to CAL 1.01 and INS 1.02 are shown in Figure 84. For reference, we provide the same spectra for Metop-A / FM3 in Figure 85 at approximately the same geo-location; similar viewing geometry but not exactly co-located. For co-located data, see next sub-section.

After the channel-overlap adjustments have been carried out (Section 4.8), there is a notable gap and slope between channel 3 and its adjacent channels. This gap develops in the reflectivity opening under some measurement conditions, while the channel-to-channel transitions in the solar spectrum are very smooth for Metop-B / FM2 (see Figure 84 and Figure 85). Originally, this gap has been associated only to certain viewing angles, which, in turn would point to the underlying viewing angle-dependent key-data, (either in κ or in χ for the applied polarisation correction for earthshine data [AD 7]) as primary cause for the anomaly. EUMETAST internal AR 14557 addresses this.

These jumps have also been observed in the mean reflectivity spectra as provided in the daily report on gome.eumetsat.int (see daily reports for target earthshine monitoring areas) for both instruments FM3 and FM2, even though the former are averages of overall viewing angles within the target monitoring region.

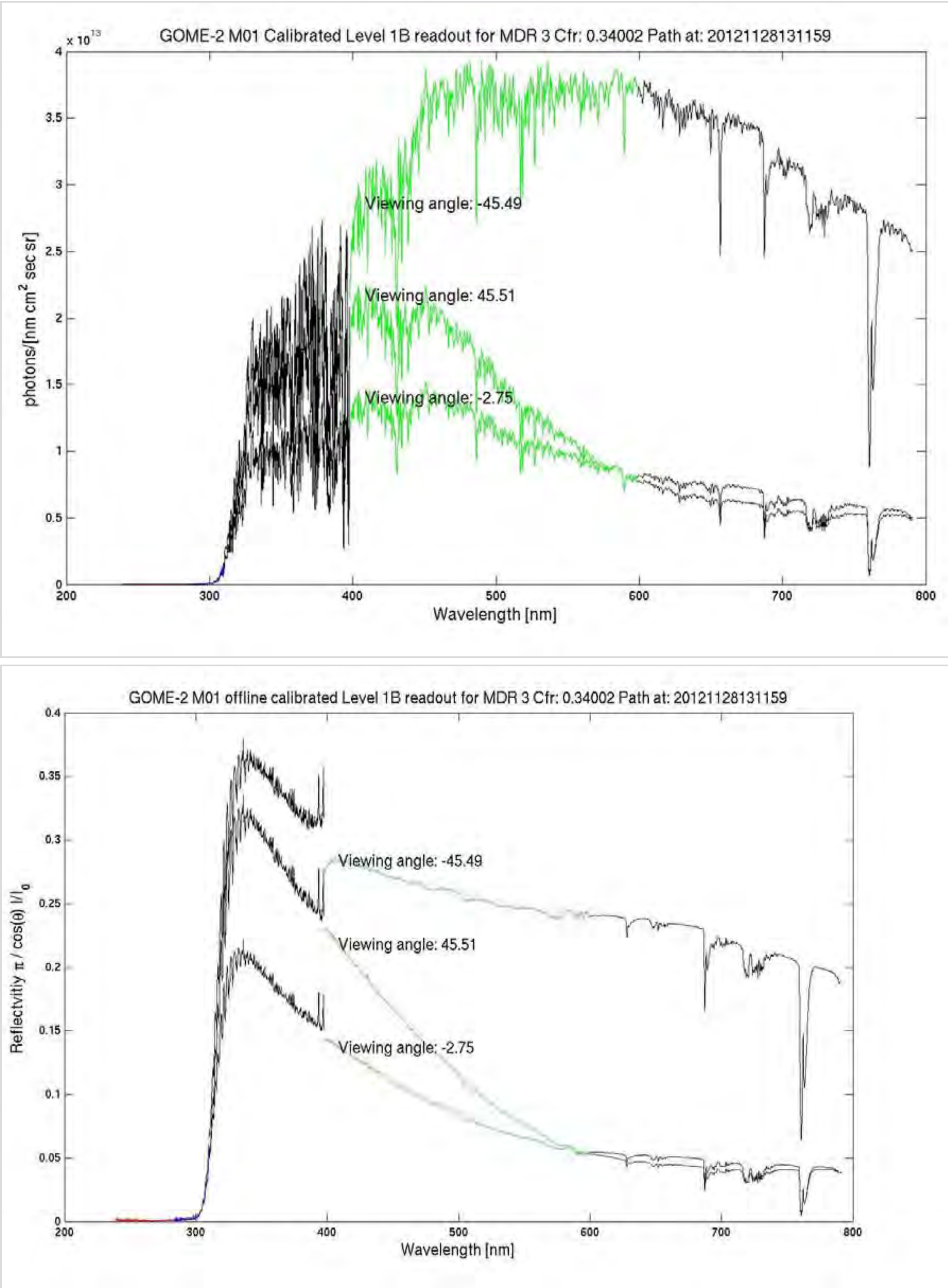

Figure 84: GOME-2 Metop-B / FM2 calibrated earthshine (upper panel) and reflectivity (lower panel) spectra for three read-outs 28 November 2012 at three different vieiwing angles (see legend).

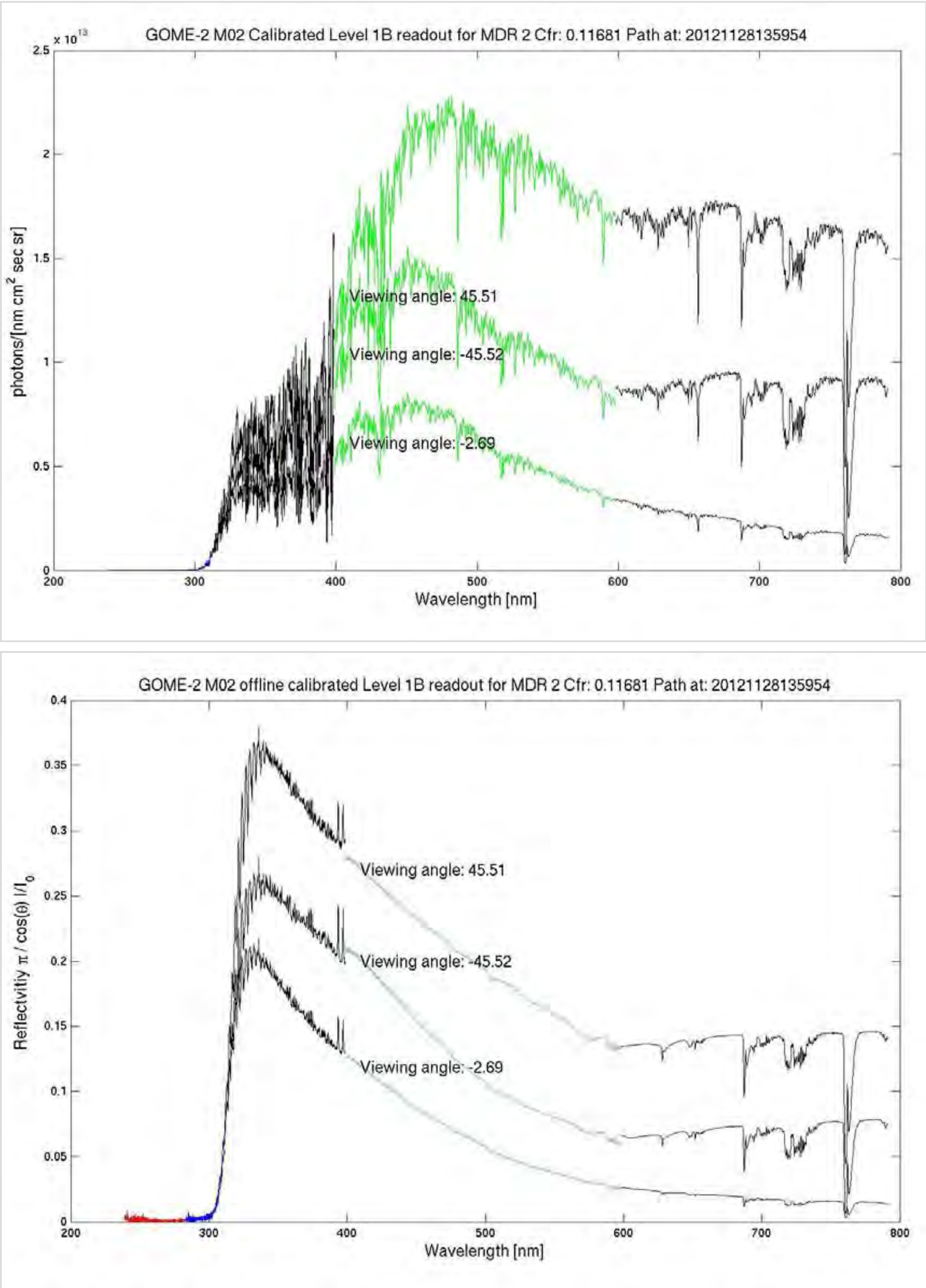

Figure 85: GOME-2 Metop-A / FM3 calibrated earthshine (upper panel) and reflectivity (lower panel) spectra for three read-outs on 28 November 2012 approximately (not co-located) at the same location, though 48 min. temporally separated.

Further investigations using different scenes for Metop-B / FM2 observations have revealed that the gap was also present for different (and opposite) viewing angles and even under some nadir conditions as shown in Figure 86. We have also added some spectra for which the polarisation correction step has been omitted to investigate the impact of the latter (and of the involved key-data for polarisation correction) and to see if this has a noticeable and identifiable effect on the gap.

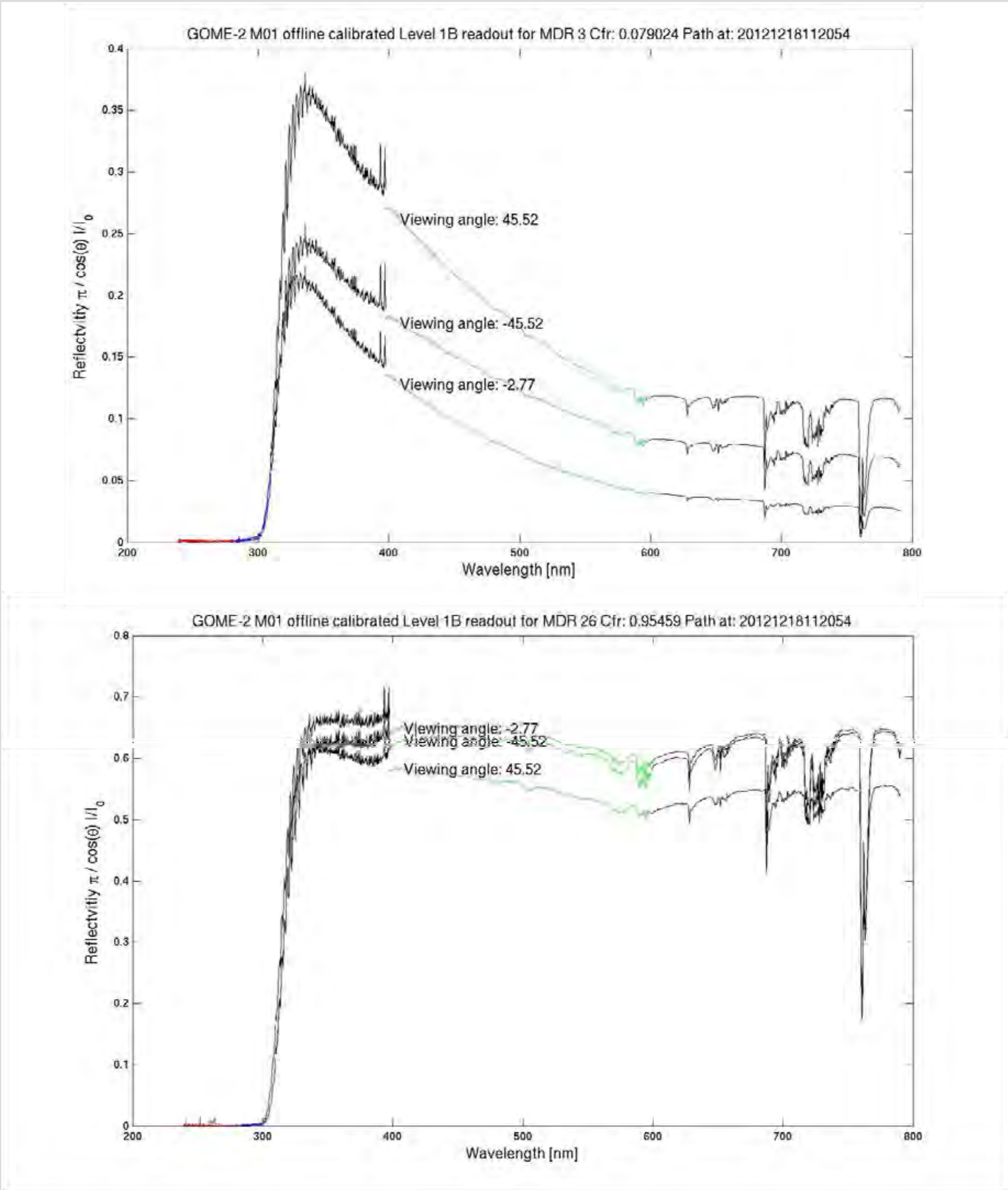

Figure 86: GOME-2 Metop-A / FM3 calibrated earthshine (upper panel) and reflectivity (lower panel) spectra for three read-outs on 18 December 2012 approximately (not co-located) at the same location, though 48 min. temporally separated.

Figure 87 shows the additional polarisation spectra overlaid as a red line. The typical spectral signatures (like the "bump" in the middle of channel 3) are visible for these spectra as a result of the polarisation sensitivity of the instrument (ζ- sensitivity). Both cases are taken at mid-latitudes where the degree of polarisation is largest for the east-viewing conditions (negative viewing angles). The two cases are for clear sky-conditions (upper panel) and for a very bright cloud under all viewing conditions. For very bright cloud, the degree of polarisation of the incoming light is significantly reduced. For all cases, the gap occurs relatively independently of the polarisation correction or conditions and under different viewing conditions.

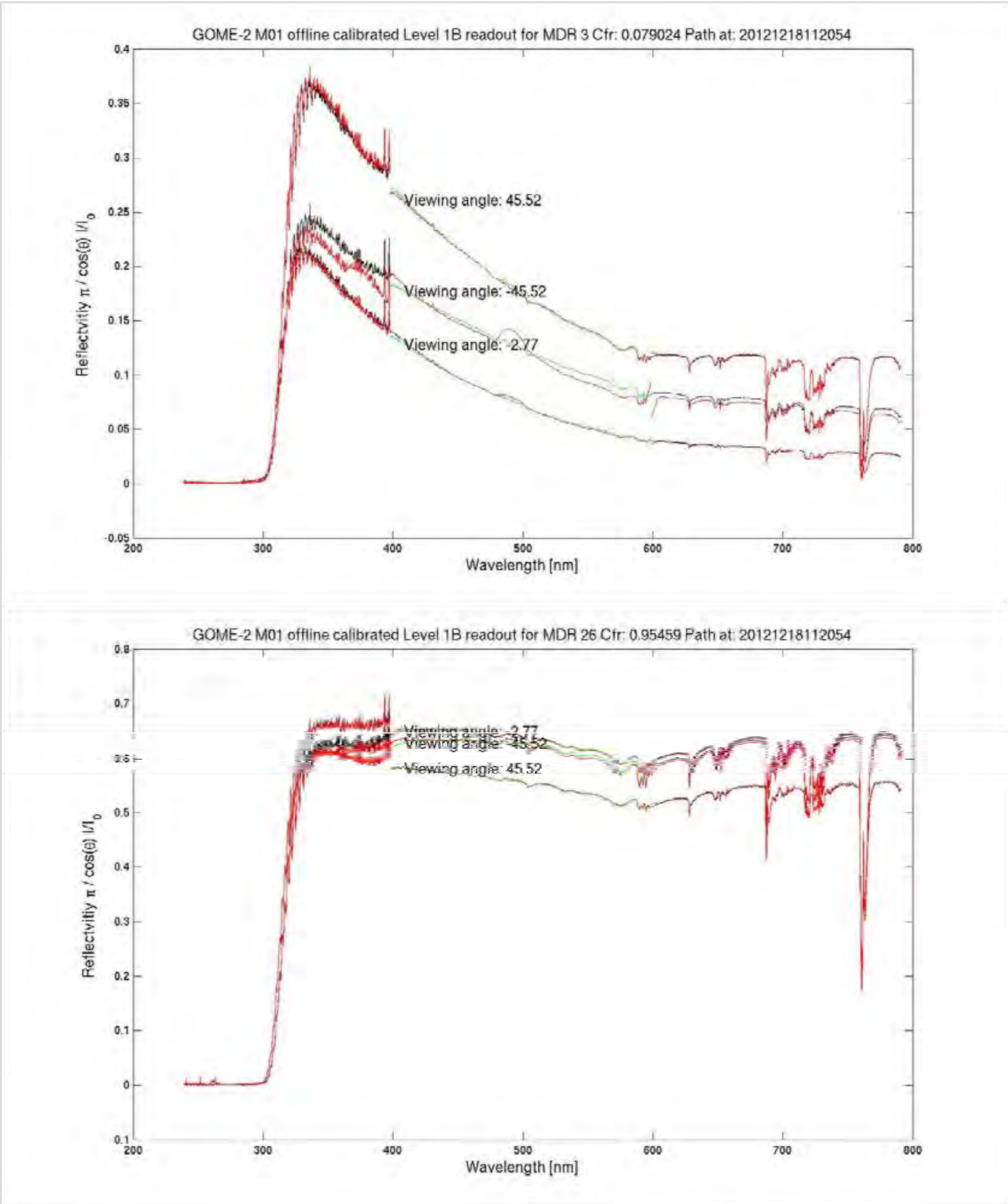

Figure 87: GOME-2 Metop-A / FM3 calibrated earthshine (upper panel) and reflectivity (lower panel) spectra for three read-outs on 18 December 2012 approximately (not co-located) at the same location, though 48 min. temporally separated. and with an additional spectrum without polarisation correction (red line) overlaid.

4.12.2.2 Metop-A/B global individual co-locations

Reflectivity spectra from Metop-B / FM2 (M01) are compared to co-located Metop-A / FM3 (M02) data using the following co-location strategy. First, for the sake of efficiency, timestamps for the closest overlaps of the swathes of both instruments are retrieved from the MPSTAR monitoring database with some temporal margin (a default spacing of 48.2 minutes between both satellites is used). Then the corresponding pdus of both satellites are read in from the rolling-archive of MPSTAR and all ground-pixel for which the centre points of Metop-B / FM2 fall into the region of one Metop-A / FM3 ground pixel are selected for further evaluation. For the latter selected pixel the area overlap in percentage to the total area of both ground pixel is evaluated. Finally only those co-located pixels from FM2 and FM3 with an area overlap fraction of more than 85 % are selected for further evaluation (see Figure 88).

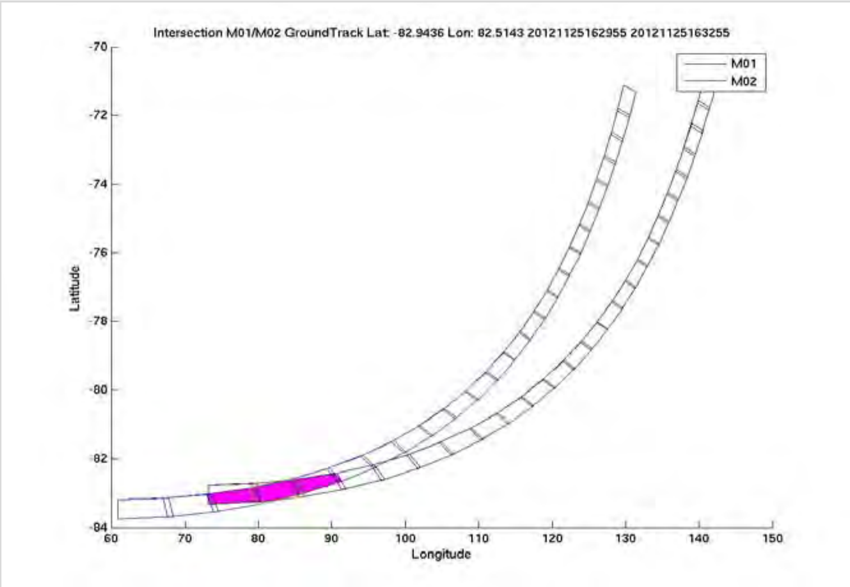

Figure 88: Co-location of Metop-A /FM3 (M02: blue track) and Metop-B / FM2 (M01, black track) ground –pixel. The shaded area shows those pixels where the centre points are inside the corner values. The pixel with the largest fractional area overlap is finally selected (red/green lines).

Figure 89 and Figure 90 show the corresponding FM2 and FM3 reflectivity and radiance spectra and their corresponding residual for a ground pixel at –82 in latitude and –80 in longitude on 25 November 2012. During this time of year, most co-locations satisfying all criteria are found over the Antarctic region. The advantage of Antarctica is that the surface albedo is stable and quite large, with very little spectral structure over the entire spectral range (which is sensitive to the surface). There are drawbacks of such geo-locations: the large solar zenith angles (related to very long-light paths and therefore to an increased contribution of a potentially varying atmosphere), as well as the difficulty in differentiating clouds from the background.

For each co-location, we evaluate the geometric light-path difference for both instruments (see legend in lower panel of Figure 89 and Figure 91) as well as the depth of the residual in the oxygen A-band region. The ratio of the background (750 nm) to the centre of the Oxygen A-Band (760 nm) in the residual provides an additional measure of light path differences. The final co-location selection is then based on a differential geometrical light path of less than 1.8 % and a residual Oxygen A-Band ratio (ROR) of smaller than 0.3.

The residual of the reflectivity spectra in the lower panel in Figure 89 shows a persistent spectral structure for most of the co-locations satisfying all quality criteria. The better the co-location, the more the residual shifts towards the 0 line–but the observed spectral structure stays essentially unchanged. There is a large deviation in channel 1 with an initial underestimation below 310 nm and a large overestimation below 280 nm for FM3 with respect to FM2. There is also a considerable, Etalon-like structure superimposed on the residual in channel 1. For channels 2 to 4, the residual structure is quite smooth but tilted in a channel-to-channel zigzag. There is some similarity with the observed "tilt" in channel 3 for different viewing angles (see previous section). This similarity requires further investigation.

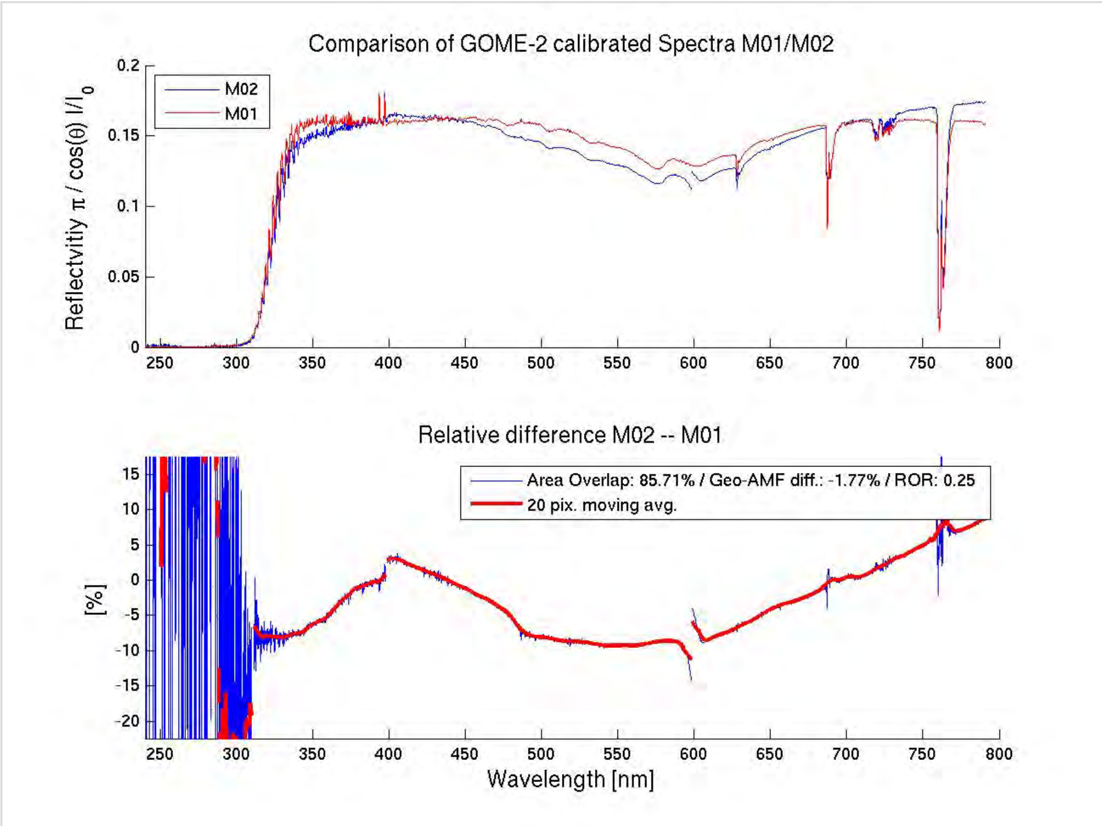

Figure 89: Co-located Metop-A / FM3 (blue line) and Metop-B / FM2 (red line) reflectivity spectra for 28 November 2012 (upper panel). The lower panel shows the residual (blue line) and a 20- detector pixel moving average (red line) together with the quality indicators of the co-location in the legend.

In contrast, the residual between the radiance spectra in the lower panel of Figure 90 clearly shows the spectral structure of the degradation of M02 relative to M01. This degradation is much larger than the individual calibration-dependent effects and the individual differential-degradation effects visible in the reflectivity residuals. Since level 2 retrievals mainly use reflectivity, we will focus on the latter data quality in the following.

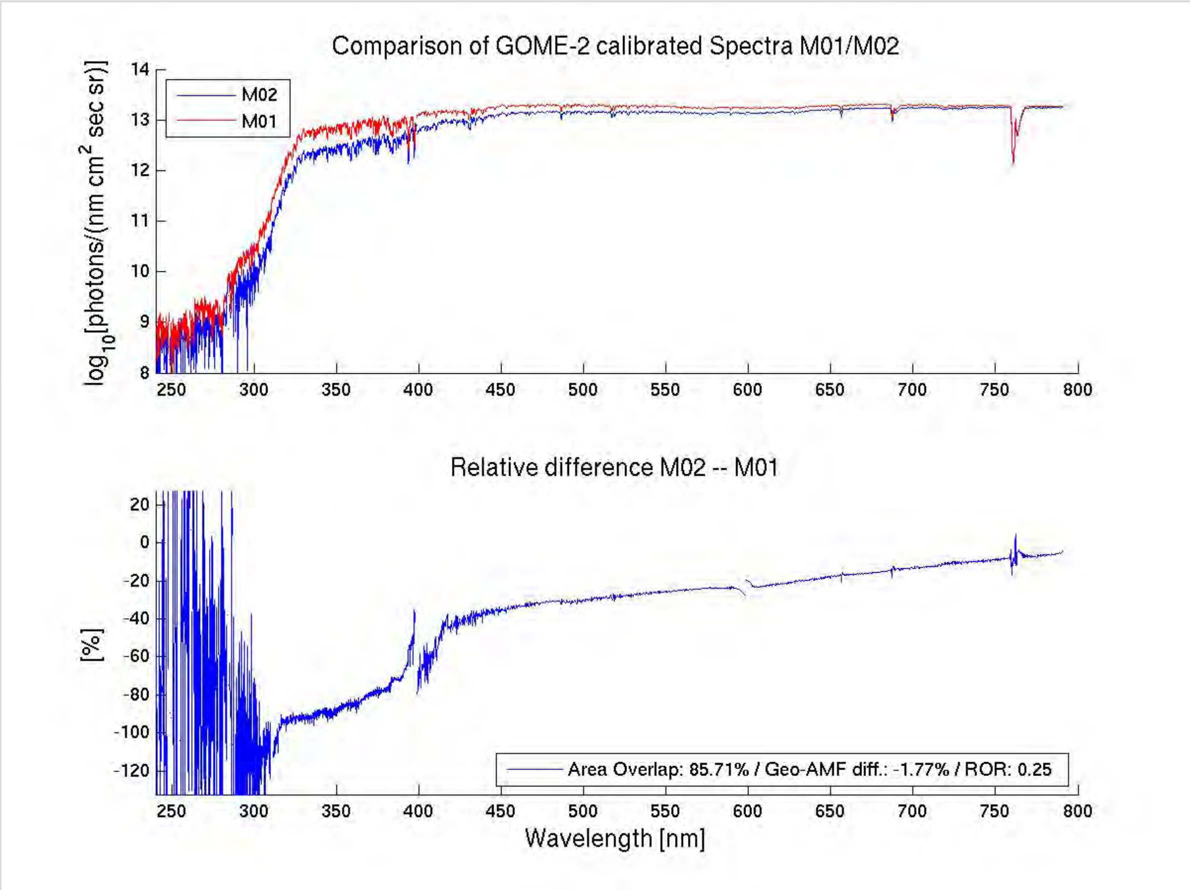

Figure 90: Co-located Metop-A / FM3 (blue line) and Metop-B / FM2 (red line) radiance spectra for 28 November 2012 (upper panel with log scale). The lower panel shows the residual (blue line) and a 20 detector pixel moving average (red line) together with the quality indicators of the co-location in the legend.

To improve the statistics, and to investigate the robustness of the residual shape using various viewing conditions and geo-locations; we collected co-location for two different days. Figure 92 shows the position of co-locations for both days separated in M01-East/M02-West and M02-West/M01-East, as well as for nadir conditions separated by +/– 20 degrees viewing angle. The co-locations are distributed similarly for the two days and there are only a few nadir co-locations along high southern latitudes.

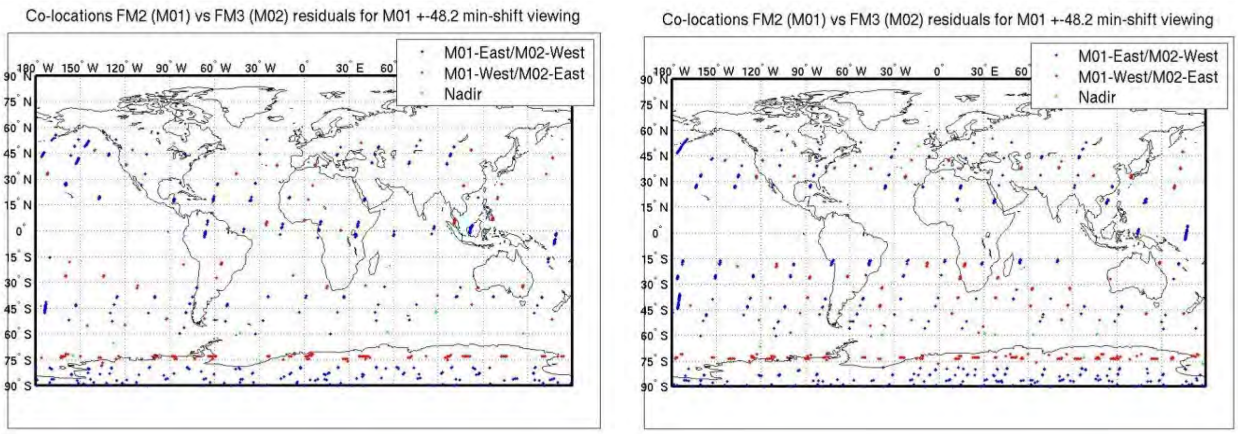

Figure 91: Individual Metop-A / FM3 and Metop-B / FM2 co-location separated at +-20 degrees viewing anlge into M01-East/M02-West, M01-West/M02-East, and nadir

Differences in the distribution are due to the residual oxygen A-band differences criterium being below a certain limit to select for similar atmospheric path length. The overall background may still vary greatly from co-location to co-location and since an offset due to larger differential degradation from M02 can be assumed, we subtract a linear background of the residual per channel. Figure 92 shows an example for the averaged residual between M02 and M01 in the Pacific box, with the linear background superimposed.

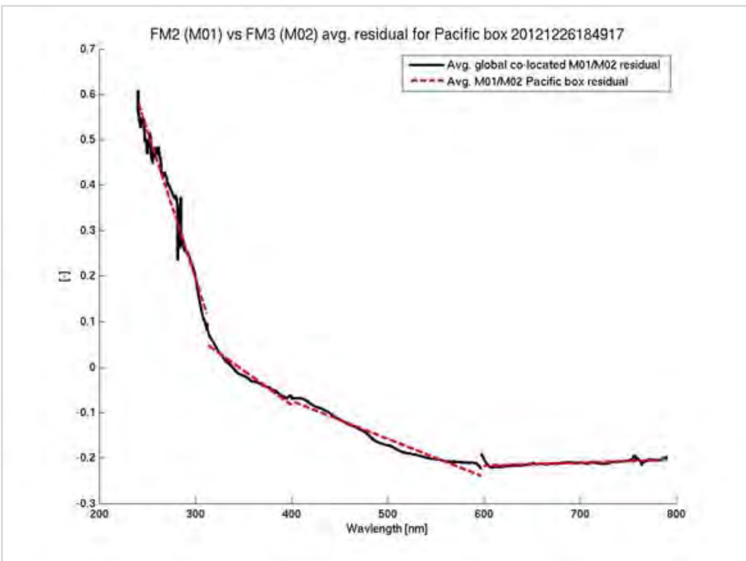

Figure 92: Residual between co-located Metop-A / FM3 and Metop-B / FM2 reflectivity spectra (black line) for 28 November2013. The red dashed line shows the linear background that is subtracted from residuals for the results presented in the following figures.

Figure 93 shows the final three types of residuals (East/West, West/East and nadir) globally averaged with background subtracted for the co-located individual measurements and for both days and for spectra with and without polarisation correction applied. All residuals show very persistent patterns for channels 2 and 3, under all conditions. The removal of polarisation correction is visible by the significant signature of η just before 500 nm, otherwise the overall signature seems to be the same.

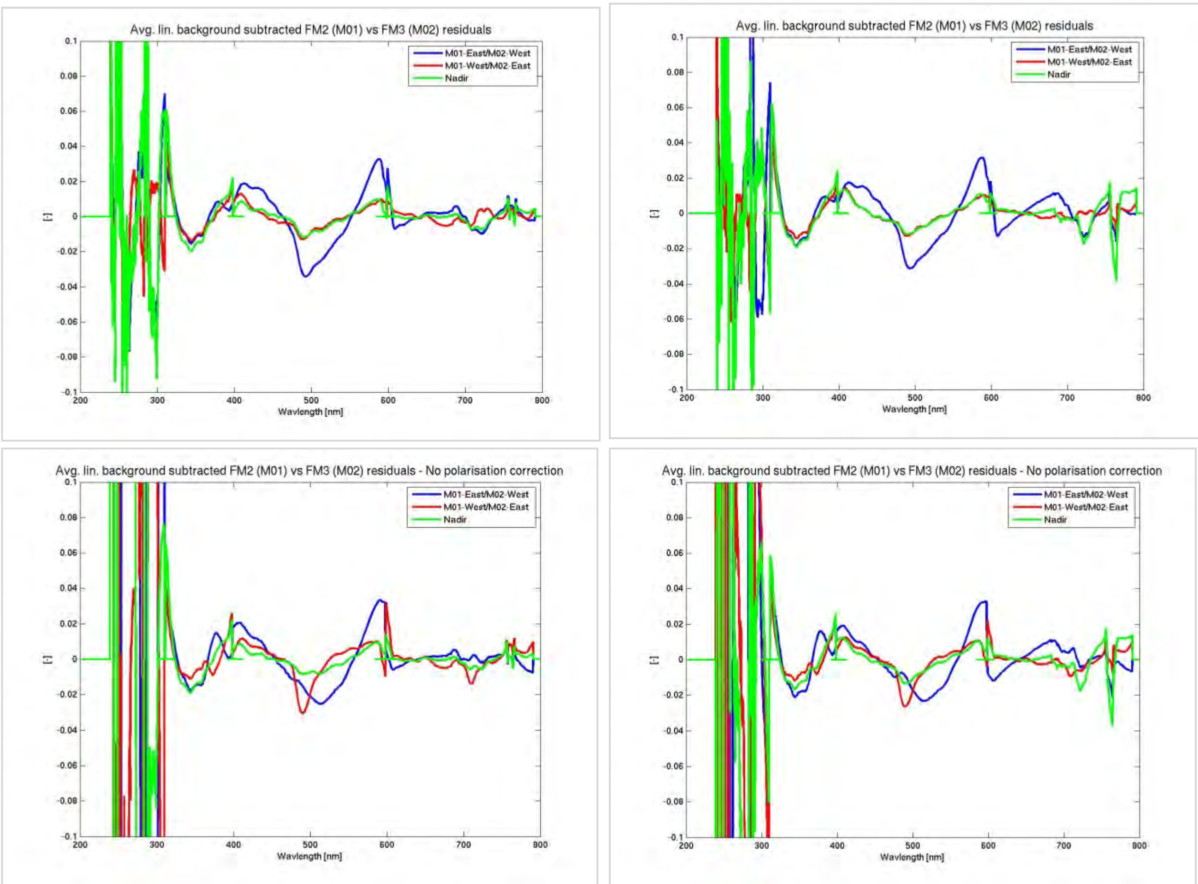

Figure 93: Co-located Metop-A / FM3 and Metop-B / FM2 reflectivity residuals of individual co-locations globally averaged on 26 November 2013 (left panels) and for 10 January 2013 (right panels). The upper panels show the residuals for the nominal level 1b reflectivity product, whereas the lower panle show reflectivity residuals without polarisation correction. Residuals are separated in M01-East/M02-West (blue), M01-West/M02-East, and Nadir (green) viewing combinations, for which the separation is made at +/– 20 degrees viewing angle.

Looking specifically at channel 4, we see there is not much broad-band persistent residual spectral visible outside the regions of strong atmospheric absorptions (predominantly water vapour at 640 nm and 700 nm, and oxygen at 630 nm and 740 nm). In channel 1, there are large variations at higher frequencies than found in channels 2 and 3. These will be examined more closely, along with the channel 2 and channel 3 residuals, in the following sections.

4.12.2.3 Metop-A/B comparison in the target boxes

In addition to the averaged residuals from the individual co-locations, we derive residuals between Metop-A/FM3 and Metop-B/FM2 from the averaged reflectivity spectra in the Pacific and Sahara stable target boxes (see Figure 83). Since here we take the average over the acquired radiances before taking the residuals we cannot discriminate for viewing angle. However the residuals are more specific to the target region.

Figure 94 shows the target box M01/M02 residuals for the Pacific and the Sahara taken 26 December 2012 and on 25 January 2013. We selected also here only those results with relatively small residuals in the O2 A-band region. The similarity to the previous derived residuals is striking. The remaining questions to be answered are as follows:

- which part of the residual may be attributed to which instrument,
- which instrument feature (key-data, degradation) may be involved,
- what influence does the subtraction of the residual offset/background have.

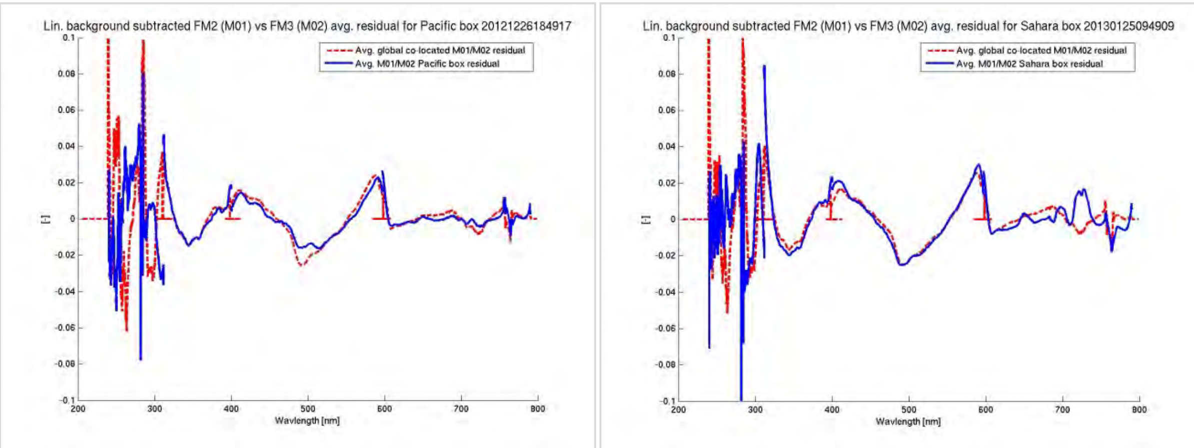

Figure 94: Co-located Metop-A / FM3 and Metop-B / FM2 reflectivity residuals (blue line) of individual co-locations globally averaged on 26 December 2012 (left panels) and for 25 January 2013 (right panels) for the Pacific and the Sahara box. The cases were also selected on the basis of small residuals ion the O2 A-band area. The globally and viewing angle averaged residuals of the individual co-locations as shown in Figure 93 are indicated by a red dashed line.

4.12.2.4 Metop-A/B comparison – the impact of instrument degradation

Since we have subtracted only a linear background from the derived co-located residuals (see Figure 92) and still must account for differences in degradation between the two instruments, the question remains if there are higher-order structures to be taken into account. Overall, the degradation for both GOME-2 instruments is a smooth function in wavelength (see references in [RD8] as well Section 4.13, Figure 102)–though not linear over the full region. Also, detailed investigations of the nature of the GOME-2 / Metop-A degradation revealed some higher frequency–though still broad-band pattern– in the degradation spectrum of GOME- 2 / Metop-A. This was especially prevalent in channel 2 between 300 nm and 425 nm, and previously was attributed to contaminating substances from conformal coatings of electronics inside the instrument [RD7]), and some “etalon” type of structures apparently not accounted for by the level-0-to-1b etalon correction in channel 1. The latter gradually appeared for both signatures over the course of the mission, possibly as a result of the degradation (see Figure 95).

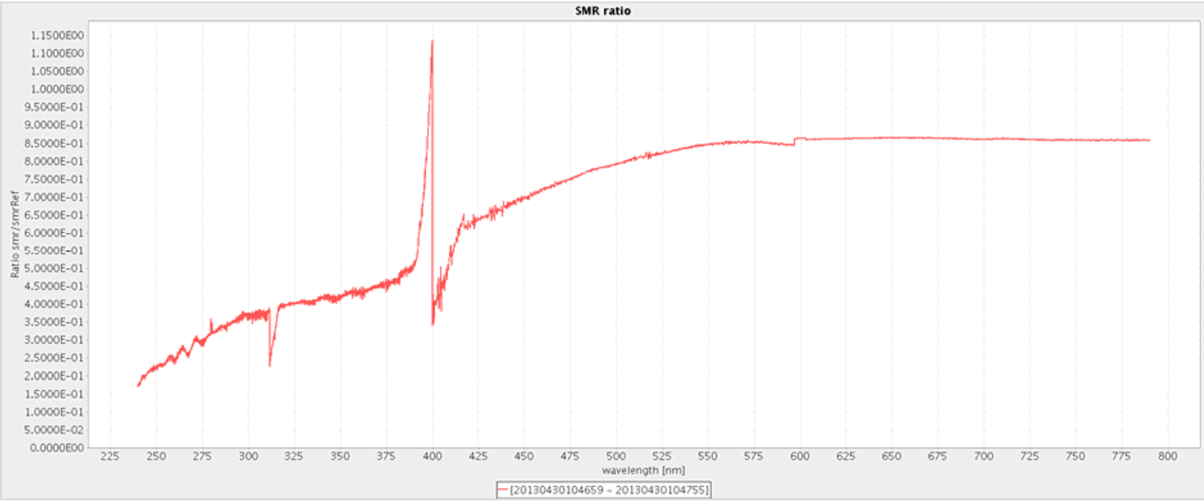

Figure 95: Metop-A / FM3 degradation pattern displaying the ratio of a solar mean reference spectrum from April 2013 with respect to Februar 2007. Smaller scale (etalon-type) structures appear in channel 1, though the individual spectra are etalon- corrected. Also between 300 and 425 a broad band trough is observed.

To further separate spectral signatures from degradation patterns in the co-located residuals, we calculate the contribution of the degradation patterns for the Metop-A instruments separately. Figure 96 shows averaged reflectivity spectra from GOME-2 Metop-A for the periods February 2007 and December 2012. The average is done within the Sahara box and for one month of data. The figure also shows the residual between both reflectivity spectra, for which a linear background is subtracted precisely as was done for the co-located residuals. Figure 97 then compares this residual with the residuals found in Figure 93 and Figure 94 when co-locating the two instruments on 26 December 2012, with consideration that FM3 has been in orbit for nearly seven years. The comparisons show striking similarities in the overall broad-band patterns (apart from the strong atmospheric absorption regions). Even the high frequency patterns in channel 1 show strong similarity. This same strong similarity holds true when comparing the observed residuals from the target boxes with co-located individual and globally-averaged residuals (Figure 98), though there are some interesting differences observed in the channel 1 residual structure. These differences are in pattern, not in frequency, and may provide an indication of its origin.

When subtracting the "degradation spectral structure" now referred to the FM3 GOME-2 / Metop-A instrument from the overall observed residual structures for the co-location results the remaining residual turns out to be very flat and generally below 1 % (Figure 99). The remaining residuals for the Pacific box are a bit larger which can be largely attributed to the fact the results, are generally noisier because of more cloud-screening and more residual cloud effects (and larger differences in viewing geometry sampling) than it is the case for the Sahara region. However, from Figure 98 one can see that the general patterns in the co-located residuals between the instruments can be mainly attributed to M02 instrument degradation for the Pacific box.

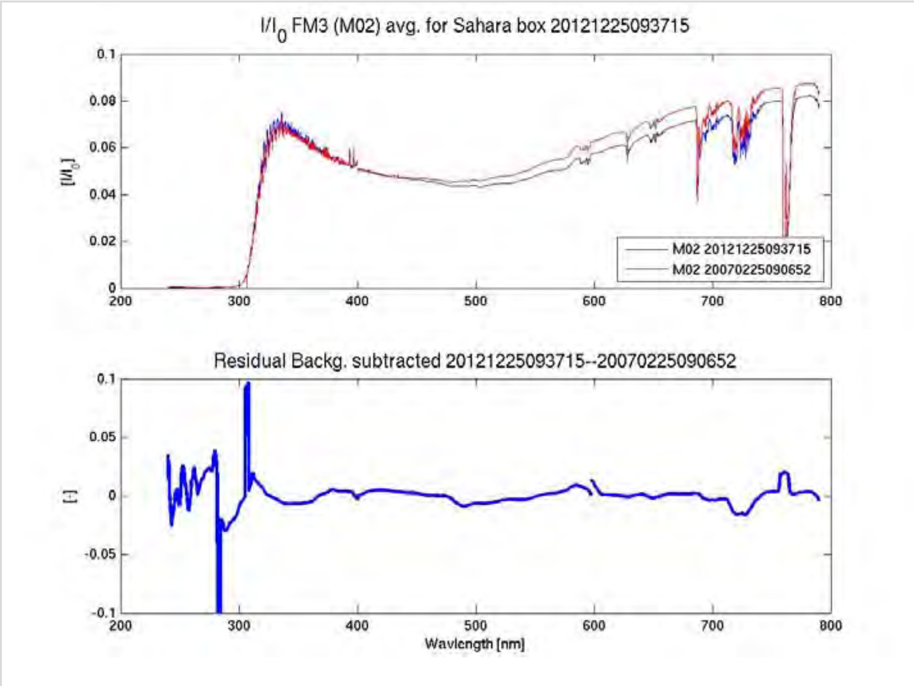

Figure 96: Metop-A / FM3 reflectivity spectra (upper panel) averaged over month and over the Sahara box in February 2007 (red line) and in December 2012 (blue line). The lower panel shows the residual between both for which a linear background has been subtraced per channel (as in Figure 92).

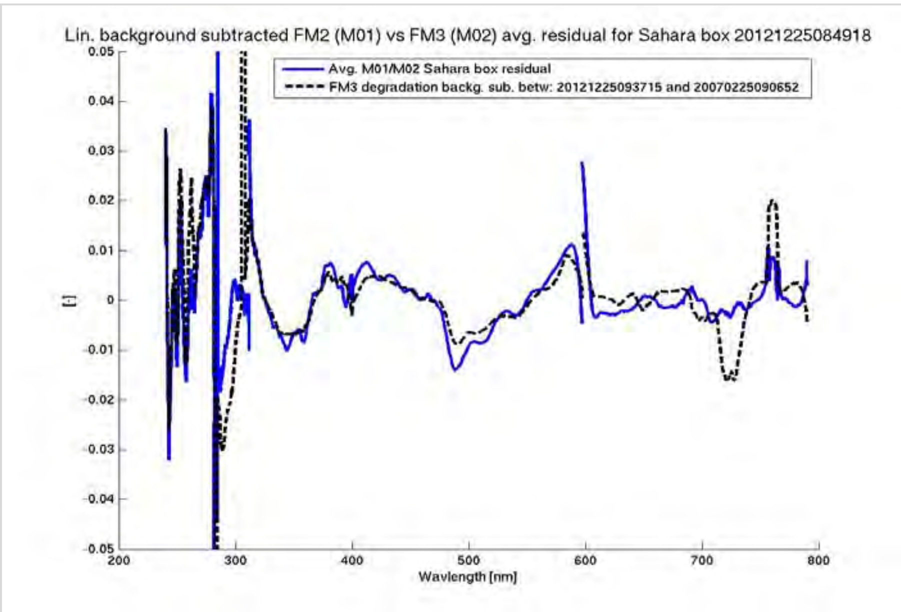

Figure 97: The lower panel residual of Figure 96 (black dashed line) is compared here with the linear backroung subtracted residual of the co-located Metop-A and B instruments as shown in Figure 93 and Figure 94 for the Sahara box.

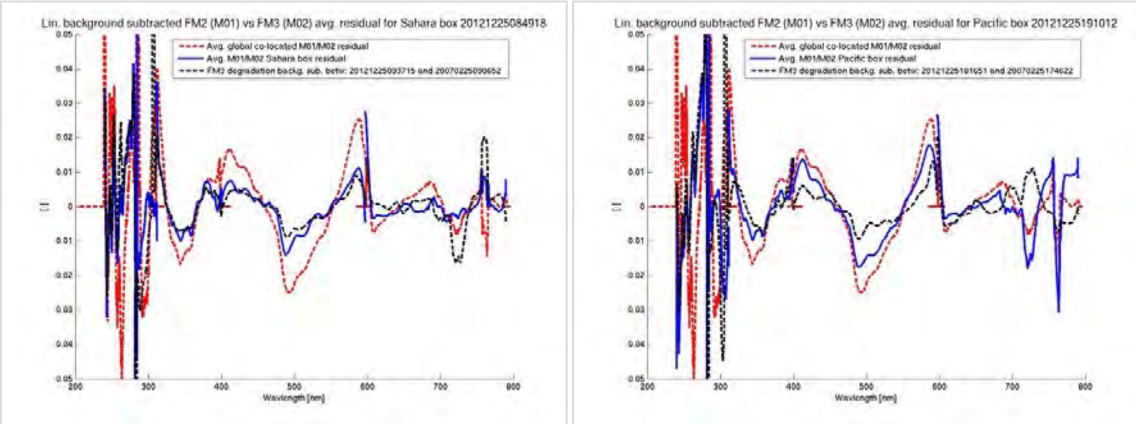

Figure 98: The lower panel residual of Figure 96 (black dashed line) is compared here with the linear backroung subtracted residual of the co-located Metop-A and B instruments as shown in Figure 93 and Figure 94. Additionally, the averaged results of the globally- averaged individual co-locations (red dashed line) and for both the Sahara (left panel) and the Pacific box (right panel)

After subtracting the “degradation spectral structure” now ascribed to the FM3 GOME-2 / Metop-A instrument from the overall residual structures for the co-location results, the remaining residual turns out to be very flat and generally below 1 % as shown in Figure 99. The remaining residuals for the Pacific box are a bit larger. This can be attributed to the fact that the Pacific box results are generally noisier; there is more cloud-screening, more residual cloud effects, and larger differences in viewing geometry sampling than in the Sahara region. However, in Figure 98 one can see that the general patterns in the co-located residuals between the instruments can be mainly attributed to M02 instrument degradation for the Pacific box.

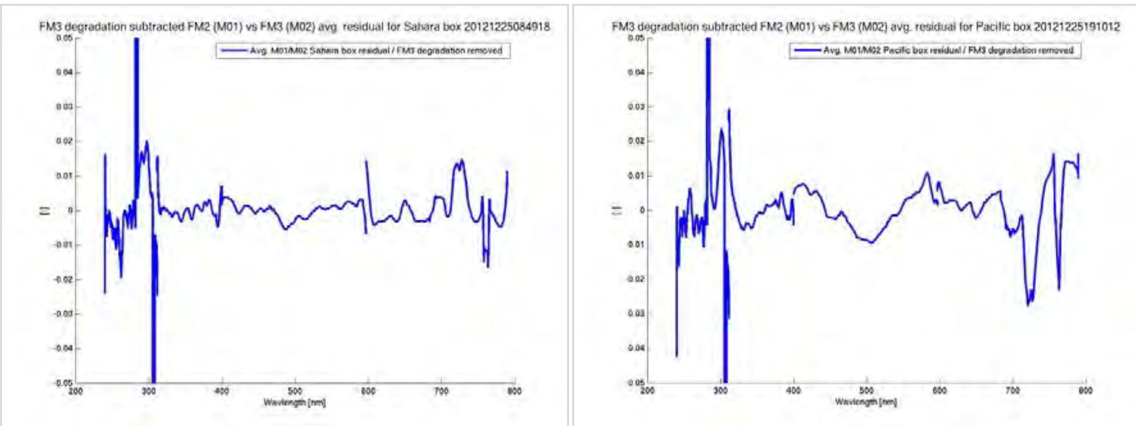

Figure 99: Difference between the residuals in Figure 97 and for both the Sahara (left panel) and the Pacific box (right panel).

The residuals that remain after FM3 degradation patterns have been subtracted are shown in Figure 99. These residuals show the expected prominent atmospheric absorption patterns, especially in channel 4 and at 475 nm (O_2-O_2 absorption) in channel 2. The observed “etalon-type” pattern in channel 1 can be completely attributed to degradation features. Since FM2 is also degrading quite fast in the early weeks after launch, it cannot be excluded that some of the remaining patterns have to be attributed to the initial degradation of FM2 (see Section 4.13.1, specifically Figure 102).

4.12.3 Comparison to Forward Model Data (V-Lidort)

In this section, we compare Metop-B / FM2 and Metop-A / FM3 reflectivity to the output of a vector radiative transfer model V-LIDORT Version 2.4 RTC [RD21] fed by six hourly ECMWF forecast model profiles, of which 19 layers are used in temperature, water vapour, ozone and humidity. We use the same two target areas (Pacific and Sahara) used before.

This installment of V-LIDORT 2.4RTC uses a lowest equivalent reflection albedo database derived from GOME-1 and attributed to Koelemijer et al. [RD18] over ocean. Over land surfaces, it uses a MERIS-based albedo database described in [RD19]. The model includes a Mie-scattering code with bi-model phase scattering distribution functions using standard atmosphere LOWTRAN aerosol optical properties. These properties are confined to a number of extinction coefficients, single scattering albedo, and asymmetry parameters defined for six wavelengths covering the GOME-2 range, and also for a selection of mixed "types": rural continental, maritime, background stratospheric, etc.) These types are described in detail in [RD21].

Figure 100 shows the results of a comparison of GOME-2 measured reflectivities with the output from V-Lidort in both target areas, and for the same times as in Figure 94. The top panels show the average over all residuals to V-Lidort per Metop-B / FM2 (M01) and Metop-A / FM3 (M02) instrument. Like the previous co-location results, a linear background has been subtracted from the individual residual per channel in order to account for degradation and broad band effects as, for example, deficiencies in the albedo value used by V-Lidort. The lower panel then provides the differences between both residuals. This should result in the same instrument-to-instrument comparison as provided previously for the co-location results.

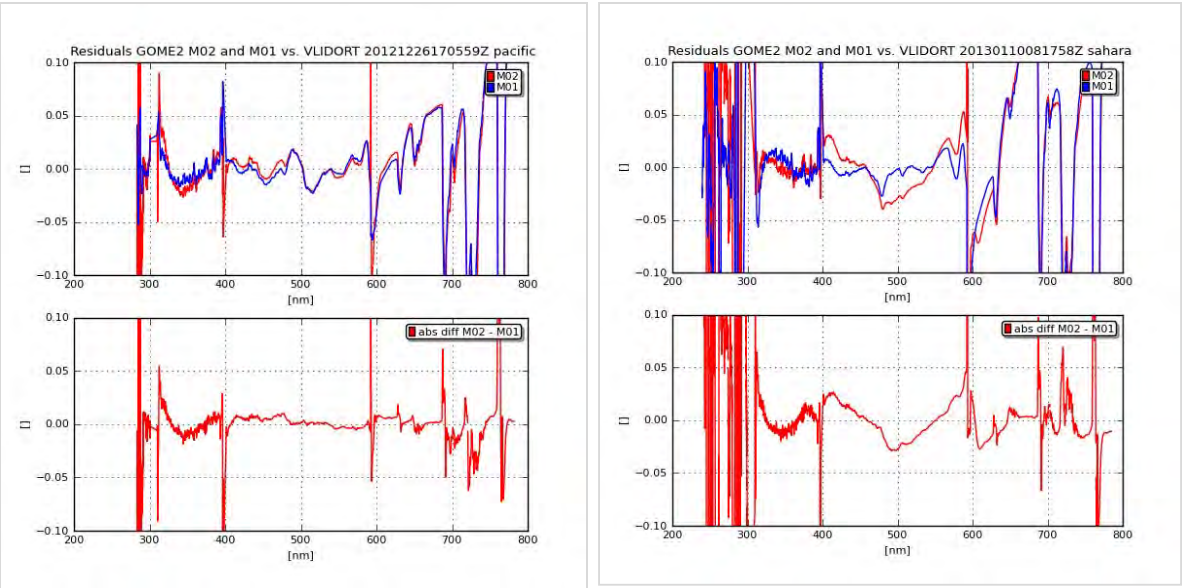

Figure 100: The top panel show Metop-A / FM3 (red line) and Metop-B / FM2 (blue line) reflectivity residuals to V-Lidort forward model results averaged on 26 December 2012 (left panels) and for 10 January 2013 (right panels) for the Pacific and the Sahara box. The lower panel show the differences between the residuals in the top panel and should therefor be conceptionally the same as the residuals shown in Figure 94.

In channel 2, the observed residuals between both measurements are similar in shape to the residuals provided for the same case for the co-located results in Figure 94. The remaining residual can be attributed to the degradation of the instrument FM3. In channel 3, where the overall degradation contribution is flatter (excluding the “artefact” introduced by the O_2-O_2 absorption around 475 nm) some of the observed broad band residual can be referred to the absorption of dust/sand which has a similar spectral signature and is consequently not observed for the Pacific box. Again channel 4 is dominated by atmospheric residual absorption patterns and does not reveal any particular additional broad-band residual effects.

The much larger spectral structures in channel 1 have been also linked to the Metop-A / FM3 degradation residuals. In addition, the forward model systematic errors are expected to become quite large below 310 nm because of the strong ozone absorption–for which small errors in the scope of the profile distribution may have large effects on the residual.

Finally, bear in mind that, generally, high-frequency spectral structures observed in the data are more problematic for DOAS-type level 2 retrievals than for broad-band structures, since they may interfere with differential spectral absorption patterns of the targeted species.

4.13 Signal levels (A4.3.5)

Degrading signal throughput levels have been a concern for FM3 on Metop-A throughout its current mission. Throughput decrease for FM3 has been quite strong before September 2009 (second throughput test) especially in channel 1 and 2, and has significantly decreased afterwards. For a detailed summary of the changing throughput level issue on Metop-A / FM3, see [RD7]. For an extensive evaluation of signal levels after reprocessing R2 of FM3 data see [RD8].

Since no fundamental single element could be identified as the cause of the degradation, it has been considered very probable that throughput degradation above the nominal level (degradation of throughput because of mirror degradation) might also be expected for FM2. During the IOV phase of Metop-B / FM2, we decided to carry out a similar throughput test as was carried out for Metop-A / FM3 in January 2009 (first throughput test). In this test, the detector temperatures have been increased from nominal operations temperature levels at 235 K up to 255 K (in increments of 5 K), just below the temperature of the optical bench. This test was meant to serve two objectives:

- To investigate if the observed immediate response of signal levels to temperature changes in FM3 was also present for FM2.
- To provide a reference for the long-term monitoring concerning the magnitude of 1. For FM3 it has been observed that this magnitude was increasing over time.

In the following section, we provide a summary of the observed FM2 signal levels for the first three months after the acquisition of the first solar spectrum 29 October 2012, and compare them to the signal levels acquired for FM3 during the same time span, early in its mission lifetime. Before looking at the data presented in 4.13.1, please read the disclaimer on the following page.

Important disclaimer

1. MPSTAR OPE FM2 data from after 28 November 2012 cannot be mixed with the data before this date without reprocessing of FM2 level 1 data with INS 1.02 and CAL 1.01 or higher versions. This is due to the adjustment of the overlap region between channel 1 and 2 and 2 and 3 introduced by 28 November 2012 in CGS1 (see Section 4.8).
2. For the period of the IOV throughput phase 7 test please note the following:
   The initial solar spectrum from the first throughput-test timeline at orbit 705 with sensing time 201211060707 should be neglected from any analysis. This is true for both main channel as well as PMD results.
   For main channel, there is a significant etalon in the spectrum visible which could not be corrected properly during the processing since in the previous obit the DSM sets (orbit 704; see IOV schedule) the main channel coolers have been switched off during the period of 05:20 to 07:00 UTC and went back to 260K (the DSM sets automatically turn all channel coolers off and since there was no new timeline after the DSM set the coolers stayed off during this orbit. However, a DSM command had been sent mistakenly to turn the PMD coolers on immediately after the DSM set, such that the PMD coolers effectively stayed on and were only switched off as planned in the subsequent pass (EUM/EPS/AR/14456). At 07:00, they were back to 235 K as planned for the first throughput test timeline in orbit 705. During this transient period, the Etalon effect due to changing layers on the optics and the detectors changes. But since the solar spectrum is taken at the beginning of the timeline and not after the WLS measurement this initial main channel solar spectrum could not be properly corrected for the changed etalon. This is a transient effect since the WLS are taken shortly afterwards and the next solar spectrum taken is fine again. For the PMDs the coolers have been triggered to ground line as planned just before the beginning of the timeline. This means that PMD detectors (both for PMD-P and S) were at 265 K at 07:00 UTC. Since no dedicated dark measurements could be taken for this first solar spectrum, the measurement has been flagged as non-valid in the database. Again this is a transient effect and is solved by the next solar spectrum for PMDs for which adequate measurements could be taken.
3. No PMD data from the solar measurements could be acquired during the IOV throughput test because of a problem in the timelines (EUM/EPS/AR/14471).
4. *The period of the "darkness-test" implemented between 14 and 28 March 2013 is outside the scope of the commissioning campaign. Evaluations by the instrument team, ESA/SSST, and the industrial partners are currently underway.*

.

4.13.1 Signal Throughput of Metop-B / FM2 – Commissioning Period

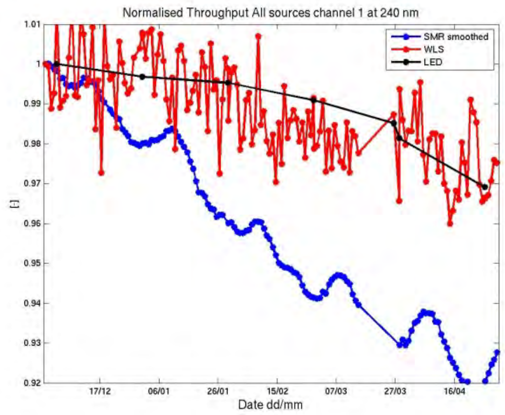

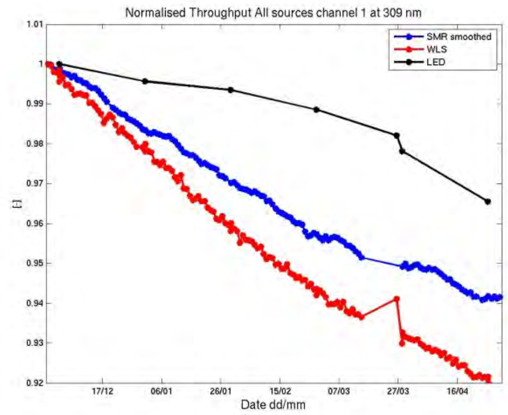

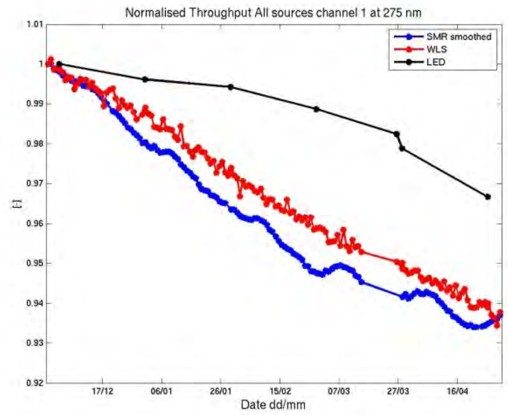

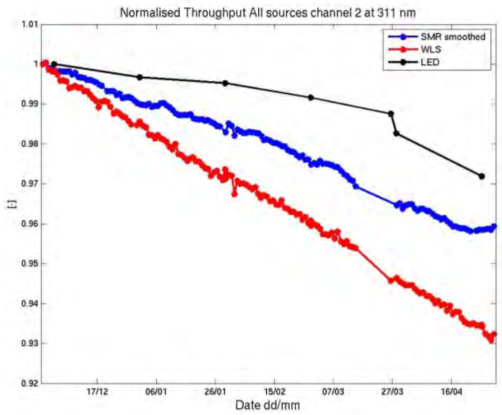

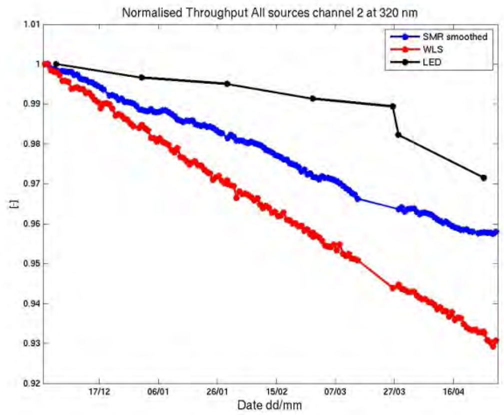

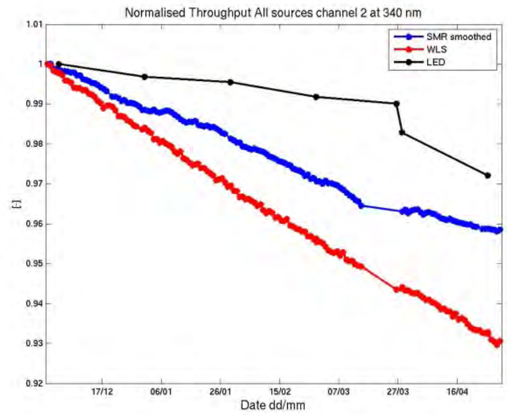

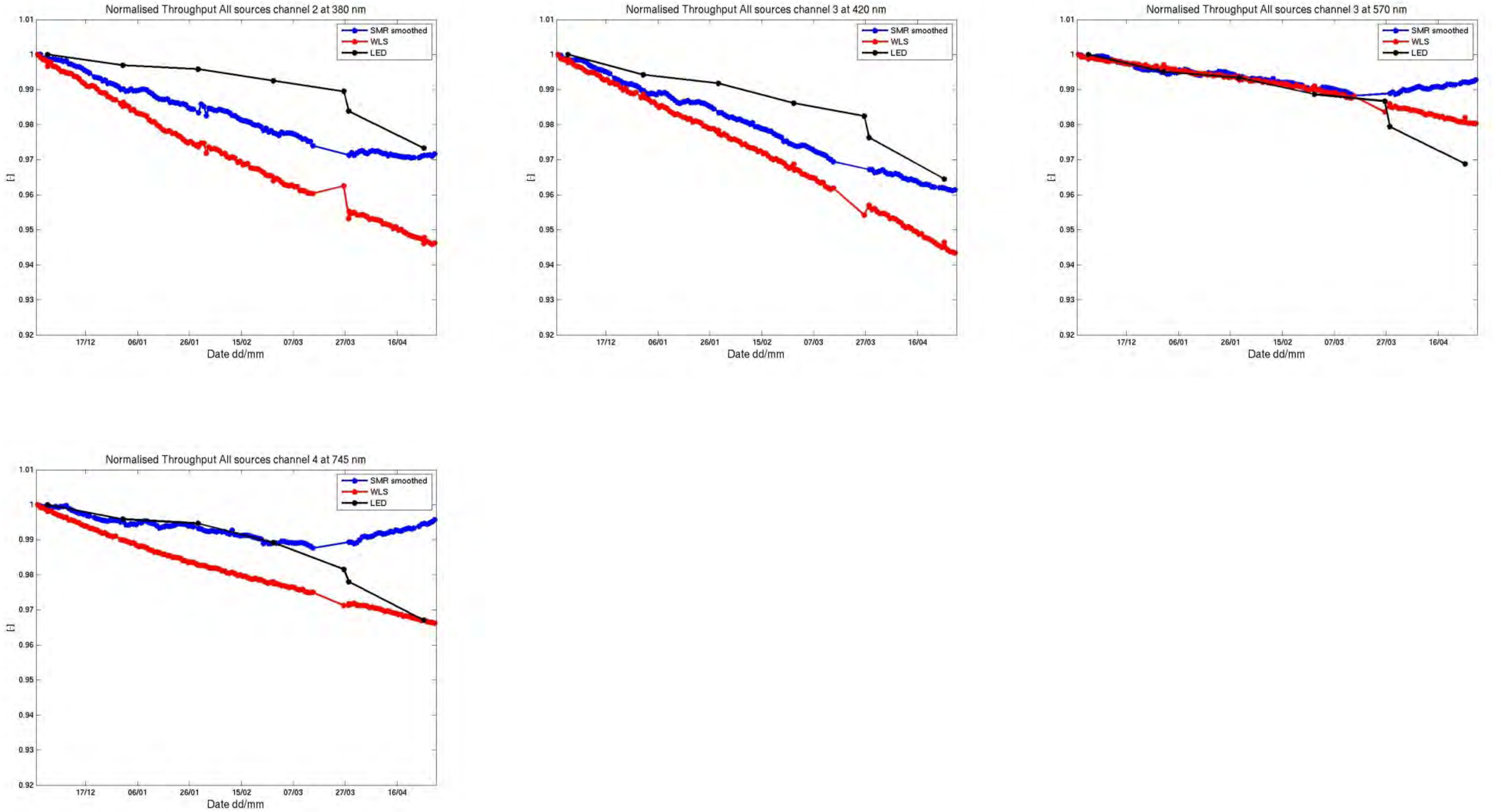

Figure 101: Signal levels for Metop-B / FM2 at various wavelength (see panel title) normalised to 28 November 2012 (for LEDs to 2 December) until 1 May2013. Solar mean reference (SMR) measurements are shown in blue, whitle light source (WLS) measurments in red and LED measurments in black (last LED measurement at 26 April 2013 during monthly calibratino). LED signals emit at 570 nm on all panels!

Figure 101 presents normalised signal levels for Metop-B / FM2 with respect to 28 November 2012 (after radiometric key-data update CAL 1.02). The results present white light source data (WLS) and solar mean reference data (SMR), as well as LED data. Spectral light source data is omitted because this source is not stable enough (as for FM3). The overall and inter-source observations are generally the same as for FM3 on Metop-A. The strongest degradation is observed in the UV with a decreasing degradation rate towards the NIR, with the exception that the WLS degrades more strongly at 745 nm than at 570 nm (as observed on FM3). The WLS source is too noisy to be considered reliable in the extreme UV and degrades generally faster than the SMR spectrum, which is, as far as FM3 is considered, to be due to additional blackening of the lamp [RD7]. The far UV also exhibits a more pronounced variation in SMR, which is due to solar activity.

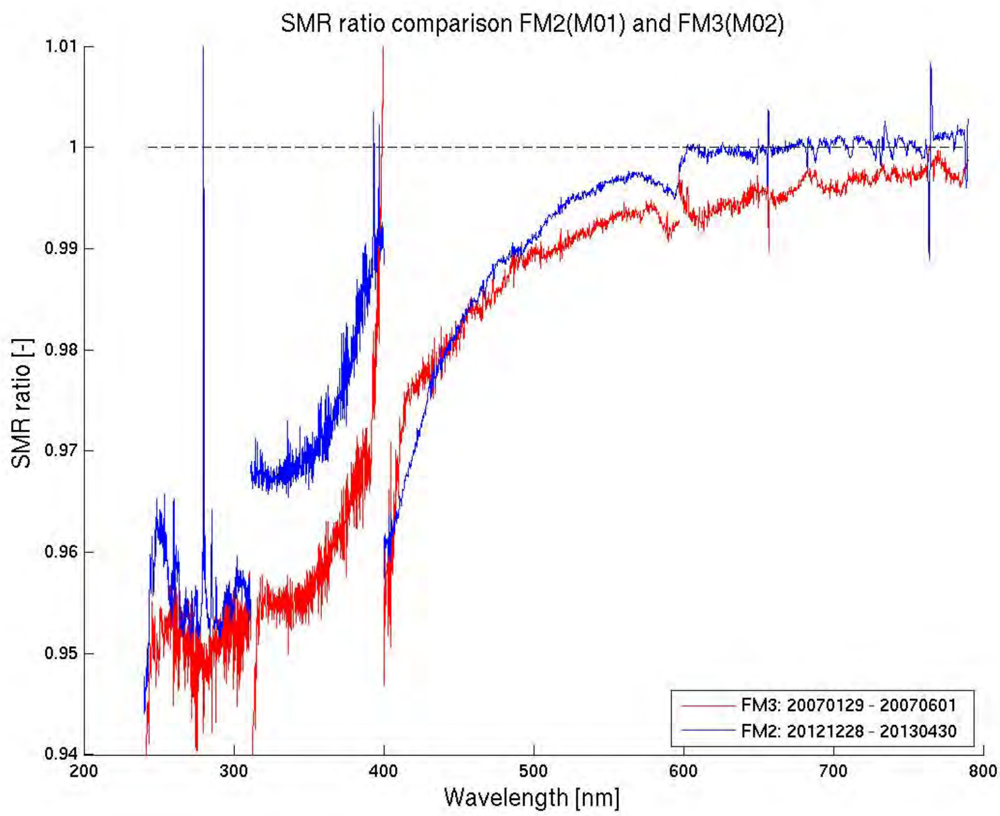

Figure 102: The ratio of the solar mean reference spectrum (SMR) of Metop-B / FM2 taken on 30 April 2013 with respect to the SMR taken at the 28 December 2012 (blue line) is compared with the SMR ratio for Metop-A / FM3 taken at the 1 June 2007 with respect to the 29 January 2007. Both instrumentsmark 102 days in orbit.The ratio covers a time span of exactly 123 days for both instruments.

Figure 102 shows the SMR ratio of both FM3 and FM2 using four month of data. Both instruments have been in orbit for 102 days. The Metop-A / FM3 ratio is based on reprocessed data R2 using the same processor version level than Metop-B / FM2. The results indicate that Metop-B / FM2 signal degradation is overall similar to that of FM3– except for channel 2. Overall, channel 2 appears to degrade differently (less) than channel 1 on the blue side. Also for channels 3 and 4 on FM2 we can conclude that degradation rates are a bit lower than for FM3. Initially, channel 4 has been degrading slightly but has recently increased its signal levels once again.

Figure 103 shows the same analysis using PMD-S and PMD-P but confirming the overall similar behaviour to the main channel degradation with a bit higher degradation rates in the UV and the visible region. PMD-P for FM2 is degrading in exactly the same way as for FM3, whereas PMD-S is degrading significantly faster for FM2 than it has been degrading for FM3, especially in the UV and visible region.

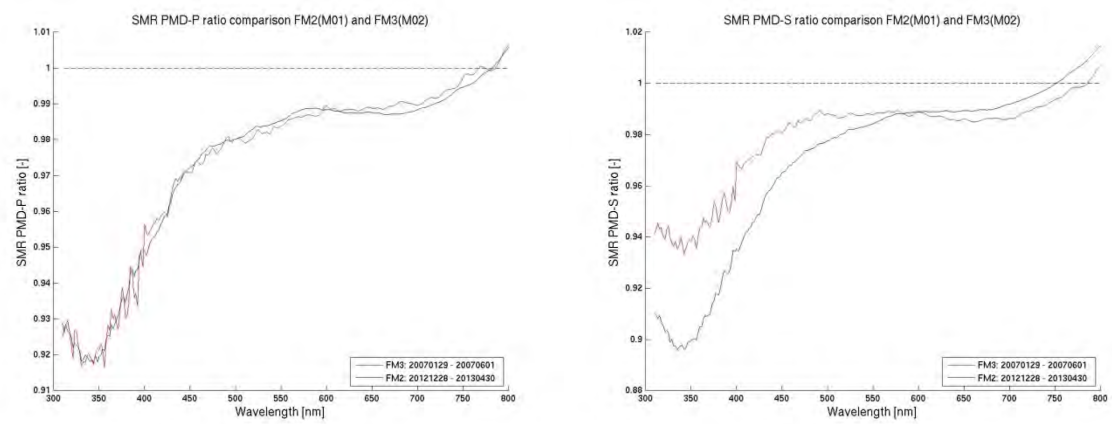

Figure 103: The ratio of the solar mean reference spectrum (SMR) PMD-P (left panel) and PMD-S (right panel) of Metop-B / FM2 taken on 30 April 2013 with respect to the SMR PMD-P and PMD-S taken on 28 December 2012 (blue line) is compared with the SMR ratio for Metop-A / FM3 taken at the 1 June 2007 with respect to 29 January 2007. Both instruments mark 102 days in orbit. The ratio covers a time -span of exactly 123 days for both instruments..

4.14 Geo-referencing (A5.1)

Geo-location parameters are processed during level 0-to-1B processing both for a fixed grid of 32 read-outs per scan and for an individual grid based on the actual integration time of an instrument band. For reference, GOME-2 channels 1 and 2 are separated into two bands each, as are the PMD channels—both short-wave and main PMD bands—such that there are ten bands in total that potentially can be commanded with different integration times, leading to different ground footprints. In practice, GOME-2 instrument timelines include only four different integration times per scan:

- IT1 for band 1a
- IT2 for band 1b to 4
- IT3 for PMD main channels
- IT4 for PMD short-wave channels.

However, IT1 and IT2 change over the orbit from longer to shorter integration times along decreasing solar zenith angles.

For GOME-2 level 1 processing, predicted orbit state vectors are used for near real-time processing. The accuracy of the predicted orbit is significantly less than 100 m. Therefore, an upper limit bias on the calculated geo-referencing parameters of 1 % of across-track pixel size for PMDs (0.25 % along track) and 0.6 % for main channels (0.25 % along track) are estimated with respect to dedicated corrected orbits for reprocessing. The effect is considered negligible with respect to the pointing accuracy of the instrument.

For the evaluation of the geo-pointing accuracy, we convolve GOME-2 radiances in channels 3 and 4 with the AVHRR spectral response function and compare the result to the averaged radiometric signal from AVHRR within one GOME-2 ground pixel (using IT2 for channel 3 and 4). The geo-location data for the GOME-2 ground pixel box is subsequently modified in an iterative process and re-fitted with the averaged AVHRR radiances until an optimal correlation between both, GOME-2 and AVHRR averaged radiances, is achieved. Along-track, the delta on the GOME-2 geo-location data should be zero, whereas across-track there is an offset of 5-15 % of the (varying) pixel size expected due to spatial aliasing. Spatial aliasing can be defined as the time that has to be accounted for during the duration of read-out of the detector arrays of GOME-2, a time period during which the spacecraft moves. For more details, see PGS 7, Section 5.3.16 and [AD3]..

Below, Figure 104 shows the along-track and across-track offsets for Metop-B / FM2 (using AVHRR Metop-B) over one orbit on 3November 2012. The scatter in the results is due to the differences in fit residuals, depending on the “information content” of the scene. For a scene with a lot of albedo variations (broken cloud fields, for example) one GOME-2 measurement covers a large variation in signal level as measured by AVHRR and therefore provides a more robust (smaller fitting error) correlation result. Note that, because of the latter, multiple pixels at the same scanner position for each product dissemination unit (PDU), (for example 30 GOME-2 measurements at a time) are used for the optimisation procedure (striping along-track). As expected, the along-track offset is close to zero and the across-track offset is around 10 % for the reference orbit due to smaller relative fraction for larger pixels at the edges and larger relative fraction for smaller-nadir ground pixels.

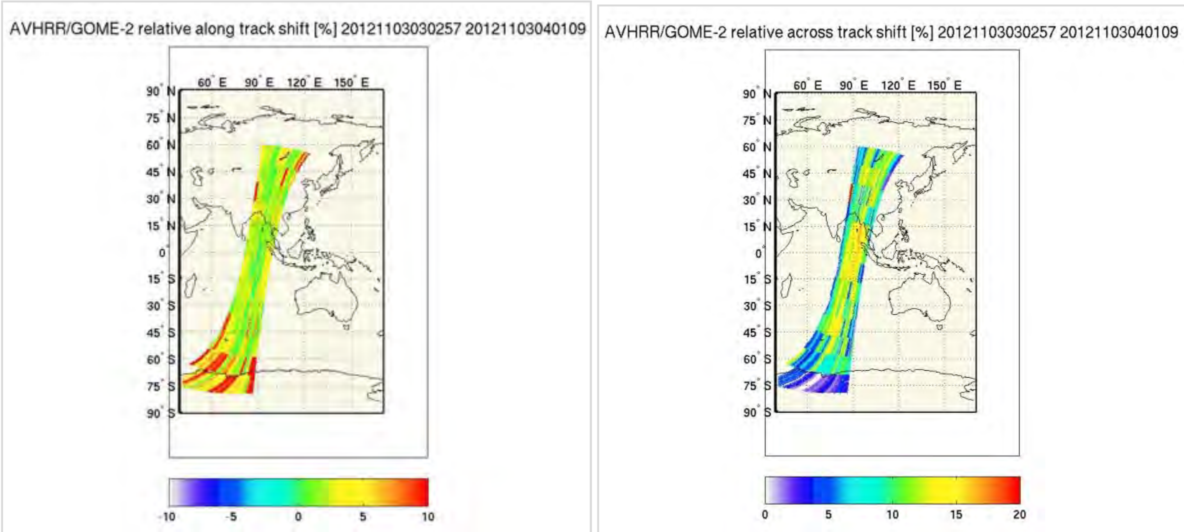

Figure 104: Metop-B / FM2 along-track (left panels) and across-track (right panels) relative shifts of the geo-location as evaluated from co-location to AVHRR signals for one orbit on 3 November 2012.

We compare the results to the corresponding orbit (in time) of Metop-A / FM3 and find similar offsets and shifts.

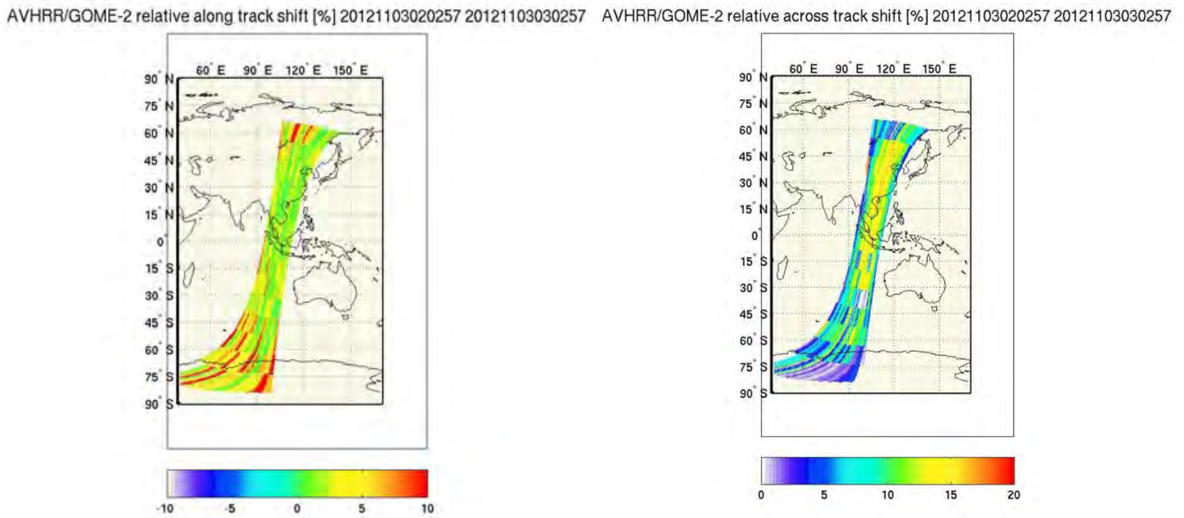

Figure 105: Metop-A / FM3 along-track (left panels) and across-track (right panels) relative shifts of the geo-location as evaluated from co-location to AVHRR signals for one orbit on 3 November 2012.

.

5 EXTERNAL PARTNER VALIDATION

5.1 Scope of Validation

External partner validation is based (and restricted to) the demonstrational and pre-operational phase of GOME-2 Metop-B / FM2 level 1 data dissemination. The list of Cal-Val partners involved in this phase included all operational level 2 data producers from the ozone SAF (o3msaf.fmi.fi) and its partners (like BIRA), the University of Bremen, the Institute for Environmental Physics, and NOAA.

In the following section, we are summarising results based on comparisons of FM2 level 2 data with current products from Metop-A / FM3, and with products derived from reprocessed (R2) level 1 data from Metop-A in early 2007. Some validations have also been focussed on sensitivity studies and fit residual evaluations, which are summarised here to the extent that they are relevant for on-going analysis on residual spectral patterns.

Note: The wavelength region provided in the header title for each product is only a rough indication, since individual products may cover slightly different spectral regions

5.2 Validation results

5.2.1 Level 2 comparison with Metop-A / FM3 results

5.2.1.1 Total ozone: 320 nm-335 nm; Channel 2

5.2.1.1.1 DLR / Operational O3MSAF product

DLR / O3MSAF observation in (Figure 106): A negative bias of FM2 total ozone w.r.t. FM3, which further increases the already observed bias of –1 % of FM3 total ozone with respect to ground based measurements [RD20]. An additional bias is further substantiated by the fact that the observed RMS fitting residual are also slightly higher than for FM3 at an early mission stage (January 2008).

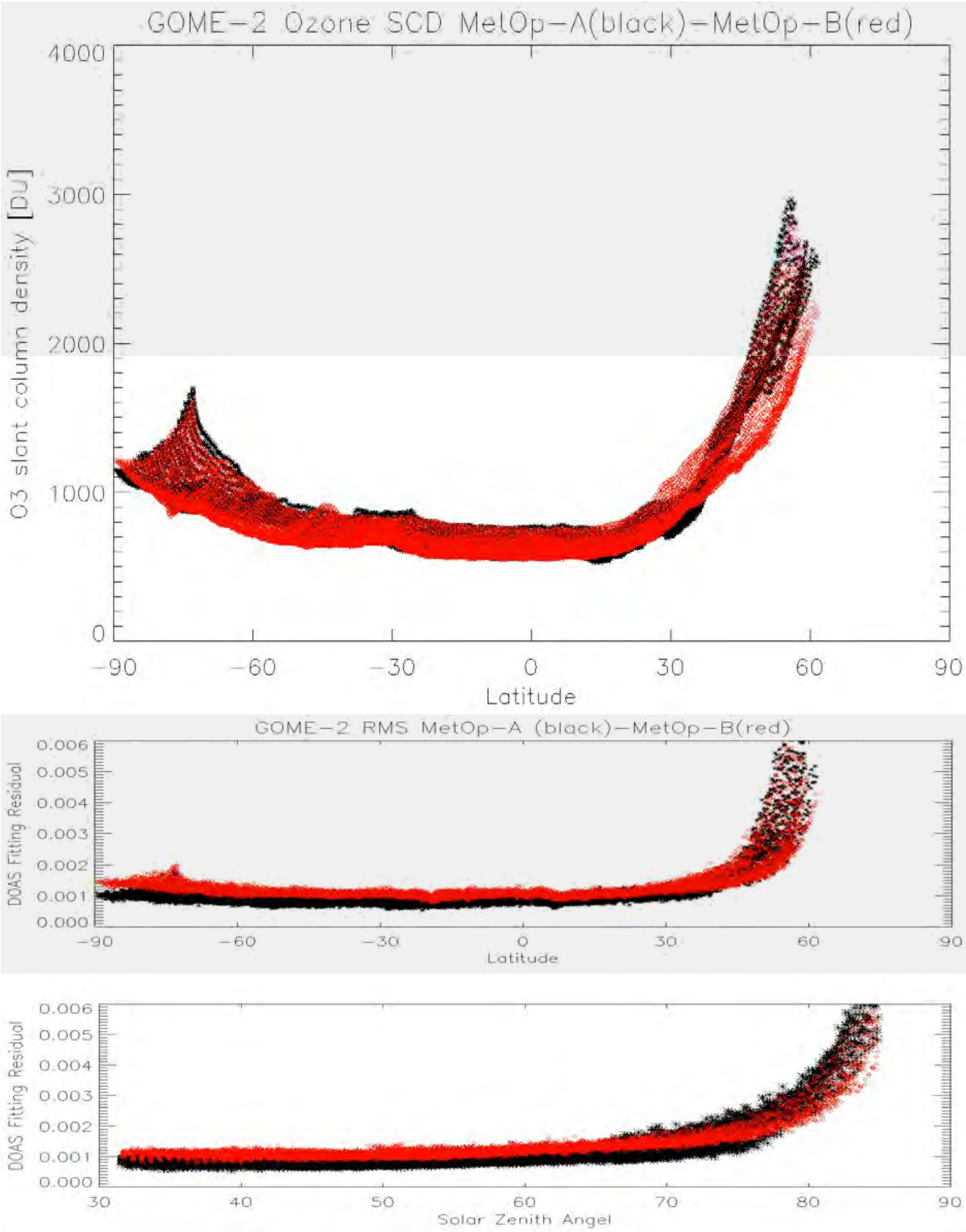

Figure 106: Total ozone column for Metop-B / FM2 (red) and Metop-A / FM3 (black) are provided in the upper panel for 5 January 2013 and 5 January 2008 respectively The middle and the lower panels show the corresponding RMS fitting residuals as order in latitude and solar zenith angle respectively.

5.2.1.1.2 Institute für Umweltphysik (IUP) Bremen

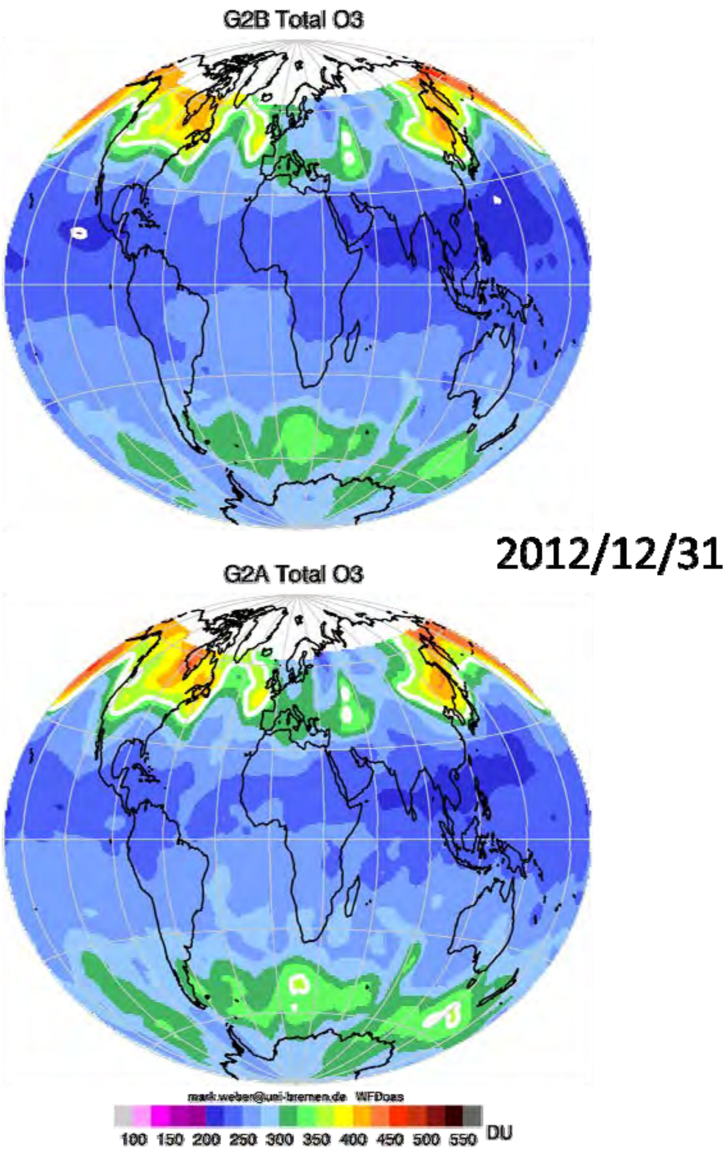

Figure 107: IUP-Bremen derived total ozone column for Metop-B / FM2 (G2B; top panel) and Metop-A / FM3 (G2A; bottom panel) 31 December 2012.

The IUP Bremen detected various offsets when comparing Metop-B / FM2 with Metop-A / FM3 total ozone along the orbit 31December 2012 depending on different instalments of cross-sections (Figure 107 and Figure 108). Best results are biases around –0.2 % and are achieved when using high-resolution measurements of ozone cross-sections (Serdyuchenko et al., [RD22], [RD23]) convolved with the official EUMETSAT/RAL FM2 dedicated slit-function measurements [RD24].

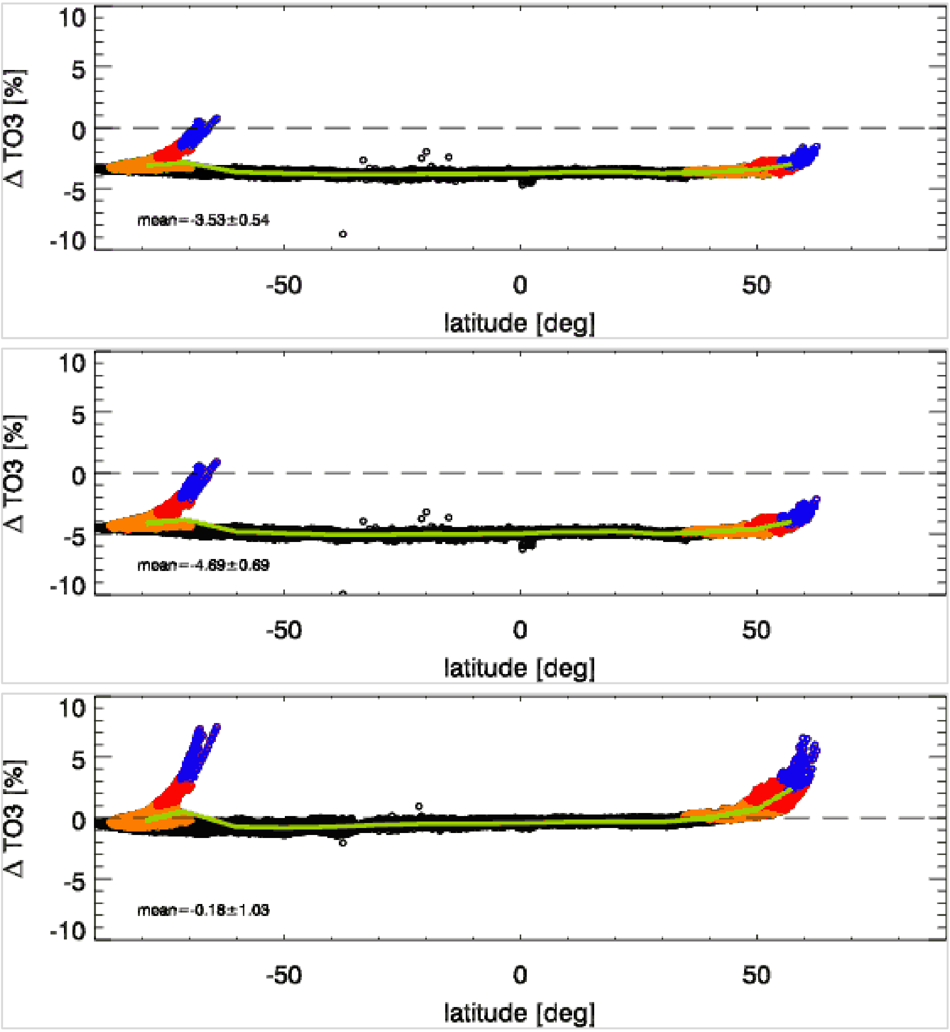

Figure 108: IUP-Bremen total ozone column differences of Metop-B / FM2 with respect to Metop-A / FM3 on 31 December 2012, and for three different instalments of ozone cross-sections. Upper panel: CATGAS FM3 cross-sections (Burrows et al.) de-convolved and re-convolved with RAL FM3 slit-function. Middle panel: CATGAS FM3 cross-sections (Burrows et al.) de-convolved and re-convolved with the official EUMETSAT/RAL FM2 slit-function. Lower panel: Cross-sections by Serdyuchenko et al. [RD22][RD23], convolved with RAL FM2 slit-function.

5.2.1.1.3 Belgian Institute for Space Aeronomy (BIRA-IASB)

The Belgian Institute for Space Aeronomy (BIRA-IASB) find differences in total ozone between Metop-B / FM2 and Metop-A / FM3 on the order of –1 %, with FM2 being lower than FM2. This is of a similar order to the ones reported by DLR. It must be noted that BIRA-IASB uses a direct fitting approach (GODFIT) which is different from the DOAS approach, which uses V-Lidort derived AMF LUTs with the operational DLR GDP4.5 processor.

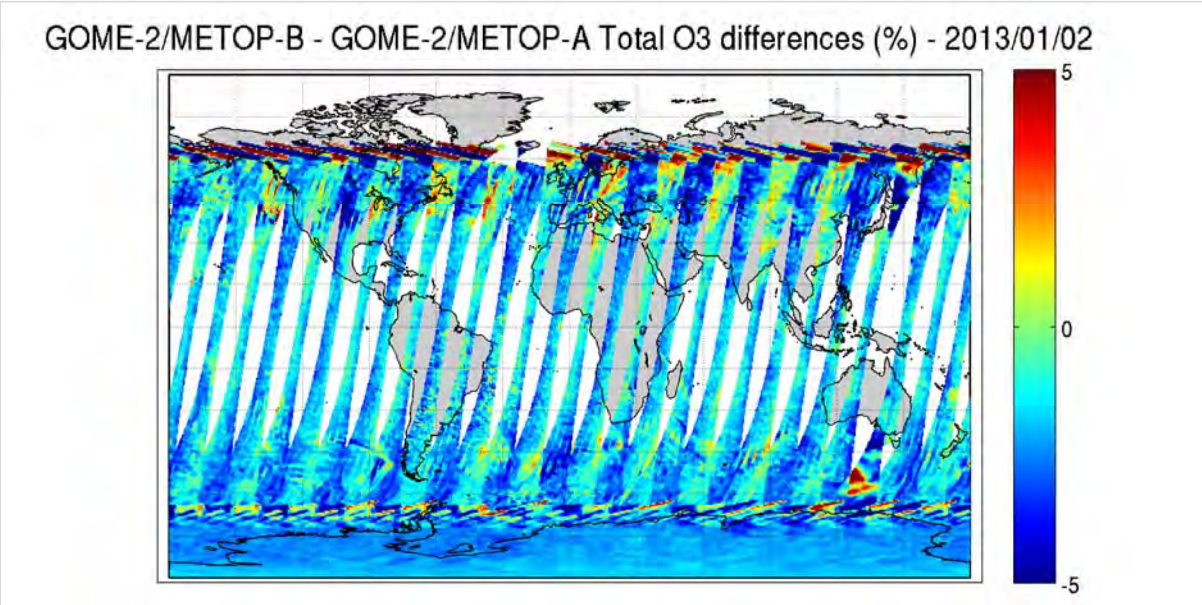

Figure 109: BIRA-IASB total ozone column differences of Metop-B / FM2 with respect to Metop-A / FM3 on 2 January 2013.

BIRA-IASB reports an offset of –3 % to –4 % with respect to the early mission FM3 situation (Figure 109). They also report that the fitting of a wavelength-dependent offset helps to reduce the fit residual (see Figure 118 in Section 5.2.2.3).

5.2.1.2 BrO: 330 nm-360 nm; Channel 2

5.2.1.2.1 Institute für Umweltphysik (IUP) Bremen

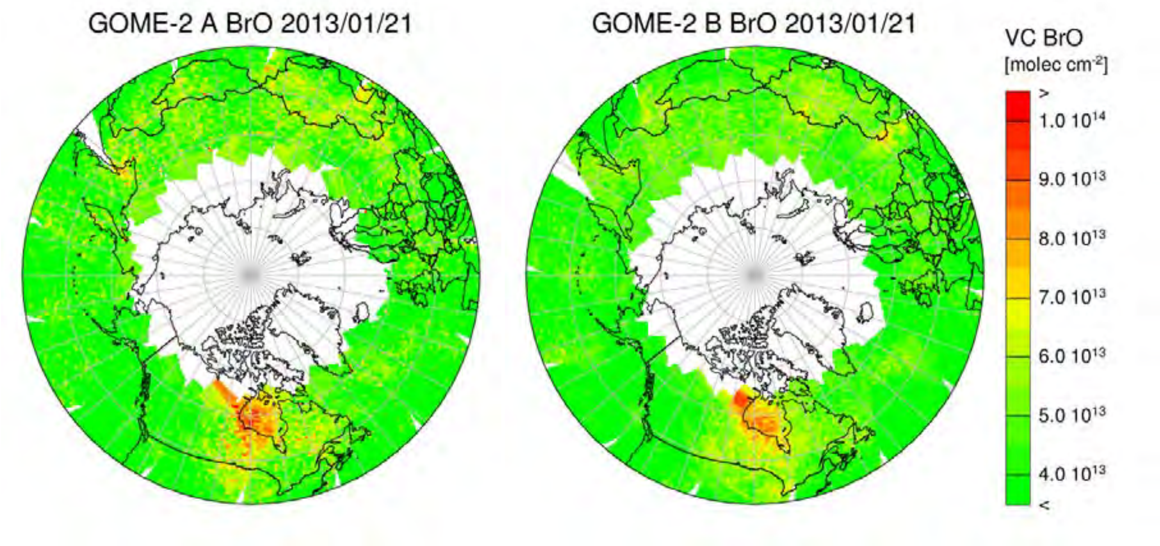

Figure 110: BrO total columns as retrieved by IUP Bremen for Metop-A / FM3 (left panel) and Metop-B / FM2 (right panel).

IUP Bremen reports similar results for BrO total column retrievals from Metop-A / FM3 and Metop-B / FM2 on 21 January 2013. See Figure 110. However, the signal-to-noise ratio for the BrO retrievals for FM2 is much higher than for FM3. These BrO retrievals for FM2 do not require any additional offset corrections at present, but this can change after further evaluation.

5.2.1.2.2 BIRA-IASB

BIRA-IASB had the same conclusion on BrO slant columns when they compared Metop-A / FM3 and Metop-B / FM2. See Figure 111. They found a small positive difference in FM2 retrievals and generally reduced scatter in slant column when compared to the segment in January 2007 for FM3. Furthermore, they find no dependence of the slant column values on the viewing angle Figure 112.

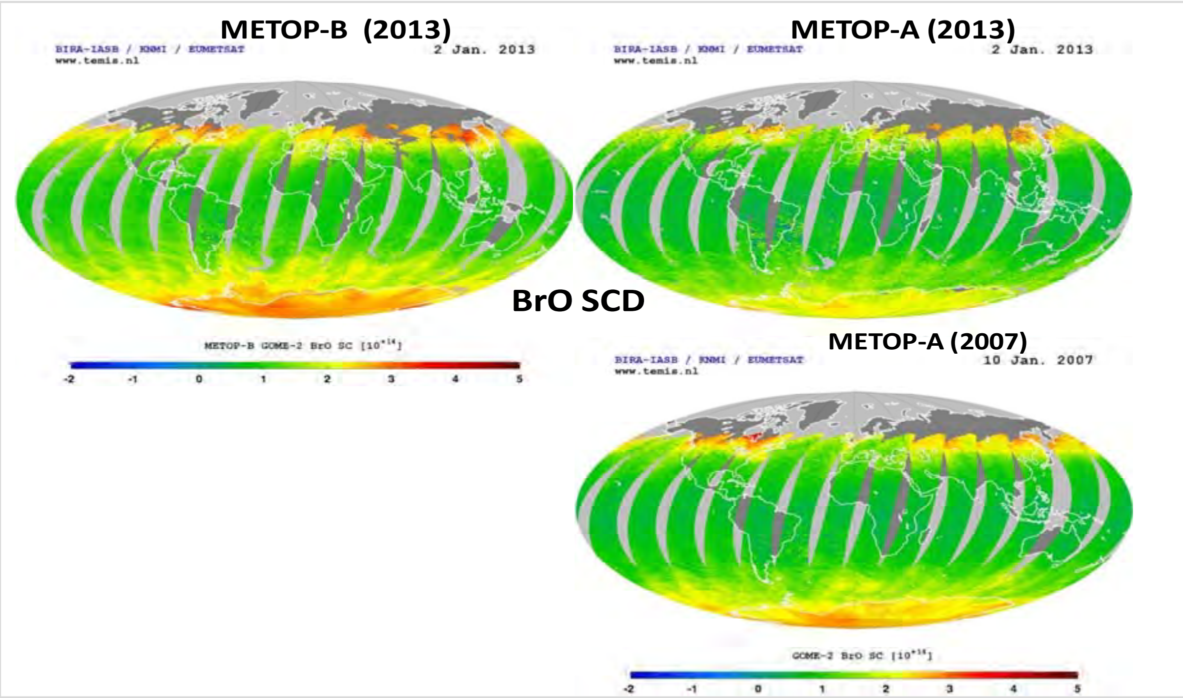

Figure 111: BrO slant columns as retrieved by BIRA-IASB for Metop-A / FM3 January 2013 (left panel) and Metop-B / FM2 January 2013 (right upper panel) and January 2007 (right lower panel).

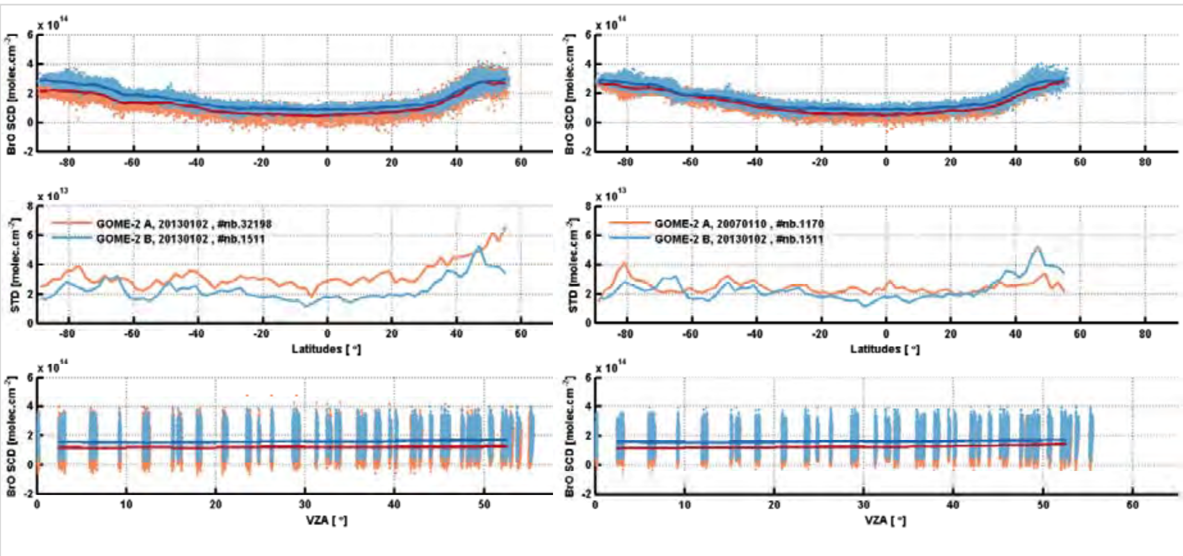

Figure 112: BrO slant columns as retrieved by BIRA-IASB for Metop-A / FM3(red) and Metop-B / FM2 (blue) with FM3 values from January 2013 (left panel) and from January 2007 (right panel).

5.2.1.2.3 DLR / O3MSAF

BrO slant-column densities as provided by the O3MSAF/DLR GDP 4.5 operational retrieval algorithm show very small differences between Metop-A / FM3 and Metop-B / FM2. FM3 data is from 15 December 2008 and FM2 data from the same day in 2012 (Figure 113). The same negligible differences can be seen for the corresponding-fit RMS residuals.

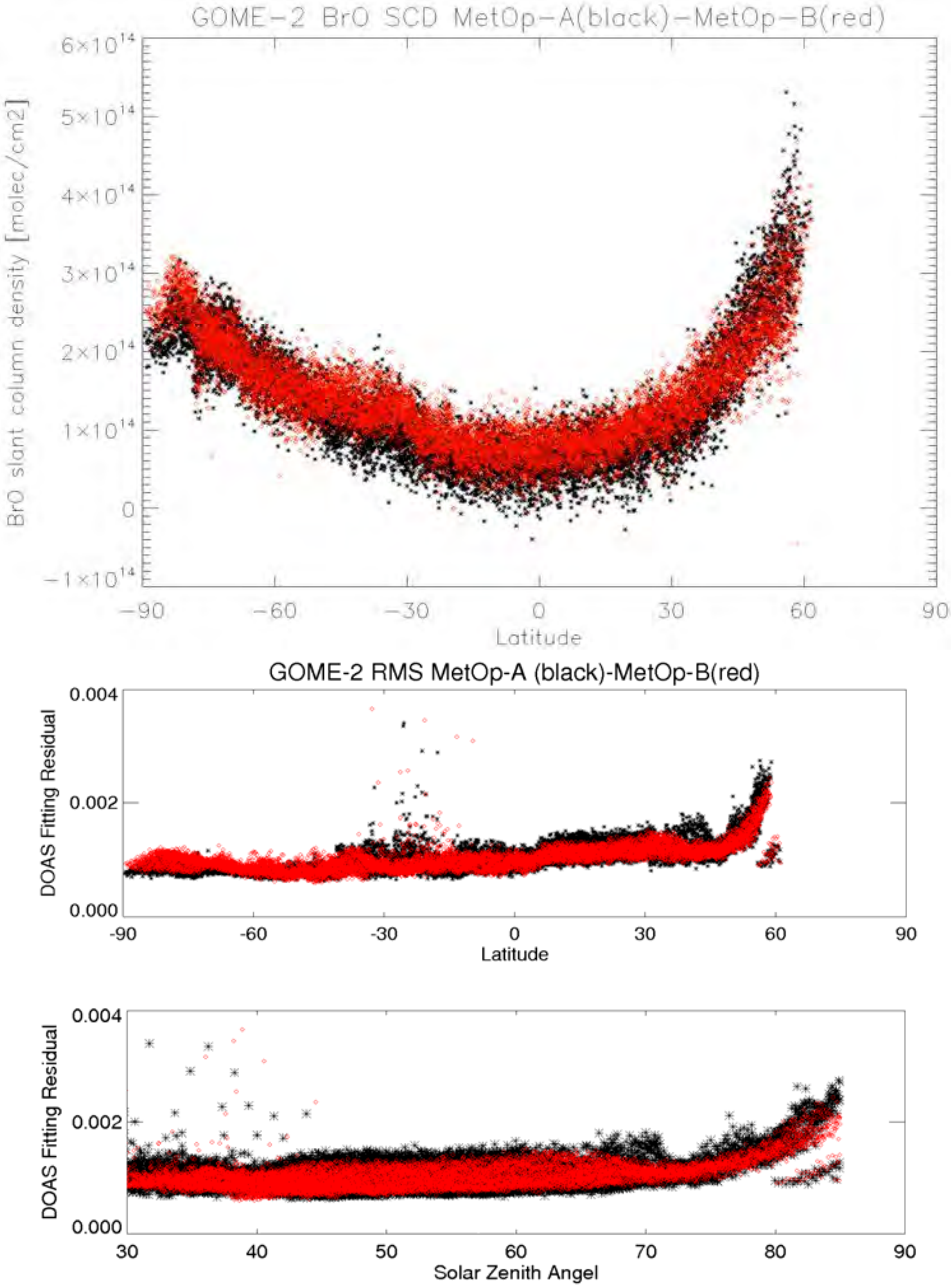

Figure 113: BrO slant columns for Metop-B / FM2 (red) and Metop-A / FM3 (black) are provided in the upper panel for 15 December 2012 and 15 December 2007 respectively. The middle and the lower panels show the corresponding RMS fitting residuals as ordered in latitude and solar zenith angle respectively.

5.2.1.3 H_2CO: 328 nm-348 nm; Channel 2

5.2.1.3.1 BIRA-IASB

BIRA-IASB retrievals of formaldehyde slant columns show similar results for both Metop-A / FM3 in January 2007 and recent Metop-B / FM2. See Figure 114. Also, the RMS-fit residual values are on the same order. BIRA-IASB also reports even slightly less noise on the slant-column values for Metop-B/FM2 than for FM3 in 2007, as observed in a pristine equatorial Pacific reference box (with “zero” signal background). The dependence of slant column values on the RMS-fit residuals and on SZA is also slightly smaller for Metop-B / FM2 than for Metop-A / FM3. For their best Metop-B / FM2 retrievals to date, they use a fitted asymmetric Gaussian slit-function shape based on TNO slit-function data from the key-data set. The correct, or yet-to-be-corrected usage, of the slit-function is an issue with the current level 2 retrievals from FM2 data and limits the interpretation of the results.

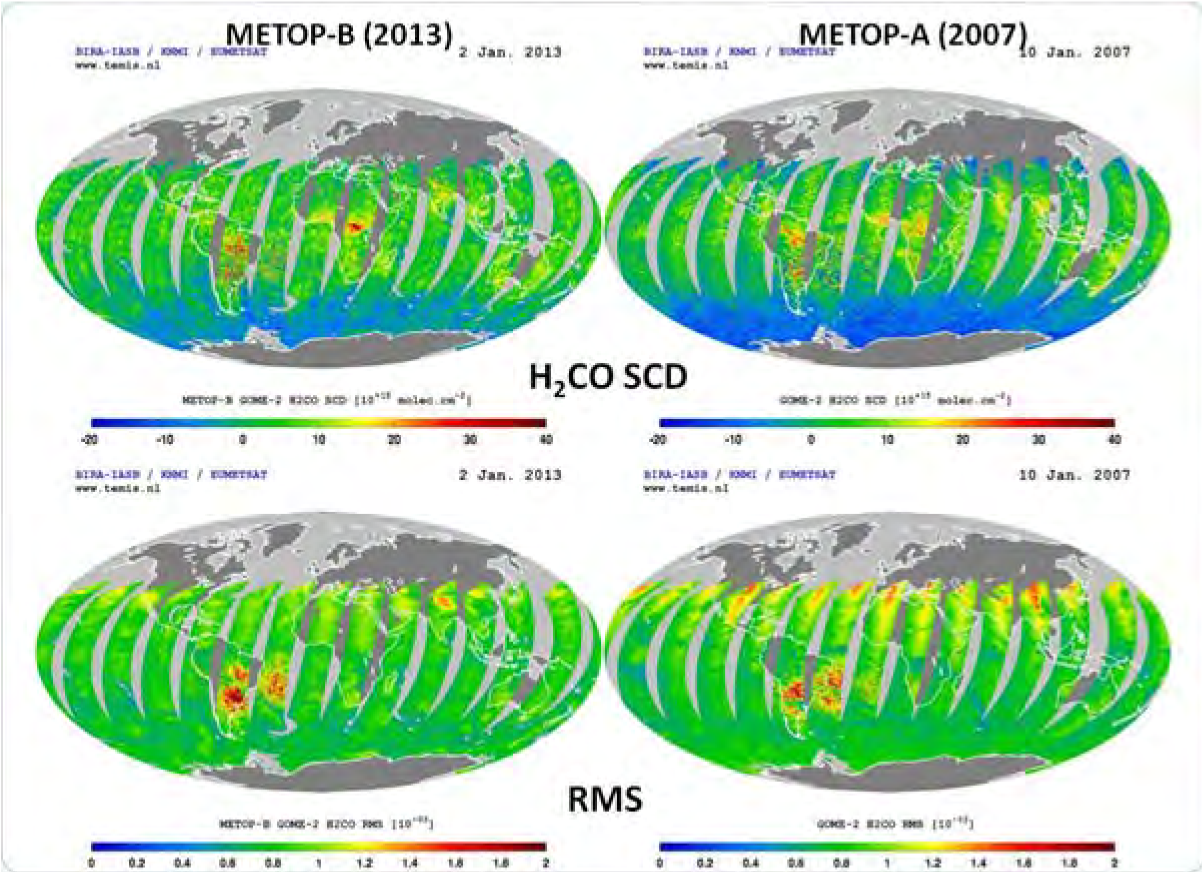

Figure 114: Formaldehyde slant columns (top panels) as retrieved by BIRA-IASB for Metop-A / FM3 (right panels) and for Metop-B / FM2 (left panels) with FM3 values from January 2007. The lower panel shows the RMS fit-residual values.

5.2.1.3.2 DLR / O3MSAF

Formaldehyde vertical column densities as retrieved by the O3MSAF/DLR GDP 4.5 operational retrieval algorithm show only minor differences between Metop-A / FM3 and Metop-B / FM2. FM3 data is from 15 December 2008 and FM2 data 15 December 2012 as shown in Figure 115. The corresponding-fit RMS residuals have the same minor differences, with Metop-B / FM2 being slightly larger on average, but with less scatter than FM3 in the corresponding in-orbit period.

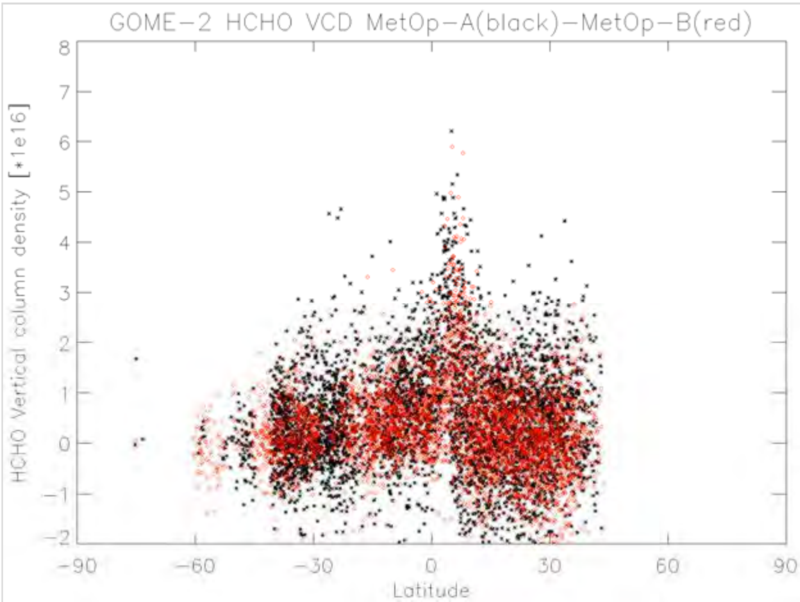

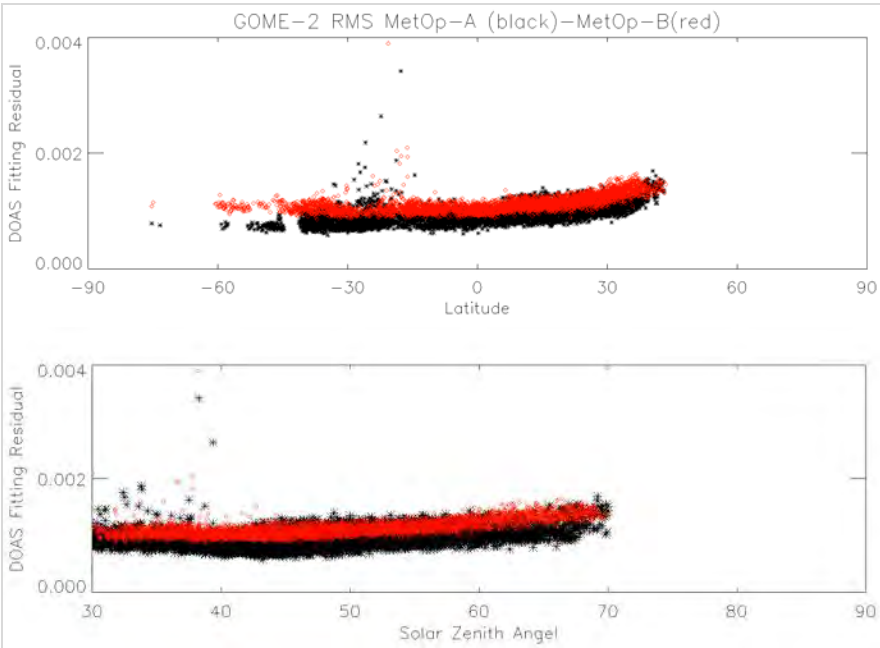

Figure 115: Formaldehyde total columns for Metop-B / FM2 (red) and Metop-A / FM3 (black) by DLR/O3MSAF are provided in the upper panel for 15 December 2012 and 15 December 2007 respectively. The middle and the lower panels show the corresponding RMS fitting residuals as ordered in latitude and solar zenith angle respectively.

5.2.1.4 NO_2: 425 nm- 450/500 nm; Channel 3

5.2.1.4.1 BIRA-IASB

The BIRA-IASB provided NO_2 slant columns and their RMS-fit residuals reports for both Metop-B / FM2 and Metop-A / FM3 for 5 January 2013 and 10 January 2007 respectively. BIRA-IASB makes use of two spectral bands for FM2–between 425 nm-450 nm and 450 nm-497 nm. The latter has been used by IUB Bremen previously to increase the retrievals sensitivity. Both retrievals show slightly or significantly higher RMS values. with significantly higher SCD for the latter. See Figure 116 on the following page. The larger retrieval window also shows signs of scan-angle-dependent patterns, the most significant of which is a sharp increase of the residual directly at the nadir point–which, in the first instance, BIRA-IASB attributes to their ζ-residual pattern. See also the following Section and Section 4.9.

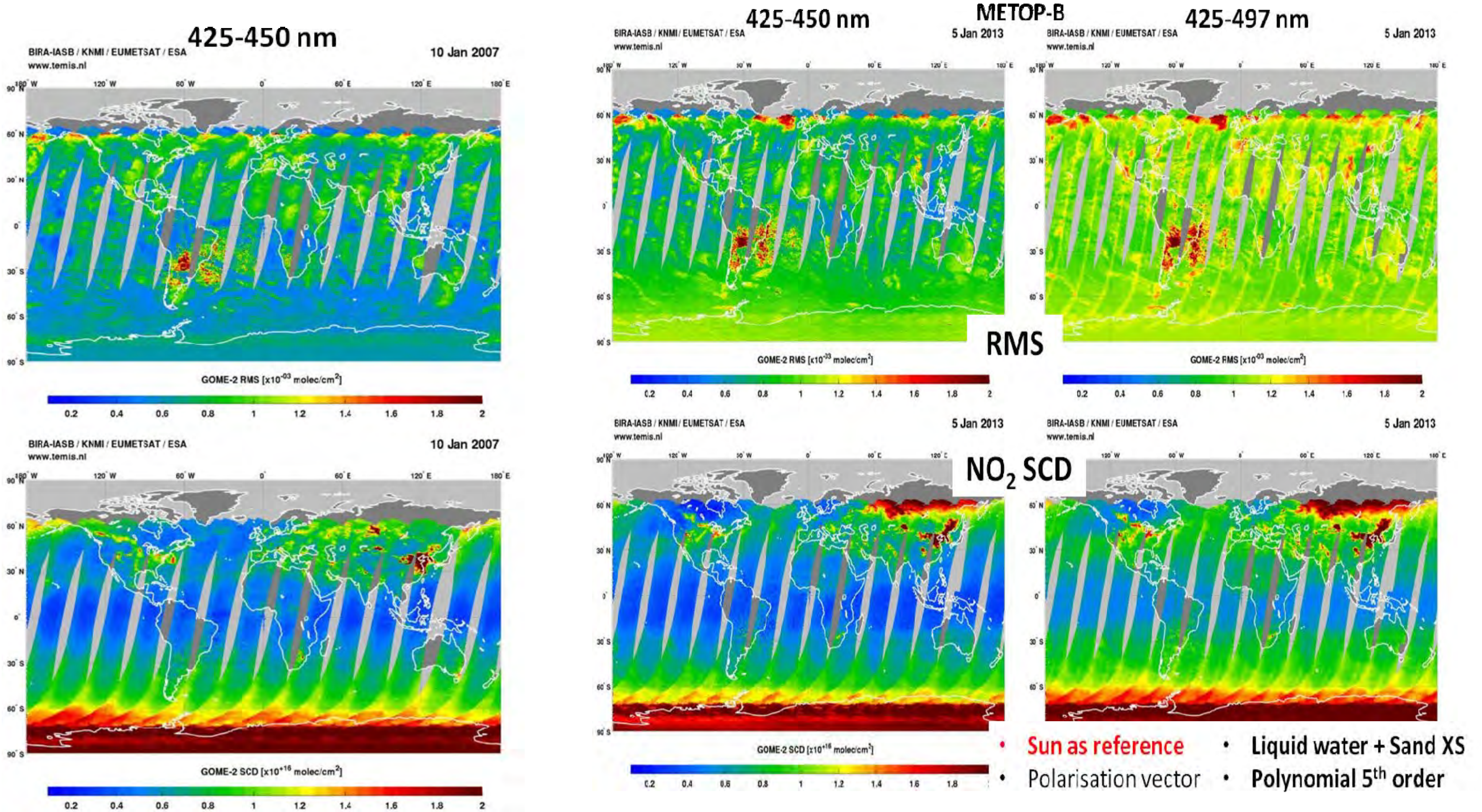

Figure 116: Retrievals of RMS fit residuals (upper panles) and ("stratospheric") slant columns (lower panels) of NO_2 by BIRA-IASB for Metop-A / FM3 (10th January 2007; left panel) and Metop-B / FM2 (5th January 2013) in two bands of 425-450 nm (middle panel) and 425-497 nm (right panel).

5.2.1.4.2 IUP Bremen

IUP Bremen retrievals show total “stratospheric” columns for NO_2 of the same order and with similar patterns for the two instruments. Generally, NO_2 columns from FM2 are lower than those from FM3 as shown in Figure 117.

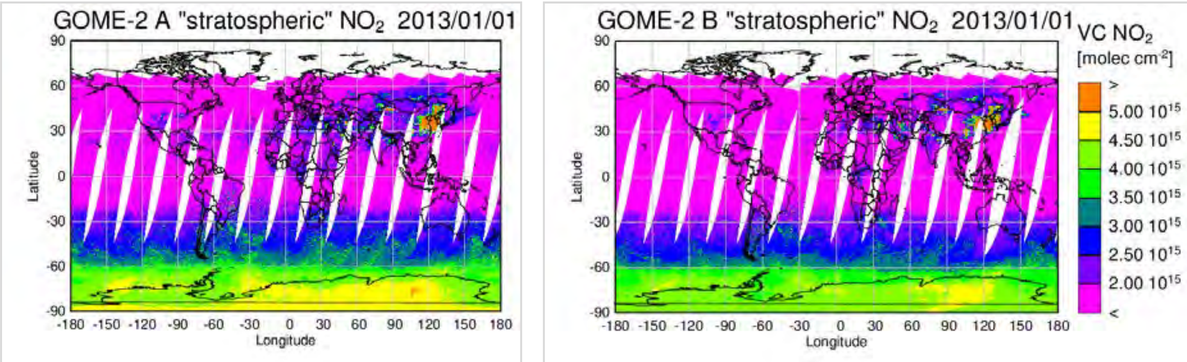

Figure 117: Retrievals of of total (“stratospheric”) columns for NO_2 by IUP Bremen for Metop-A / FM3 (1st January 2013; left panel) and Metop-B / FM2 (1st January 2013; right panel).

The slant columns show a viewing-angle-dependent offset after correction for LOS. It is important to note that IUP Bremen does not observe a cloud-dependent effect in this respect; there is no indication of a polarisation-correction-dependent offset. See Figure 118.

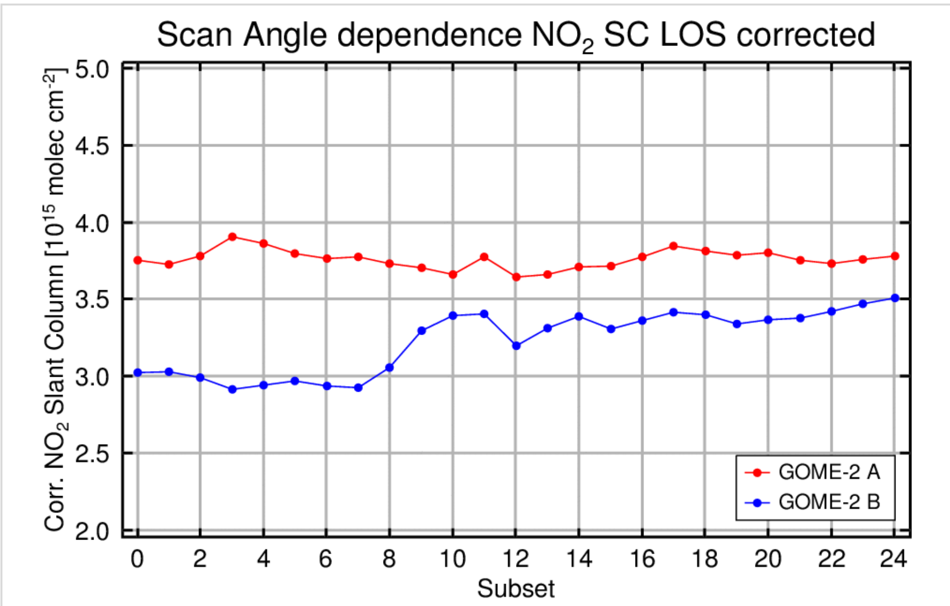

Figure 118:Viewing angle (line-of sight; LOS) dependent columns after bias correction for (“stratospheric”) slant column values of NO_2 as observed by IUP Bremen for Metop-A / FM3 (red line) and Metop-B / FM2 (blue line).

5.2.1.4.3 DLR / O3MSAF

DLR/O3MSAF GDP 4.5 retrievals of NO_2 show differences of +/– 5° molec./cm^2 between Metop-B / FM2 and Metop-A / FM3 for 1 January 2013, depending on viewing angle. See Figure 119. The fit residuals of Metop-B / FM2 are also significantly larger than those for Metop-A / FM3 at similar times in orbit as shown in Figure 120.

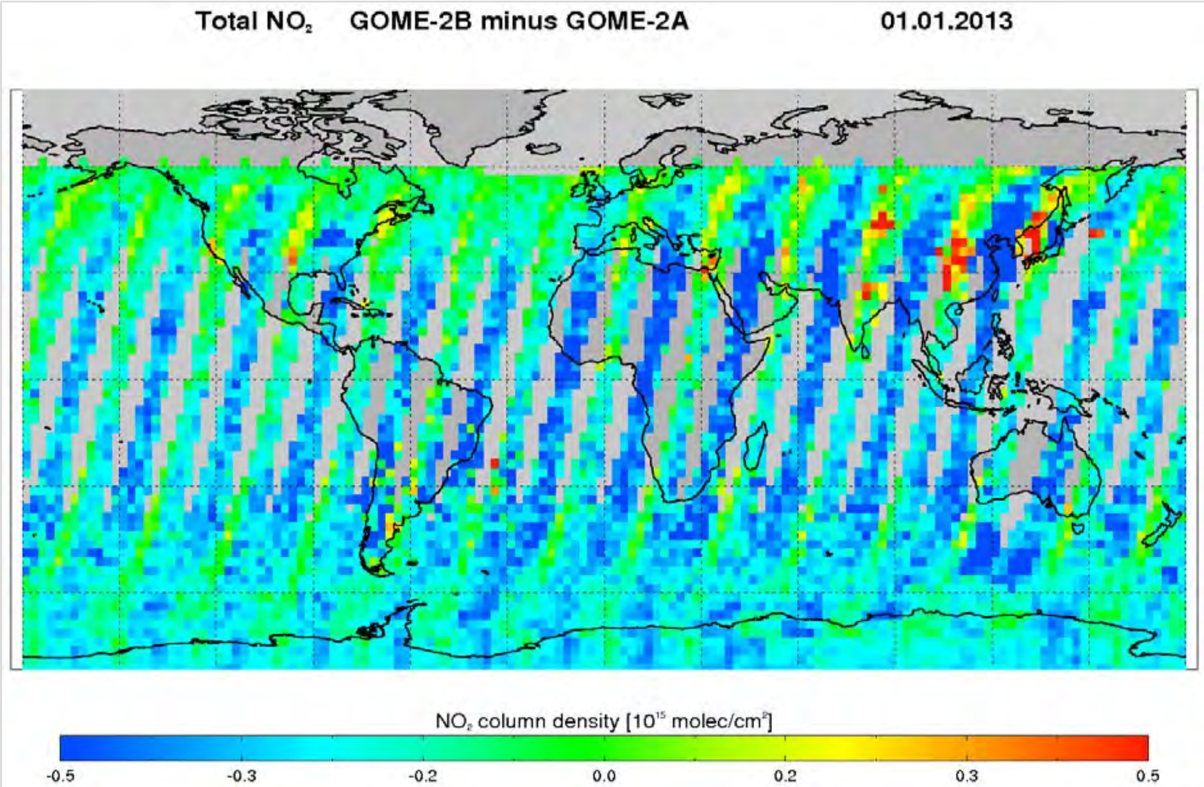

Figure 119: Differences as observed in the retrieved total ("stratospheric") columns for NO_2 by DLR/O3MSAF between Metop-B / FM2 and Metop-A / FM3.

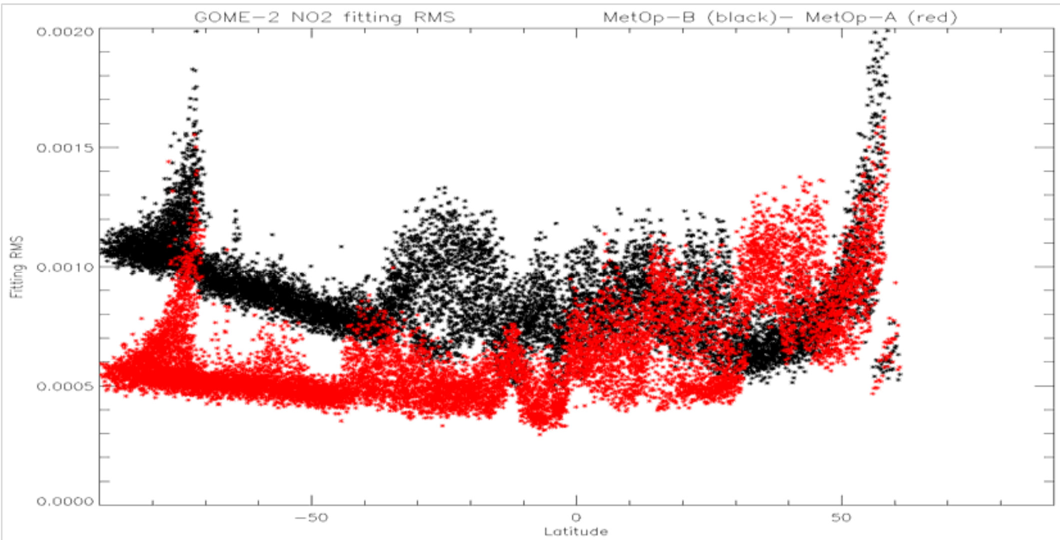

Figure 120: Fit residuals as observed in the retrieval of total "stratospheric" columns for NO_2 by DLR/O3MSAF for Metop-B / FM2 (30 December 2012) and Metop-A / FM3 (30 December 2007).

5.2.2 Investigations of fit residuals

5.2.2.1 NO2: 425 nm-450/500 nm; Channel 3

5.2.2.1.1 BIRA-IASB

BIRA-IASB provides individual components as fitted during their retrieval of slant-column NO_2 values. See Figure 121 and Figure 122. They observe a larger offset in the spectrum compared to Figure 126 in Section 5.2.1.1.3, in case they use the SMR of the FM2 level 1b product as reference, instead of using a reference Earthshine spectrum as retrieved from a Pacific “background” atmosphere.

Both spectral bands are fitted to include a weighted ζ- (both bands) and a weighted η-vector (only 425 nm-497 nm), both of which are provided from the FM2 instrument polarisation key-data. The ζ-fit contribution panel has an arrow pointing to it in both Figure 121 and Figure 122. This shows a peculiar small-scale spectral structure for version 1.03 of the key-data used for level 1 processing. These structures are known to interfere to some extent with the NO_2 spectral signature shown in the first row, third column of Figure 122. This issue has been resolved with the introduction of calibration key-data version 1.03. For details and results see Section 4.9.

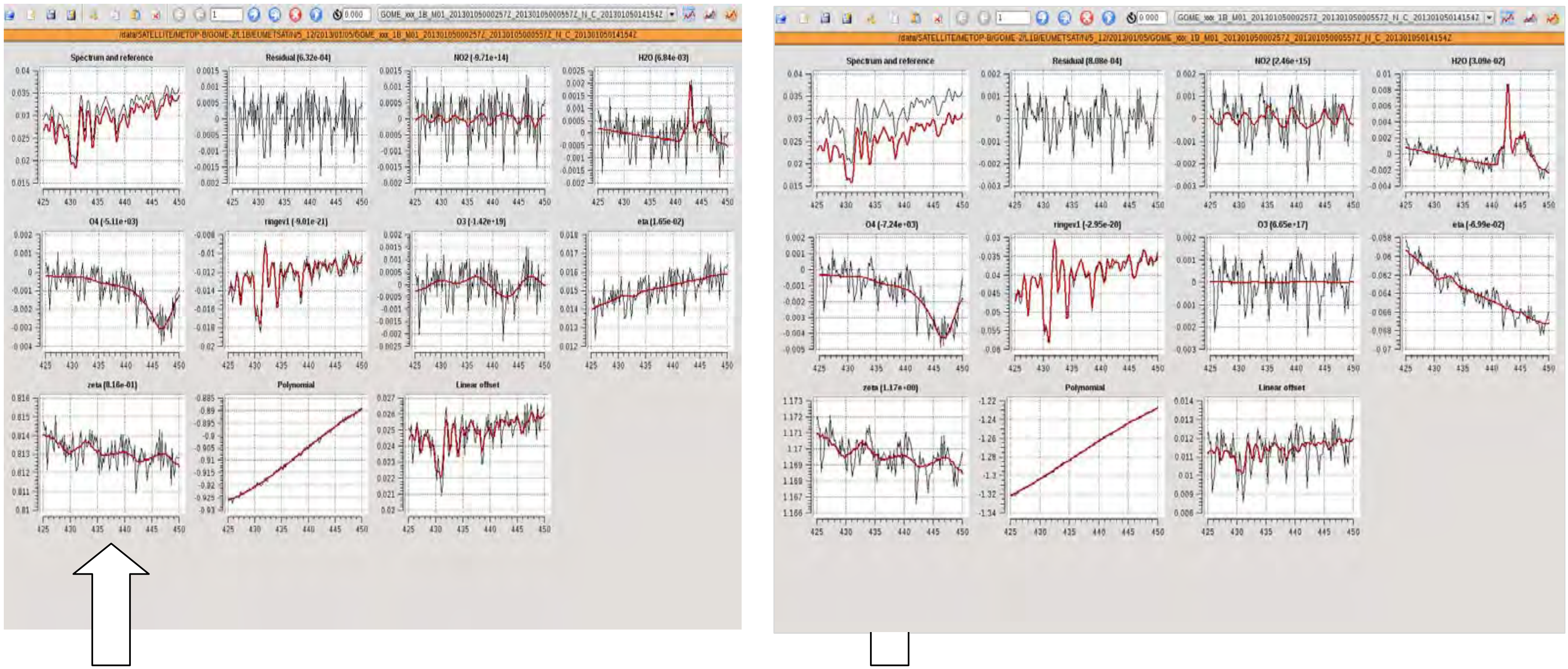

Figure 121: Fit residual components for the retrieval of "stratospheric" slant columns of NO_2 as reported by BIRA-IASB for Metop-B / FM2 on 5 January 2012 for the 425nm -450 nm retrieval band. The right panels show all components used for a fit for which the product SMR is used. The left panel shows the same but for a fit with a reference Earthshine spectrum derived from the pacific area.

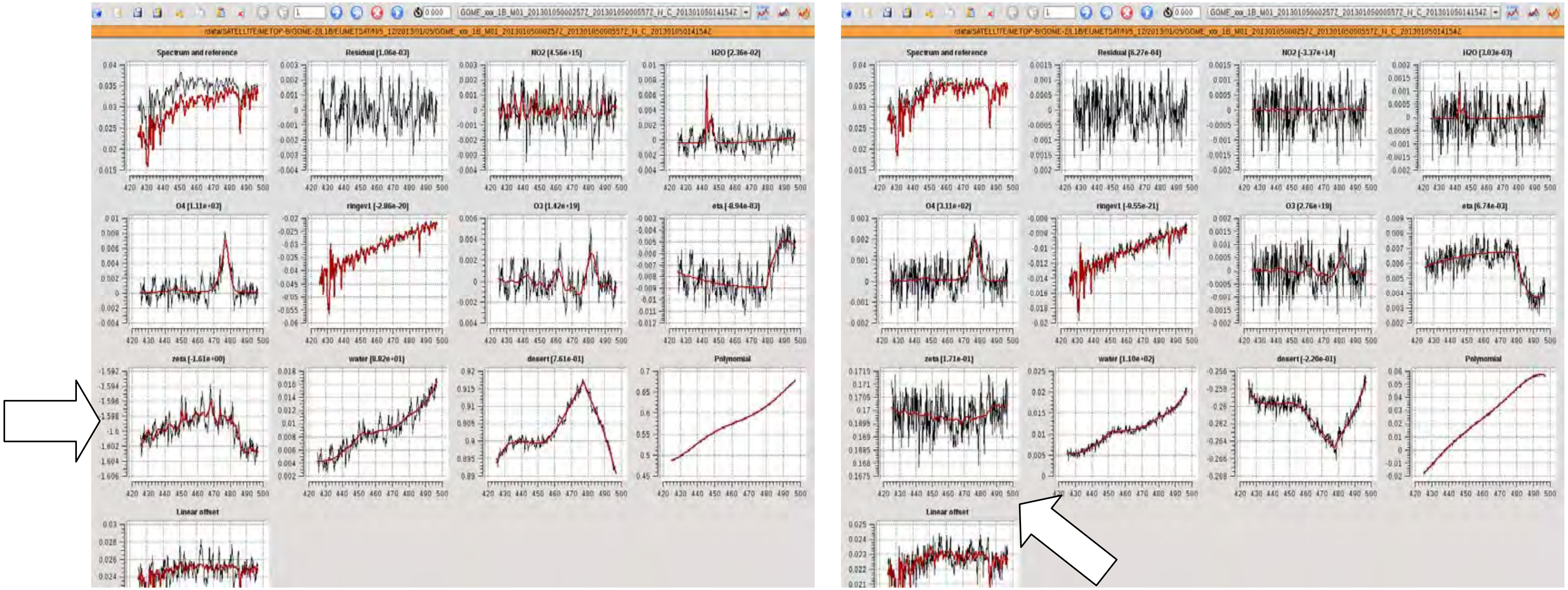

Figure 122: Same as Figure 121 but for the wavelength region of 425 nm- 497 nm. This fit includes also an η-residual component in addition to the ζ-signal also fitted in the smaller wavelength band.

5.2.2.2 Ozone: 290 nm-380 nm

5.2.2.2.1 BIRA-IASB

BIRA-IASB uses a GODFIT direct-fitting approach to retrieve ozone total columns in the spectral region between 325 and 335 nm. They observe slightly larger spectral structures for Metop-B / FM2 direct fitting results than for Metop-A / FM3 at least in their early month in orbit. See Figure 123.

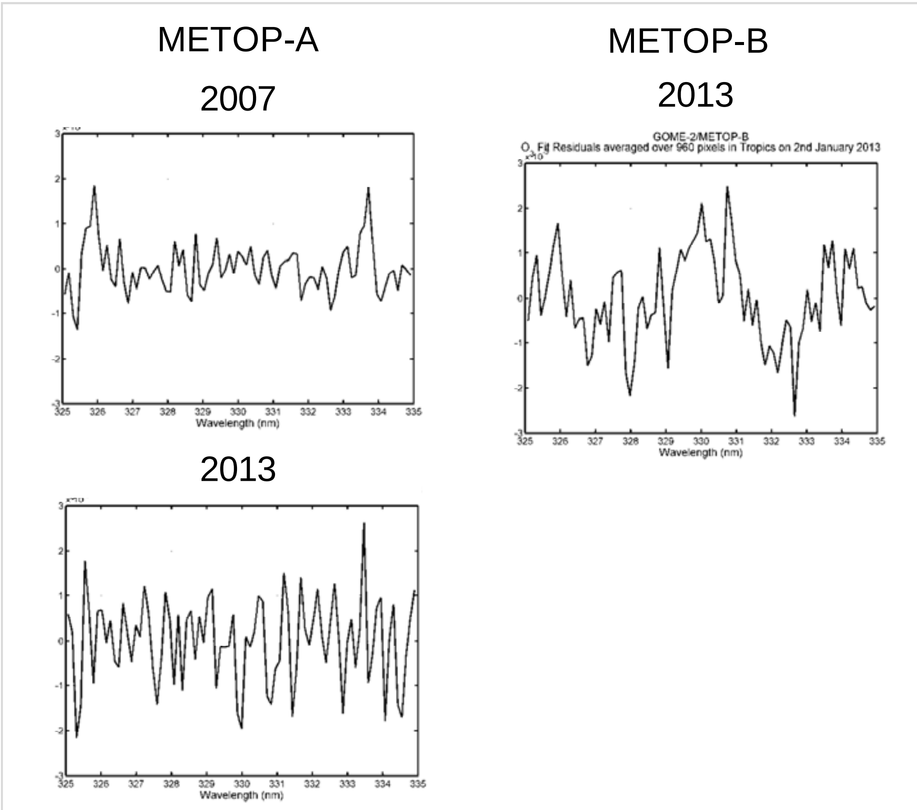

Figure 123: Metop-A / FM3 (left panels) and Metop-B / FM2 (right panels) direct fitting residuals for total ozone column fits by BIRA-IASB as taken in 2013 and 2007 (see title).

Results from BIRA-IASB show that FM2 total column retrieval residuals are markedly different to those from early FM3 retrievals in the region between 325 nm and 335 nm, whereas other regions in channel 2 look more similar.

A wavelength dependent offset fitted to the data, as illustrated in Figure 124, helps to reduce the fit-residual, as evidenced in Figure 125.

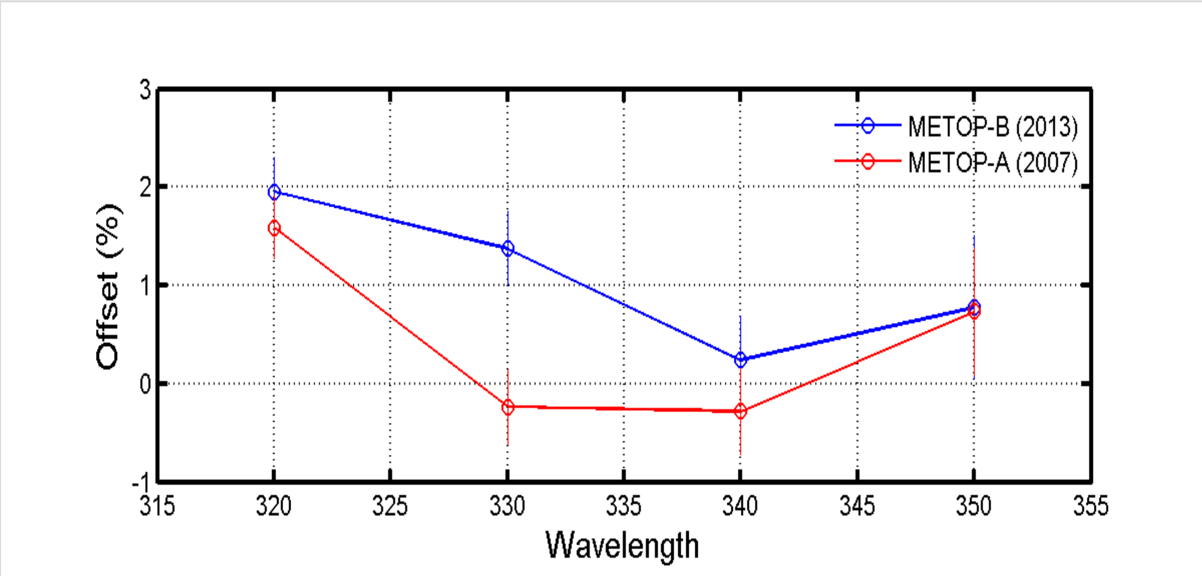

Figure 124: BIRA-IASB fitted wavelength dependent offset in GODFIT total ozone column retrievals for 2013 Metop-B / FM2 and for 2007 Metop-A / FM3 retrievals. The offset is fitted in 4 successive intervals (10 nm wide, centered at given wavelength). Results are then averaged over 2 orbits in a -30°/+30° latitude band in Pacific area

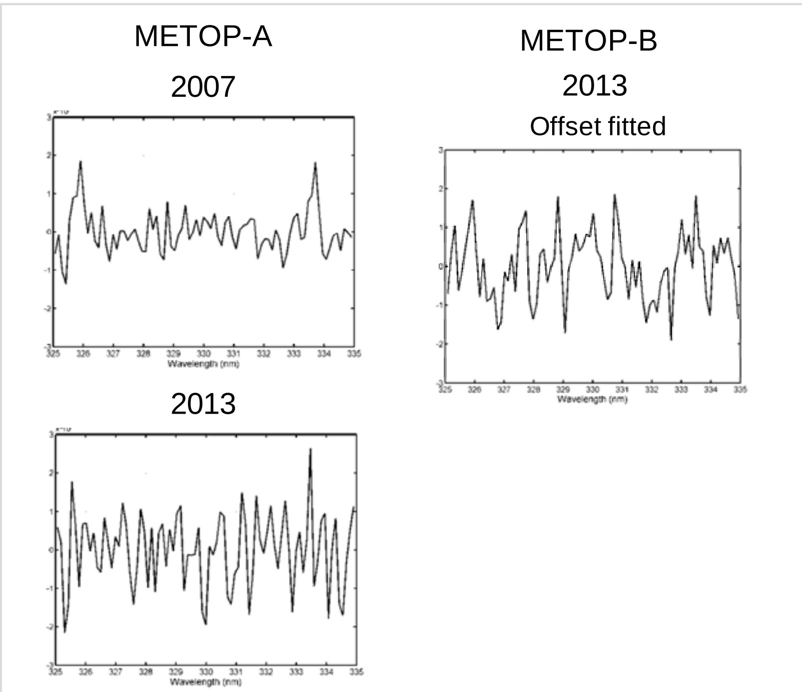

Figure 125: Metop-A / FM3 (left panels) and Metop-B / FM2 (right panels) direct fitting residuals for total ozone column fits by BIRA-IASB as taken in 2013 and 2007 (see title). but with a wavelength- dependent offset as shown in Figure 124 fitted to reduce the residual for Metop-B / FM2 retrievals.

5.2.2.2.2 KNMI / O3MSAF operational product

The KNMI observes spectral patterns in their remaining fit residuals from their operational ozone profile retrieval code (Opera). To date, they have restricted their analysis to the region between 300 nm and 330 nm. Figure 126 shows the measured and simulated (Opera-tailored LIDORT-based forward model) spectra along with the residual patterns in both absolute and relative quantities.

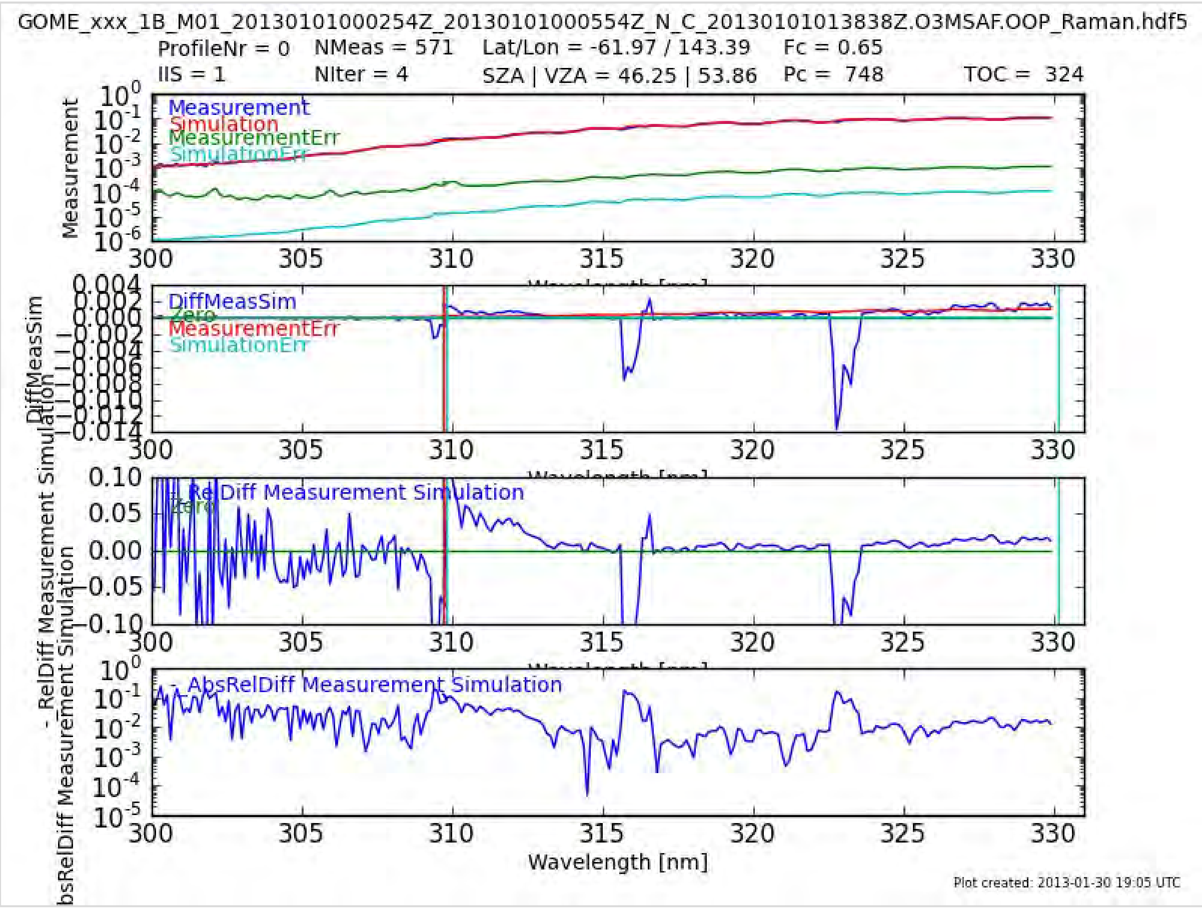

Figure 126: Opera (LIDORT based) forward model simulation (top-panel red line) and Metop-B / FM2 measurements (top-panel blue line) along with their corresponding errors (light blue and green respectively). The remaining panel shows the relative and absolute differences between the measured and simulated data.

Overall, the observed residuals look similar to the ones observed by NOAA-NESDIS (especially in the overlap region)–except for some abnormal spectral structures observed around 316 nm and 323 nm which are not visible in the NOAA-NESDIS data. Those patterns are currently the subject of investigations concerning the slit-function or the use of the slit function at RAL.

5.2.2.2.3 NOAA-National Environmental Satellite and Data Information Service (NESDIS)

The NOAA-NESDIS bases its analysis on a principle component evaluation of the retrieval co-variance matrices over a large spectral region, 290 nm-380 nm. A key element in the process is the first three or four principal component patterns and their Eigen-value Orthogonal Functions (EOFs). Depending on the spectral region, these usually represent the main and expected atmospheric signals, including the ozone profile and clouds. Once these are removed, the remaining significant principle components with significant regular patterns may be related to underlying issues in the retrieval model or in the calibration of level 1 radiance data.

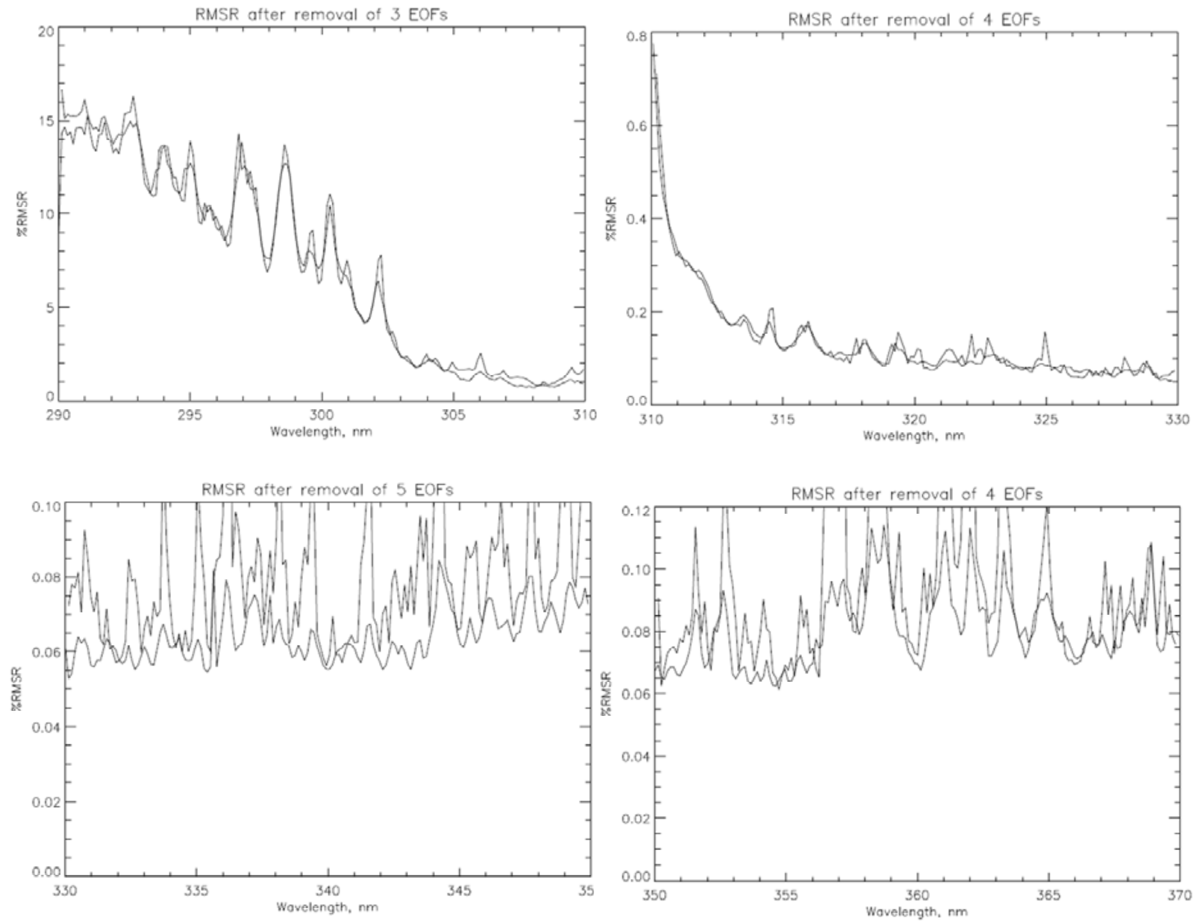

Figure 127: RMS residual values in percent of the averaged measured spectrum. The residual is the reconstructed spectrum for the first couple of EOFs (see title above each plot) with respect to the observed averaged spectrum. For higher wavelength, more identifiable atmospheric EOF components are visible in the spectrum (like surface contributions) than at lower wavelength.

From the data in Figure 127, we may conclude that, as has been observed for Metop-A / FM3, there is a significant increase in the observed radiometric bias towards lower wavelength, below 305 nm. This may be related to Stray-light contributions ([RD12]). There is also an increased residual towards the channel 2 to channel 1 boundary in channel 2, which is expected due to the steep gradient of the radiometric response function and the large associated errors in this region. The same is probably true for the channel 1 boundary towards 310 nm, but this is not clearly visible because of the different scale in the plot provided in Figure 127. The observed residuals are usually larger at solar Fraunhofer line positions because of the large difference in the signal-to-noise ratio in these lines.

5.2.3 Level-2 User Status Summary after the 48th and 49th Joint GSAG/O3MSAF Meetings

The overall status of level 2 retrieval accuracy has initially been summarised at the 48th GSAG meeting at EUMETSAT, which took place on 14 February 2013.

Channel	*Status*	*Issue/Action*
Channel 1	OK	
Channel 2	Some issues with level-2 offsets and persistent residuals identified	Slit-function ghosts (RAL) Cross-section (GSAG/O3MSAF)
Channel 3	Persistent residual structures and angular offsets in total column and residuals identified	Cleaning of key-data (EUM) in spectral and angular direction
Channel 4	OK	

Table 12: Summary of level-2 product status at the 48th GSAG 14 February 2013 using demonstrational level 1 data.

5.2.3.1 Channel 1 and 2

The GASG and O3MSAF operational product producers confirmed that the observed channel 2 issues are very likely due to problems related with the level-2 retrievals themselves: cross-section or slit-function related issues. This has been summarized in Section 5.2. For the profile retrievals for ozone in channel 1 and 2 only preliminary indicative results have been presented to date. This demonstrates the improved signal-to-noise and, therefore improved information content from FM2 because of higher overall signal levels. The stray-light level in channel 1 and 2 is a concern here, though this probably has to be dealt with as a “design” feature of the instrument. Mitigating actions for this have so far been mostly implemented at the level-2 level (c.f. [RD12]).

5.2.3.2 Channel 3

From the level-2 perspective, channel 3 has been identified to show some clear instrument key-data related-problems. Consequently, these problems have been addressed with the update of calibration key-data version 1.02 to 1.03 (7 May 2013). This update served to solve at least the main issues in channel 3. This was detailed in a presentation during the 49th GSAG special meeting on tandem operations, which took place on 25 April 2013 at EUMETSAT.

5.2.3.3 Status by End of Commissioning and Conclusion

By the 48th GSAG, the users had already expressed their satisfaction with the observed data quality [RD25]. The issues then identified and summarised in Table 12 were not considered serious enough to block the start of operations in February 2013. After the most recent updates were finished, the users confirmed this status and encouraged EUMETSAT to release the data in operational status at the 49th GSAG [RD26]. Table 13 summarises the status from a level-2 perspective as presented at this 49th GSAG on tandem operations, which took place on 25 April 2013 at EUMETSAT.

Channel	***Status***	***Issue/Action***	***Comments***
Channel 1	OK		OK with respect to the requirements for operational status. Outstanding issues as addressed in the text will need to be done as part of normal work cycle.
Channel 2	Some issues with level-2 offsets and persistent residuals identified	Slit-function ghosts (RAL) Cross-section (GSAG/O3MSAF)	NOT Blocking
Channel 3	Some issues with level-2 offsets and persistent residuals identified	Slit-function ghosts (RAL) Cross-section (GSAG/O3MSAF)	NOT Blocking
Channel 4	OK		OK with respect to the requirements for operational status. Outstanding issues as addressed in the text will need to be done as part of normal work cycle.

Table 13: Summary of level-2 product status at the 49th GSAG 25 April 2013 using pre-operational level 1 data.

6 CONCLUSIONS

6.1 Product Validation Summary

We consider the current level 1B GOME-2 / FM2 product of sufficient quality for calibrated radiances, spectral calibration as well as geo-referencing parameters. . Currently, the product is of similar quality and often significantly better quality than the operational level 1B product released in July 2007 for Metop-A / FM3. It should be released with operational status to all users.

6.2 Product Validation Issues

Tasks to be undertaken:

Task	*Done during*
Monitoring offset (Stray-light) and instrument degradation levels	**routine operations**
Improve if possible the goniometric key-data for the solar diffuser	**Normal work assignment for FM3**
Detailed evaluation of the observed level-2 fit residuals and product offsets in relation to remaining key-data deficiency need to be carried out during the evaluation of the SAF products for operational status	**SAF review cycle**
Coordinate, implement, and oversee the recommendation for tandem operations (see recommendation by the 49th GSAG),	**normal work based on GSAG/STG-SWG/OPSWG recommendations**

6.3 Actions for Product Rollout

Dissemination to all users with “operational” status can start without further updates.

6.3.1 Time Schedule

We propose the notification to users on the operational status update by the 7 May 2013.

6.3.2 User Notification

Users have already been notified on the overall planned timeframe for change of status via the regularly issued news letter and dedicated e-mails, as well as via the weekly UNS message.

A dedicated e-mail to inform the users on the start of dissemination has already been sent more than two week ahead of the proposed date indicating that the start is pending a positive decision by the PVRB board.

6.3.3 Web Update

The product navigator will be updated as needed. This validation report will be published in the technical documents section on the EUMETSAT web-pages.

7 RECOMMENDATION

Based on the analysis and verification contained in this product validation report, we recommend updating the status to operational.